PHD

Thermo-hydro-mechanically modified cross-laminated Guadua-bamboo panels

Archila Santos, Hector Archila

Award date:
2015

Awarding institution:
University of Bath

Thermo-hydro-mechanically modified cross-laminated Guadua-bamboo panels

by

Hector F. Archila Santos

A thesis submitted for the degree of
Doctor of Philosophy

University of Bath
Department of Architecture and Civil Engineering
March 2015

I am not reinventing the wheel,
I just think that it would be much better if it were round,
symmetric and with a centred axle…

Acknowledgments

I would like to express my gratitude to Dr. Martin Ansell for his balanced supervision approach during the course of my PhD. I still do not understand how he manages to be always there when required, comply with all his many academic and administrative duties, write books, papers and reports, complete sponsor forms, read this whole thesis, explain to me engineering and material science concepts, which I could not get my head around, and to distance himself enough to let things flow. My special thanks to Prof. Pete Walker for offering me the PhD position on the first place and for setting a good example of how to be respectable and modest at the same time. Thanks also goes to all the technicians at the civil and mechanical engineering labs, the wood workshop, and to the administrative and support staff in the Departments of Architecture & Civil Engineering and Mechanical Engineering: Glen, Walter, Will, Rob, David W., Neil, David A., Claire, Sophie and Nigel; you have literally made it possible, easier and more enjoyable. A big thank you to Dr. Graham Ormondroyd at Bangor University for allowing me access to the 'big hot press' used for densifying my material and assembling the 'large' panels; as well as to his team at the Bio-Composites Centre in Mona, Nick, Bronia, Dave and all the rest who provided outstanding support, working extra-hours and ensuring the work was done on time at to a high standard.

Special thanks to Wilson, Adiela and all the family ARME for their friendship, motivational and valuable support in materials and logistics; to Prof. Caori Takeuchi who supported my application to this PhD and has always been there.

I am extremely grateful to all my fellow colleagues at 4.15 (the lab space designed as office and sometimes labelled as electrical cupboard), who have rightly become good friends. There is not any other place I would have rather worked at; Gianluca, Tom, Jun-zhe, Dragos,

Daniel, Manuel, and Lizette, you more than made up for the lack of light, tidiness and space! I also have to acknowledge the joint work undertaken with two of them: Gianluca and Daniel who provided remarkable support on the use of EDXS and FIB techniques and on the development of the FEM, respectively. Results of their contribution have been included in this thesis.

A huge thank you goes to Anyela for giving me the Gung Ho!. I wouldn't have started this journey if it were not for you, to you '*ibid*' .

I am profoundly grateful to my family for giving me a line to earth, Sophie, Pao, Caro, Má, Pá, Nona, and to Louise for putting up with this sometimes stubborn man, forcing him away from his work addiction and engulfing me with loving melodies.

Finally, I would like to thank all the Colombian tax payers that have indirectly and most likely, unknowingly paid for most of my PhD studies and provided me with a generous stipend for almost four years; in spite of priority needs to be covered in the country. I hope, I can honour their contribution with equal generosity and through material actions. I am also grateful to Amphibia Group Ltd, Colciencias and Colfuturo, Colombian organisations that sponsored my research at the University of Bath. Thanks also go to Santander, The worshipful company of Armourers and Brasiers and the Forest Products Society for sponsoring research and conference trips to different parts of the world.

Abstract

Guadua angustifolia Kunth (Guadua) is a bamboo species native to South and Central America that has been widely used for structural applications in small and large-scale buildings, bridges and temporary structures. Currently, its structural use is regulated within seismic resistant building codes in countries such as Peru and Colombia. Nevertheless, Guadua remains a material for vernacular construction associated with high levels of manual labour and structural unpredictability. Guadua buildings are limited to two storeys due to the overall flexibility of the slender and hollow culms and its connection systems. Its axial specific stiffness is comparable to that of steel and hardwoods, but unlike wood, Guadua's hollow structure and lack of ray cells render it prone to buckling along the grain and to transverse crushing. As a result, Guadua's mainstream use in construction and transformation into standard sizes or engineered Guadua products is scarce. Therefore, this work focussed on the development of standardised flat industrial structural products from Guadua devising replicable manufacturing technologies and engineering methods to measure and predict their mechanical behaviour. Cross-laminated Guadua panels were developed using thermo-hydro-mechanically modified and laminated flat Guadua strips glued with a high performance resin.

Guadua was subjected to thermo-hydro-mechanical (THM) treatments that modified its microstructure and mechanical properties. THM treatment was applied to Guadua with the aim of tackling the difficulties in the fabrication of standardised construction materials and to gain a uniform fibre content profile that facilitated prediction of mechanical properties for structural design. Densified homogenous flat Guadua strips (FGS) were obtained. Elastic properties of FGS were determined in tension, compression and shear using small-clear specimens. These properties were used to predict the structural behaviour of G-XLam panels comprised of three and five layers (G-XLam3 and G-XLam5) by numerical methods.

The panels were assumed as multi-layered systems composed of contiguous lamellas with orthotropic axes orientated at 0° and 90°. A finite element (FE) model was developed, and successfully simulated the response of G-XLam3 & 5 panels virtually loaded with the same boundary conditions as the following experimental tests on full-scale panels. G-XLam3 and G-XLam5 were manufactured and their mechanical properties evaluated by testing large specimens in compression, shear and bending. Results from numerical, FE predictions and mechanical testing demonstrated comparable results. Finally, design and manufacturing aspects of the G-XLam panels were discussed and examples of their architectural and structural use in construction applications such as mid-rise buildings, grid shells and vaults are presented.

Overall, this research studies THM treatments applied to Guadua in order to produce standardised engineered Guadua products (EGP), and provides guidelines for manufacturing, testing, and for the structural analysis and design with G-XLam panels. These factors are of key importance for the use of Guadua as a mainstream material in construction.

Table of contents

List of Figures

List of Tables

Symbols and abbreviations

Symbols

B	Biomass
C	Carbon content
w_g	Green-weight of the measured biomass
ρ	Density
L	Length
ΔL	Change in length per unit of original length
l_0	Initial length of the extensometer
l_1	Final length of the extensometer
l	Dpan, gauge length (A-B length of the virtual extensometer)
b	Width
h	Thickness
m	Slope $(F_2 - F_1)/(a_2 - a_1)$
A	Cross sectional area of the panel
λ	slenderness ratio
N	Neutral axis
Z	Half the total thickness of the panel
z_i	Distance between the centre point of each layer and the central axis of the panel.
I	Second moment of area of the cross section
I_o	Second moment of area of the cross section about its neutral plane
C'	Shear stress correction factors by Pierron & Vautrin 1994
S'	Shear strain correction factors by Pierron & Vautrin 1994
V_f	Volume fraction
ε	Engineering strain
$\mu\varepsilon$	Microstrain
X_1	Geometric axis corresponding to the longitudinal (L) orientation
X_2	Geometric axis corresponding to the tangential (T) orientation
X_3	Geometric axis corresponding to the radial (R) orientation
f_c	Compressive strength
E_1	Modulus of elasticity along the X_1 (longitudinal orientation)
E_2	Modulus of elasticity along the X_2 direction (tangential orientation)
E_3	Modulus of elasticity along the X_3 direction (radial orientation)
E_b	Local modulus of elasticity in bending
E_t	Young's modulus (longitudinal)
E_0	Longitudinal modulus of elasticity
E_{90}	Transverse modulus of elasticity
E_m	Modulus of elasticity in bending

$E_{C,0}$	Compression moduli of elasticity in the longitudinal direction (at 0°).
$E_{C,90}$	Compression moduli of elasticity in the transverse direction (at 90°).
Ep_m	Panel modulus of elasticity in bending
Ep_{m-0}	Panel modulus of elasticity in bending parallel to the main direction of the panels (outer layers at 0°).
Ep_{m-90}	Panel modulus of elasticity in bending perpendicular to the main direction of the panels (outer layers at 90°).
Ep_{c-0}	Panel modulus of elasticity in compression along to the main direction of the panels (outer layers at 0°).
Ep_{c-90}	Panel modulus of elasticity in compression along the transverse of the panels (outer layers at 90°).
F_{max}	Maximum permitted load
$F_{\max est}$	Estimated maximum permitted load
G^{app}	Apparent shear modulus
G^{chord}	Shear chord modulus of elasticity
G_0	Panel shear modulus parallel to the grain
G_v	Panel shear modulus
MOR_b	Modulus of rupture in bending
υ	Poisson's ratio
υ_{12}	Ratio of passive strain along X_2 (ε_2) to active strain along X_1 (ε_1).
υ_{13}	Ratio of passive strain along X_3 (ε_3) to active strain along X_1 (ε_1).
υ_{21}	Ratio of passive strain along X_1 (ε_1) to active strain along X_2 (ε_2)
υ_{32}	Ratio of passive strain along X_2 (ε_2) to active strain along X_3 (ε_3)
Υ	Shear strain
Υ^{av}	Average shear strain
τ	Shear stress
τ^{av}	Average shear stress
CoV	Coefficient of variation
d.w.	Dry weight
MC	Moisture content
ppm	Parts per million

Subscripts

m	bending
t	tension
c	compression
v	panel shear
n	number of layers of the panel (from top face to bottom face)
I	rank of layers from top face
0	parallel to length of the panel (direction of the grain of the face layers)
90	perpendicular to the length

Abbreviations

ACE	Department of Architecture & Civil Engineering (University of Bath)

AIS	Asociación Colombiana de Ingeniería Sísmica
B.C.E.	Before the Common Era
BRE	Building Research Establishment
BS	British Standard (EN: European Norm)
BSI	British Standard Institution
CARDER	Corporación Autónoma Regional de Risaralda
CDM	Clean Development Mechanism
CER	Certified Emission Reductions
CICM	Centre for Innovative Construction Materials
COLCIENCIAS	Departamento Administrativo de Ciencia Tecnología e Innovación (Colombia)
COLFUTURO	Fundación para el futuro de Colombia
COP	Colombian pesos ($)
CORPOCALDAS	Corporación Autónoma Regional de Caldas
CORTOLIMA	Corporación Autónoma Regional del Tolima
CRQ	Corporación Autónoma Regional Del Quindío
DBH	Diameter at breast height
DIC	Digital Image Correlation
EMC	Equilibrium moisture content
EDXS	Energy Dispersive X-ray Spectrometer
FAO	Food and Agriculture Organization of the United Nations
FE	Finite elements
FIB	Focussed Ion Beam
FOREC	Fondo para la Reconstrucción y desarrollo social del Eje Cafetero
FPL	Forest Products Laboratory
FSP	fibre saturation point
GHG	Greenhouse gas
IAC	Interface Analysis Centre
ICC	International Code Council
ICONTEC	Instituto Colombiano de Normas Técnicas
ICPCC	Intergovernmental Panel on Climate Change
IAC	Interface Analysis Centre of the University of Bristol
INBAR	International Network for Bamboo and Rattan
IPCC	Intergovernmental Panel Climate Change
IPGRI	International Plant Genetic Resources Institute
LCA	Life cycle assessments
LVDT	Linear variable differential transformer
MAS	Microscopy analysis suite at the University of Bath
MOE	Modulus of elasticity in bending
MinAmbiente	Ministerio de Ambiente Vivienda y Desarrollo Territorial
MechEng	Departments of mechanical engineering within the University of Bath
MEng	Master of Engineering
NSR 2010	Norma Sismo Resistente 2010 (Colombian code of seismic resistant constructions)
NTC	Norma Técnica Colombiana
NWFP	Non Wood Forest Product

OSB	Oriented Strand Board
PVC	Polyvinylchloride
PW	Primary cell wall
REDD	Reduce Emissions from Deforestation and Degradation
SEM	Scanning Electron Microscope
SIP	Structural Insulated Panels
SWB	Strand Woven Bamboo
TH	Thermo-Hydro (treatment)
THM	Thermo-Hydro-Mechanical (treatment)
TM	Thermo-Mechanically (treatment)
UNEP	United Nations Environment Programme
UNFCCC	United Nations Framework Convention on Climate Change
UN-HABITAT	United Nations Human Settlements Programme

Chemical formulas

$CaCO_3$	Calcium carbonate
$Ca(OH)_2$	Calcium hydroxide
CO_2	Carbon dioxide
C-S-H	Calcium silicate hydrate
H_3BO_3	Boric acid
NaOH	Sodium hydroxide
SiO_2	Silicon dioxide (silica)

Materials

CLT	Cross-laminated timber
EBP	Engineered bamboo products
EGP	Engineered Guadua products
ETP	Engineered timber products
FGS	Flat Guadua strips/sheets
G-XLam	Guadua cross-laminated
G-XLam3	Guadua cross-laminated comprising three layers
G-XLam5	Guadua cross-laminated comprising five layers

1. Introduction

Background

Traditional construction with round culms of the bamboo species *Guadua angustifolia* Kunth (Guadua) is regulated by the seismic-resistant building code (norma sismo resistente NSR) for structural applications in Colombia (MinAmbiente, 2010a). Figure 1-1 illustrates the structure of a holiday house that uses Guadua as mainstream material complying with NSR regulations. This house combines structural Guadua frames and wall framing systems using round and opened-flat (riven) Guadua.

Figure 1-1. Structure of López house by Hector Archila, La Mesa, Cundinamarca, 2005.

Traditional Guadua construction has demonstrated structural stability during earthquakes, architectural design flexibility and eco-friendly attributes. Nevertheless, there are several factors concerning buildability, standardisation, durability and sustainability of building systems with Guadua. For instance, Guadua construction is regarded as handcrafted. Guadua's natural variability along and across its section and its hollow and tapered structure require the expertise of experienced craftsmen during construction. Skilled expertise in carpentry is essential when making cuts, connections and fitting conventional building elements (e.g. doors and windows). Frequently structural design needs to be adjusted during construction or validated through full-scale testing. In addition, the bio-deterioration of the material presents a challenge for the protection of externally exposed Guadua elements. Furthermore, despite being widely promoted as an environmentally friendly building system, traditional Guadua systems make an intensive use of aggregates, cement and steel in walls and foundations, which contributes to about 95% of the environmental impact. Particularly, the use of a thick sand/cement render in structural wall framing systems using Guadua contributes to 85% of the wall mass (Murphy *et al.,* 2004). In addition, end of life processes for recycling or reusing the material have not been addressed and the CO_2 stored within Guadua is released back to the atmosphere in relatively short periods of time with no real contribution to the carbon sink (Murphy *et al.,* 2004).

Engineered Guadua products have been developed to tackle these issues. However, research and development on these type of materials is scarce and has been limited to replicate Chinese products and technologies developed for the bamboo species Moso mainly for flooring applications. One of the most employed technologies is the lamination of unidirectional strips of Guadua for the production of beams and panels. This fabrication method results in an energy intensive process due to the machining of round culms into rectangular strips that produces high amounts of waste (de Flander & Rovers, 2009; Vogtländer *et al.,* 2010). Moreover, the discarded material (about 50%) includes the densest fibre section along the wall cross section, which possesses the highest tensile strength in bamboos (Amada *et al.,* 1997). Consequently, commercialization is hindered and the structural potential of the material is certainly unexploited. Hence, the development of engineered Guadua products needs to exploit its remarkable features, tackle the issues regarding manufacture, short life span and buildability. It also has to enhance the material's compatibility with conventional building systems and reduce the wastage and environmental impact in the built environment.

Projections have been made which demonstrate that one laminated Guadua home could

be built by utilising one hectare of a managed Guadua forest per year (de Flander & Rovers, 2009). This means that with the bamboo resources available worldwide, in just one year 31.5 million houses could be built without affecting or increasing the amount of established bamboo plantations. This is just 14% short of the 36.5 million homes required annually by 2025 (UN-HABITAT, 2009). Guadua construction could also sequester about 285.39 million tonnes of carbon per year and improve indoor air quality thanks to its natural permeability. However, the development of efficient and feasible processing methods for manufacturing engineered Guadua products and structural systems that integrate to conventional construction systems, need to be devised.

Cellulose based resources have increasingly been used as replacements for conventional construction materials reducing the negative carbon footprint (Sutton *et al.,* 2011; Yates *et al.,* 2013). For example multi-storey timber buildings have demonstrated their potential to store up to 80% more carbon than reinforced concrete buildings, reduce energy bills and provide high living standards (Sutton *et al.,* 2011). Cross-laminated timber (CLT) systems reduce the anisotropy of wood properties, minimise the impact of natural defects and provide a standardised and highly processed flat panel product for construction. Adhesives used for CLT guarantee a strong interface between cross layers. Modern frame walling systems known as light-frame construction are widely accepted for their favourable response during earthquakes due to their low mass and effective dissipation of energy through fastened shear walls (Lindt, 2004). Improved environmental performance by the reduction in the use of dimensional lumber, increased durability and reduced labour time are some key features of this system (PATH, 2006). In addition, features such as weather tightness, fire performance and thermal comfort can be explored by insulating the boards in the same way as Structural Insulated Panels (SIP) where a thick core is sandwiched between two boards of plywood, OSB (oriented stranded board) or fibre-cement.

This work aims to develop engineered Guadua products for structural applications via straightforward processes with low environmental impact and wastage. Engineered Guadua products can potentially reduce structural design uncertainties, improve durability, facilitate modularity and prefabrication, enhance the carbon footprint of traditional Guadua construction and offer an alternative to wood products. These are key factors for achieving standardised systems for Guadua construction for the new built environment.

Aim and Objectives

The main aim of the project was to develop standardised flat industrial structural products from Guadua devising replicable manufacturing technologies and engineering methods to measure and predict their mechanical behaviour.

The objectives of the research project were to:

- Characterize the microstructure, chemical composition and mechanical properties of Guadua in order to understand the factors determining its physical features and mechanical behaviour.
- Investigate alternative methods to the conventional processes used for the conversion of round Guadua culms into standard flat pieces.
- Study *state of the art* wood modification techniques that can be applied to bamboo and Guadua for improving its mechanical and physical properties as well as its resistance to decay.
- Apply conventional treatments used for the manufacture of commercial engineered bamboo products to Guadua, and assess their feasibility for Guadua's modification.
- Develop engineered Guadua products that tackle material limitations concerning its irregularity, bio-deterioration short life-span and environmental impact.
- Devise adequate testing methods for the characterisation of the main elastic values of Guadua for the prediction of flat sheet laminated engineered Guadua products.
- Develop numerical and analytical methods for the prediction and/or simulation of the engineered Guadua products' response to set load conditions.
- Devise structural systems for the application of the developed engineered Guadua products in construction.
- Determine opportunities for scaling up the manufacturing technology of the developed engineered Guadua products in Colombia

Programme of work

To pursue the main aim of the research project and its specific objectives, eight main modules of the research were identified:

1. Appraisal of the scientific literature available and current practical knowledge on wood, bamboo and Guadua's transformation into engineered products.
2. Experimentation with modification treatments of wood, bamboo and Guadua.
3. Microstructural imaging of specimens to assess treatments applied.
4. Characterization of small specimens through mechanical testing for wood, bamboo and Guadua.
5. Developing numerical methods and FE models for predicting the mechanical response of engineered Guadua products.
6. Manufacture of engineered Guadua products.
7. Characterization of large-scale panel products through mechanical testing.
8. Assessment of buildability, industrial scalability and design alternatives.

Thesis Outline

The thesis follows the programme of work previously described. With the aim of setting the scene of the work undertaken during the research project, the following three Chapters of this thesis provide essential background to the subject and a comprehensive literature review. Chapter 2 includes a review of general features of bamboo and Guadua's anatomy and morphology, its physical and mechanical properties, availability, environmental impact and carbon sequestration. A comparison of the microstructure and physical properties of bamboo and wood is also presented in this Chapter. Chapter 3 is mainly dedicated to Guadua and its uses in construction. In this Chapter, processing methods and issues regarding construction with Guadua and standardised building systems are reviewed. Engineered bamboo and Guadua products and their manufacturing processes are also reviewed. In Chapter 4, wood modifications involving thermo-hydro-mechanical (THM) treatments and their implementation on bamboo are discussed. Key concepts concerning THM modifications of wood are presented in this Chapter with the aim of understanding the chemical,

physical and mechanical changes occurring during THM treatments. Adequate temperatures, pressures and preparation methods for densifying wood and bamboo, together with some recommended post-treatments to avoid spring-back recovery are reviewed. Chapter 5 provides a transition between the conceptual and the experimental Sections of the research. It presents some of the practical experimentation carried out in order to define the THM modifications applied to Guadua. Further experimentation on manufacturing methods is also discussed. The following Chapters are then, the core of the research work undertaken with Guadua. Chapter 6 focusses on the micro-imaging of Guadua and THM modified Guadua specimens. The results of microscopy observation using optical, scanning electron microscopy (SEM) and focussed ion beam (FIB) techniques are presented in this Chapter. Image analysis undertaken in this Section generated information regarding the level of densification achieved during THM treatment and some of the resulting micro-structural changes. Chapter 7 assesses the mechanical properties of densified flat Guadua sheets (FGS) and non-densified small scale specimens of Guadua in instrumented tensile, compressive and shear tests. Chapter 8 describes the transformation process of FGS into cross-laminated Guadua panels (G-XLam). Chapter 9 presents numerical and finite element (FE) analysis to predict the structural performance of G-XLam panels, whilst Chapter 10 assesses the same structural response through mechanical testing of large G-XLam panels. Chapter 11 provides alternatives for the utilization of the G-XLam panel technology in construction applications and analyses their scalability into industrial processes in Colombia. Concluding remarks are given at the end of each Chapter, and are summarised in the final conclusions in Chapter 12. References and information about the author are included at the end of this document.

2. A review of the literature on bamboo & Guadua

Introduction

A giant grass not a tree, hollow, tapered and fast growing, bamboo develops its adult height, diameter and wall thickness in as little as six months. Then, instead of producing new cells as in trees, bamboo consolidates its internal structure for around ten years until decay. This gives bamboo the ability to produce remarkable quantities of biomass and capture large amounts of carbon in less time than trees do. Furthermore, bamboo provides benefits for soil erosion control, water conservation and land rehabilitation. All these features add to the environmental and commercial value of bamboo. However, its potential is commonly overlooked. Bamboo is generally considered as an invasive plant for low-key and temporary applications in gardening, decoration, kitchenware or temporary applications in shelters or scaffolding in the developing world.

Therefore, with the aim of understanding the attributes of this plant and its prospects as an alternative building material, its differences and similarities to trees and other cellulosic plants are explored. This Chapter reviews some of the characteristic features of bamboo in general and the bamboo species *Guadua angustifolia* Kunth (Guadua) in particular. Its anatomical and morphological features and the variation of physical and mechanical properties along and across its grain are explained. The carbon fixation capacity of bamboo plantations and their potential as carbon sinks is also discussed. Its availability, diversity of uses and potential as alternative material to wood are also highlighted. Finally, the case for bamboo as a renewable material that can sequester carbon into long-lasting construction applications and help reduce the pressure over wood forest resources is made.

2.1 Bamboo

Commonly referred to as a giant grass, bamboo is an Angiosperm plant from the *Poeceae – Gramineae* family (grasses) which propagates rapidly by the expansion of underground rhizomes. It is a monocotyledon that can grow for 50 years or more but flowering results in the death of the whole plant in some species (Hidalgo-López, 2003; Liese, 1998). Such delay in the flowering process is attributed to the considerable energy demand of this fast growth plant (Clark, 1997 cited by Lybeer *et al.,* 2006).

Figure 2-1. Bamboo plant from the species *Guadua angustifolia* Kunth

Bamboos are frequently associated with trees and despite both being living organisms with cellulosic structures they possess distinctive physical and mechanical properties, which relate to their morphology, anatomy, growth process, chemical composition and location in the globe.

2.2 Morphology of bamboo

Although the 75 genera of bamboo with about 1250 species possess distinctive features (Liese, 1998), morphologically bamboo can be generally described as a hollow tapered tube (culm), with internodes separated by nodes, which is supported by an intricate root system (rhizome). The culm is the main organ of the aerial part of bamboos (Figure 2-2), which is also comprised of branches, sheaths and foliage leaves (flowering occurs sporadically). The rhizome and culm neck form the subterranean part (Figure 2-3). Culms store about 80% of the carbohydrates required by young plants for their growth, whilst rhizomes store the remaining 20% (Kleinhenz & Midmore, 2001).

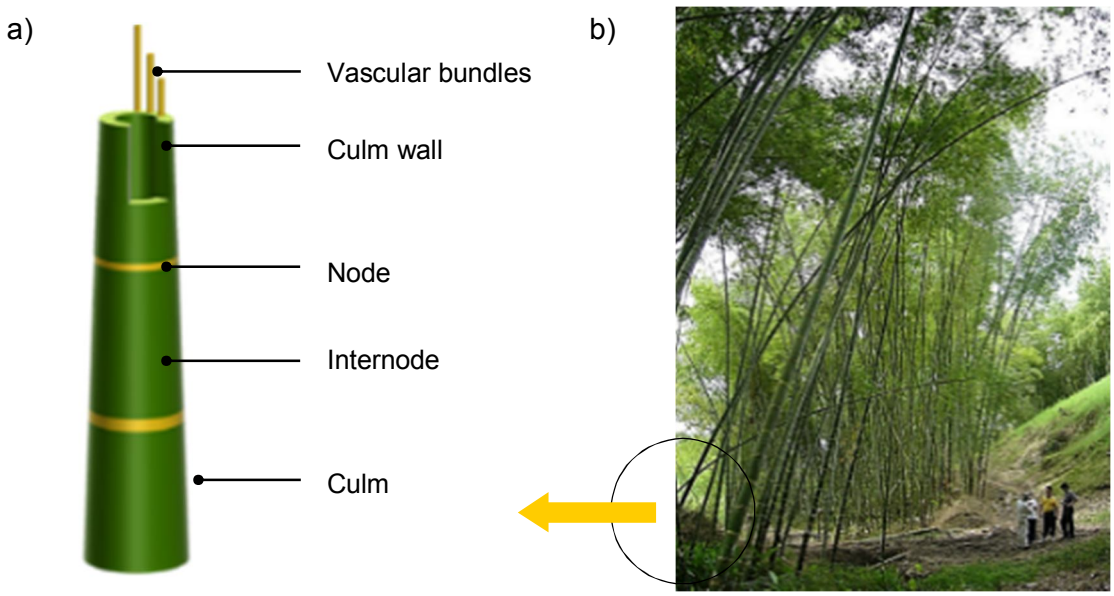

Figure 2-2. (a) Part of the culm, (b) Bamboo plantation.

Depending on the rhizome structure, tropical and temperate bamboos are classified as sympodial and monopodial (Figure 2-3). Both possess characteristic anatomical and morphological features, which determine their physical and mechanical properties (density, strength, bending behaviour, shrinkage and splitting) and thus their end uses. Sympodial bamboos in tropical areas have been widely used as raw material for construction and monopodial bamboos in subtropical regions are finely processed for non-structural applications.

For example, the sympodial species *Guadua angustifolia* Kunth (Guadua) used for construction in South and Central America has large vascular bundles with fibre bundles of variable sizes that confer it with a coarse finish. In contrast, the monopodial *Phyllostachys heterocycla pubescens* (Moso) endemic to Asia is more suitable for smooth finishes for parquet, furniture and decorative applications (Liese, 1998). This is due to its smaller vascular bundles with fairly even distributed fibres around the conductive tissue. Some species such as *Oligostachyum sp.* and from the genus Indocalamus are classified as amphipodal, which combines sympodial and monopodial rhizomes

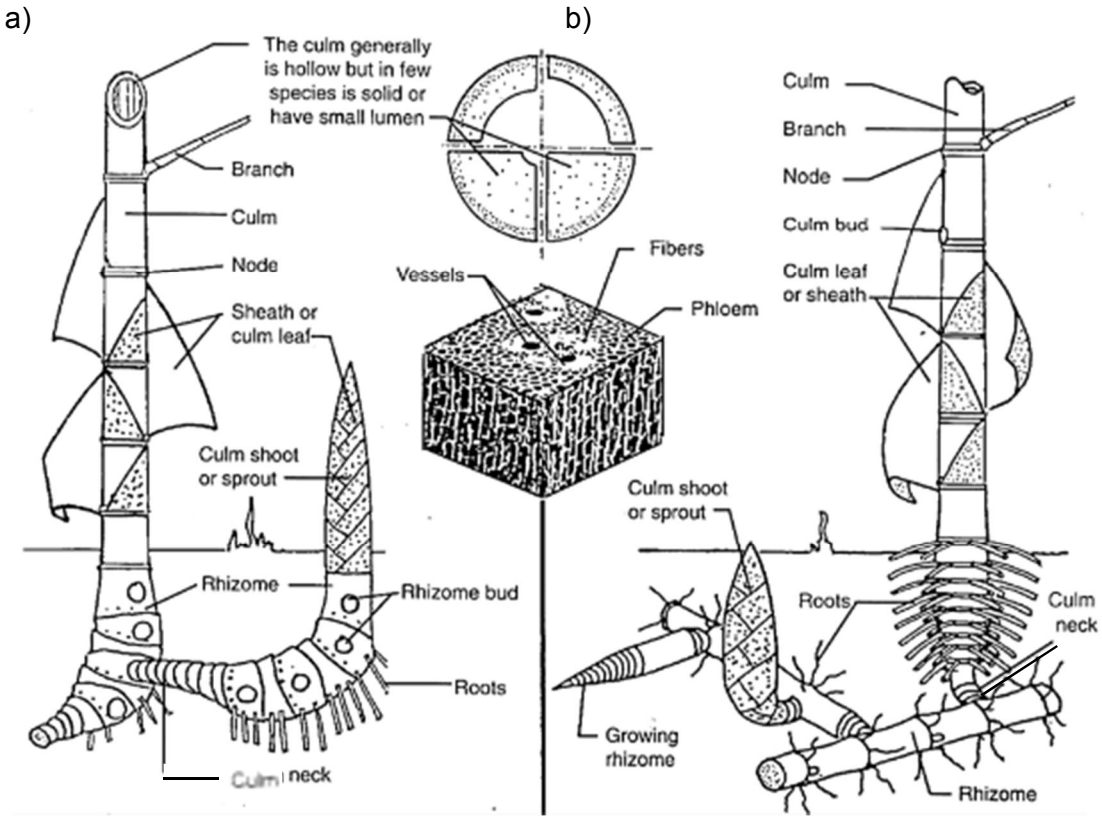

Figure 2-3. Bamboo morphology, (a) Tropical bamboos (sympodial). (b) Temperate bamboos (monopodial) (Hidalgo-López, 2003).

2.3 Anatomy of bamboo

At the cellular and tissue level, the composition of bamboo culms consists of 52% parenchyma cells, 40% fibres and 8% conductive tissues (Liese, 1998). Their simple arrangement in vascular bundles (Figure 2-4) along the stem (Figure 2-5a) allows cellular differentiation and rapid flow of nutrients, which results in the fast elongation of the culm. The main function of parenchyma cells is the storage of starchy nutrients within their large lumens (Liese, 1998), whilst fibres provide structural support to the plant. Unlike heartwood cells in

wood, parenchyma and fibre cells in bamboo remain alive until maturity maintaining a living protoplasm (Gritsch *et al.,* 2004; Liese, 1998).

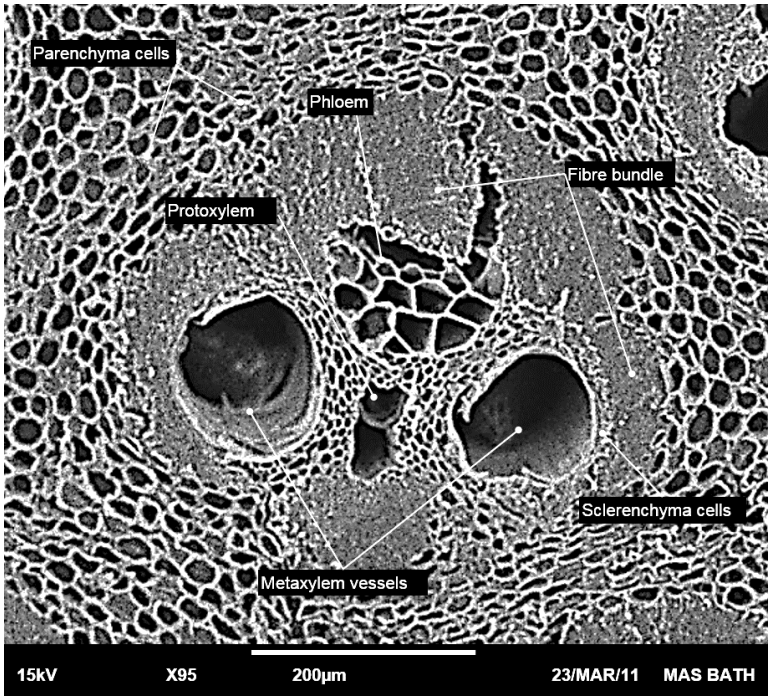

Figure 2-4. Vascular bundle of *Guadua angustifolia* Kunth (Guadua) taken at the University of Bath.

Contrary to wood, bamboo does not possess ray cells and radial conduction of fluids and nutrients is done through pit openings within the cells (Figure 2-5b). The only transversal connection of the vascular system take place at the nodes, which interrupt the continuity of the culm (see Section 2.2).

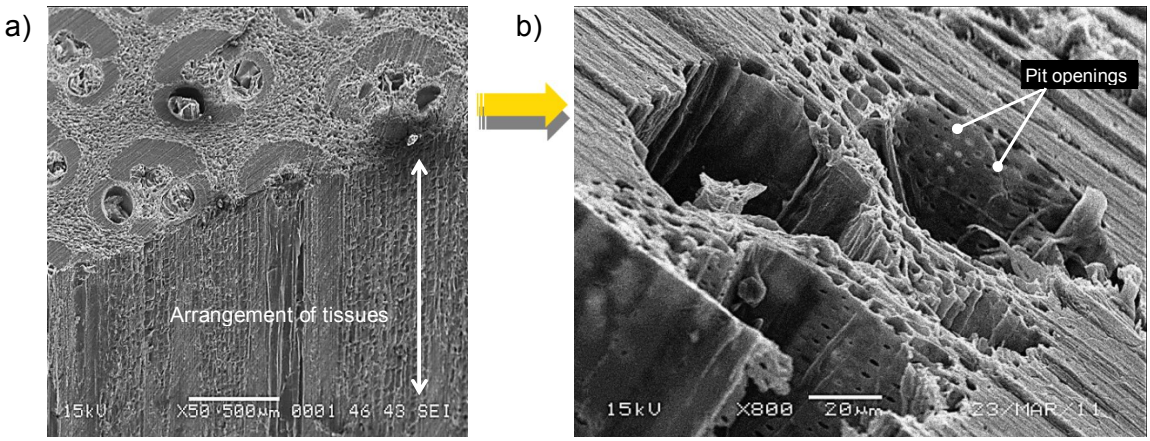

Figure 2-5. Three dimensional scanning electron microscopy images illustrating the microstructure of bamboo. a) Axial arrangement of tissues in *Guadua angustifolia* Kunth. b) Isolated vascular bundle of *Guadua angustifolia* Kunth.

Figure 2-6 illustrates some of the differences between wood and bamboo at the microstructural level. No medullar rays are present in bamboo and the area of conductive tissue in this giant grass (e.g. metaxylem vessels and phloem) is small compared to diffuse porous vessels in hardwood (20-30%) and tracheids in softwoods (60-70%) (Liese, 1998).

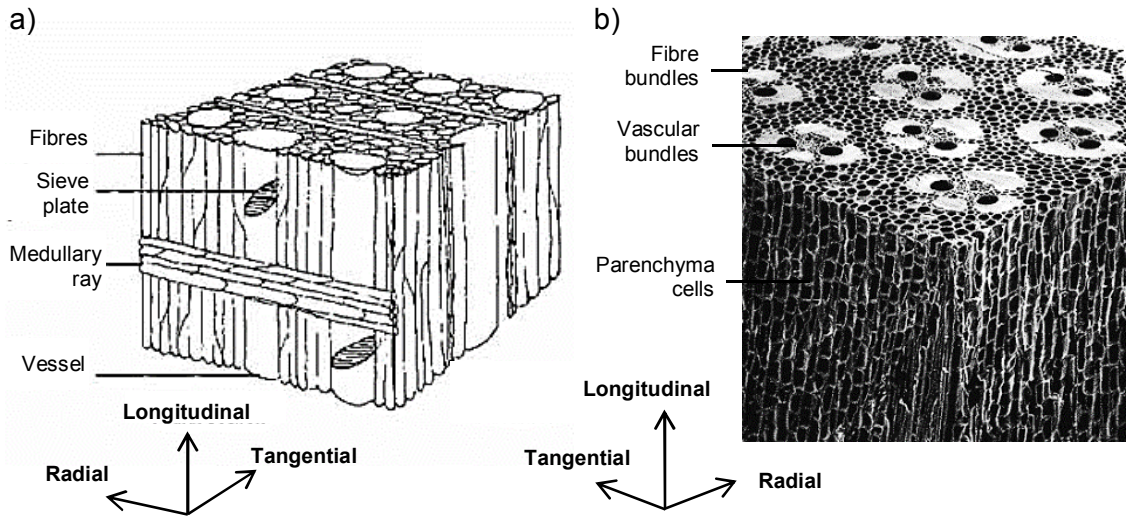

Figure 2-6. a) Wood crosswise features b) Bamboo crosswise features (Liese, 1998).

As previously discussed, production of new cells does not occur but, lignification of multiple layers (polylamellation (Gritsch *et al.,* 2004; Liese, 1998)) occurs (Figure 2-7b). Throughout the first two years of life, bamboo cells with lignified cell walls are developed; subsequently a process of lignification of new lamellas occurs on top of the already lignified cell walls (secondary walls in Figure 2-7 & 1-6) (Liese & Weiner, 1996).

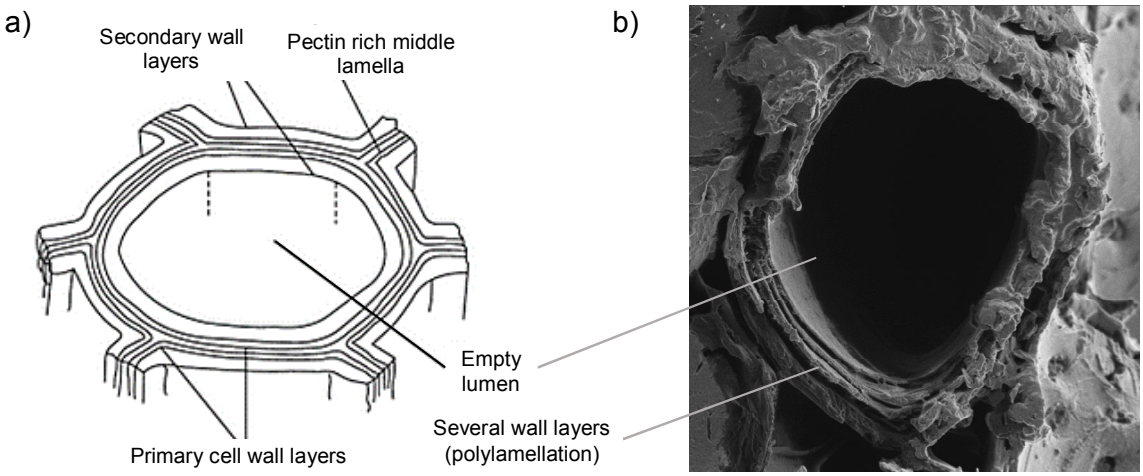

Figure 2-7. a) Secondary thickening on a plant cell (Ansell & Mwaikambo, 2009). b) Detail of the cell wall thickening (polylamellation) in a parenchyma cell of *Guadua angustifolia* Kunth.

Figure 2-7a illustrates the cell thickening within a plant cell drawn by Ansell & Mwaikambo (2009) which relates to that of a bamboo cell in Figure 2-7a & c.

Three sections can be identified across the section of the bamboo culm: cortex (bamboo green), ground tissue and pith ring (bamboo yellow). These sections are labelled in Figure 2-8 as A, B, and C, respectively. The cortex is rapidly consolidated with a high content of lignin and small amounts of silica, providing protection to the plant during growth (Liese, 1998).

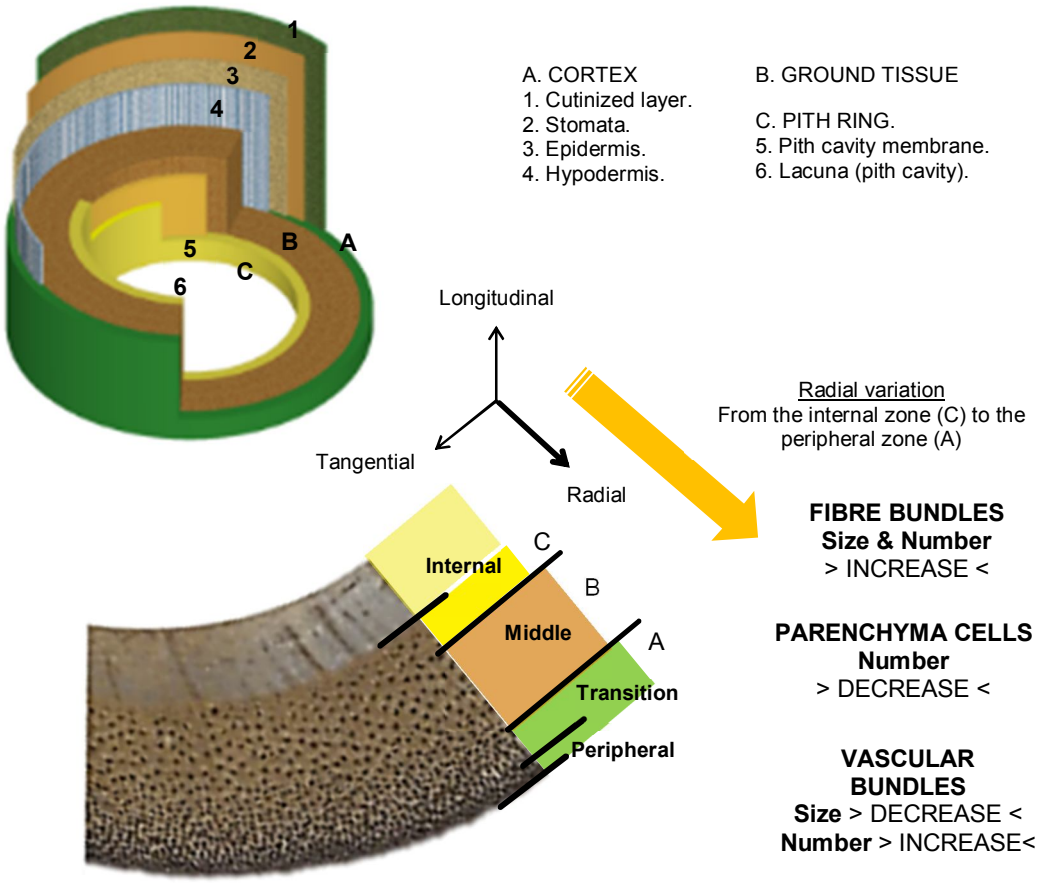

Figure 2-8. Crosswise anatomy of the bamboo culm (left) including the radial variation of its anatomical features (indicated by the arrow) and its subdivision into zones according to the fibre content.

Overall, fibre and parenchyma percentages are inversely proportional, whilst the first decreases towards the pith, the second decreases towards the cortex (Figure 2-8). Fibres in bamboo occur in packs (fibre bundles in Figure 2-4) within individual vascular bundles. The size and the number of fibre bundles increase in the radial direction towards the cortex (Figure 2-8). The increase in number and the decrease in size of vascular bundles leads to

denser areas of fibre towards the cortex with few or non-metaxylem vessels. Liese & Grosser (1971) divided the culm wall of bamboo into four zones as a function of the fibre content per unit area. The first two sections are the peripheral and transition zones, which constitute the cortex (A); whilst middle and internal zones comprise the ground tissue (B) and pith ring (C), respectively (Figure 2-8). The fibre content of these zones within individual vascular bundles in the bamboo species *Guadua angustifolia* Kunth (Guadua) is estimated at 97.2% (peripheral zone), 89.9% (transition zone), 87.2% (middle zone) and 64.8% (internal zone), respectively (Table 2-1) (Londoño *et al.,* 2002).

Table 2-1. Variations in the fibre content across the thickness in *Guadua angustifolia* Kunth (Londoño *et al.,* 2002).

Zone	Cross section	Culm width (mm)	Culm thickness (%)	Vascular bundles per cm^2	Fibres per vascular bundle (%)
CORTEX	Periphery	0.65-0.77	4.5	346-530	89.9
	Transition	1.2-2.55	10.7		97.2
GROUND TISSUE	Middle	4.9-16.34	73.9	81-194	87.2
INNER	Inner	1.3-2	10.9	52-96	64.8
	Total	**8.05 - 21.66**	**100%**	**479-820**	

Gritsch *et al.* (2004) investigated the polylamellation of fibre cell walls close to the phloem in the bamboo species *Dendrocalamus asper*, which occurs towards the cell lumen (inside of the cell) as illustrated in Figure 2-9. The same authors quantified the number of fibres and multiple layers from the elongation of the culm at <6 months through to the first and third year of life (Figure 2-10). Their findings evidence the growth process of bamboo and microstructural changes as a function of time.

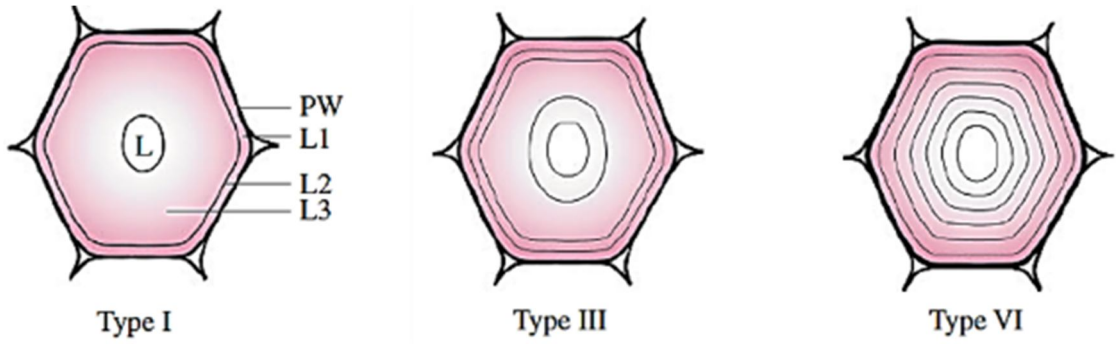

Figure 2-9. Layering (polylamellation) in fibre cells close to the phloem in *Dendrocalamus asper* (Gritsch *et al.,* 2004) PW: primary cell wall; L1, L2, L3: secondary cell wall and L: Lumen. Type I, III and VI refers to the author's classification of the different cell wall layering patterns encountered in <6 months, 1 and 3 year-old-culms.

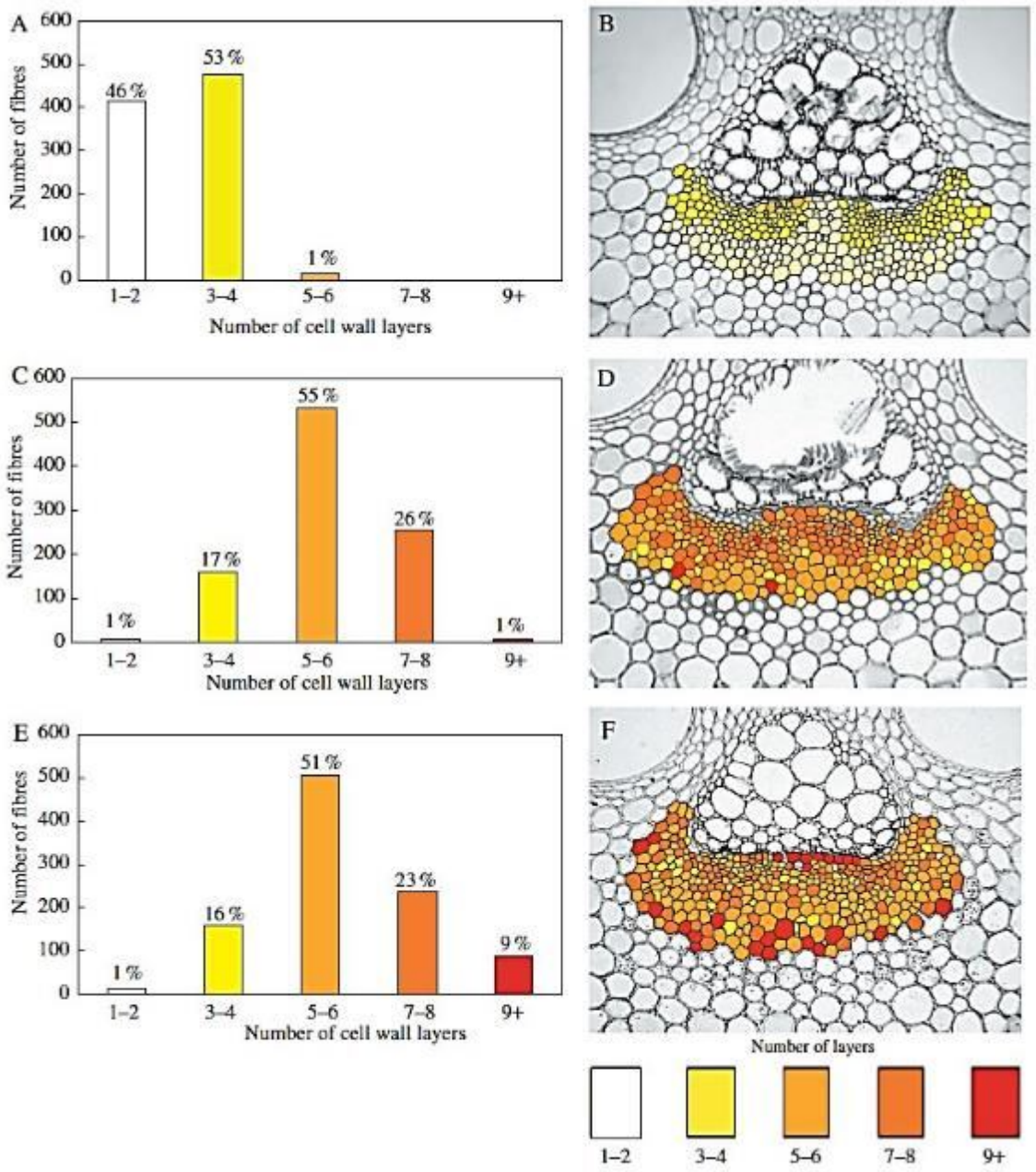

Figure 2-10. Layering of fibre cell walls close to the phloem expressed in percentages (left) and colours in a microscope image (right) for: A) and B) Elongating culm (<6 months); C) and D) One-year-old culm; and E) and F) Three-years-old culm (Gritsch *et al.,* 2004).

A similar pattern of cell wall consolidation can be appreciated in Figure 2-11 for a fibre bundle of Guadua with variable fibre lumen sizes.

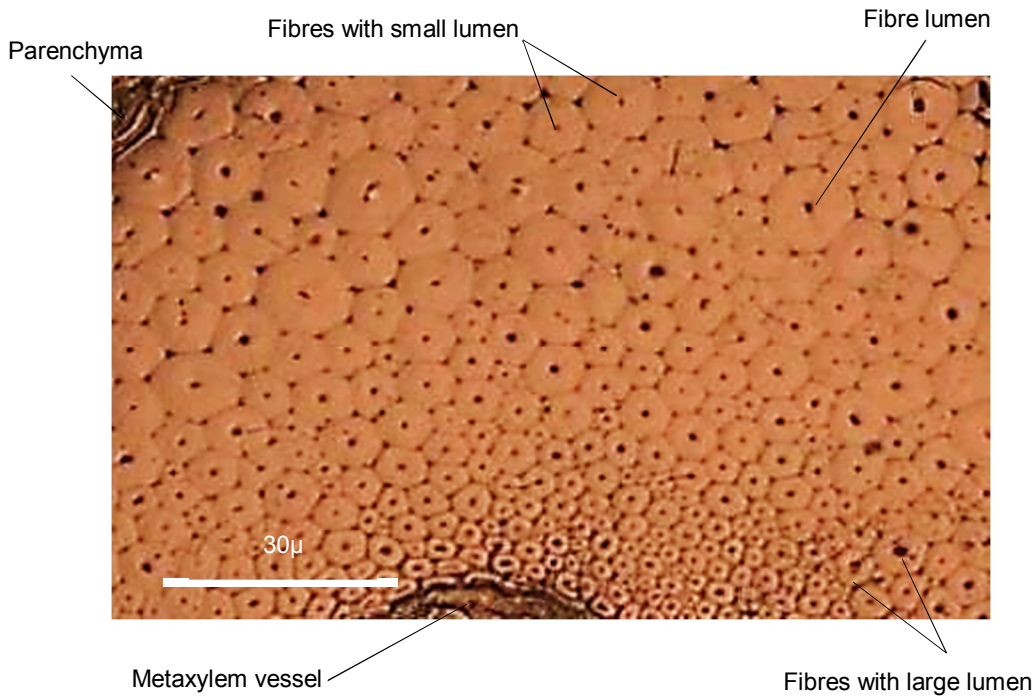

Figure 2-11. Fibre bundle in a section of vascular bundle of *Guadua angustifolia* Kunth

2.4 Growth

Bamboo shoots emerge from the ground with their definitive/adult diameter and wall thickness and develop in approximately 30 days (sprouting). Unlike trees, bamboos have only one growth stage (Hidalgo-López, 2003; Liese, 1998) where the culm (stem) reaches its full height, during the first four to six months of life (e.g. Figure 2-12 for Guadua). The fast elongation of the culm is a result of the simple structure of fibres, conductive tissue and parenchyma cells (Figure 2-8b) arranged axially along the stem, which allows cellular differentiation and rapid flow of nutrients (see also Figure 2-5c).

Subsequently, consolidation of tissue occurs by secondary cell thickening until maturity, which results from a process of lignification of acquired cell wall layers in bamboo (polylamellation). Bamboo does not continue producing cells along its life (Lybeer, 2006) nor it possess cambium zone, annual rings or bark as in wood. No growth occurs in the longitudinal, tangential or radial direction in the following years (as it occurs in trees). Growth of new shoots and young culms (≤1 year old) which do not possess photosynthetic leaf area, is supported by older culms (≥1 year old) through the export of carbohydrates (Kleinhenz & Midmore, 2001; Riaño *et al.,* 2002). This exchange of nutrients is possible thanks to the intricate underground rhizome system that connects young and old culms.

2.4.1 *Guadua angustifolia* Kunth

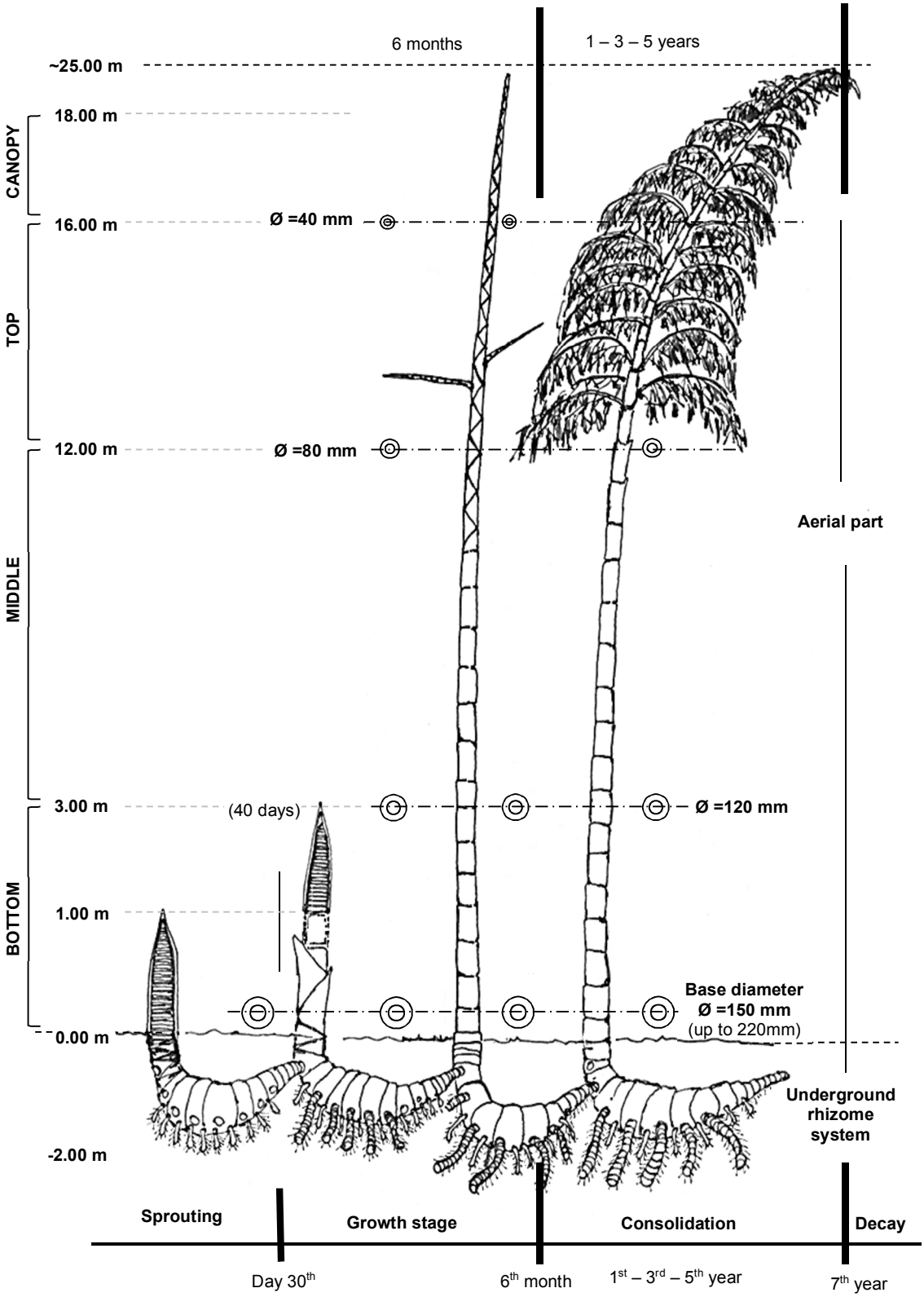

Figure 2-12. Growth of *Guadua angustifolia* Kunth with timeline and average diameter and height dimensions.

The genus Guadua is a tropical species of bamboo that commonly grows at altitudes between 500 and 1500m, in the temperature range 18 to 24°C and relative humidity between 80 to 90% in regions with precipitation varying from 1200mm to 2500mm per year (Riaño, *et al.,* 2002). This sympodial bamboo can grow at a maximum rate of 21cm per day to an average height of 25m in the first 6 months (Figure 2-12).

Its base diameter can reach 22cm, becoming mature between the third and fifth year. More details regarding its mechanical properties and chemical constituents are given in the following sections.

2.5 Chemical composition of bamboo

Bamboo consists of a blend of mainly three elemental compounds: carbon, oxygen and hydrogen. These elements form polymer chains that build the cell structure of the plant and constitute the majority of its mass. Other elements such as nitrogen and silicon appear in smaller amounts alone or in combination with other compounds providing diverse benefits and characteristics to the plant.

Carbon, oxygen and hydrogen account for approximately 50%, 43% and 6% of composition by weight, respectively (Scurlock *et al.,* 2000). A similar elemental compositions is found in wood in fairly identical proportions (Bodig & Jayne, 1982). These elements form the molecular structure of α-cellulose (cellulose), hemicellulose and lignin, which makeup over 90% of the total mass of bamboo (Li *et al.,* 2007).

The content of cellulose by mass in bamboo ranges between 40-50%, whilst lignin and hemicellulose account for 20-26% and 30-14% by mass, respectively (Li *et al.,* 2007; Lybeer, 2006). Average values for cellulose and hemicellulose content in bamboo are commonly presented in the literature as holocellulose (the carbohydrate fraction of lignocellulosic materials, which includes both cellulose and hemicellulose (Bodig & Jayne, 1982)). This is due to difficulties associated with the separation of hemicellulose from lignin (Liese, 1985). Furthermore, the variability of the compounding polymers forming the hemicellulose within different bamboo species (*e.g.* pentoses and hexoses) hinders its quantification (Wahab *et al.,* 2013). Some variation between the contents of xylose and mannose (the primary compounding polymers in hemicellulose) is also reported for softwoods and hardwoods (Bodig & Jayne, 1982). Nevertheless, their average hemicellulose content is assumed as 30% of the total biomass.

Another elemental compound present in bamboo is nitrogen; however, it constitutes only 0.4% of the total composition by weight. Silicon is present in an amorphous form as silica (SiO_2), which is the primary component of the ash content in bamboo. This compound is known to cause wear of cutting tools and hinder fibre pulp production processes (Li *et al.,* 2007; Liese, 1998). Other metals such as calcium, magnesium and potassium are found within the ash content of bamboo. Ash content accounts for about 1.5% by mass of the total chemical constituents in the bamboo species *Phyllostachys pubescens* (Moso) (Li *et al.,* 2007), whilst in other species such as *Phyllostachys makinoi* or *Guadua angustifolia* Kunth, it exceeds 2% of the total weight of the plant. Table 2-2 illustrates the chemical compositions of some lignocellulosic materials including bamboo and wood.

Table 2-2. Chemical composition by weight of selected lignocellulosic materials from several authors

Material	Fibre type	Species	Cellulose (%)	Hemicellulose (%)	Lignin (%)	Pectin (%)	Ash (%)	Others (%)
Bamboo	stalk	Moso[1]	47	24.4	22.8		1.5	5*
	stalk	*P. heterocycla*[2]	49.1	27.1 (Pentosan)	26.1		1.3	4.6*
	stalk	*P. nigra*[2]	42.3	24.1 (Pentosan)	23.8		2.0	3.4*
	stalk	*P. reticulata*[2]	41	26.5 (Pentosan)	25.3		1.9	3.4*
	stalk	*P. makinoi*[3]	45.3	24.3 (Polyoses)	25.5		2.3	2.6*
	stalk	*Chusquea culeou*[6]	51.4	21.7	22.3		1.2	3.5*
	stalk	*Guadua*[7]	37-44	13-20	23-27		0.92-2.93	
Plants	bast	Hemp[4]	70-92	18-22	3-5	1		
	bast	Kenaf[4]	44-87	22	15-19	2		
	fruit	Banana[4]	60-65	6-19	5-12	3-5		
	leaf	Sisal[4]	43-78	10-24	4-12	0.8-2		
	seed	Cotton[4]	82-96	2-6.4	0-5	<1-7		
Wood	stalk	Hardwood[5]	45	30	22		0.2-0.3	5
	stalk	Softwood[5]	41	30	28			3

[1] (Li *et al.,* 2007) [2] (Scurlock *et al.,* 2000) [3] (Lybeer, 2006) [4] (Ansell & Mwaikambo, 2009) [5] (Bodig & Jayne, 1982) [6] (Poblete *et al.,* 2009) [7] (Sánchez-Echeverry *et al.,* 2014)
P. = *Phyllostachys*. *Extractives

As shown in Table 2-2 bamboos in general possess a higher content of cellulose and ash than wood. Despite having a lower heating value than wood, the high yield per unit area and the low ash and sulphur contents in bamboo make it a potential biomass fuel (Montaño *et al.,* 2012; Scurlock *et al.,* 2000). Low lignin content in plants with bast, fruit, leaf and seed fibres makes them easier to process into pulp. Lignin content in wood and bamboo are in the same range, between 22% and 28% by weight. Overall, wood and bamboo possess very similar contents of cellulose, hemicellulose and lignin.

Cellulose, hemicellulose and lignin contents in bamboo vary with age influencing its anatomy and physical and mechanical properties. Chemical changes with ageing and their influence on the mechanical, physical and anatomical properties of bamboo have been studied by many authors (Crow & Murphy, 2000; Gritsch *et al.,* 2004; Hisham *et al.,* 2006; Li *et al.,* 2007; Lo *et al.,* 2008; Lybeer, 2006; Poblete *et al.,* 2009; Sánchez-Echeverry *et al.,* 2014; Scurlock *et al.,* 2000; Wahab *et al.,* 2013). Significant statistical correlation between changes in chemical composition, age and density in Moso and *Gigantochloa scortechinii* have been reported by Li *et al.* (2007) and Hisham *et al.* (2006), respectively. Values of density and contents of hollocellulose and lignin (Klason lignin) in one-year-old culms were lower than three-year-old and five-year-old culms (three and five-year-old culms presented low variation). Furthermore, Li *et al.* (2007) found a higher concentration of cellulose and lignin in the outer layer of three-year-old Moso specimens. This layer has the highest concentration of fibres per unit area, thus contributing significantly to the structural support of the culm.

Lignin has a key role in the consolidation of tissues (polylamellation process) that occurs in bamboo during growth. Lignin blends with hemicellulose to form a matrix for the cellulose fibres (Wegst & Ashby, 2004). As discussed in Section 2.3, lignin consolidates new lamellas forming on top of the primary cell walls (Gritsch *et al.,* 2004) and provides the plant with resilience to decay. Nevertheless, lignin is prone to photodegradation (Krause & Ghavami, 2009); hence, if exposed to weathering, it can cause fibres to detach from the surface (a phenomenon call erosion in wood (FPL, 2010; Krause & Ghavami, 2009)).

Another important substance found in bamboo is starch. Granules of starch in bamboo are found in parenchyma cells (Figure 2-13) and their content also varies with age (Hisham *et al.,* 2006; Lybeer, 2006). Older culms accumulate more starch whilst, young culms (<1year) have little or no starch content (Liese & Weiner, 1996). High starch contents make the culms

prone to insect attack and fungi decay. Starch is broken down into nutrients that are transferred from older culms to growing/young culms (Section 2.4), which need them the most. This is the reason why no starch deposition is found in young culms. In addition to ageing, starch content in bamboo also fluctuates between species, culm height, location and season. Therefore, starch content is an indicator of the readiness of bamboo for harvesting, its growth stage and decay. As in wood, starch can trigger bacterial degradation and formation of fungi (FPL, 2010).

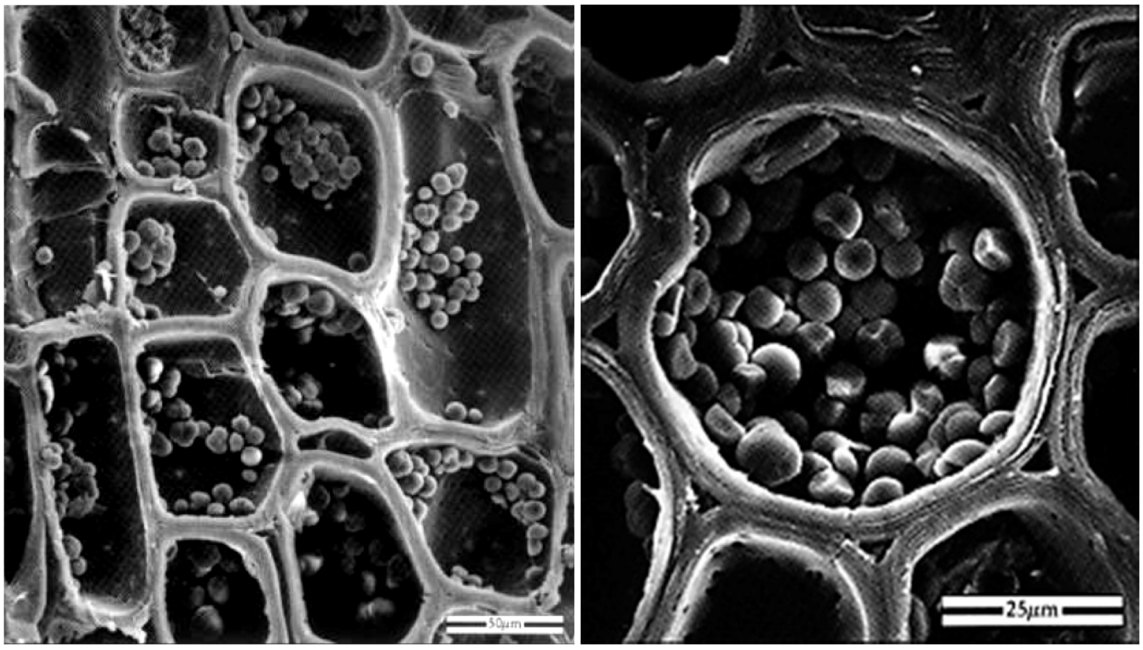

Figure 2-13. Parenchyma cells filled with starch granules in *Phyllostachys viridiglaucescens* (Liese, 1998)

2.6 Physical and mechanical properties

The physical and mechanical properties of bamboo are closely related to its microstructure, chemical composition and age. Wegst & Ashby (2004) define bamboo as a composite material of cellulose fibres joined by a lignin-hemicellulose matrix and remark its prismatic arrangement of cells with different thickness. Hence, factors such as cell wall thickening, fibre density and cellulose and lignin content have a significant influence on its specific gravity, modulus of elasticity and ultimate strength.

Although parenchyma and fibre cells become lignified and acquire several layers through poylamellation (see Section 2.1), the main structural support to the culm is provided by highly lignified and compact fibre bundles. Parenchyma cells are hollow and are arranged vertically in alternating long and short cells Figure 2-14). This, together with their foam-like

arrangement around fibres can help withstand compression loads and avoid fibre buckling.

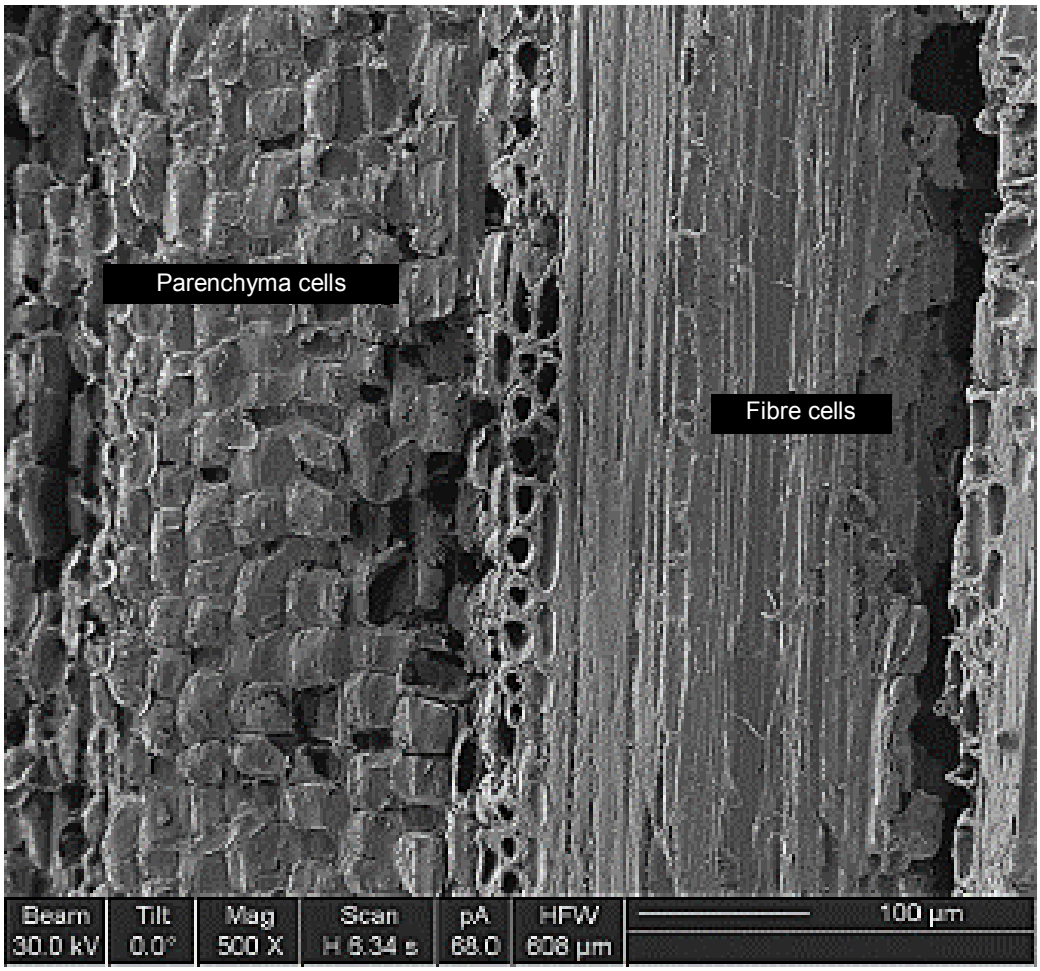

Figure 2-14. Transverse section of Guadua illustrating fibre bundles and parenchyma cells.

Fibres are the denser cells within the culm structure; they possess several layers and small lumen (see Figure 2-9). An isolated fibre cell is composed of several layers originated by polylamellation. These cellulosic layers with variable microfibril orientations (Figure 2-15a) are cemented by lignin and their thickness and number varies with age (Section 2.1). As in wood and other plants, single fibres of bamboo are multi-directionally reinforced (Figure 2-15b).

The number and occurrence of fibres in bundles define the specific gravity of the culm (Liese, 1998). Furthermore, their distribution across the section and along the length of bamboo culms influence its response to static and dynamic loads such as self-loading, rain-water and wind. Fibre proportion increases from bottom to top of the culm and decreases towards the lacuna (Figure 2-8 & Table 2-1). Londoño *et al.* (2002) reported a two-fold increase in the percentage of fibres from the bottom (29%) to the top part (58%) of the culm of Guadua.

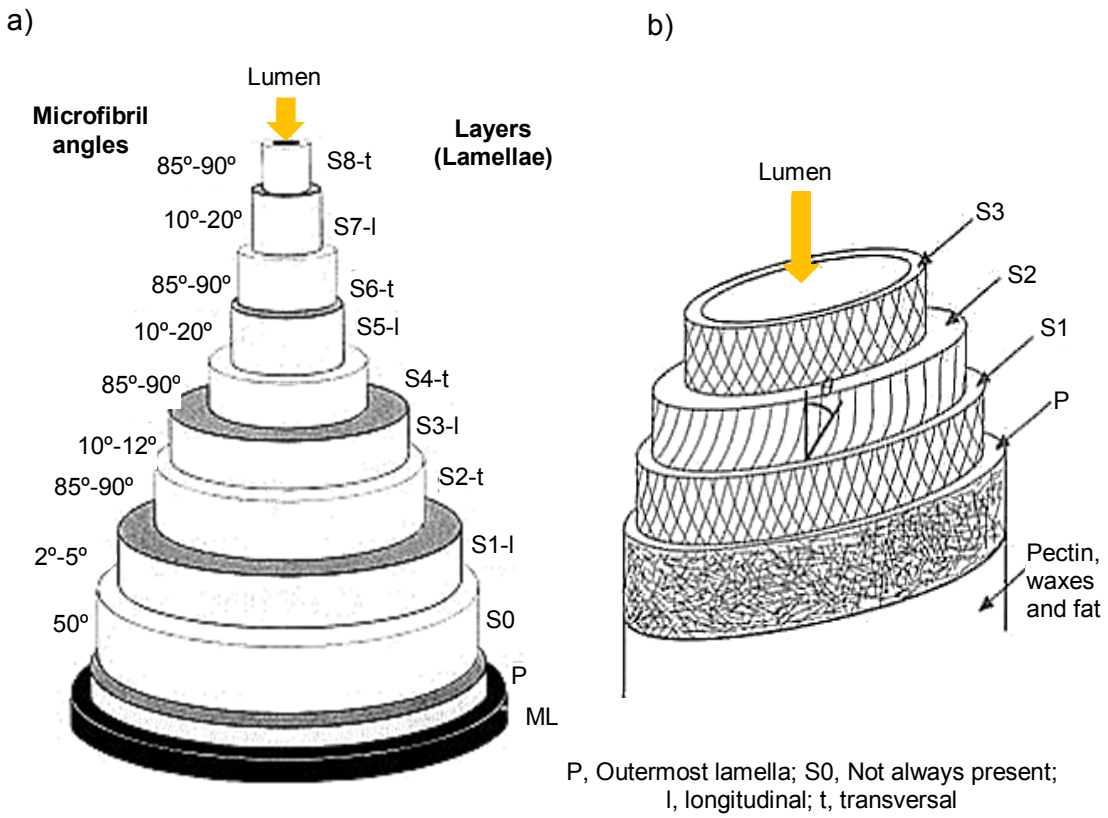

Figure 2-15. a) Polylamellate structure model of a thick-walled fibre of bamboo (Liese, 1998). b) Generalized plant fibre cell wall structure (Aziz & Ansell, 2004)

The graded organisation of fibres, parenchyma and other tissues in bamboo and plants in general, responds to global and local stresses determined by gravity and the environment (Amada *et al.,* 1997; Weinstock, 2006). The increase of fibre volume towards the top part of the plant (where the culm of bamboo tappers) can be correlated to the reduction in cross section (diameter and wall thickness), the extra weight provided by branches and leaves and the stresses added by wind and rain.

Amada *et al.* (1997) assessed the tensile strength of slices of Moso bamboo extracted from various locations across the thickness and along the height of the stem. The height was determined by the number of internodes from bottom (internode no. 0) to top part of the culm (internode no. 50), and the thickness by the distance from the inner surface (r-a). They found a strong influence of height and distance from inner surface on the results of tensile strength (Figure 2-16). Tensile strength increased towards the top of the stem and decreased from the outside (cortex) to the inside of the culm (across the thickness). Accordingly, the volume fraction of fibres increased as a function of height and distance to the outer cortex (Figure 2-17).

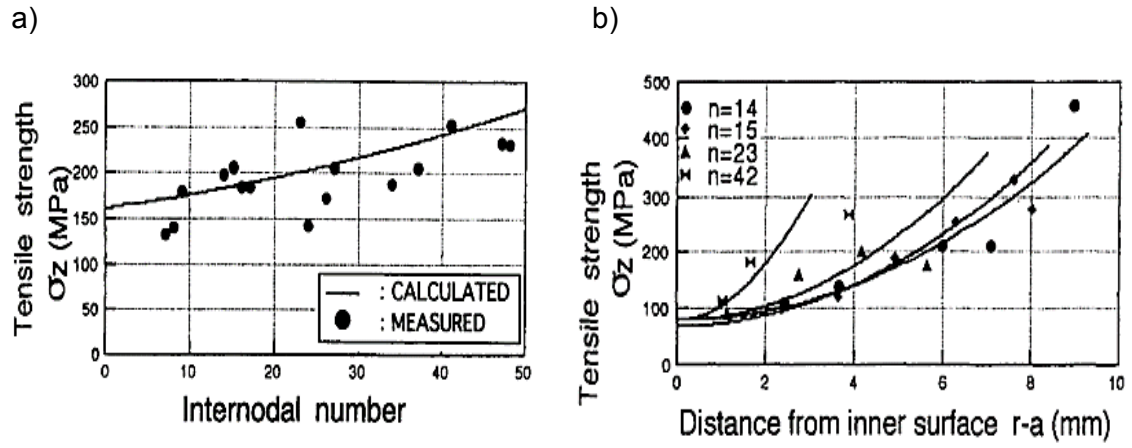

Figure 2-16. Tensile strength of Moso bamboo a) Calculated and experimental along the height. b) Along the radial coordinate from inner (lacuna=0mm) to outer (cortex=10mm) surface (Amada *et al.,* 1997).

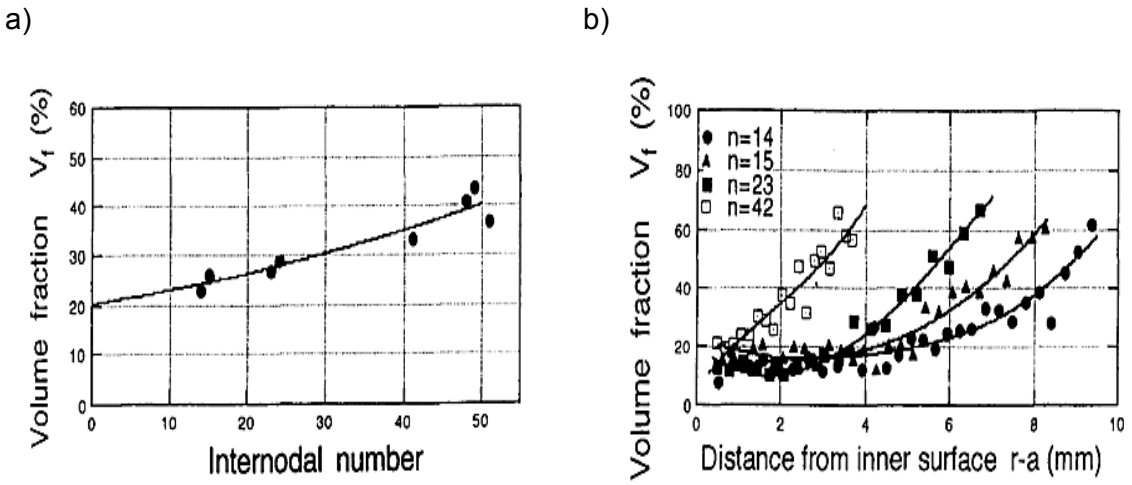

Figure 2-17. Volume fraction variation in Moso a) with height; b) with thickness from the inner (lacuna=0mm) to the outer (cortex 10mm) surface (Amada *et al.,* 1997).

Similarly, Li & Shen (2011) measured the Young's modulus and tensile strength of Moso bamboo slices and confirmed the dependence of stiffness and strength on the fibre volume fraction and position across the thickness. The stiffness and strength variation across the radial direction is illustrated in the stress versus strain characteristics of Figure 2-18a, whilst the variation in volume fraction (V_f) with distance from the inner surface measured by the same authors is displayed in Figure 2-18b.

In Guadua, values of Young's modulus range from 8GPa for the basal section to 16.25GPa for the top part of the culm which also depends on the presence or not of nodes and the fibre volume fraction (Ghavami & Marinho, 2005). Similarly, the tangential Poisson's ratio

(the ratio of passive strain along the tangential direction to active strain along the longitudinal direction) varies from 0.19 for the bottom part to 0.35 for the top part (Ghavami & Marinho, 2005; Osorio-Saraz *et al.,* 2007).

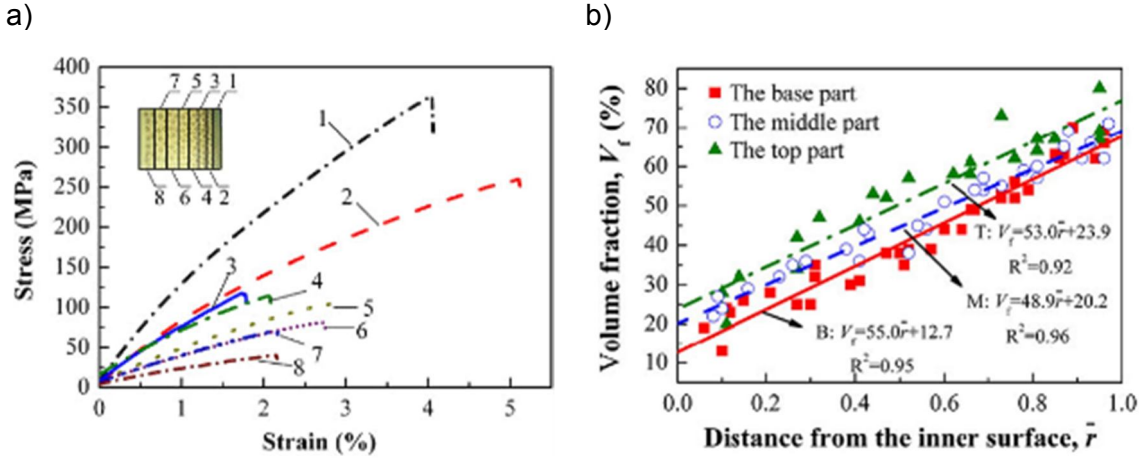

Figure 2-18. a) Tensile longitudinal stress vs strain characteristics for bamboo slices cut from layer 1 (outer) to layer 8 (inner) of a Moso-bamboo culm wall across the section. b) Volume fraction variation of vascular bundles across the culm thickness and along the height in Moso (Li & Shen, 2011).

Mechanical properties of Guadua also vary across the wall thickness. For instance, external fibre bundles from mature culms of Guadua possess higher Young's modulus values than those from the middle and the internal layers (Moreno, *et al.,* 2006). It is in part explained by the increase of fibre content from the inner part to the outer part (see Figure 2-8); approximately 50% of the fibre content is situated in the cortex. Recent studies have reported that the ratio of bamboo's lengthwise to crosswise strength is 30:1, which is 50% higher than that of wood (INBAR, 2002).

Therefore, density has a significant effect on the overall mechanical properties of bamboo. Specific strength and specific modulus denote the ratio of tensile strength (σ_z) and elastic modulus per unit density, respectively. The specific modulus of bamboo is usually compared to that of mild steel (25 x 10^6 m^2/s^2); for instance, the species of bamboo Moso and Guadua possesses values of about 30 x 10^6 m^2/s^2 (Table 2-3). Furthermore, specific strength and stiffness values of bamboo are fairly similar to those of glass fibre (E-Glass). In general, plant fibres, wood and bamboo possess a high stiffness and strength to weight ratio along the fibres (Table 2-3); however, due to their orthotropicity the same figures cannot be achieved in the radial or tangential directions as with steel or aluminium, which are isotropic materials. As seen in Table 2-3 the specific modulus of bast fibres such as hemp and kenaf, fruit fibres such as banana, and stalk fibres of Spruce and Pine trees have similar values to those

of Moso and Guadua.

Table 2-3. Characteristic mechanical properties of lignocellulosic and conventional materials used in construction (values for clear, straight grained specimens of wood and bamboo at ~12% moisture content).

Material	Type/Species	Tensile strength (MPa)	Tensile modulus (GPa)	Density (10^3 kg/m^3)	Specific strength (10^6 m^2/s^2)	Specific modulus (10^6 m^2/s^2)
Bamboo	Moso[1]	206.2	20.1	0.66	0.31	30
	Guadua[7] (fibres)	~806	~43	1.44	0.56	30
Plant fibres	Hemp[4]	310 - 750	6-10	1.4-1.5	0.22-0.5	20-41
	Kenaf[4]	295 - 1,191	22-60	1.2-1.4	0.25-0.85	18-43
	Banana[4]	529 - 914	27-32	1.3-1.35	0.4-0.68	20-24
	Sisal[4]	80 - 840	9-22	1.3-1.5	0.05-0.6	6-15
	Cotton[4]	300 - 700	6-10	1.55	0.2-0.45	4-6.5
Hard-wood	Meranti[2] (*Shorea spp.*)	129.6 (MOR) 46.6 (COMP) [3]	14.5	0.68	0.19	21
	Oak, Pin red[2] (*Quercus palus-tris*)	112.4 46.6 (COMP)[3]	11.9*	0.63	0.18	19*
Softwood	Sitka spruce[2]	70 (MOR) 88.2 (COMP) [3]	10.8*	0.40	0.17	26
	Pine[2] *(Pinus radiata)*	80.7 (MOR) 41.6 (COMP) [3]	10.2	0.42	0.09-0.19	25
E-Glass fibre[6]		1,200-1,500	70	2.5	0.48-0.6	28
Carbon fibre (PAN)[6]		4,000	230-240	1.4	2.86	164.2-171.4
Steel[5]		2,000	200	7.9	0.25	25
Aluminium[5]		600	69	2.8	0.21	26
Concrete[5]		2-5 [5] (40 COMP)	20-25[5]	2.4	0.005	17

[1] (Li *et al.,* 1994). [2] (FPL, 2010). [3] The wood database (www.wood-database.com). [4] (Ansell & Mwaikambo, 2009). [5] Commercial information. [6] (Osorio-Serna *et al.,* 2010). [7] (Trujillo De Los Ríos *et al.,* 2010)

*MOE from bending. (s=side; m^2/s^2 in SI = Pa/(kg/m^3) or dimensionally equivalent to N.m/kg).
Meranti in table is from baulau group, some species of *Shorea* are known as Philippine mahogany.

Another factor influencing the physical and mechanical properties of bamboo is ageing. Research into the influence of ageing on the anatomy and mechanical properties of bamboo has been performed by several authors (Hisham *et al.,* 2006; Kamruzzaman *et al.,* 2008;

Liese & Weiner, 1996; Lo *et al.,* 2008; Londoño *et al.,* 2002; Lybeer, 2006). Studies conducted on Guadua have assessed its compressive strength, shear and bending properties for specimens of different ages and segments as a function of height (Moreno *et al.,* 2006; Montoya, 2007; Osorio, *et al.,* 2010). Castaño (1992) and Londoño, *et al.* (2002) define maturity at between the 4th and 6th year; also the Colombian building code (NSR 2010) specifies culms harvested in this range of age for structural applications. Hidalgo-López (2003) states that the appearance of small dots over the culm surface of Guadua after the 3rd year signals the initiation of maturity and that the increase in size of the dots during the 4th and 6th year indicates its readiness to be used in construction applications (Hidalgo-López, 2003).

Table 2-4 illustrates some of the variations in density and mechanical properties of mature specimens of Guadua as a function of height investigated by different authors.

Table 2-4. Properties variation of round culms of *Guadua angustifolia* Kunth as function of age at three heights.

			Guadua in green condition (MC ≥ 30%) (Correal & Arbeláez, 2010)					(Takeuchi-Tam & González 2007)*
Property	units	Section	2nd year	3rd year	4th year	5th year	Average by height	5th year
Density (ρ)	g/cm^3	Bottom	0.6745	0.6819	0.6173	0.6769	0.6626	NR
		Middle	0.6781	0.7055	0.7800	0.7800	0.7359	NR
		Top	0.7030	0.8286	0.7741	0.7354	0.7602	NR
		Average	**0.6873**	**0.7480**	**0.7259**	**0.6861**		**NR**
MOE (Bending)	GPa	Bottom	16.9	16.7	17	18	17.15	17.48
		Middle	17.7	15.8	17	18.7	17.3	18.13
		Top	16.1	19.4	18.3	15.5	17.32	17.75
		Average	**16.9**	**17.1**	**17.4**	**17.4**		**17.85**
Compressive strength (f_c)	MPa	Bottom	39.9	38.1	37.6	32.1	36.93	50.6
		Middle	27.2	42.1	41.5	34.7	36.38	56.4
		Top	20.4	42.6	42.1	39.0	36.03	59.7
		Average	**28.6**	**41.0**	**40.4**	**35.2**		**56.2**

NR = Not reported; * MC was not reported by (Takeuchi-Tam & González 2007), but their specimens were air dried.

As seen in Table 2-4 and Figure 2-19, density increases with height but decreases with age; compressive strength is strongly affected by age and moderately influenced by height. Conversely, MOE values appears not to be significantly affected either by age or height, although maximum compressive strength values are reported for the top segment when compared to the middle and bottom segments of the culm (Correal & Arbeláez 2010; Takeuchi-Tam & González 2007).

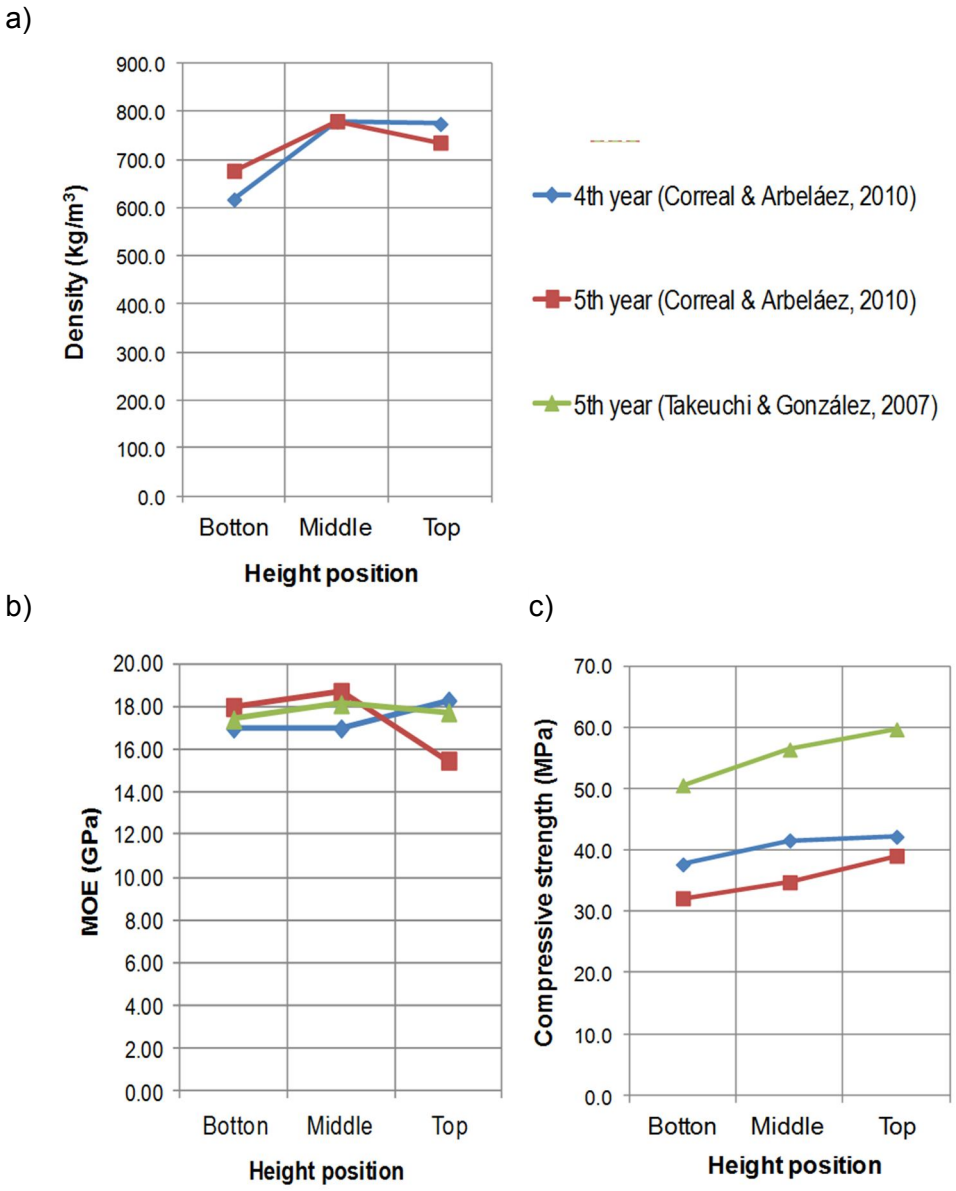

Figure 2-19. Variation of density (a), MOE (b) and compressive strength (c) as function of age in four and five years old specimens of *Guadua angustifolia* Kunth (Correal & Arbeláez 2010; Takeuchi-Tam & González 2007).

Factors such as soil quality and clump density affect these values. Mechanical properties of Guadua drop sharply after the sixth year of life when the culm is considered over-mature and starts to die. Tissue decay starts with degeneration of the cell structure.

In addition to the microstructural variations along and across the bamboo culms, their morphology (conical-tapered tubes) influences their mechanical properties. Janssen (2000) compared the structural efficiency of the tubular cross-section of bamboo and the high distribution of fibres at the outside of the culm to an I-shape beam profile (Figure 2-20). Having the material away from the neutral axis (as in I-beam sections) is an efficient way to

withstand bending stresses along the beam. The flanges resist the bending moment and the flange resists the in-plane shear forces experienced by the beam.

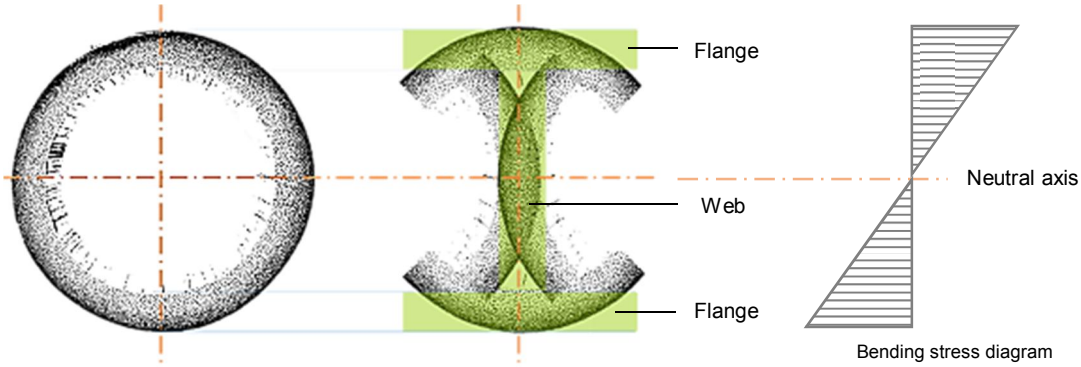

Figure 2-20. Conversion of the round cross section of bamboo into an I-profile.

Overall, bamboos and Guadua in particular have been defined as functionally graded materials (Amada *et al.,* 1997; Ghavami *et al.,* 2003; Ghavami, 2005; Wegst, 2011; Weinstock, 2006) with micro and macro structures that respond to their need to withstand static and dynamic loads such as self-loading and wind.

2.7 Resource availability

Bamboo resources have been recently listed as Non Wood Forest Products (NWFP) and a wood substitute in the last Forest Resource Assessment report (FAO, 2010b) compiled by FAO (Food and Agriculture Organization of the United Nations). This report collected updated information on forest resources from 233 countries around the world and analysed trends in forest management and expansion and loss of resource. Figures for biomass production and carbon storage are also presented. It includes the most up to date assessment of forest resources worldwide, although there is almost no agreement with the data from several previous reports from the International Network for Bamboo and Rattan (INBAR), United Nations Environment Programme (UNEP) World Conservation Monitoring Centre and FAO (Bystriakova, *et al.,* 2003; Bystriakova *et al.,* 2004; Hunter & Junqi 2002; Lou, *et al.,* 2010).

Countries such as China and India have a more thorough inventory of their natural and planted bamboo areas whereas countries such as Brazil and Nigeria – that account for the biggest resource in America and Africa, respectively – rely on historical estimations (e.g. figures for Brazil are dated 1990). The lack of information systems and the presence of

bamboo resources in patches with other plants within forests and along streams and rivers hinder the assessment process (FAO, 2010b). This situation reflects the relative economic insignificance of the bamboo resource in Africa and America. From a total bamboo forest resource of about 0.8 % of the world's land area (31.5 million ha), China possesses 5.7 million ha (FAO, 2010b) where Moso bamboo (*Phyllostachys heterocycla var. pubescens*) covers about 70% of its total bamboo forest (Lou, *et al.,* 2010). With 300 thousand hectares less than China, India occupies the second place in Asia and its principal bamboo variety is from the tropical genus *Dendrocalamus*. Brazil has the biggest diversity of bamboo in America with 230 native species and 32 introduced (FAO, 2006) and its resource estimation reaches 9.3 million hectares (mainly of the genera Guadua) in the south-eastern part of the Brazilian Amazon region (state of Acre). *Guadua angustifolia* Kunth resources in Colombia account for only some 51.5 thousand ha (Riaño, *et al.,* 2002).

Although there are some small plantations in Portugal and Belgium, Europe and the United Kingdom do not report figures on bamboo forests. A scattered presence of the resource across Oceania and North & Central America accounts for 1% of the total distribution of bamboo resources. The worldwide distribution of bamboo is summarised in Figure 2-21.

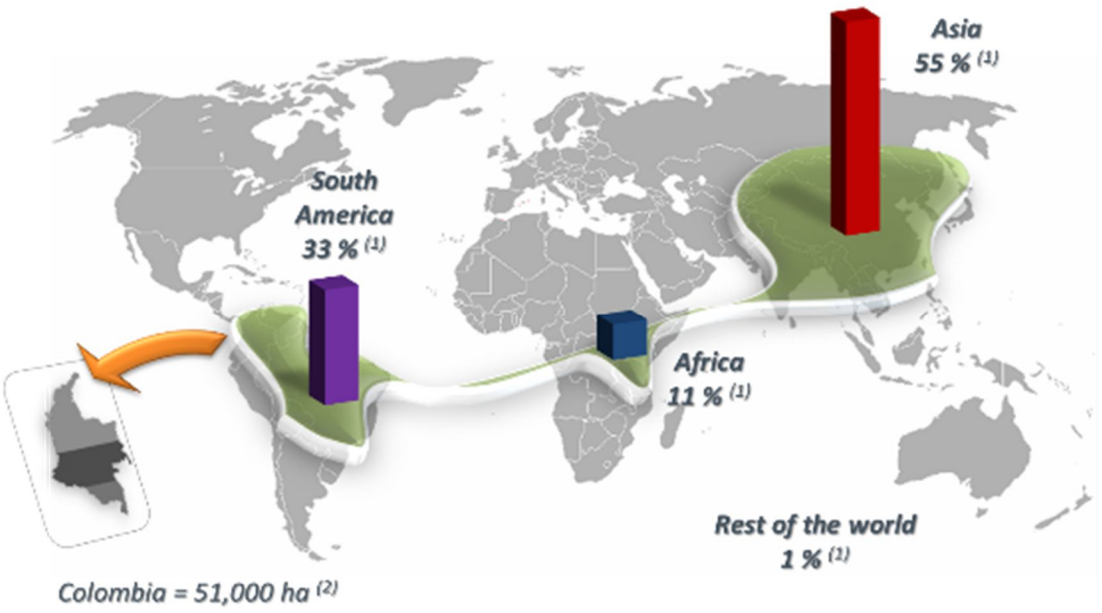

Figure 2-21. Worldwide distribution of bamboo, 2010. Information for bamboo extracted from [1](FAO, 2010b) Guadua [2](Riaño *et al.,* 2002).

2.8 Uses of bamboo.

Bamboo has been used for centuries in countries where it is endemic. A complete and informative review of bamboo and its diverse uses worldwide is presented by Hidalgo-López (2003) in his book *'Bamboo: The Gift of the Gods'*. The author showcases the most traditional applications in food, handicrafts, architecture, engineering and medicine, and various developments in composite materials, aeronautics and other disciplines (Figure 2-22).

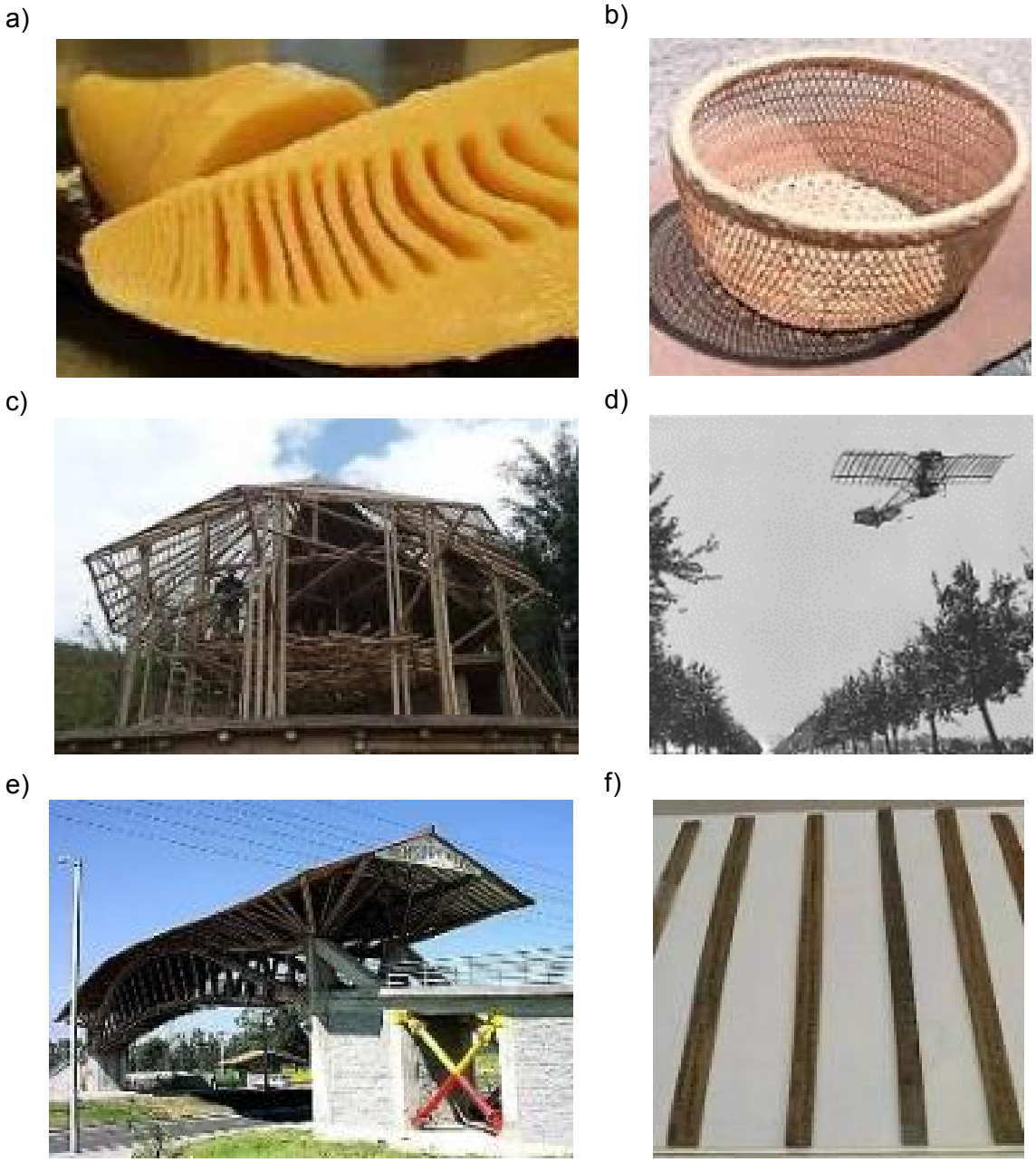

Figure 2-22. a) Fresh bamboo shoot for cooking (Source: www.laocook.com). b) Woven bamboo basket. c) Guadua-bamboo structure. d) The Demoiselle by Alberto Santos Dumont, 1909 (Source wikimedia). e) Guadua-bamboo pedestrian bridge, Bogotá. f) Bamboo strips with ancient inscriptions in Beijing, China.

Rao *et al.* (1998) reported on the general features of twenty selected species of bamboo considered by INBAR and the International Plant Genetic Resources Institute (IPGRI) as priority species for research and development. Amongst them were Moso and Guadua; these two species demonstrated high commercialization potential and high impact on environmental rehabilitation and development of rural industries (see Table 2-5).

Table 2-5. Priority species of bamboo evaluated by their potential commercial and local use (Rao *et al.,* 1998)

Taxa	Value			Domestication	Climate & Ecology		Genetic resources				
	C	R I	E		CI	SI	GE	S	I V	E	Survey
Bambusa balcooa	++	++	++	D	h, d	m r	H	H*	H	H	H
Bambusa bambos	++	++	++	D	h, d, s	c m, P	H	L	M	M	H
B. blumeana	++	++	++	D	h, d, s	r, m, P	H	L	H	H	H
B. polymorpha	+	+	−	D	h, d	r, m	H	H	M	H	H
B. textilis	+	++	+	D	st	r, m	M	L	H	H	L
B. tuida	+	++	+	D	h, d	r, m	H	M	H	H	H
B. vulgar-is	−	−	++	D	h, d, s	r, m, P	L	L	L	L	L
Cephalostachyum pergracile	+	++	+	W	h, d	m	M	L	M	H	M
Dendrocalamus asper	++	+	++	D	h, d		H	H	M	H	H
D. gigan teus	+	+	+	D	h	r	H	H	M	H	H
D. la tiflorus	++	+	+	D	h	r	M	L	M	H	L
D. strictus	++	+	++	D	d, s	m, P	M	L	L	H	M
Gigantochloa apus	+	++	++	D	h	r	H	H	M	H	H
G. levis	+	++	++	D	h	r	H	L	H	H	H
G. pseudoarundinacea	++	+	+	D	h, d		M	L	H	H	L
Guadua angustifolia	++	++	++	W	h	r, m	H	H	H	H	H
Melocanna baccifera	+	++	+	W	h		H	M	H	H	M
Ochlandra sps	+	+	+	W	h	r	H	H	M	H	H
Phyllostachys pubescens	++	++	++	D		r, m	M	M	L	L	L
Thyrsostachys siamensis	++	++	++	D	d. (h)	m, (r)	M	M	L	H	L

KEY *Value*
C = commercialization potential: High (++), medium (+), and little (-).
Survey = need for further field survey: High (H), medium (M), low (L).
RI = rural industries: High (++), medium (+), and little (-).
E = environmental rehabilitation: High (++), medium (+), and little (-).

Genetic resources
GE = genetic erosion: High (H), medium (M)., low (L).
S = need for research on seed storage: High (H), medium (M), low (L).
IV = need for research on in vitro storage: High (H), medium (M), low (L).
E = need for wider exchange. High: (H), medium (M), low (L).

Domestication
Wild = W, domesticated = D.

Climate and ecology
CI = climate: humid tropics (h), dry tropics (d), subtropics (St), semi-arid (s), temperate (t).
SI = soils: rich (r), medium (m), poor (p)

On the basis of this priority list of species Jayanetti & Follett (1998) highlighted the role of Guadua as one of the most suitable bamboo species for specific uses in construction (listed in ten out of twelve different applications). Framing, walling, roofing, sheathing, concrete formwork and scaffolding are some of the most relevant uses of this bamboo species in traditional construction (see Chapter 3) mainly in South and Central America, where this species is native. Chinese Moso-bamboo on the other hand, is recognized as the species with the highest industrial development in the production of flooring, car interiors, kitchenware, charcoal, engineered products, and many other miscellaneous applications such as toothpicks, handcrafts, bikes, beer, helmets, mobile phone cases, surfboards, clothing, etc.). Bamboo uses can then be classified depending on the degree of transformation of the raw material and the manufacturing process to which it has been subjected. Three material transformation stages are identified: non-processed, moderately processed and highly processed. Figure 2-23 illustrates the processes applied to bamboo and the transformation stage attained for certain applications. Overall, traditional uses require less intensive processing, whilst industrialised uses require high levels of transformation.

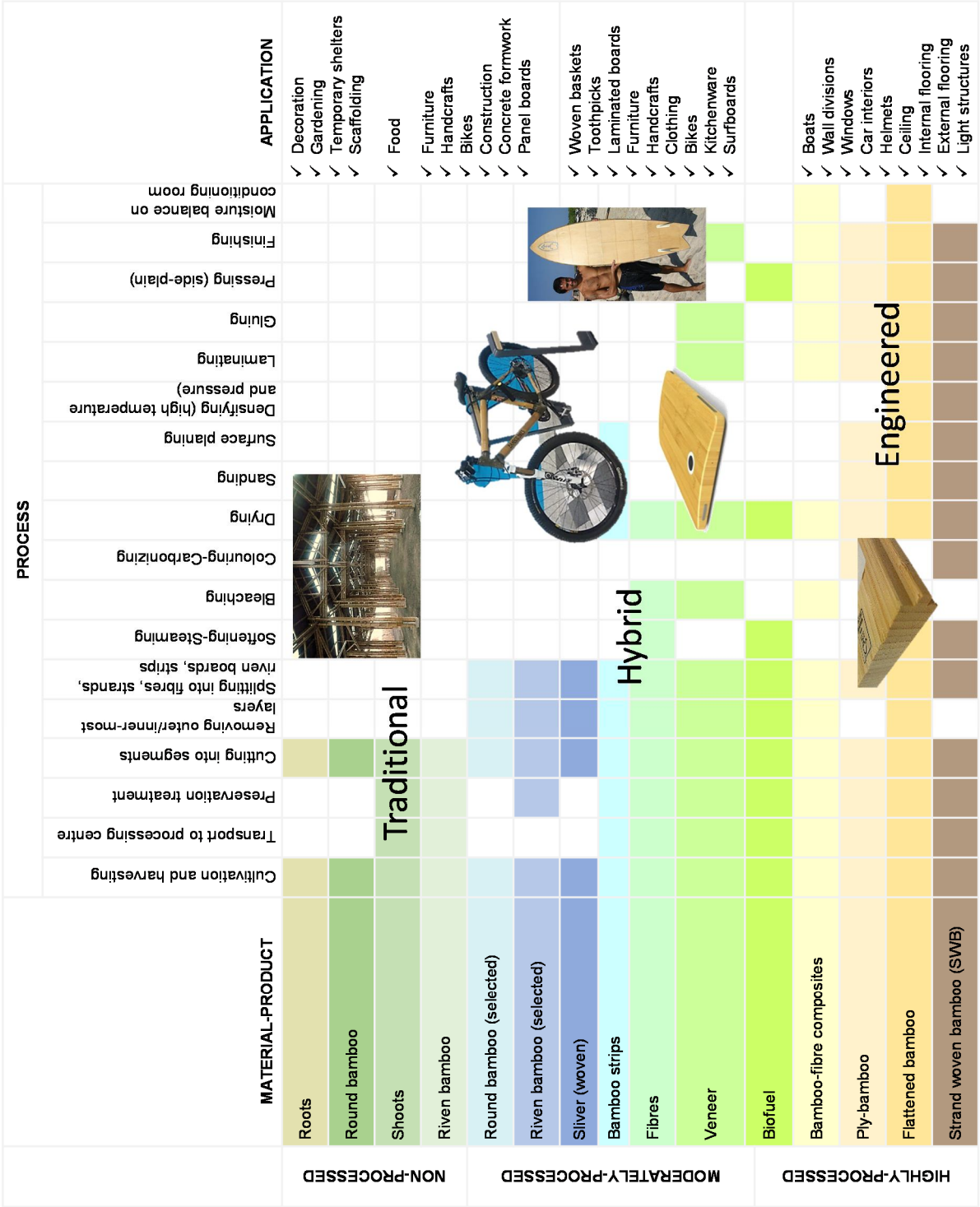

Figure 2-23. Uses of bamboo depending on its transformation degree.

Non-processed raw bamboo is commonly used for low added value and short-term applications (temporary shelters, scaffolding, handcrafts, food, etc.) usually where the material is abundant and durability is not a concern –because rotten material can be easily replaced. Moderately processed mature bamboo is preserved and dried mainly for its use in traditional construction in countries where bamboo-building systems (Guadua) are regularized (e.g. Colombia, Ecuador and Peru). In addition, some handcrafts and furniture applications make use of these type of bamboo in which, manual and non-intensive industrial processes are involved (hybrid). Highly processed bamboo products that add high value to the plant through different transformation processes can be classified into strip laminates (bamboo plywood or plyboo), woven strands and heat-pressed bamboo panels and beams (flattened bamboo and strand woven bamboo-SWB in Figure 2-23). The Chinese industry is the main supplier of these products with Moso-bamboo as the raw material. Finally, some hybrid bamboo products are made by combining different processing stages to achieve aesthetic appeal.

2.9 Environmental impacts of bamboo.

The intricate arrangement of bamboo rhizomes that spread shallowly underground provides a stable support for soils and riverbanks, preventing landslides and controlling erosion. The capacity of Guadua forests to store and regulate water is comparable to that of wood forests. This capacity has been measured at 530m^3/ha for Guadua and 572m^3/ha for wood by Camargo-García *et al*. (2009); results for mixed crops and silvopastoral systems are in the same range (~550m^3/ha), whilst lands with pasture cover have values below 500m^3/ha. Conversely, the same authors found that the resistance to erosion in soils of Guadua forests was twice that provided by mixed crops and pasture, and 64% higher than the resistance provided by wood forests.

The contribution of bamboo to soil erosion control, water conservation and land rehabilitation have a positive impact on the environment. For instance, the self-renewability and fast growth rate of bamboo enable commercial plantations of Moso and Guadua to be effective rehabilitators of degraded lands (Table 2-5 in Section 2.8). These features, together with bamboo's capacity for storing carbon contribute significantly to the mitigation of global warming and its negative effects on the planet (Henley & Yiping, 2009; Zhou, *et al.,* 2005). Among these effects are: sea level rise, heavy precipitation and flooding, wildfires, heat waves, severe draughts, forest death, health impacts, disruption of food supplies, biodiversity loss and destruction of coral reefs. Their impact on life in the planet, resource availability

and human civilization is monitored through nine measurable planet boundaries (Steffen *et al.,* 2015). One of these boundaries is 'climate change', which is measured in atmospheric concentration of CO_2 in parts per million (ppm) and has a minimum value set at 350ppm CO_2 (with an uncertainty threshold between 350 and 450 ppm CO_2). Recently, this value has been exceeded and is calculated at 396.5ppm CO_2, which Steffen *et al.* (2015) suggests have caused an increase in the intensity of rainfall, droughts, mass loss in Greenland and Antarctic ice sheets, as well as heat waves worldwide. Surpassing the set threshold for these planet boundaries can drive the planet to unhospitable conditions for human civilization to subsist (away from the current Holocene state). Hence, the importance of devising effective ways of fixing CO_2 in fast growing and highly renewable bamboo forests, which will contribute to keep the planet boundaries within safe levels.

Recent afforestation and reforestation projects with bamboo under international initiatives such as the Clean Development Mechanism (CDM) of the Kyoto Protocol have also proved the importance of this resource to alleviate the pressure on wood forests and to act as a highly significant carbon sink (FAO, 2010a, 2009). Therefore, the carbon sequestered within plant tissues enhances the environmental impact of bamboo (Zhou *et al.,* 2005). Currently, several projects from the United Nations Framework Convention on Climate Change (UN-FCCC) and Intergovernmental Panel on Climate Change (ICPCC) are considering the managed exploitation of bamboo forests in tropical and subtropical zones as a potential contributor to reduce the pressure on forestry resources (FAO, 2010a; Lou, *et al.,* 2010; FAO, 2009).

2.10 Carbon sequestration of bamboo.

The role of the bamboo forest within the carbon cycle has gained relevance in a period of increasing concerns about climate change. Carbon dioxide (CO_2) is the major greenhouse gas (GHG) causing an increase in global temperature (FAO, 2009). Throughout photosynthesis, plants absorb and release CO_2 during respiration, part of it remains fixed in leaves, branches, roots and tissue as hydrocarbons. Generally, fifty percent (50%) of the dry weight of these biomass components is estimated to be stored carbon (C). The content of carbon in bamboo and wood is equivalent to 0.5kg C of the plant dry biomass weight (Broadmeadow & Matthews, 2003; Riaño *et al.,* 2002). Biogenic CO_2 fixed in bamboo and bamboo products results from the ratio of the molar weight of CO_2 (44.01g/mol) to the molar weight of carbon (12.01g/mol). Calculations of biomass (B), carbon content (C) and biogenic CO_2 values are made using the following expressions:

$$\boldsymbol{B = w_g - (w_g \cdot MC)} \quad 2\text{-}1$$

$$\boldsymbol{C = B \cdot 0.5} \quad 2\text{-}2$$

$$\boldsymbol{CO_2 = C \cdot 3.67} \quad 2\text{-}3$$

where
(w_g) is the green-weight of the measured biomass;
(MC) is its moisture content, estimated as the difference between the initial weight and the dry weight divided by the initial weight;
(C) the carbon content and (CO_2) is the biogenic carbon dioxide assumed to have been sequestered by the plant.

Estimates of forest total carbon storage reach 650Gt C (Gigatonnes carbon), where biomass accounts for 44%, dead wood and litter for 11% and soil for 45% (FAO, 2010a). Estimations of the total carbon stock in bamboo forest in China range between 0.605 and 0.837Gt C, which corresponds to about 0.09 to 0.13% of the total forest carbon storage, and the carbon density for bamboo lies between 130.4 and 173.0ton C/ha (Lou, *et al.,* 2010). Lou *et al.* report a carbon storage capacity of a Moso bamboo forest within the soil layer of between 19-33% and above ground between 67-81%, whilst Riaño *et al.* (2002) assert that 19.9% corresponds to the soil and 80.1% to the aerial part in a Guadua plantation. Figures for carbon fixation in different organs of the Guadua plant measured by Riaño *et al.* 2002 are presented in Figure 2-24 (branches, caulinar and foliage leaves and culms constitute the aerial part).

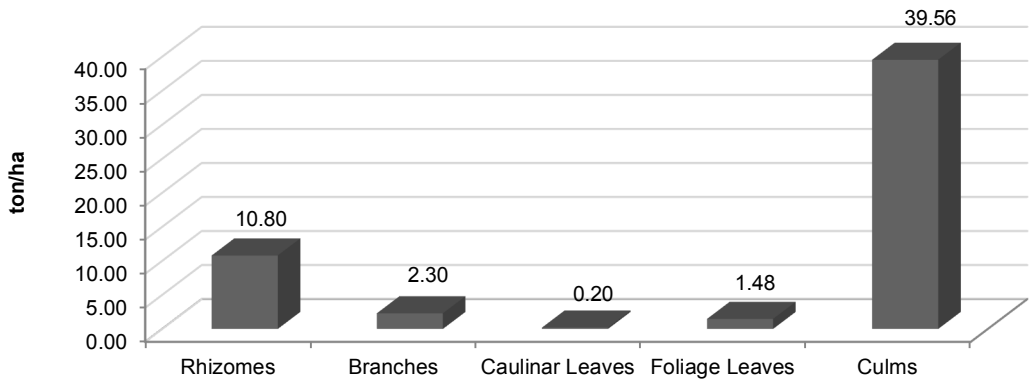

Figure 2-24. CO_2 fixed by 1ha of Guadua during 6 years on the different organs of the plant. Source (Riaño *et al.,* 2002)

Bamboo's high rate of biomass production and carbon sequestration above and below ground has been compared to fast growing trees. INBAR's report '*Bamboo and climate change mitigation'* by Lou, *et al.* (2010), estimates that a fairly equal amount of carbon is stored by Moso bamboo (*Phyllostachys heterocycla var. pubescens*) and the wood species

Chinese Fir (*Cunnighamia lanceolata*) – *both subtropical specie*s - during the first 30 years of controlled exploitation. An increase in carbon storage of about 20% was calculated for Moso over a period of 60 years. However, on un-managed bamboo plantations the result was 30% less storage capacity. Similar carbon storage over a period of ten years was found when comparing Ma bamboo (*Dendrocalamus latiflorus*) – a sympodial tropical species - with Eucalypt (*Eucalyptus urophylla*) – one of the fastest growing trees on the planet - 128ton C/ha and 115ton C/ha, respectively (Lou, *et al.,* 2010) (Table 2-6).

Table 2-6 provides information on carbon stored, yield class and normal rotation years for different commercial wood and bamboo species. Yield class (YC) refers to the potential productivity of the forest/plantation in volume per year and per hectare; these values in trees vary with factors such as age, top height, thinning and location (Moore, 2011). The term 'rotation years' refers to the period of felling or harvesting in years depending on the yield class. For instance, commercial Sitka spruce stands can grow at YC 14, 16 or 18-24 over typical commercial rotation periods of 35-45 years (Moore, 2011).

Table 2-6. Carbon stored by British and Chinese-grown trees and bamboos from China and Colombia.

Location	Species	Yield class (m^3/ha/year)	Equivalent carbon yield (ton/ha/year)	Rotation (years)	Carbon yield in rotation years (ton/ha)	Period to max. carbon storage (years)
UK Uplands (trees)[1]	Sitka spruce	14	1.70	35-45	68	110
	Scots pine	8	1.40	70	98	140
	Birch	4	1.00	45	45	90
UK Lowlands (trees) [1]	Scots pine	10	1.70	65	110.5	130
	Corsican pine	16	2.70	50	135	100
	Oak	6	1.50	150	225	300
South East China (temperate regions) [2]	Chinese Fir	-	3.2	30	96	-
	MOSO bamboo	-	3.1	(10)	31	-
South Asia (Tropical China)[2]	Ma bamboo		12.8	(10)	128	-
	Eucalyptus uroph.	20-30[7]	11.5	(10)	115	-
Colombia[3] (coffee region)	Guadua (aerial part-modelled)	(304)	26	5	130	-
Colombia (Valle del Cauca)	Guadua (aerial part)	- (188.5)[5]	7.26 [4] (12.04)[6]	5	36.3 (60.2)[6]	-
	Guadua (culms)	45*	6.59	5	33	-

[1](Thompson & Matthews, 1989) and (Moore, 2011); [2](Lou *et al.,* 2010); [3](Kleinn & Morales-Hidalgo, 2006), [4](Riaño *et al.,* 2002); [5](Arias-Giraldo *et al.,* 2008) on a plantation of 6,284 culm/ha (including young, mature and dry); [6] is based on van der Lugt & Brezet (2009) update of Riaño *et al.* (2002) calculations -estimated 33% increase in biomass on the plantation once it reaches its mature phase; [7] (Mead, 2001).
*Results from a plantation where 1,500 mature culms produced 0.03m^3 of commercial 'wood' volume that are felled yearly.

As shown in Table 2-6 the tropical bamboos Ma bamboo and Guadua and tree species *Eucalyptus urophylla* have the highest tonnage of carbon fixed per hectare, per year with the lowest rotation period. Guadua culms alone account for almost double the carbon content of the whole Moso bamboo plant, when comparing their annual yield in tons per hectare (Figure 2-25). Tropical species show a higher rate of biomass accumulation: *e.g.* stored carbon per ha after 10 years for subtropical and tropical bamboos (Moso and Ma bamboo) was 31ton and 128ton C/ha, respectively (Lou, *et al.,* 2010).

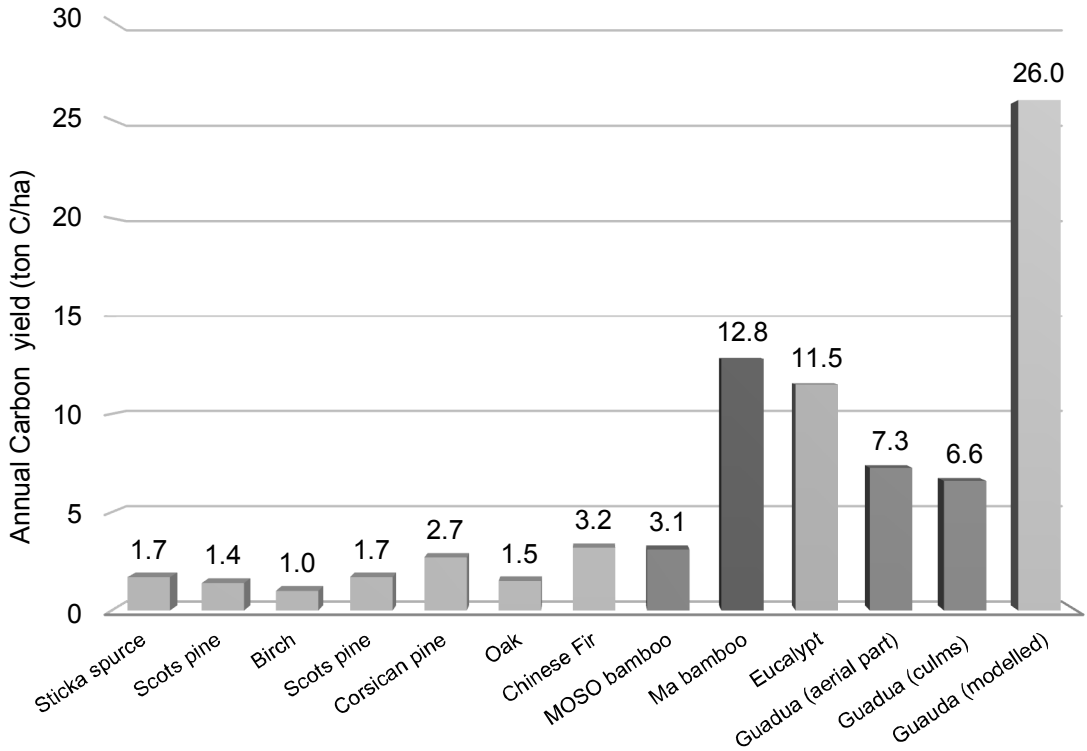

Figure 2-25. Annual Carbon fixation in wood and bamboo species in tons per hectare. Source for trees: (Thompson & Matthews, 1989) for bamboo: (Lou *et al.,* 2010) & (Kleinn & Morales-Hidalgo, 2006; Riaño *et al.,* 2002) for Guadua.

This figure of above ground carbon stock for Chinese Ma bamboo is similar to that obtained by Kleinn & Morales-Hidalgo (2006) for *Guadua angustifolia* Kunth in Colombia. The authors calculated a total above ground carbon stock in Guadua of 156ton C/ha on a six-year period (26ton C/ha/year). Although Ma bamboo and Guadua are tropical bamboo species, the rotation period for Ma bamboo is 10 years; thus, the lower resulting annual carbon yield (12.8ton C/ha). By contrast, for a six-year period, Riaño *et al.* (2002) estimated a total of 43.5ton C/ha (7.26ton C/ha/year) fixed in the aerial part (above ground) of a managed plantation of Guadua. This significant difference between the results of Kleinn & Morales-Hidalgo (2006) and Riaño *et al.* (2002) could be explained by the different methods used

by each study and the different regions and type of plantations chosen (*e.g.* the first study predicted the density of natural occurring plantations using aerial photographs and the second did it on-site in a reforested stand). Moreover, evidence suggests that naturally occurring bamboo forests possess higher capacity of storing carbon (Arango-Arango, 2011). The conservative results of Guadua's carbon sequestration reported by Riaño *et al.* (2002) have been updated by van der Lugt & Brezet (2009), who estimated an increase of 33% of biomass on the same plantation once it reaches its mature phase. The final values for Guadua are presented in parenthesis with the superscript '6' in Table 2-6 (e.g. 12.04ton C/ha/year).

Carbon storage in plants and particularly in bamboo depends on the different methodologies used including species, climate, natural features of the plantations (such as soil quality) and variability in yield per ha, diameter at breast height (DBH), number of culms per hectare, etc. For example, managed Guadua plantations have a denser composition of clumps (average 5,000 culms/ha for Guadua vs. 3,300 culms/ha for Moso), superior biomass production and faster maturation (four to six years in Guadua compared to nine to ten years in Moso).

Biogenic CO_2 sequestration in wood and bamboo depends on the annual yield in cubic meters per hectare (m^3/ha) and varies with harvesting practices and forest management. Vogtländer *et al.* (2010) assert that Guadua has about twice the yield of Moso and that use of their biomass could be made at 2 year cycles (as both bamboo species have branched out and reached their adult size by that time –see Section 2.4) for some highly processed bamboo products (see Section 2.8). Furthermore, maturity in bamboos occurs faster than in most wood species, which makes bamboo plantations an attractive option for high biomass yield and rapid CO_2 fixation compared to fast growing softwood species.

In Table 2-6 an estimated yield of 45m^3/ha was calculated for only mature culms of Guadua, assuming that in total 1,500 culms/ha are commercially exploited. Arias-Giraldo *et al.* (2008) calculated a yield of 188.52m^3/ha for 6,284 standing culms of Guadua of 20m in length and 11cm in diameter, which results in a volume of 0.03m^3/culm. van der Lugt & Brezet (2009) on the other hand, estimated a total volume of 0.0235m^3/culm for Guadua of 10.66m in length and a yield of 117.5m^3/ha for a total of 5,000 standing culms of Guadua.

Bamboo forests ability to sequester carbon and potential to act as carbon sinks (fix that carbon into CO_2) when converted into durable products have been highlighted by several authors (de Flander & Rovers, 2009; Henley & Yiping, 2009; Lou *et al.,* 2010; Murphy *et al.,*

2004; Riaño *et al.,* 2002; Rojas-Quiroga *et al.,* 2013; van der Lugt *et al.,* 2003; Vogtländer & van der Lugt, 2014; Vogtländer *et al.,* 2010; Zea-Escamilla & Habert, 2014). Well-managed bamboo and wood forests are able to maintain a balance between release and sequestration of CO_2 (zero carbon) from the atmosphere. Adequate plantation management together with appropriate disposal of these long lasting bamboo products at the end of their life (*e.g.* energy production through burning (Vogtländer *et al.,* 2013)) could significantly contribute to reduce greenhouse gases emissions responsible for global warming and climate change.

However, as discussed by several authors, in addition to fixation of CO_2 into durable products, real contribution to carbon sinks has to consider three key aspects (Broadmeadow & Matthews, 2003; Düking *et al.,* 2011; Vogtländer & van der Lugt, 2014; Vogtländer *et al.,* 2013). Firstly, the increment of forest area (afforestation); secondly, optimization of processing (less use of fossil fuels); and thirdly, increase in the use of these products (use in construction). When all these elements come together, the carbon footprint of wood and non-wood forest products becomes carbon negative.

2.11 CO_2 fixation and carbon footprint of bamboo and bamboo products.

Carbon footprint is usually measured through life cycle assessments (LCA) over a determined life cycle of a product (cradle to grave, cradle to gate, cradle-to-cradle, etc.). Depending on the methodology and life span chosen, LCA can assess the environmental impacts caused during cultivation, harvesting, manufacture, transport, use and disposal of bamboo and bamboo products. This allows the determination of the carbon footprint of these products and their comparison with other renewable and non-renewable materials.

Through a LCA using the Ecoinvent database, Vogtländer *et al.* (2013) estimated that 1kg d.w. (dry weight) of Moso and Guadua bamboo biomass above the ground (stem) originates from 3.1kg d.w biomass above and below the ground and that 1kg d.w of biomass in standing European softwood trees originates from 1.25kg d.w of biomass in the forest. By using Equations 2-2 and 2-3 to calculate the carbon content (0.5kg C/1kg d.w.) and the CO_2 storage in the forest (3.67kg CO_2), respectively, it is estimated that 1kg d.w of bamboo biomass and European softwood are related to 5.69kg CO_2 in the bamboo plantation and 2.30kg CO_2 in the wood forest, respectively (Table 2-7). These values could be used to assess the net weight of CO_2 sequestered by non-processed bamboo (see Section 2.8) and wood products (e.g. bamboo stems and wood logs).

The reason why CO_2 sequestered by bamboo in the whole plant is higher than the CO_2 sequestered by a whole tree in a European softwood forest is due to the high amount of carbon stored by bamboo's underground rhizome system and soil. This increment of CO_2 sequestered is also reflected in the CO_2 sequestered by highly processed bamboo and wood products.

Table 2-7. Equivalent $C0_2$ sequestration in bamboo and wood forest for different bamboo based products. Data from (Vogtländer *et al.,* 2013).

Product/Material		weight d.w. (kg)	Equivalent Biomass d.w. (kg)	Equivalent C (kg)	Equivalent CO_2 storage in forest/plantation (kg)	
	European softwood	1.0	1.25	0.62	2.30	
	Bamboo stem (Moso)	1.0	3.1	1.55	5.69	
	Plybamboo	1.0	7.05	3.52	12.85	
	Strand woven bamboo (SWB)*	1.0	5.7	2.85	10.5	

* For outdoor applications.

In the same study Vogtländer *et al.* (2013) found that for highly processed bamboo products such as plybamboo and outdoor strand woven bamboo (SWB) (Table 2-7) the amount of CO_2 sequestered per 1kg d.w. of product was equivalent to 12.85kg CO_2 and 10.5kg CO_2 storage in the bamboo plantation, respectively. These two bamboo products originate from 7.05kg d.w. and 5.7kg d.w. biomass in the bamboo plantation and use 5% and 23% content of resin by weight. The higher weight of dry matter biomass used per 1kg d.w. of each product explains the increase on the CO_2 storage when compared to the CO_2 sequestered by low-processed bamboo. In addition, the lower carbon storage of SWB compared to plybamboo is due to the higher use of resin in the first.

A LCA from cradle to grave undertaken by Vogtländer & van der Lugt (2014) assessed the

full carbon footprint of highly processed bamboo products including plybamboo and SWB. This assessment comprised the positive CO_2 emitted (debit) during production and negative CO_2 stored (credit) by the reuse of the product at the end-of-life in power generation. Additional credits were given to these products by factors contributing to CO_2 storage in the product related to land-use change, extra stored carbon in bamboo plantations (Broadmeadow & Matthews, 2003) and extra stored carbon in buildings (by increased use).

illustrates the results obtained by the authors.

Table 2-8. Carbon footprint of various bamboo products (MOSO International BV) and other conventional construction materials over their life cycle expressed in kg of CO_2 per kg and m^3 of product assessed (Vogtländer & van der Lugt, 2014).

Product	Density	CO_2 debit / kg product	CO_2 credit/ kg product		CO_2 / kg product	
		Production	End of life (burnt in power plant)	Land use change + extra CO_2 plant. and building	Total	Total
	kg/m³	kg CO_2	kg CO_2	kg CO_2	kg	m³
Bamboo stem (locally used)	700	0.20				
Bamboo stem	700	1.37				
Flattened bamboo	850	0.62	-0.70	-0.63	-0.72	-613
Plybamboo	700	1.01	-0.70	-0.62	-0.31	-220
SWB indoor	1,080	0.87	-0.70	-0.62	-0.44	-484
SWB outdoor	1,200	1.19	-0.70	-0.60	-0.11	-141
Sawn timber softwood (planed and kiln dried)	460	0.26	-0.81	-0.17	-0.72	-334
Meranti plantation (hardwood)[1]	640	0.71	-0.70	0.00	0.006	4
PVC (Polyvinylchloride) [1]	1,380	2,104			2,104	2,904
Steel[1]	7,850	1,838			1,838	14,429
Aluminium[1]	2,800	11,580			11,580	32,423
Reinforced concrete[1]	2,400	0.23			0.23	554

[1] Values extracted from Idemat 2014 database modified from Vogtländer & van der Lugt (2014)

In Table 2-8, the cradle to gate assessment of the CO_2 emitted during production (third

column) estimates all the processes involved from harvesting in a Chinese plantation (cradle) to transport of the product to a warehouse in the Netherlands (gate). It is remarkable to note that the same assessment for moderately-processed bamboo stems transported to Europe by sea have a carbon footprint equivalent to 1.369kg CO_2 per kg of stem. This is higher than the carbon footprint of any of the highly-processed bamboo products presented in Table 2-8 (e.g., it is 2.2 times higher than the carbon footprint of flattened bamboo). However, if the same stem is used locally (in China) the carbon footprint is only 0.20kg CO_2 per kg of stem. This occurs due to the low weight to volume ratio of bamboo stems, which increases the cost of transport.

Overall, highly-processed bamboo products such as flattened bamboo and plybamboo, whose physical properties (e.g. density, durability, hardness) have been improved through industrial processes outperform conventional materials in terms of their contribution to the overall CO_2 sequestration. Additionally, highly-processed bamboo products sequester more CO_2 than moderately-processed bamboo products.

Three key reasons support the carbon footprint results obtained by Vogtländer & van der Lugt (2014) for highly-processed bamboo products; firstly that more biomass goes into their manufacture (if compared to moderately-processed bamboo stems); secondly the assumption that the products will be used to generate electricity at the end of their life; and thirdly the additional credits given for land use, afforestation and use of these products in buildings.

Vogtländer *et al.* (2013) stated that increasing the use of carbon sequestered by forests on housing will translates into extra carbon sequestration; however, as the authors also remark, this will not happen by the use of tropical hardwood but, of softwood from northern areas (boreal or temperate) and/or bamboo. These forests are commonly well managed and have a higher yield of carbon per hectare with less negative impact on biodiversity. It can then be concluded that the transformation of bamboo into durable products for the construction industry could have a remarkable effect on the reduction of global carbon emissions.

Concluding remarks

Bamboo is a natural material with a functionally graded arrangement of tissues that respond to the plant vital requirements. For instance, the graded distribution of highly lignified fibres around the periphery (cortex) and less dense tissues towards the inner part of the culm (pith ring) of bamboo's tubular shape provides structural support and insect protection. Bamboo cortex possesses high tensile strength and hardness with silica cells and highly consolidated tissues (mainly fibres) that provide support during growth. Bamboo tissues towards the pith ring have a foam-like organisation of vascular bundles surrounded by vertically alternated short and long parenchyma cells that contribute to resist axial compressive loads and are in charge of the flow of nutrients. This results in a combined action for resisting lateral loads and self-weight; as well as in insects finding it more difficult to penetrate the cortex and access the soft and nutrients-rich tissues inside. Overall, the anatomical arrangement of bamboo is closely related to its morphology, growth and its chemical composition, which together define its general features. These features require more study in order to realize the potential of bamboo as an alternative renewable material for engineering applications.

The use of bamboo as a wood substitute in the construction industry can enhance the availability of wood forest resources for the future and reduce CO_2 emissions. *Guadua*-bamboo has an extraordinary growth rate with a higher production of biomass and CO_2 storage than most wood species and Moso-bamboo. These features can be exploited to develop long lasting products for the construction industry, which is one of the sectors that significantly contributes to environmental deterioration and depletion of natural resources.

3. A review of the literature on bamboo & Guadua in construction

Introduction

The mainstream use of bamboo has been widespread in construction. It is estimated that more than a billion people live in bamboo houses worldwide. In Bangladesh alone, more than 70% of the houses use bamboo in walls and roof structure. Mainly used by low-income communities, bamboo provides an abundant and low cost mainstream material for these houses. In countries such as Ecuador, Peru and Colombia the structural use of the bamboo species Guadua is currently regulated by national building codes. The construction of large structures such as warehouses and retail stores, and housing complexes complying with the Colombian code have demonstrated Guadua's potential as a mainstream material. However, issues such as its natural variability, poor design, labour intensive building processes and inadequate preservation treatments have hindered its widespread use as a standard construction material. Bamboos in general present the same issues. Bamboo is regarded as a temporary building material and because of its wide availability, ease of processing and low cost little attention has been paid to its preservation, detailing and maintenance post-construction in mainly low-income communities. Buildings constructed from bamboo with a long design life require thorough selection and preservation, along with high skilled workmanship and quality architectural and engineering design, all of which usually increases cost. Despite its limited availability in countries in South and Central America, Guadua is probably the most extensive bamboo used for construction worldwide. This Chapter explores the use of Guadua in traditional building systems and unconventional structures, highlighting its potential for engineering applications in construction and discussing potential flaws.

3.1 Guadua in construction

Several authors have described the versatility of Guadua as a building material along with its multiple transformations into fibre-cords, woven mats, riven culms, longitudinal strips, etc. (Figure 2-23) (Jayanetti & Follett, 1998; Janssen, 2000; Hidalgo-López, 2003; Villegas, 2003; Xiao *et al.,* 2008; van der Lugt & Brezet, 2009; Minke, 2012). Guadua's high biomass production, renewability and high strength-to-weight ratio make it a material of particular interest for structural purposes.

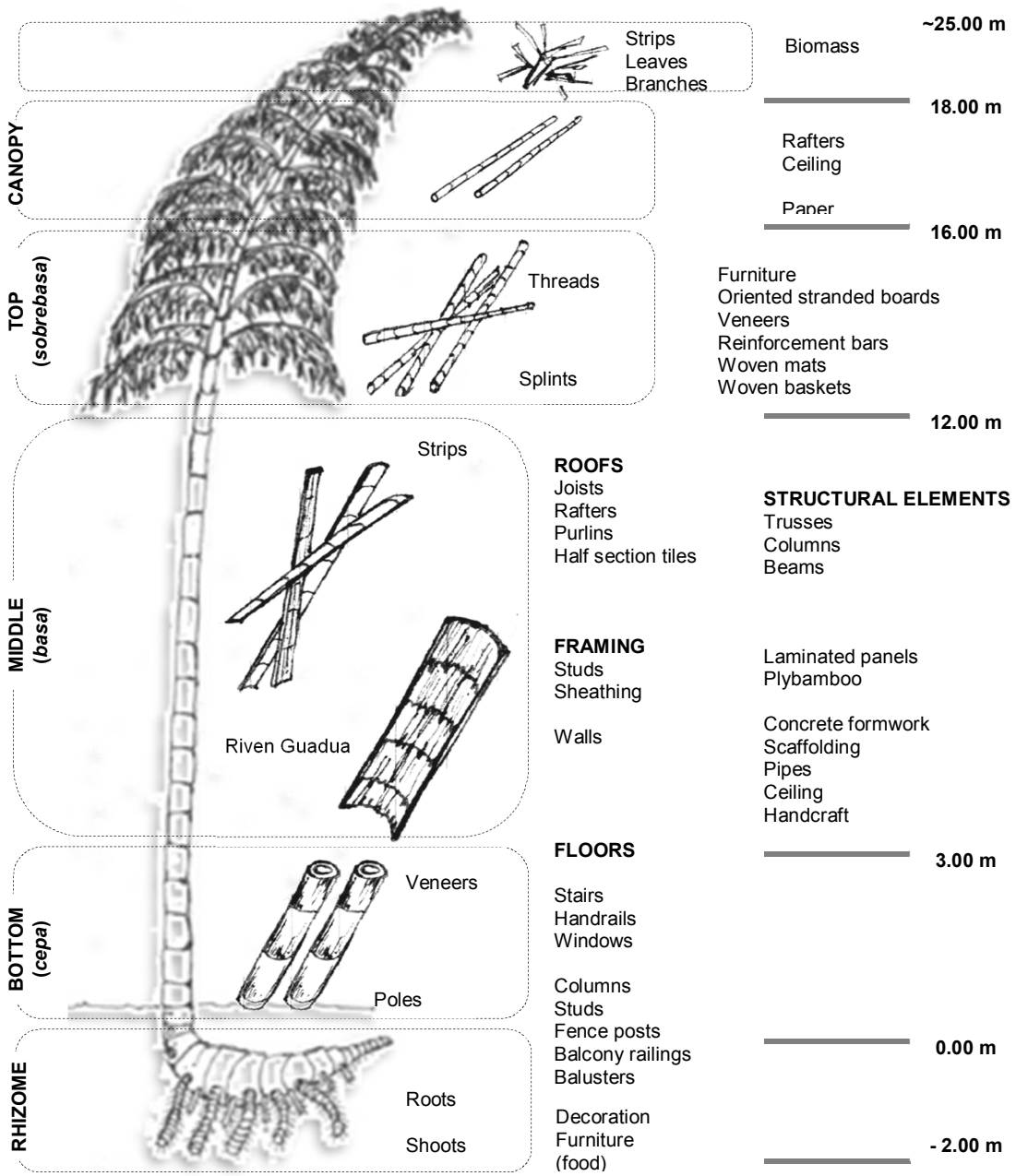

Figure 3-1. Uses of Guadua in construction as a function of the part of the culm utilized.

In construction, different parts of the Guadua culm are used for different purposes. Commercially, the culm is divided into three sections: the bottom, middle and top parts. Their common uses in construction are illustrated in Figure 3-1. These uses are dependent on the typical external diameter, culm-wall thickness, internode length and the straightness of the section. The bottom part (*cepa*) is the section with the widest diameter (~150mm and up to 220mm, Figure 2-12), the thickest culm-wall and the shortest internodes. These features make it ideal for structural elements which experience high compressive stress such as columns and studs in walls. The middle section (*basa*) has an almost constant diameter and culm-wall thickness along its 8 to 9 meters average length (Figure 3-1), and it is the straightest section. Thus, it is extensively used for beams and trusses subjected to high bending moments. Furthermore, this section is greatly used for highly processed products such as laminated panels and flooring. The top part of Guadua culms has a small cross section with a high content of fibre, which is mainly used for rafters and ceilings.

According to building regulations in Colombia, any section of Guadua for use in construction needs to be carefully selected and moderately-processed. Broadly speaking, two material forms (usually from the middle part of the culm) are used for traditional construction applications in this country: round and riven Guadua.

3.1.1 Preparation of round culms of Guadua

Prior to using Guadua for structural applications a series of simple processes are followed to ensure the quality and durability of the material. Despite some traditional beliefs concerning moon-phase and harvesting time for Guadua, it is exploited throughout the year following silvicultural practices (CARDER *et al.,* 2007). Felling between midnight and sunrise during the waning of the moon is believed to increase the durability of Guadua culms (due to the low starch content). During this phase, the lowest gravitational effect of the moon upon the earth means minor attraction of water inside the culms. Furthermore, the period during the night corresponds to the lowest levels of photosynthetic activity. However, study of the chemical components of bamboo culms after felling has not shown significant differences among moon phases (Liese, 2003). Starch content is reported to be at its lowest level in bamboo culms during rainy and winter seasons in tropical and temperate countries, respectively. Hence harvesting is advised during these seasons (Jayanetti & Follett, 1998; Liese, 2003).

Preservation techniques for using bamboo and Guadua in construction have also been studied and standardized (ICONTEC, 2007; Jayanetti & Follett, 1998; Liese, 2003; Montoya,

2005; Morán-Ubidia, 2011). Seasoning, preservation, drying, sectioning, flattening and selection processes are applied to the round bamboo culms depending on their final use.

The first process for the preparation of Guadua is curing, which takes place about 20 days after felling, allowing the plant to release water and sap (MinAmbiente, 2010b). Parenchyma cells remain alive after felling and the stored sap content continues to be used for the plant (branches and leaves) decreasing the sugar content (Jayanetti & Follett, 1998).

In the second process, four commercial pieces of four meters are sectioned as follows: one piece from the bottom, two pieces from the middle part and one piece from the top (Figure 3-1). The uppermost part with the leaves and branches (canopy) is usually chopped off and left on the plantation as organic matter. At this stage, some pieces of the middle are converted into riven Guadua (*esterilla de Guadua* by its name in Spanish, see Section 3.1.2) and the remaining material is pre-selected by diameter depending on their final application (columns, beams and rafters).

The third process is the preservation against xylophage insects (wood eating insects e.g. wood boring beetle), where different methods are implemented by using chemical solutions. Immersion of the material in a boron-based preservative and injection of the same preservative are the most popular techniques used. Immersion consists of soaking the material under water with a solution of boric acid (H_3BO_3 or $B(OH)_3$) and borax (sodium borate) for 7-10 days which requires the breaking of internal nodes to allow the flow of the solution along the cane. The injection process involves the drilling of small holes close to the nodes and along the culm with injection of the solution, which allows the preservative to be absorbed by the internal layer which is the most vulnerable to the fungi attack (Liese, 2003). Both methods rely on the axial diffusion of the boric acid and borax solution through the conductive tissue and its penetration across the cells by capillarity (radial cells as in wood does not exist in bamboo). Another process that uses the same borax and boric acid solution known as Boucherie consists of the displacement of the sap material contained inside the vascular bundles of Guadua by using a pressure system (Jayanetti & Follett, 1998; Liese, 2003; Montoya, 2005). This method has been scarcely studied and used for preservation due to some restrictions on the lengths that can be preserved and the cost associated with this process.

Other methods used for preserving bamboos are (a) smoking which consists of placing bamboo in chambers at 55°C for 15-30 days (Liese, 2003) and (b) whitewashing using slaked lime, which consists of a soaking process on saturated solution of $Ca(OH)_2$ in water

that during drying reacts with CO_2 to form calcium carbonate ($CaCO_3$) (Montoya, 2005). However, the efficiency of these two methods and the final appearance of the material are aspects that need more investigation (Jayanetti & Follett, 1998). Jayanetti & Follet (1998) also mention a combined preservative and fire retardant treatment produced by mixing different chemicals dissolved in water (Ammonium phosphate, Boric acid, copper sulphate, zinc chloride and sodium dichromate). Liese (2003) highlights the use of plasters of mud, clay or cement in walling as a way to protect the material.

Once the material has been preserved the fourth stage is the drying of the culms. Water is present in Guadua culms in free, fixed and hygroscopic forms and as water vapour (Montoya, 2005). The dimensional changes (swelling) of Guadua stops when free water is released and the culm reaches a 30% water saturation point, which is commonly achieved through air drying. Therefore, the moisture fixed within the cell wall needs to be removed by technical means. Solar drying and dehumidification in adapted chambers are the most frequent systems for drying Guadua (Montoya, 2005).

3.1.2 Preparation of riven Guadua.

The standardized frame-walling building system in Colombia (*bahareque*) makes an intensive use of a processed form of the culm known as riven Guadua or flattened Guadua for the sheathing of the walls. This material is widely used due to the low skilled and low energy process of manufacture (it just requires one person to do the job; see Figure 3-2). A sequence of the handicraft process for producing riven Guadua is shown in Figure 3-2.

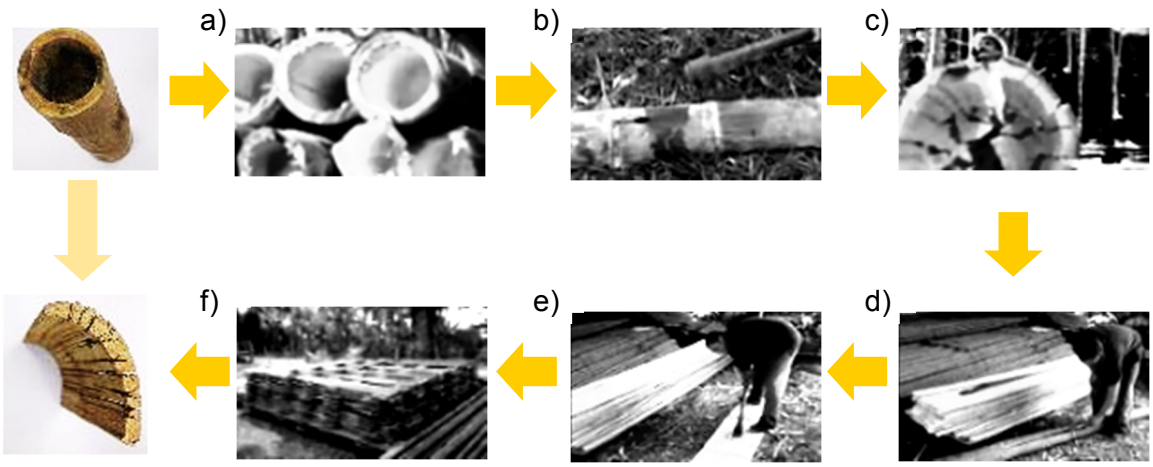

Figure 3-2. Handicraft manufacture of riven Guadua. (a) Cutting and selection of the round Guadua, (b) Splitting of nodes, (c) Splitting of internodes along the culm, (d) Riven Guadua before being opened flat, (e) Removing of internal diaphragms (nodes) and (f) Storing and drying of riven Guadua.

Its flat shape allows the configuration of different surfaces for boards (Figure 3-3d), slabs (Figure 3-3b) and walls (Figure 3-3a). The ability to bend riven Guadua also gives some manoeuvrability for more complex arrangements (Figure 3-3e). Commercial dimensions range between 300mm to 350mm wide and 4,0m to 4,5m long. Low added value uses are commonly given to this material due to its low cost, which ranges between £1.5 per linear metre for green specimens to £2.5 per linear metre for mature ones (£1~$3,000 COP). Furthermore, due to its low weathering exposure when used in walls, preservation processes are not usually applied but preservation is recommended. The fabrication of Guadua formwork 'boxes' (*casetón de Guadua*, Figure 3-3c) for concrete structures is the most popular use for riven Guadua boards in Colombia. These form the cavities (voids to reduce weight) in reinforced concrete hollow-core slabs that can be left to decay or removed after the concrete is cured.

Figure 3-3. Riven Guadua uses in construction. a) Wall sheathing, b) Roof & Ceilings, c) Floors, d) Slab formwork and (e) Arc configuration.

3.1.3 A brief history

Vernacular and traditional architecture in Colombia have made use of different material forms of Guadua. For instance, strips and riven culms were used in wattle and daub indigenous huts. Plastered cane system for walls (*bahareque*) from 1,300 B.C.E. in Ecuador, are reported as some of the most ancient bamboo structures in South America (Hidalgo-López, 2003) (Figure 3-4).

a) b)

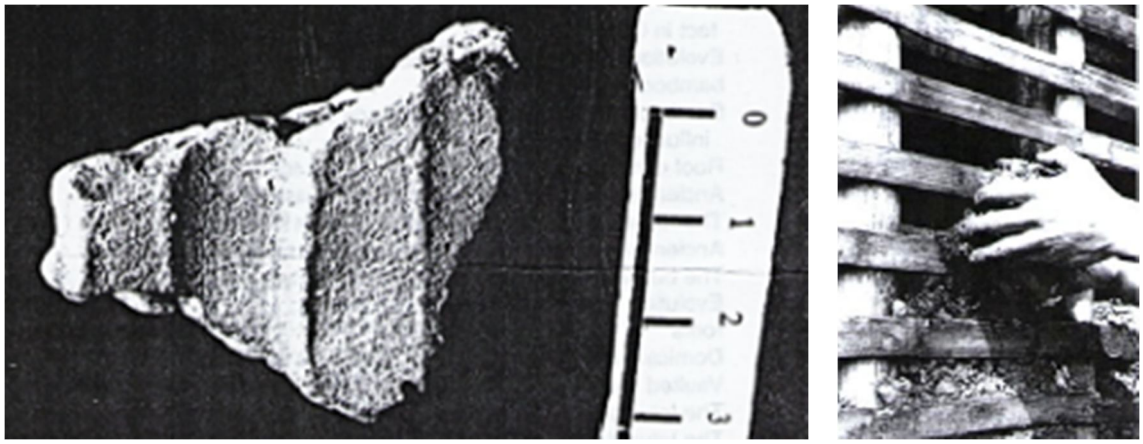

Figure 3-4. a) 3,500 years old Fossilized clay with bamboo slats impressions. b) Wattle and daub technique -*bahareque* (Hidalgo-López, 2003)

The abundance of bamboo was the reason for its widespread use for everyday objects in Central and South American pre-Columbian civilizations such as the Incas and Mayas. Hidalgo (2003) describes how the uses of bamboo for '*quincha*' (traditional construction system in Peru composed of wood, bamboo, mud and straw or grass fibres), *bahareque* and adobe walls among other vernacular technologies and structural models were adopted and adapted by the Spanish for the establishment of their new colonies. The combination of indigenous knowledge of construction with bamboo and natural materials, and the Spanish building methods along with historical and cultural processes shaped the new colonial style of the Spanish-colonized Americas.

In Colombia, after independence from the Spanish, an internal migratory phenomenon known as the "*colonización Antioqueña*" during the 18th century marked the birth of an architectural identity with a structural system which intensively used timber and bamboo (Robledo-C., 1996). This migration occurred in the area known as the coffee growing zone, where these materials were locally available. Figure 3-5a illustrates a farm house from this period.

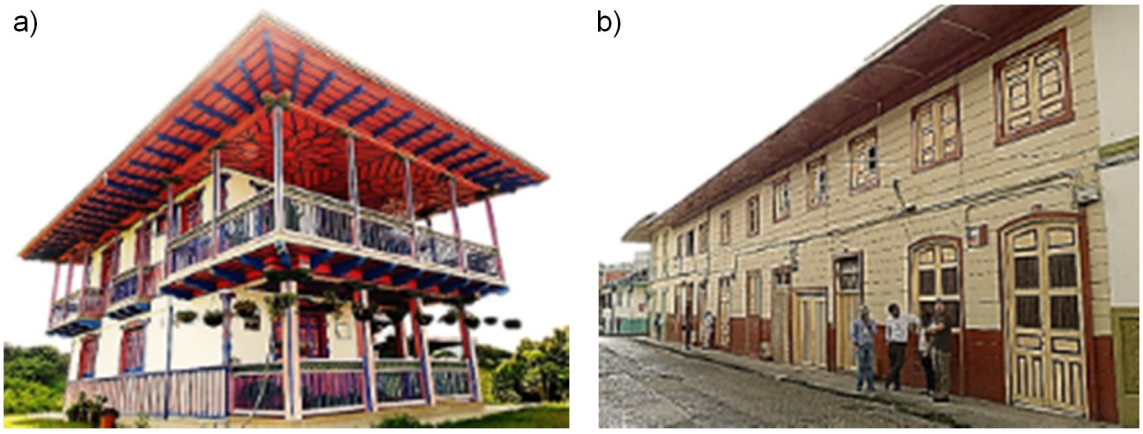

Figure 3-5. a) Typical farm house of the '*colonización antioqueña*' style (picture by Marco A. Ramírez, https://yoreportoarquitectura.wordpress.com/). b) Façade of a two-storey urban house with metallic *bahareque*.

Between the end of the 19th century and the beginning of the 20th 'modern' materials such as steel and cement were introduced to the architectural style of the region. For instance, cement mortars and metallic sheets were used for covering traditional *bahareque* systems (*bahareque encementado* and *bahareque metálico* (Figure 3-5b), respectively). Furthermore, the rapid growth of cities such as Manizales, Armenia and Pereira at the start of the 20th century and their location within the steep Andes mountain range generated Guadua structures of several stories (Figure 3-6). Round Guadua for the frame structure and riven Guadua boards for walling, flooring and ceiling were the most used forms for these type of structures (Figure 3-6).

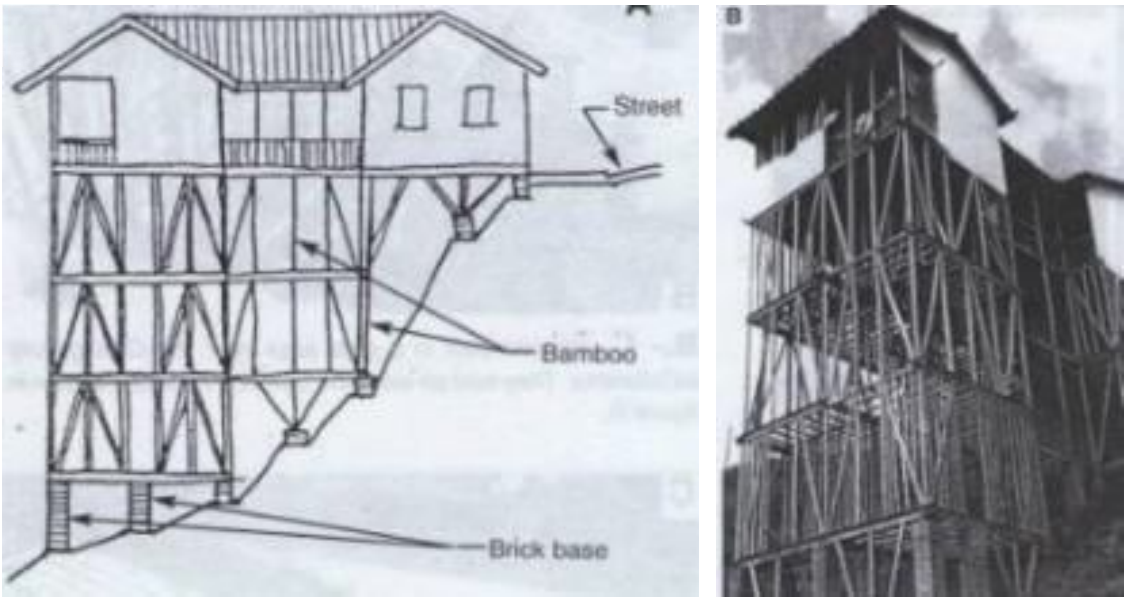

Figure 3-6. Four storey Guadua building in Manizales with *bahareque encementado* in the top floor, Colombia (Hidalgo-López, 2003).

Throughout the 20th century, carpenters, practitioners, architects and engineers mastered building and connection techniques that are still in use today. In the 1980s architects such as Simón Vélez took inspiration from *bahareque* systems and in particular from the *'colonización Antioqueña*'s style. He started a trial and error experimentation with round culms of Guadua for large structures. Vélez designed and successfully built cantilever roofs of up to six-meter using traditional collar and tie systems. He has also built forty-metre-span bridges (Figure 3-7b) and large structures mainly for farms (Figure 3-7a) and holiday houses in remote locations where building regulations were not a concern. Vélez also introduced the use of cement mortar filled internodes in bolted connections, which allowed for more rigidity in the overall structure of Guadua.

a)

b)

c)

d)

Figure 3-7. Bamboo buildings using Guadua by Simón Vélez in Colombia. a) Cantilevered roof of a stable by Simón Vélez (Villegas, 1989). b) Forty-meter span pedestrian bridge in Bogotá. c) Hoilday house in the coffee growing region and d) Roof structure detail.

Simón Vélez is the most renowned architect worldwide who is expert in the use of bamboo and Guadua in construction. His designs are based on three simple principles that are illustrated in Figure 3-8: wide roof, façade protection and ground insulation; or in his own words 'a big hat, broad poncho and wellies'.

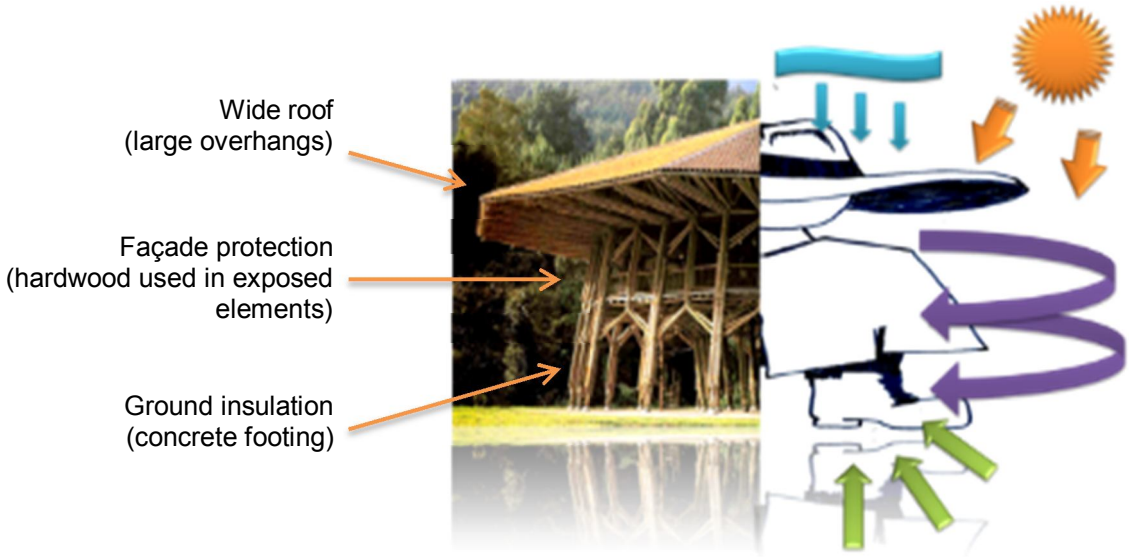

Figure 3-8. Principles of Simón Vélez architecture in response to the weathering effects produced by sun, rain, wind and humidity in Guadua constructions.

In 1999, traditional Guadua-constructed buildings withstood or suffered only minor damage during an earthquake that reached 6.2 on the Richter scale and had its epicentre in the coffee growing region of Colombia. This event attracted the attention of engineers, architects and researchers and led to the improvement of the building form (AIS & FOREC, 2002b) and the standardization of Guadua buildings in the seismic-resistant Colombian code or NSR-10 (MinAmbiente, 2010a). Nowadays, within this code, two traditional building technologies are regulated; (a) dwellings of one and two stories using *bahareque encementado* and (b) structures for residential, commercial and institutional buildings using round Guadua with bolts and filled internode connections (MinAmbiente, 2010b). A determining factor for the inclusion of these systems within the NSR-10 has been the use of cement renders for (a) and cement mortars for (b).

3.2 Building systems

Low weight and high ductility are desirable for buildings in earthquake prone areas where the dissipation of energy through structural elements with little or no damage is crucial.

Bahareque encementado and Guadua structures with in-filled internodes provide high-energy dissipation throughout nailed and bolted connections.

3.2.1 Plastered cane building system (*Bahareque encementado*)

Structural wall framing systems with Guadua for one and two storey dwellings are referred as to as '*Bahareque encementado'* in the Colombian construction code (NSR-10). It is defined as a system composed of a Guadua or Guadua and timber skeleton, and a sheathing made out of riven Guadua (Figure 3-9), nailed to the skeleton and covered with a cement render applied over a steel mesh (AIS & FOREC, 2002; MinAmbiente, 2010a). Both elements together result in a shear wall response.

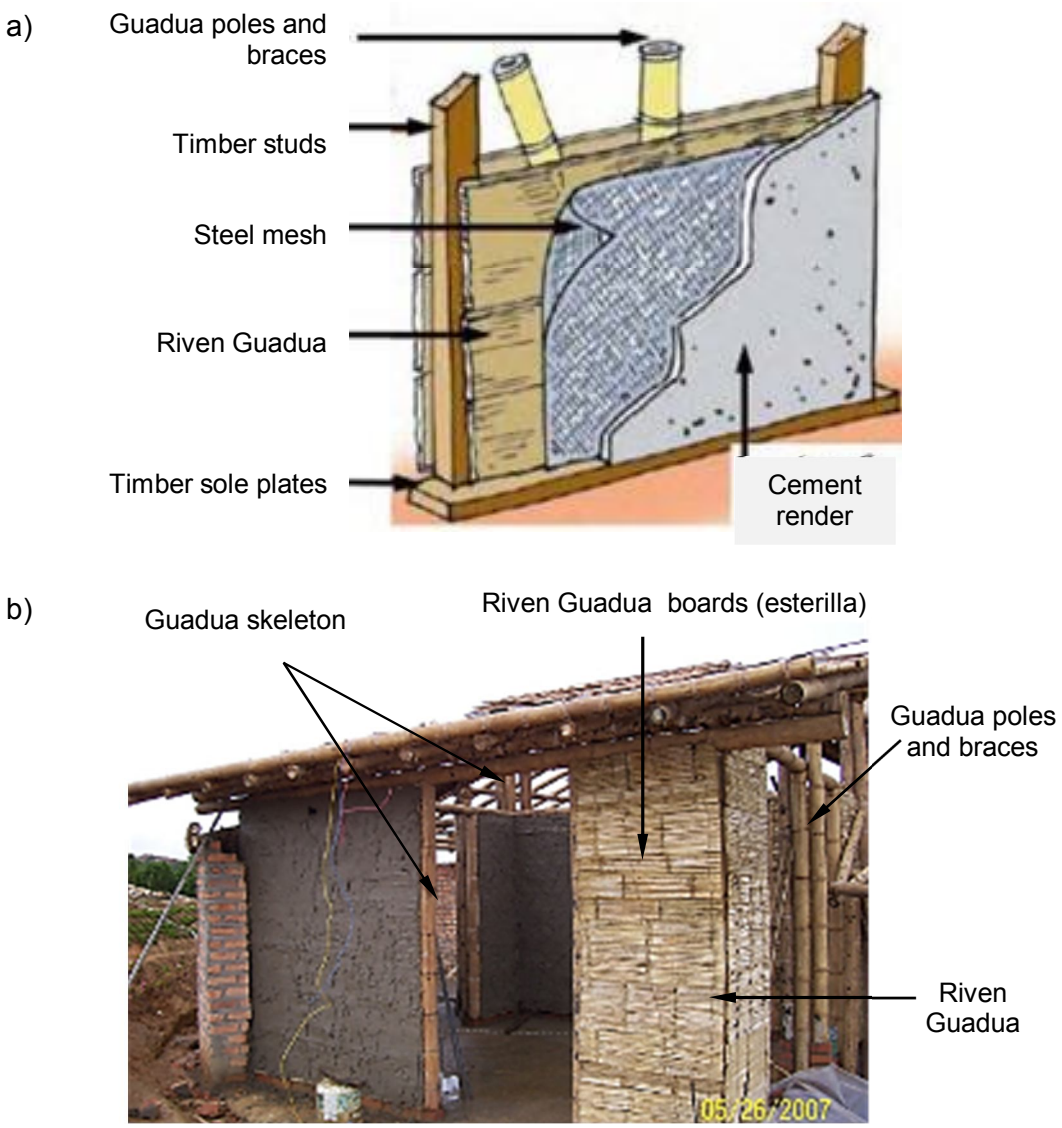

Figure 3-9. Plastered cane wall-framing system with parts diagram. Image (a) taken from (AIS & FOREC, 2002a)

This system uses Guadua intensively (approx. 12 linear meters per sq. meter) where 50% of the material is round Guadua used for the skeleton (frame) and the other 50% is riven Guadua boards used for the sheathing. Different configurations of walls depend on their function and structural performance. Structural braced walls are designed to resist vertical, horizontal and wind loads and must be located on the corners of the building and at the ends of every set of structural walls. Non-braced structural walls withstand vertical loads and must not be located at the ends of the wall system. In addition, non-structural walls are used as divisor walls and must not bear any shear or vertical loads (do not need to be continuous or to be anchored to the foundations). A series of images in Figure 3-10 depict the building process with this Guadua wall framing system.

Figure 3-10. Construction process of the plastered cane wall framing system (picture (h) by Arme Ideas en Guadua Ltd).

Within the frame structure, head and sole plates in timber are strongly recommended instead of Guadua due to crushing perpendicular to the grain (see Figure 3-9); these

constitute the horizontal elements. The studs must be separated by between 300 mm and 600 mm and the diameter of Guadua must not be less than 80 mm. The diameter of the steel wire mesh nailed to the riven Guadua (esterilla) must not exceed 1.25 mm (curtain mesh). The sheathing of the wall skeleton should be applied to both sides.

Overall, this system has been conceived to: a) minimize the effect of collapse during strong seismic events of low probability; b) ensure low damage during moderate seismic events; and c) avoid any damage from minor seismic events of high probability. Therefore, slab, roofs, columns and additional structural elements must be designed to contribute to the stability of the main load bearing system, *bahareque encementado*, following the requirements for each variation considered within the Colombian Code for seismic resistant construction (Chapters E7, E8, E9 are dedicated to this building system). As stated previously, this system is restricted to two storey buildings.

3.2.2 Larges structures with Guadua

The infill of Guadua internodes with a cement mortar (Figure 3-11) has led to increased rigidity of the connections, which otherwise will fail by shear parallel to the grain or crushing perpendicular to the grain.

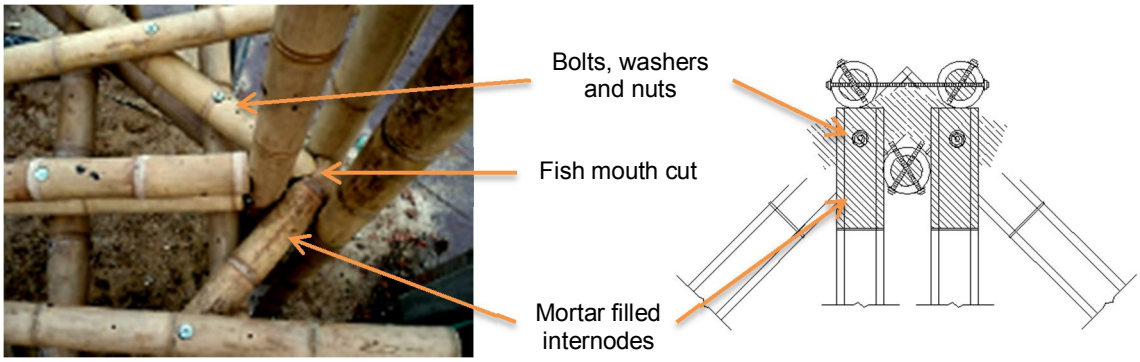

Figure 3-11. Detail of connections in a Guadua structure

This gain in rigidity has allowed the construction of large structural frames for commercial and institutional buildings and hybrid structures for holiday houses such as those in Figure 3-12a & b, respectively.

Isolated examples of large Guadua structures such as the bridge in Figure 3-7b and the dome in Figure 3-13, which use in-filled internodes and different structural concepts to the traditional collar and tie initially introduced by Simón Vélez, have spread within South and Central America.

a) b)

Figure 3-12. a) Warehouse in Bogotá, Colombia by Hector Archila. b) Bohio, holiday cottage in Villeta, Colombia by Hector Archila.

Others structures have demonstrated the potential of round *Guadua angustifolia* Kunth as an engineering material for large structures including the replica of the Indian Pavilion for the Shanghai Expo 2010 (Figure 3-13) recently built in Bogotá, the Zeri Pavilion for the Expo Hannover in 2001 and a pedestrian bridge in Holland.

a) b)

Figure 3-13. Replica of the Indian pavilion for Expo-Shangai 2010 by Simón Vélez in Bogotá, 2014. a) Interior view of the structure. b). Exterior view.

3.2.3 Boom and decline of traditional construction with Guadua in Colombia and its current opportunities and issues.

As discussed in Section 3.1.3 at the beginning of the 20th century Guadua was a construction material of widespread use in the coffee growing region of Colombia. However, events such as the 1925 fire in Manizales that devastated as much as 50% of the city (Robledo-C.,

1996) and the introduction of 'modern' construction materials (nowadays, known as conventional construction materials e.g. cement and steel) contributed to the almost complete decline of its use. Additionally, the prevalent use of non-processed Guadua by low-income communities for temporary shelters, due to its ease to use, resource accessibility and low price, branded this bamboo as 'a material for the poor'. Consequently, throughout the rest of the 20th century, natural plantations lost their value and were gradually replaced by crops such as coffee and plantain or cleared for cattle.

At the end of the 20th century, the use of Guadua in construction experienced a renaissance in interest, development and research. Around the 80s, Guadua structures built by architect Simón Vélez for affluent clients showcased the material's versatility, structural capacity and visual appeal. These captivated the interest of fellow builders, architects and engineers, as well as researchers in the field; for instance, in 1996 a dissertation by Jenny V. Garzón (referenced in Arbeláez *et al.,* (2001)) validated Vélez's mortar filled connections through mechanical test. However, it was not until the 1999 earthquake that devastated the city Armenia that Guadua became a subject of high quality research in Colombia and worldwide. Following the severe test of *bahareque* constructions during the earthquake, intensive investigation resulted in the standardisation of the two building systems described in Section 3.2.1 and 3.2.2: the plastered cane system and large Guadua structures, respectively. As a result, several examples of construction with Guadua in this earthquake prone country and other parts of the world can be found.

A number of issues have been identified associated with construction with Guadua (Kaminski, 2013; MinAmbiente, 2010b; Trujillo *et al.,* 2013; Xiao *et al.,* 2008). These issues and their determining flaws (design, material, processing and usage) are listed in Table 3-1 (1 to 14)

One of the most common issues in construction with Guadua is the use of non-processed/green material (item 1 in Table 3-1). Due to the poor selection of mature culms, the lack of preservation and absence of drying procedures, these culms experience severe dimensional changes (radial swelling) and are rapidly attacked by xylophage insects (Ghavami in Xiao *et al.,* 2008). As a consequence of the deficient drying and selection processes, cracks are generated on culms and walls (when using rendered riven Guadua) and connections become loose adding excessive flexibility to the structural system used (item 12, e.g. loss of rigidity on shear walls). On the other hand, the effective cross-section of the culm is drastically reduced by the attack of insects that feed from the 'soft' and nutritious internal

and middle sections of the culm wall. Internal and middle sections constitute about 80% of the culm thickness and are rich in starch-storing parenchyma cells (Figure 2-8 and Table 2-1in Section 2.3).

Table 3-1. Common issues in construction with Guadua

	Issue	Flaws			
		Design	Material	Processing	Usage
1	Use of non-processed material		X	X	
2	Poor design and detailing	X			
3	Deterioration by weathering and decay		X	X	
4	Temporary constructions become permanent				X
5	Inadequate material combinations and building modifications				X
6	Intensive labour (handcraft)		X	X	
7	Non-compatibility with building elements		X	X	
8	High material variability - Irregularity		X	X	
9	Deficient maintenance				X
10	Low added value	X	X	X	
11	High environmental impact of cement renders		X	X	
12	Highly flexible joints	X			X
13	Insufficient or non-fire proofing	X			
14	Structure unpredictability		X		

The use of non-processed Guadua usually occurs in suburban (shanty-towns) and rural areas, and mainly amongst low-income communities, which utilize Guadua together with salvaged low quality materials for building temporary shelters. These self-built constructions are frequently placed on unstable soils (Figure 3-14a & b), have bad weather protection (items 2-3) and unsafely combine heavy materials such as bricks and concrete on lightweight slender Guadua structures (Figure 3-14c). Furthermore, these buildings usually become permanent (it is easier to build on top of what exists) and there is lack of maintenance (item 9) (Gomez-Buitrago, 2002). During the 1999 earthquake in Armenia, Colombia there were two main reasons for collapse or severe damage in constructions using Guadua. Firstly, there was a lack of reinforcement and structural connection between building elements (slabs,

roofs, walls, etc.) in *bahareque* systems and secondly, there were unreliable combinations of more rigid and heavier materials (item 5) such as brick and concrete within Guadua buildings (Yoshimura *et al.,* 1999).

Figure 3-14. Construction with Guadua prior and post the 1999 earthquake in the coffee region, Colombia (Gomez-Buitrago, 2002). a) Shanty-town building. b) Collapse of a Guadua building due to unstable soil. c) Collapse due to discontinuity and inadequate combination of materials. d) & e) Houses that did not suffer collapse thanks to the correct use of building techniques with Guadua.

Plastered cane and structural Guadua systems that comply with building regulations and utilize appropriately processed Guadua tackle most of these issues (Figure 3-14d & e). However, there are some common flaws in both systems associated with the construction process and resulting from inadequate design and usage decisions. These have also been listed in Table 3-1.

Generally, the construction process of Guadua buildings relies on the abilities of high skilled

'artisan builders' (Figure 3-15a). The inherent dimensional irregularity of the material (Figure 3-15b) challenges the fitting of conventional building elements (item 7 in Table 3-1) such as windows (Figure 3-15c), doors and kitchen units, which must usually be custom-made. Therefore, construction with Guadua is regarded as a monumental and expensive handcraft (item 6).

Figure 3-15. Some common issues in construction with Guadua. a) Intensive labour. b) Material irregularity. c) Incompatibility with building elements. d) Thick cement renders that generate a high environmental impact.

In addition, the high variability of round and riven Guadua results in irregular surfaces that need thick cement renders to achieve uniform wall surfaces (Figure 3-15d). The use of a thick sand/cement render in the Guadua structural wall framing system contributes to 85% of the wall mass (Murphy *et al.,* 2004). This means that the sand/cement render corresponds to 238kg/m, whilst the total weight of Guadua used is 42kg/m (considering dry weight of Guadua = 3.5kg/m). Murphy *et al.* (2004) also highlights that the overall use of aggregates, cement and steel contributes to about 95% of the environmental impact in Guadua construction. This impact is mainly attributed to the foundations and walls that use these materials. Cement renders are therefore, a key topic for environmental impact reduction

(item 11).

Inadequate design decisions also result in negative effects during construction usage and undermine the public acceptance of Guadua as mainstream material. Poor architectural design and detailing contributes to the rapid deterioration and decay of exposed Guadua elements. Conversely, insufficient structural analysis of Guadua constructions and inappropriate combination of materials affect the structural integrity of the building (item 5). Typically, the structural design of Guadua structures has to account for the high variability of the material, use extremely conservative design values and frequently assisted by full scale structural testing.

Another factor related to design flaws is the insufficient or non-fireproofing of Guadua buildings (item.13) - with the catastrophic consequences for the city of Manizales, Colombia, discussed previously in this Section.

Overall, the issues regarding the use of Guadua in construction are strongly influenced by the inherent characteristics of the material such as its dimensional irregularity, high variability of physical and mechanical properties and natural decay. In addition, due to the little development achieved on the industrial processing of Guadua for construction applications, building methods rely on intensive manual labour. This adds to the structural unpredictability of Guadua structural systems and eventually, increase the building cost. Finally, flaws associated with the design and usage of the material post-construction are easier to tackle throughout appropriate design and improvements to the building system. Figure 3-16 & Figure 3-17 illustrate some of the new approaches to construction with round bamboo and Guadua in which improved connections and building systems are used.

Figure 3-16. Improved connections with glass fibre wrapping and combination of building systems at the bamboo straw-bale house by Susanne Korner & Tilman Schaeberle, Germany (Henrikson & Greenberg, 2011).

a) b)

c)

Figure 3-17. Stainless steel connections. a) German-Chinese House at Expo-Shanghai 2010 (ww.in-habitat.com). b) Connections and domes by Guaduatech (Guaduatech Inc.)

As an alternative to tackle the common issues in construction with Guadua, industrial processes applied to Moso-bamboo have been employed. Fibre and strip lamination techniques together with heat and pressure treatments have been used for developing engineered bamboo products.

3.3 Engineered bamboo-Guadua products and manufacturing technologies.

In general, engineered bamboo products (EBP) are scarce and require intense processing. Their development started with the manufacture of bamboo panel boards in China around

1940; however, it was not until the end of the last century, during the 80s and 90s, that research and commercial interest in this type of materials increased (Ganapathy *et al.,* 1999). Currently, the use of the bamboo species: *Phyllostachys heterocycla* pubescens (Moso) for the production of EBP is widespread. Commercially available EBP such as ply-bamboo, flattened bamboo and strand woven bamboo (SWB) illustrated in Figure 3-18a-c are industrially manufactured in China through several processing stages (Figure 2-23). Due to their elevated degree of transformation these EBP are referred to as highly processed bamboo products in Section 2.8 (Chapter 2).

Figure 3-18. Engineered bamboo products. Commercially available from: a) Ply-bamboo, b) SWB, c) Flattened bamboo (MOSO International B.V.); and other non-commercial EBP developed using Moso and Guadua: d) Bamboo plastic composite (www.bambooindustry.com), e) Riven Guadua panels, f) Laminated Guadua (www.agenciadenoticias.unal.edu.co).

Despite some research and industrial development of EBP using *Guadua angustifolia* Kunth (Guadua), fully developed, standardised and commercially available engineered Guadua products (EGP) are almost inexistent. Figure 3-18e & f illustrate two EGPs developed in Colombia. Overall, their advance is incipient and relies on the adoption of the same processing techniques used for Moso. Currently, the most widespread practices in the manufacturing of EBP are the machining and lamination of longitudinal strips and the hot-pressing of fibre strands under elevated temperatures (Table 3-2).

Table 3-2. Processes involved in the manufacture of some engineered bamboo products and their mechanical properties.

	Product	Density	Species	Process	MOE	MOR
					Bending	
		kg/m^3			GPa	MPa
Lamination Strips	Sulastiningsih & Nurwati [1]	710-750	G. apus/ G. robusta	Cold press+ clamped	7 - 10	39 - 95
	Mahdavi *et al.*,[2]	510	Moso	Cold press	9	77
	Plybamboo (Plyboo) [3]	666	Moso	Cold press	-	135
	Laminated Guadua [4]	728 - 796		Cold press	-	82
	Xiao *et al.*, 2013 [5]	800 - 980	Moso	Hot press	9	99
	Flattened bamboo [3]	850		Steam + Hot press	-	-
Hot pressing Fibre strands	LBL (zephyr mat) [1]	940	Moso	Roller crushing + Hot press	10.1 - 11.6	66.5 - 81.2
	Bamboo scrimber [6]	1240	*Melocanna Baccifera*	Roller crushing + Glue impregnation + Hot press	15.2	266
	Huang *et al* [7]			Hot press	13	89
	SWB outdoor [3]	1,200	Moso	Hot press	-	-

[1] (Sulastiningsih & Nurwati, 2009) [2] (Mahdavi *et al.*, 2011) [3] MOSO International BV (Vogtländer & van der Lugt, 2014) [4] (Correal *et al.*, 2014) [5] (Xiao *et al.*, 2013) [6] (Nugroho & Ando, 2000) [7] (Huang *et al.*, 2013)

During the strip lamination process, the round culm is first split into six to eight concentric sections; secondly, the trapezoidal-like section of the strips is sanded down into a rectangular form after removal of about two thirds of the total material and finally the strips are longitudinally oriented and glue laminated into beams, boards or flooring slats. One of the biggest drawbacks of this process is the high amount of material discarded. Usually, the

strongly consolidated outer layer of the bamboo/Guadua culm with the highest specific gravity is removed and its mechanical properties are no longer comparable to steel. The negative influence on the mechanical properties of bamboo due to removal of the outer skin as well as the considerable material wasted through the strip lamination process has been highlighted by Nakajima *et al.* (2008) and Tanaka *et al.* (2008). Both studies have undertaken modifications to the cell structure of bamboo by thermal softening, the former without pressure and the latter with elevated temperature and pressure. These type of heat and pressure treatments are currently applied to bamboo with the aim of achieving flat sections of high density and hardness. Mechanical properties of lamination and heat and pressure processes are presented in Table 3-2 and will be further discussed in the next Chapter.

Concluding remarks

Traditional Guadua building systems are not adequate for the requirements of the new built-environment. Further processing methods of the material will contribute to the creation of new building systems that tackle the common issues of traditional construction.

Engineered bamboo products have demonstrated their ability to tackle issues such as bamboo's dimensional irregularity and structural unpredictability; however, refinement of processing and modification technologies is necessary.

Current lamination processes with Moso and Guadua result in high amounts of waste material. Processing with heat and pressure allows the use of the high-density material within the outermost layer of bamboo and largely eliminates the generation of waste.

4. A review of the literature on thermo-hydro-mechanical modification in wood and bamboo

Introduction

Although research on the modification of bamboo through the use of heat and temperature was reported by Li *et al.* (1994), it was not until recently that the bamboo industry implemented these processes for the development of engineered bamboo products (EBP). Among them are bamboo hot-pressed products such as SWB (strand woven bamboo) and flattened bamboo, which were introduced in Chapter 3. The main motivations for the use of high temperature and pressure during the bamboo processing are the achievement of flat surfaces and enhancement of mechanical properties, density and hardness. Thermo-hydro-mechanical (THM) modification processes have been widely applied to wood for tissue consolidation and in particular to softwoods to increase their density, improve weather resistance and reduce fungal decay and hygroscopicity (Ansell, 2011; Fang *et al.,* 2010; Heger *et al.,* 2004; Kutnar *et al.,* 2008a; Sandberg & Navi, 2007). Despite the microstructural differences between wood and bamboo discussed in Chapter 2, both materials have comparable cellular porous structures and chemical compositions, which can result in similar changes when applying THM modifications to bamboo. Nevertheless, this is a fairly new area of research applied to bamboo processing that requires further study.

This Chapter reviews the existing knowledge on densification of wood and bamboo and explores its potential application for the processing of Guadua. The aim is to define adequate THM treatments to be used in the development of engineered Guadua products (EGP).

4.1 THM modifications

Table 4-1 presents the three main types of modifications that can be applied to wood for altering its natural characteristics: chemical, thermo-hydro (TH) and thermo-hydro-mechanical (THM) modifications (Homan & Jorissen, 2004; Sandberg & Kutnar, 2014; Sandberg & Navi, 2007). Chemical treatments such as acetylation modify the hygroscopic behaviour of wood into a hydrophobic one by replacing hydroxyl groups with acetyl groups. Amongst the TH modifications of wood are processes such as wood drying, heat treatments and the reconstitution of wood into new materials (e.g. composites and biomass products). Finally, bending, densification, welding, and shaping are part of the THM modifications in which heat, pressure and water interact to achieve the desired effect. Densification treatments are of particular interest for this review, due to its multiple benefits on the mechanical and physical properties of wood.

Table 4-1. Chemical, thermo-hydro (TH) and thermo-hydro-mechanical (THM) modifications of wood.

WOOD MODIFICATION	Chemical modification	Etherification, Olification, Acetylation, Furfurylation, Formaldehydation, etc.	
	Thermo-Hydro (TH) modifications	Wood drying	
		Wood ageing	
		Heat treatment	Thermowood
			Plato Wood
			Retification & Perdure
			Oil Heat Treatment (OHT)
		Reconstituted wood	Composites
			Fibre webs
			Veneer processing
			Biomass processing
	Thermo-Hydro-Mechanical (THM) modifications	Bending	Solid wood
			Laminated wood
		Wood shaping	Surface
			Cross-sectional
		THM densification	Open system (TM & THM)
			Closed system (THM)
		Wood welding	

Unlike chemical modification of wood, in THM modifications usually no chemicals are involved in the main transformation process. Nonetheless, some resins are occasionally used

to fix the modification (*e.g.* commercial TM and THM laminated products such as Lignofol, Jicwood, Panzerholz, Permawood and Permali are impregnated in resin to stop shape recovery/spring-back effect (Kamke & Sizemore, 2008; Sandberg & Kutnar, 2014)). Depending on the configuration of these elements throughout the duration of the process, alteration of its primary chemical components and mechanical properties occur at different levels (Esteves & Pereira 2009). These enable microstructural changes to occur when bending, shaping, welding, drying and in general, modifying wood.

4.1.1 Bending

Bending is probably the most common technique used and longest known THM process in human history; the use of steam-bent techniques for manufacturing canoes, tools, hunting arches, skies and other equipment have been dated ~3,000 BC (Sandberg & Kutnar, 2014). Different strapping methods were used to keep the set shape and reduce tension stresses. Strips or veneers of wood are also bent to achieve curved shapes for diverse applications. Figure 4-1a & b illustrates some applications of the bending of solid wood and veneers.

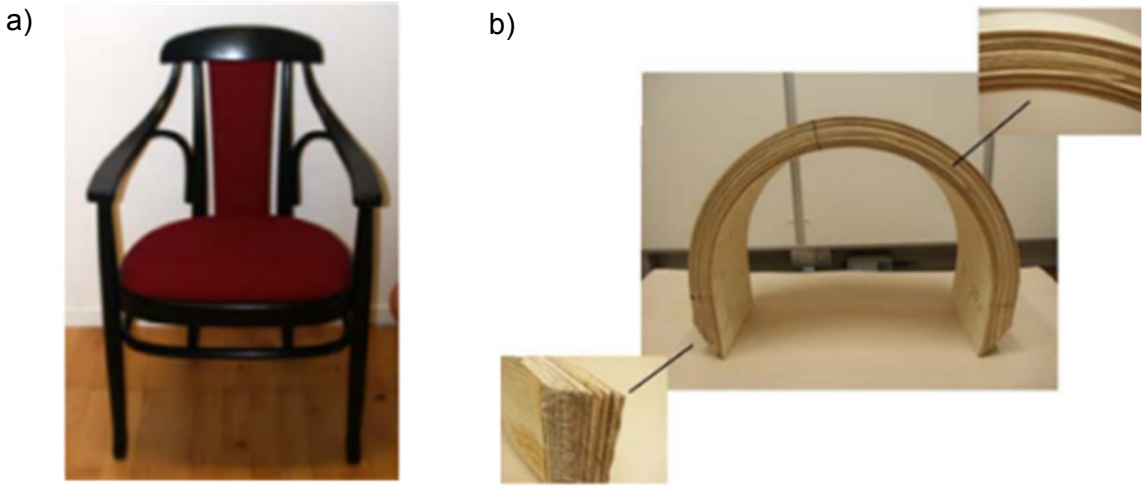

Figure 4-1. Wood bending. a) Arm chair made through steam bending of solid wood. b) Laminated bending (Sandberg & Navi, 2007).

THM processes have also been used for bending round and laminar bamboo, mainly for decorative, furniture and sport equipment applications (Figure 4-2). Vernacular techniques using heat and force have also been applied in traditional construction with bamboo and Guadua to achieve desired aesthetic effects (Figure 4-3). Bamboo in green condition (with high moisture content) is used.

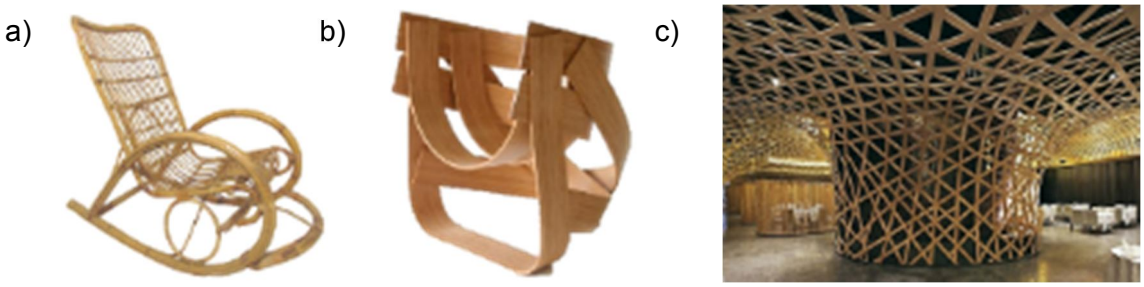

Figure 4-2. a) Italian bent bamboo rocker by Modhaus (www.1stdibs.com). b) bamboo laminated chair by Tejo Remy and Rene Veenhuizen (www.remyveenhuizen.nl/). c) Bamboo lattice wall and ceiling (www.dreamfundesign.com/).

Figure 4-3. a) Bending round bamboo with a gas flame burner. b) Bending green Guadua by manual force (www.guaduabamboo.com). c) Bent Guadua construction temporary built in Pereira after the 1999 earthquake in Colombia.

4.1.2 Shaping

Wood and bamboo can also be shaped (Figure 4-4 & Figure 4-5). Figure 4-5 illustrates the hot-pressing process of a wood log into a squared shape through a method developed at the Nara experimental research station (Morsing, 2000). The logs are in a green condition, preheated and then pressed at approximately 1MPa.

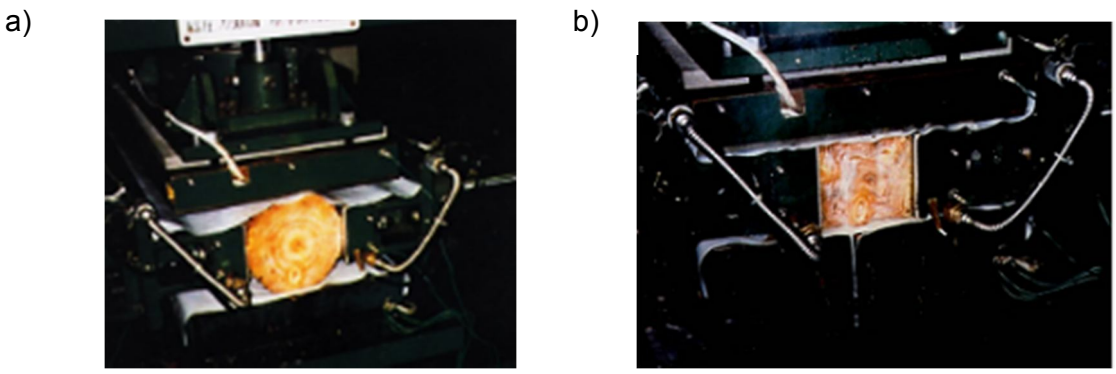

Figure 4-4. Wood shaping. a) Round log of wood prior shaping, and b) Squared log post-shaping. Photograph by Morsing (2000).

Kitazawa *et al.* (2004) utilized metal forming technologies (Figure 4-5a) with the aim of transforming the irregular and oval-like section of bamboo Madake (*Phyllostachys bambusoides*) into a continuous circular section. Round pieces of bamboo were pre-heated at about 110°C and forced to pass through a nosing device at a rate of 1.5mm/s. The nosing device was heated in an oven at 105°C, prior to processing (nosing). Subsequently, the nosed canes of bamboo were kept on an oven at 105°C for two hours after the treatment, with the aim of fixing the deformation.

a)

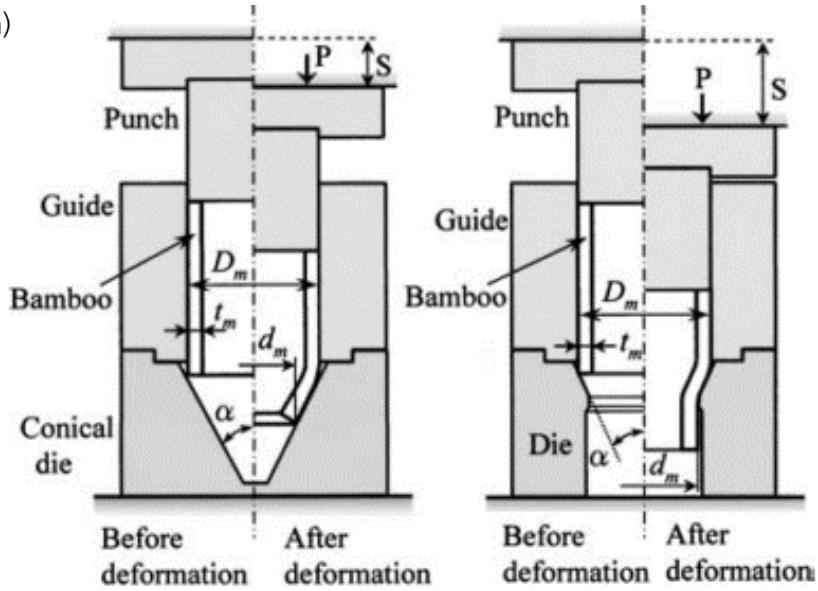

b)

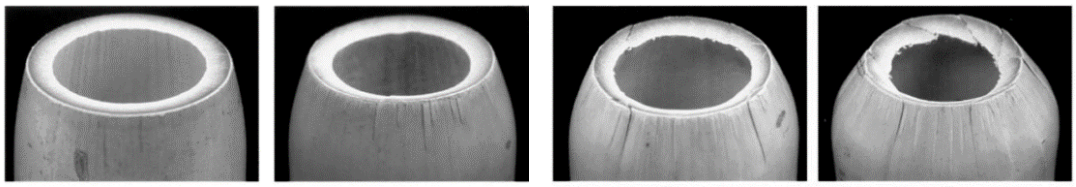

Figure 4-5. Wood and bamboo shaping. a) Round log of wood prior shaping, and b) Log post-shaping. Photograph by Morsing (2000). c) Nosing device for bamboo shaping and d) Nosing sequence at α=45° (Kitazawa *et al.,* 2004).

Both shaping applied to wood and bamboo (above) were undertaken in Japan and used microwave irradiation to thermally soften the material prior to shaping.

4.1.3 Densification

Wood and bamboo can be modified also by applying a transverse compressive force (either in the radial or tangential orientation of the grain). TM (thermo-mechanical) & THM densification methods are applied to wood for reducing void cellular spaces (lumens) within its

constituent tissues (e.g. conductive vessels, fibres, parenchyma and tracheid cells). The main aim of the densification of wood is the improvement of mechanical and physical properties such as stiffness and hardness without cell damage (Sandberg & Kutnar, 2014).

TM densification is commonly undertaken in open systems (hot-presses) where moisture content (MC) of the specimen or relative humidity (RH) of the environment cannot be controlled during the process. Hence, the use of stabilized wood at 13% MC is preferred to avoid explosion (Heger *et al.,* 2004). Staypak is a product developed during the 1950s made through this method. Seborg *et al.* (1956) conducted extensive research on the TM densification of Staypak, the effects of moisture and the dimensional stabilization of the product post-processing. The authors densified yellow-poplar with 6, 9, 12% MC for approximately two hours at temperatures between 150-180°C, and pressure of ~14MPa along the radial direction. Similar TM densification processes were used for the development of solid products such as Lignostone and Compreg (Figure 4-6) or laminated products such as Lignifol, Jicwood and Jablo. However, unlike Staypak, these products use resins (e.g. phenol formaldehyde-PF) instead of heat and pressure to avoid the spring-back effect, which results in increased brittleness of the product (Kamke & Sizemore, 2008).

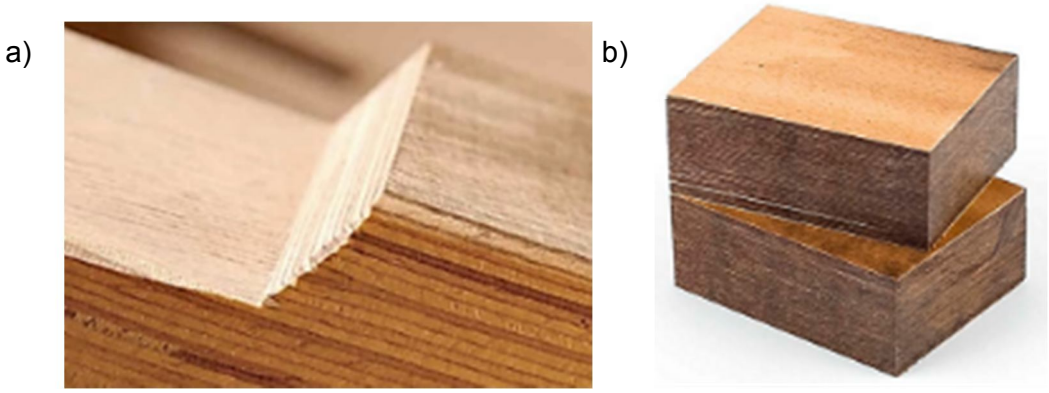

Figure 4-6. TM densification. a) Lignostone® Transformerwood® (Rochling Engineering Plastics KG). b) Compreg, hardwood (beech, birch) veneers with phenol resin at high temperature and pressure (www.sklejkapisz.pl).

The characteristic shape recovery of wood through moisture in-take or spring-back effect is a common issue with TM and THM densification processes. Several research studies on open THM densification treatments (Figure 4-7) have tackled these issues, nevertheless, issues relating to the industrial reproduction of the applied processes remain (Kamke & Sizemore, 2008; Kutnar & Sandberg, 2015; Kutnar *et al.,* 2008b; Sandberg & Navi, 2007).

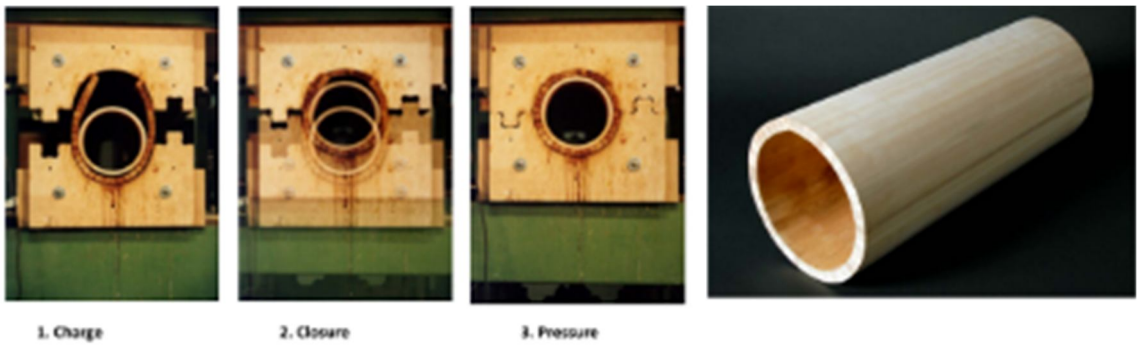

Figure 4-7. Manufacture of a tube of spruce by densification in an open system by Haller (2008) presented in (Sandberg & Kutnar, 2014).

THM densification methods in closed systems allow a strict control of temperature, moisture and pressure in sealed chambers, which results in efficient densification processes with permanent dimensional stability (Heger *et al.,* 2004). However, its use nowadays is restricted to small wood specimens in specialized laboratories.

Overall, THM & TM technologies offer attractive solutions for manufacturing engineered timber with higher resistance to decay and insect attack as well as improved mechanical performance.

4.1.4 Welding

Welding is a technique broadly used in the metal and plastic industries. In wood, welding can be achieved through oscillating or linear friction (Figure 4-8a); however the interfacial bonding strength is much lower than commercial glues (Sandberg & Navi, 2007).

Figure 4-8. THM wood modifications. a) Layers of beech and spruce bonded by circular friction welding (www.ibois.epfl.ch). b) Torrefied wood briquettes (www.cfnielsen.com). c) Wood veneer processing by steaming and boiling of logs prior to peeling (www.madehow.com).

4.1.5 TH treatments in brief

Research on heat treatments (TH) started early in the 1920s with the study of wood drying and extended along the 20th century with the experience on the development of densified

products such as Lignostone, Compreg Staypak, and Lignifol. Recently, TH processes have gained more interest as a way of tackling the restricted use of harmful chemicals, optimizing the use of wood and coping with the demand of more sustainable eco-materials (Esteves & Pereira, 2009).

TH processes are designed to increase the durability and dimensional stability of wood-products (Figure 4-9); however, their main disadvantage is the considerable reduction in strength (Welzbacher *et al.,* 2007). Products such as Thermowood® are commercially available and modify the chemical composition of wood through a three-step process. Firstly, wood is heat treated in a closed chamber at ~190ºC, which dries it. Secondly, the temperature in the chamber is raised to up to 212ºC to stabilise the modification. Thirdly, the temperature is dropped and the material is left to cool down. This heat treatment claims to reduce shrinkage to around 6-8% after drying and 5-6% after stabilising.

Figure 4-9. TH treatment of wood. Non-treated (left) and TH treated (right) ByThermoholz vergleich / Anubis100 (commons.wikimedia.org)

Zhang *et al.* (2012) applied TH treatments to *Phyllostachys pubescens* (Moso) and found a strong relationship between mass loss and the reduction of the modulus of rupture (MOR) at temperatures over 160ºC. In addition, at temperatures above 200ºC the modulus of elasticity (MOE) suffered a considerable reduction.

The joint use of TH treatments and densification processes contribute to tackle common challenges with these treatments such as strength reduction on TH and spring-back on densification. For instance, Welzbacher *et al.* (2007) applied oil-heat-treatments (OHT) to TM densified Norway spruce (*Picea abies* Karst) and achieved almost complete dimensional stability after natural weathering for 30 months Figure 4-10. Large pieces of Norway spruce were densified for 0.5, 1, 2 and 4 hours at 140, 160, 180 and 200ºC and 5.0MPa of pressure and then, subjected to OHT treatment in heated rapeseed oil at 180, 200 and 220ºC for two and four hours. The best results were obtained by the OHT process at 200ºC for four hours.

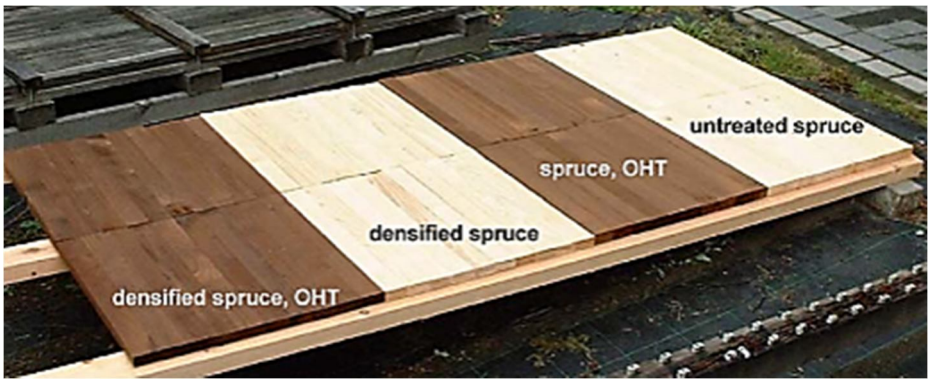

Figure 4-10. Specimens of un-treated, densified, OHT treated and densified Norway spruce with OHT treatment (Welzbacher *et al.,* 2007).

OHT have also been applied to bamboo. Cherdchim *et al.* (2004) & Parkkeeree *et al.* (2014) studied the thermal softening of black-sweet bamboo (*Dendrocalamus asper* Backer) culms in linseed oil and produced flat sheets after applying load. Both studies used the same specimen dimensions and OHT setup. Half sections of 3mm in thickness and 150mm in length of mature black-sweet bamboo without their inner and outer layer were prepared for the treatment. Prior to OHT, the specimens were immersed in water until reaching 46±8 MC. Subsequently, the specimens were immersed in linseed oil at temperatures ranging from 80 to 180°C, and loads up to of 25N were applied until the half section of bamboo was completely flat. The stages of modification of black-sweet bamboo through the OHT are illustrated in Figure 4-11.

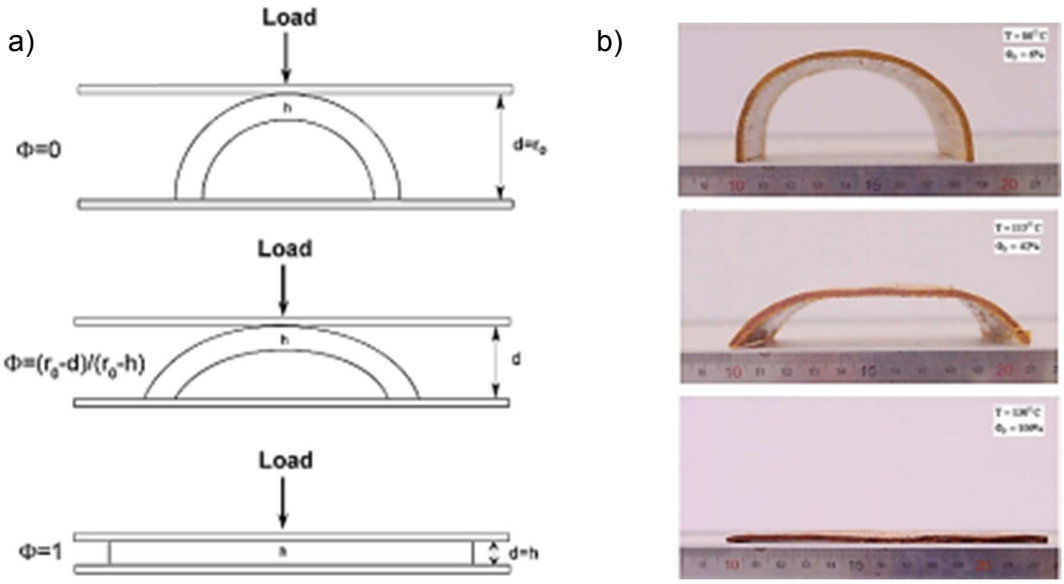

Figure 4-11. Oil heat treatment (OHT) applied to bamboo (*Dendrocalamus asper* Backer) by Cherdchim *et al.* (2004).

Under the conditions above mentioned, Cherdchim *et al.* (2004) reported that the optimum temperature of linseed oil for obtaining flat plates of bamboo without cracks was 130ºC and 20N for a period of approximately 150 seconds. In contrast, Parkkeeree *et al.* (2014) found the ideal temperature and load configurations of the OHT for flattening black-sweet bamboo to be 130ºC and 15N. Finally, these authors applied a densification process to avoid spring-back of the flattened specimens. A diagram of their OHT device is shown in Figure 4-12.

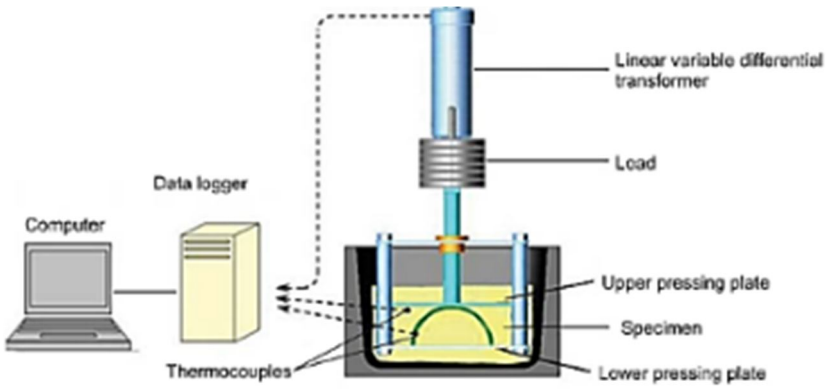

Figure 4-12. OHT experimental device for treating black-sweet bamboo (Parkkeeree *et al.,* 2014)

Other TH treatments largely used in wood (Figure 4-8b) such as torrefaction have been applied to Guadua for enhancing its fuel capacity. The potential of Guadua as biomass-energy source has been researched by Montaño *et al.* (2012), but its industrialisation potential is still untapped. TH processes are also applied during the manufacture of wood veneer. The trunk is subjected to thermo-hydraulic (TH) treatment to soften its structure and facilitate the peeling process (Figure 4-8c).

Wood modifications by chemical treatments have been extensively researched and applied to wood. Homan & Jorissen (2004), Hill (2007), Esteves & Pereira (2009) & Ansell (2011) present useful literature reviews on the subject. Nevertheless, the effects of THM modifications on the thermal softening of lignin, hemicellulose and cellulose are discussed in the following Section.

4.2 Glass transition temperature (T_g)

The term glass transition temperature (T_g) refers to the temperature at which amorphous polymers will begin to experience changes of state: from hard and brittle (glassy) to soft and flexible (rubbery) (Figure 4-13a).

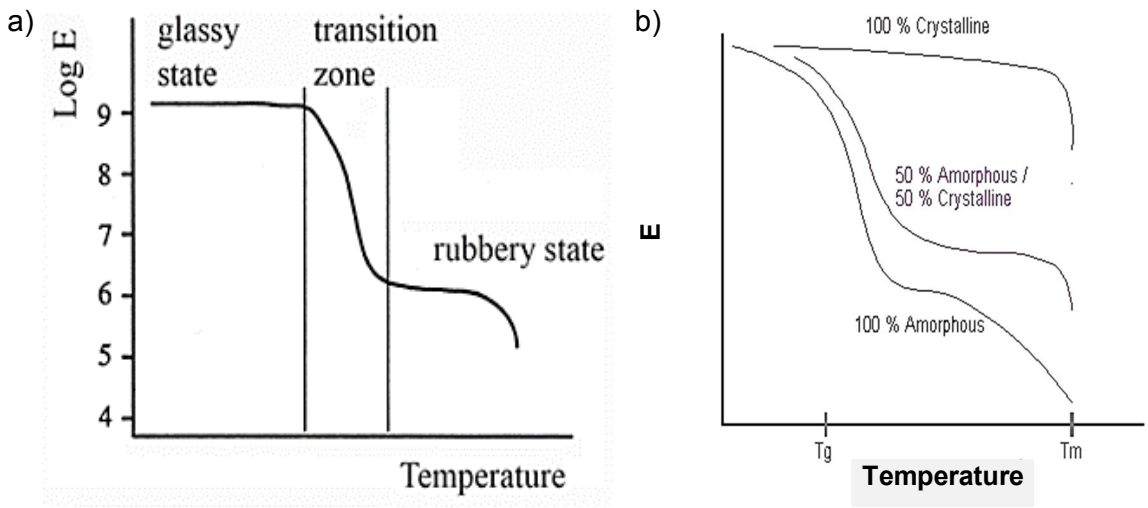

Figure 4-13. a) Logarithmic modulus of an amorphous polymer as a function of temperature, with its different state zones. b) Modulus of elasticity (E) as a function of temperature for crystalline, semi-crystalline and amorphous polymers (Western Carolina University at paws.wcu.edu).

The amorphous (hemicellulose and lignin) and the crystalline (cellulose) polymers constituting wood and bamboo are thermo-plastics that deform at different temperatures (Figure 4-13b). Although not initially amorphous, the crystalline structure of cellulose becomes amorphous at high temperatures. As seen in Figure 4-13 the transition between glassy and rubbery states caused by the increase in temperature, results in the alteration of the physical and mechanical properties of these amorphous polymers.

Micro-molecular movements occurring in the glassy state are of low amplitude and maintain the molecular cohesion of the polymer with no change in properties. However, an increase in temperature affects the molecular stability and mechanical and physical properties of the polymer. Large amplitude molecular (macro-molecular) movements are then possible in the rubbery state of amorphous polymers and factors such as the elastic modulus are severely decreased; e.g. three to four orders of magnitude lower than in the glassy state (Figure 4-13a). These inter- and intra-molecular changes within the wood polymers are related to the molecular attraction/repulsion forces (van der Waals' forces) and the hydrogen bond interactions of its functional hydroxyl (-OH) groups (Sandberg & Navi, 2007).

The glass transition temperatures (T_g) of the main compounds in wood and bamboo dictate the chemical, physical and mechanical changes occurring during THM modification. The average T_g values for cellulose, lignin and hemicellulose in the anhydrous condition are approximately 230°C, 210°C and 180°C, respectively (Sandberg & Navi, 2007). These figures

represent the T_g of the three compounds in the absence of water; however, as will be discussed in the next Section, T_g can be reduced by the increase of the moisture content of wood or the relative humidity of the environment.

4.3 Chemical alterations of wood and bamboo compounds by THM modifications.

According to Esteves & Pereira (2009) the chemical changes occurring in wood as a function of temperature can be classified into three categories: low temperature (20-150°C), medium temperature (150-250°C) and high temperature (above 250°C). These temperature ranges have different effects on the chemical composition of wood.

Low temperature levels are used for drying wood with the initial release of free water followed by the loss of moisture fixed within the cell walls. Medium temperature is the most commonly used range for heat treatments, in which significant chemical transformations occur. These changes will depend on the processing time; Sandberg & Navi (2007) state that short processing times at temperatures between 140°C and 160°C have little effect on the molecular arrangement of wood and that temperatures above 200°C start to degrade its chemical compounds. Therefore, temperature exposure over long periods or the use of high temperatures can cause significant damage to the wood structure, including its fibres (FPL, 2010). At 250°C carbonization of wood initiates and CO_2 is released; overall, high temperature levels cause severe degradation of wood (pyrolysis).

Due to its crystalline structure and large number of hydroxyl groups (-OH), cellulose is the compound least affected by heat treatments, whilst hemicellulose is the most affected. The amorphous structure of hemicellulose with weak hydrogen bounds, means that it can be easily hydrolysed. Some hydroxyl groups in semi-crystalline cellulose microfibrils are strongly bound by a hydrogen bridge, which makes them less accessible to water than the hydroxyl groups in hemicellulose (Esteves & Pereira, 2009; Sandberg & Navi, 2007).

On the contrary, lignin possesses fewer hydroxyl groups and is less affected by water. Although lignin can degrade at lower temperatures, the degradation process is slower than with hemicelluloses (e.g. T_g of lignin is ~85°C). Overall, lignin has the highest T_g at high moisture contents (MC) (Figure 4-14). Hence, the softening process of wood is highly dependent on its moisture content (MC), which relates to the relative humidity (RH) of the environment (Esteves & Pereira, 2009). Figure 4-14 illustrates the changes in T_g as a function of wood MC and RH of the environment.

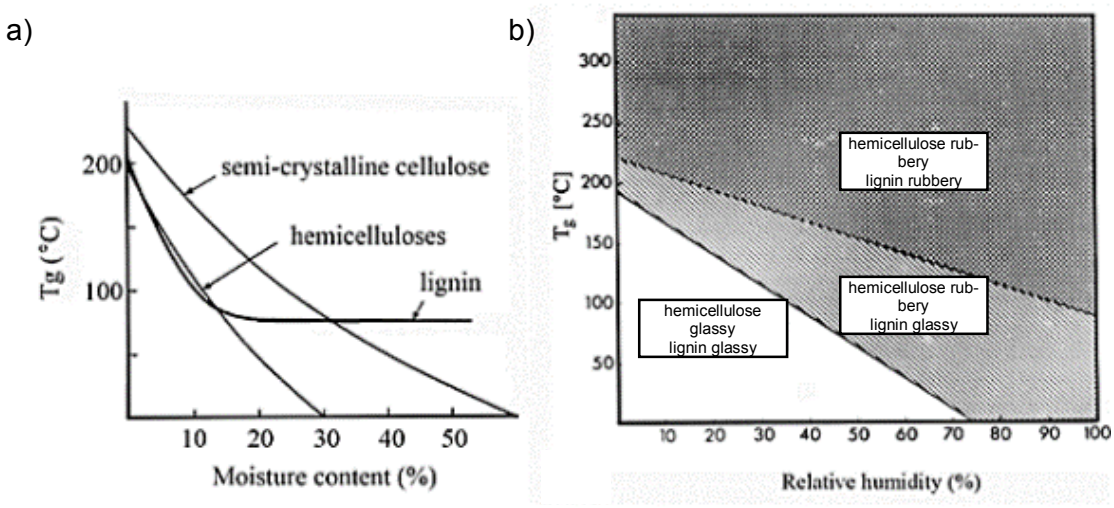

Figure 4-14. Glass transition temperature of the chemical compounds of wood: a) as function of the moisture content of wood and b) as a function of the environmental relative humidity (RH) by Salmén (1982) extracted from Sandberg & Navi (2007).

This behaviour can also be appreciated in the diagram presented by Olsson *et al*, (1997) (Figure 4-15 taken from Morsing (2000)) of the relationship between storage modulus (measure of the energy retained) and temperature for hemicellulose and lignin under dry and wet conditions.

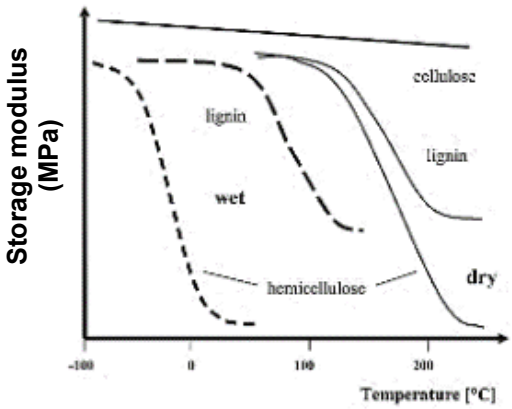

Figure 4-15. a) Reduction in the storage modulus of hemicellulose and lignin in wet and dry conditions as a function of temperature elaborated by Olsson *et al*. (1997) taken from (Morsing, 2000).

The softening process of wood through THM modifications is known as plasticization, in which water is the widest used plasticizer. Urea, liquid ammonia (NH_3), dimethyl sulfoxide $(CH_3)_2SO$, and low-molecular-weight phenol formaldehyde (PF) resin are commonly used chemicals for wood plasticization (FPL, 2010). In the case of PF resin, its molecular weight is modified to allow penetration in wood and contribute to its plasticization. Saturated and

super-heated steam, together with boiling water are alternative methods for increasing the MC of wood and bamboo during THM modifications. For wood plasticization, Sandberg & Navi (2007) recommend using a temperature of ~110°C (T_g of lignin + 25°C) under moisture-saturated conditions (20-25% MC) and ~140°C at 80% RH; additionally, they recommend that steaming processes should be applied for two minutes per millimetre of thickness for wood softening.

Regarding the plasticization of bamboo, Nakajima *et al*. (2008) suggest that under moisture-saturated conditions, temperatures above 60°C start to soften the lignin and decrease the storage modulus of the material. The material used by them to assess this softening behaviour was bamboo Madake (*Phyllostachys bambusoides*). On the other hand, Matan *et al*. (2007) reported a minimum plasticization temperature for black-sweet bamboo of 85±10°C under moisture-saturated conditions (MC_{fs}~30%) and a maximum plasticization temperature of 194±10°C for oven dried specimens. Figure 4-16 illustrates the decrease of the softening temperature of bamboo and other wood species, lignin and hemicellulose as a function of the increase on MC.

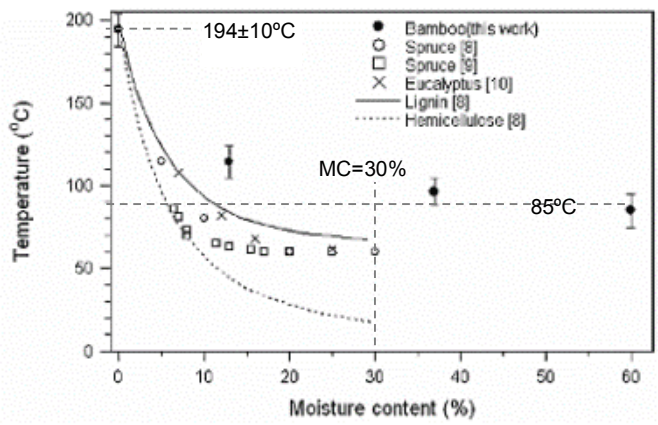

Figure 4-16. Softening temperature vs. moisture content of various materials and chemical compounds by Matan *et al*. (2007).

By contrast, Cherdchim *et al*. (2004) and Parkkeeree *et al*. (2014) reported thermal softening on linseed oil (OHT) of black-sweet bamboo at temperatures between 115°C and 130°C, respectively. The MC of this bamboo prior to processing was 46±8% (Figure 4-11).

Zhang *et al*. (2012) demonstrated the significant degradation of holocellulose and α-cellulose compounds of bamboo *Phyllostachis pubescens* at temperatures above 160 °C (Figure 4-17). This degradation was linked to reductions in mass loss, MOR and MOE of the material.

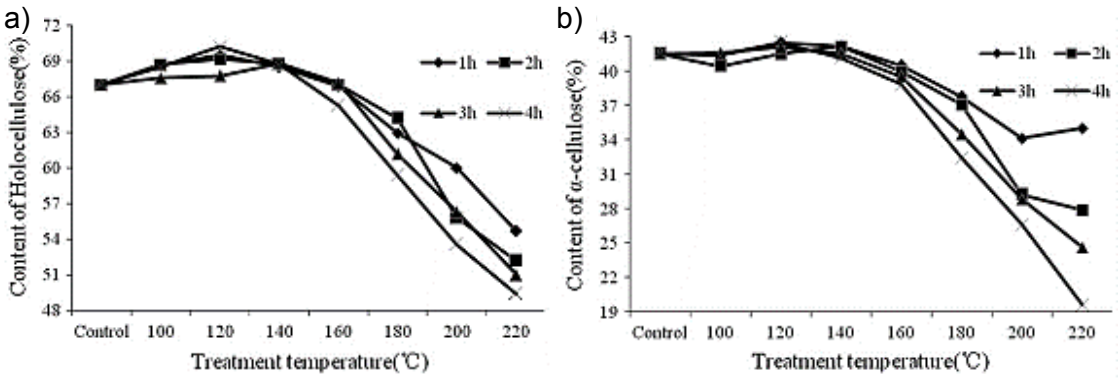

Figure 4-17. Changes occurring in the holocellulose (a) and α-cellulose (b) content of the bamboo species *Phyllostachis pubescens* as a function of temperature (Zhang *et al.,* 2012).

In general, at high RH the T_gs of cellulose, hemicellulose and lignin decrease drastically (Figure 4-14) and wood and bamboo can be moulded, shaped, densified, extruded and bent. (Morsing, 2000) outlined the temperature ranges for achieving softening of cellulose, hemicellulose and lignin, and their degradation under wet and dry conditions (Table 4-2).

Table 4-2. Variation in the softening and degradation temperatures for the main compounds of wood depending on their wet (FSP where MC_{fs}~30%) or dry state (MC ≤13%) (Morsing, 2000).

	T_g (°C)		Temperature of severe degradation (°C)	
	dry MC ≤13%	wet MC ~30%	dry MC ≤13%	wet MC ~30%
Cellulose	>230	>220	>200	>200
Hemicellulose	160-220	<25	>160	>160
Lignin	>150	60-90	>160	>160

In addition to the variations in MC, RH and temperature, the results of THM modifications are also dependent on the wood and bamboo species and the pressure applied during processing. All of these factors cause a mechanosorptive effect that is independent of time (Grossman, 1976). THM modifications exploit the characteristic viscoelastic behaviour of wood and bamboo over time by selecting MC, RH, temperature and pressure for the required effect.

4.4 Viscoelastic behaviour of wood and bamboo under THM modifications.

Wood and bamboo have comparable cellular structures and chemical compositions (Liese, 1998), which respond similarly to chemical and physical modifications. These responses are

influenced by their unique anatomical and morphological features, which ultimately determine their characteristic mechanical properties. Wood can be described as an anisotropic, cellular, polymeric and porous material, which exhibits time-dependent elastic and viscous behaviour under loading (Bodig & Jayne, 1982; Dinwoodie, 1989; Sandberg & Navi, 2007). Bamboo on the other hand, is made out of the same natural polymers as wood and possesses a graded hierarchical arrangement of cells that respond to its functional requirements within a porous structure along the culm (Amada & Lakes, 1997).

The elastic and plastic responses of wood and bamboo differ according to the duration of the load and the direction of the applied stress, whether it is along the longitudinal (L), radial (R) or tangential (T) axes. Initially their structure will deform elastically and then plastically (creep) as a function of time. These linear elastic and viscous responses are characteristic of their constituent polymers and depend on the applied load, temperature, moisture conditions and time (Kutnar *et al.,* 2008b). Based on results by Roussel (1997) for specimens of poplar under compressive load along the L, R and T axes, Sandberg & Navi (2007) illustrate an example of the typical viscoelastic behaviour of wood (Figure 4-18).

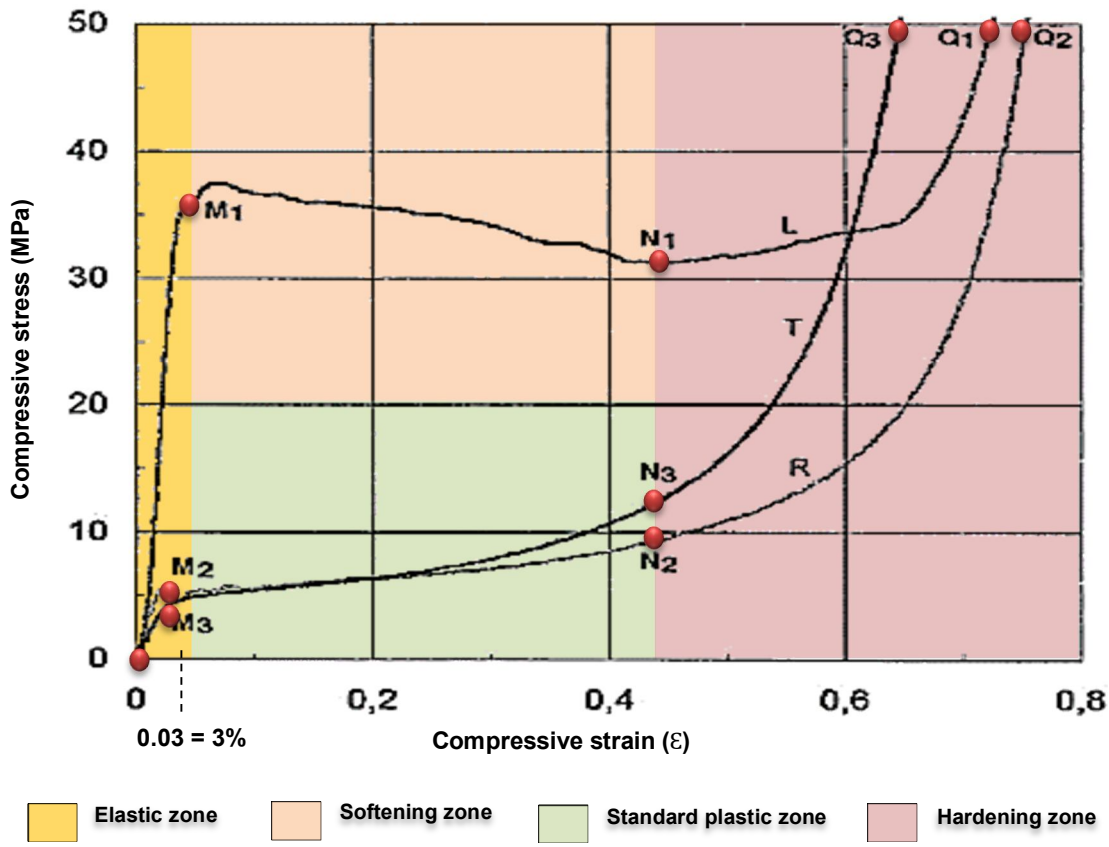

Figure 4-18. Stress vs strain behaviour of poplar specimens (25x25x5mm) under compression along the longitudinal (L), radial (R) and tangential (T) directions under constant displacement of 1 mm/min. After Roussel (1997) taken from Sandberg & Navi (2007).

The authors identify a three-phase behaviour (from zero through to M, N and Q in Figure 4-18) for the three orientations (L, R and T). Specimens under compression along the R and T axes follow the same three stages, whilst those under compression along the L axis have a different middle phase.

The first stage is the linear phase, where under short-term compressive load at low strain levels (ε), wood behaves elastically along the L, R and T axes and up to the elastic limit (0-M1, 0-M2 and 0-M3 in Figure 4-18). It then yields at a strain $\varepsilon \leq 3\%$ and starts to deform plastically if load is maintained. During the second stage, specimens under compression along the L axix suffer strain softening with considerable decrease of the gradient (M1-N1 in Figure 4-18), whilst for the specimens under compression along the R or T axes standard plastic deformation with reduced modulus occurs (M2-N2 and M3-N3 in Figure 4-18). The final stage is again similar for all the three orientations (L, R and T). During this phase the stiffness of the wood structure is steadily increased (densified) as seen in Figure 4-18 between points N1-Q1, N2-Q2 and N3-Q3.

Up to the elastic limit, elastic deformation is almost fully recovered on unloading. Above the elastic limit, deformation becomes permanent and is known as irrecoverable plastic deformation (Dinwoodie, 1989).

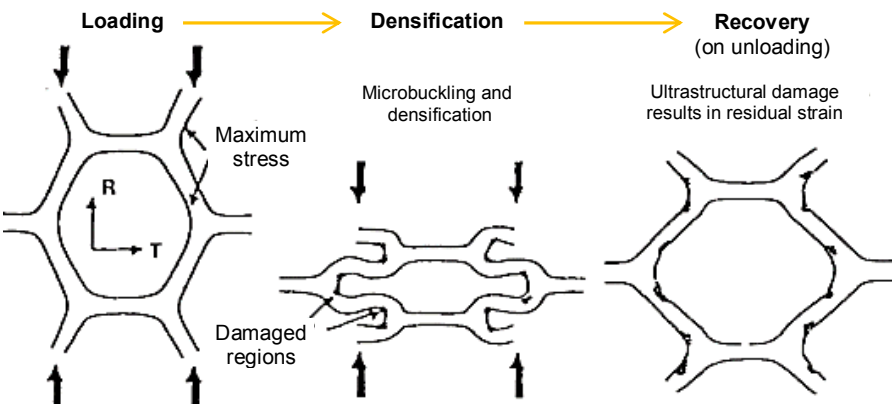

Figure 4-19. Cell structure damage and resulting residual strain from compression along the radial direction (after Gril *et al.* (1994) in Morsing (2000)).

Different mechanisms of failure of the cell structure have also been proposed by Sandberg & Navi (2007) (Figure 4-20); these mechanisms depend on factors such as wood species and density, and the direction of the load applied. For instance fibre cell rupture (Figure 4-20b) is common in low density wood (<330kg/m^3), whilst shear failure of cell walls or cell wall buckling (Figure 4-20c) is common in high density wood

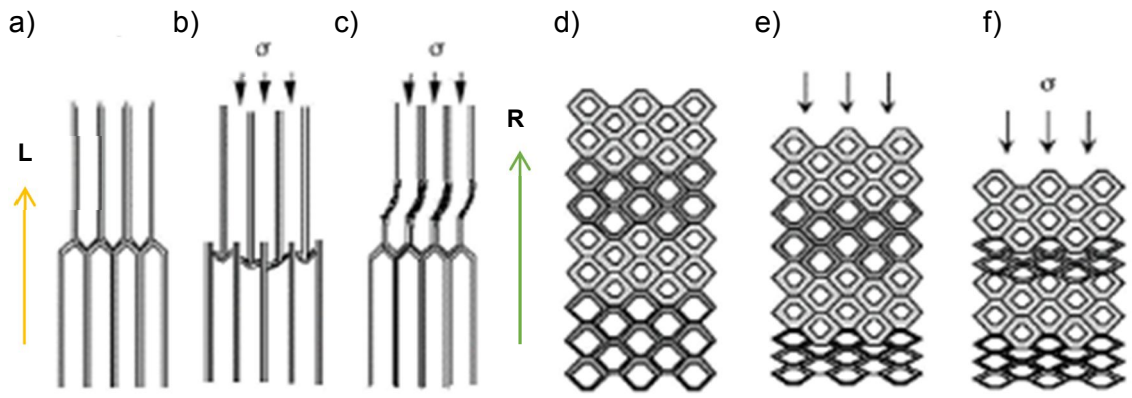

Figure 4-20. Failure mechanism of wood under compressive load along the longitudinal (L) and the radial direction (R). a) Wood prior to compression. b) Cell wall rupture. c) Cell wall buckling. d) Wood prior to compression. e) Cell crushing starting in the weakest interface (deformation localisation) and partial densification. f) Continuation of the crushing until densification. (Sandberg & Navi, 2007).

On the other hand, cell wall crushing or flexural buckling occurs initially at the weakest cellular interface (e.g. void vessels within the early-wood section) and propagates across the thickness of the piece of wood under compressive load along the radial axis. Cell wall crushing is illustrated in Figure 4-21; green and red dots indicate cell wall faces in opposition.

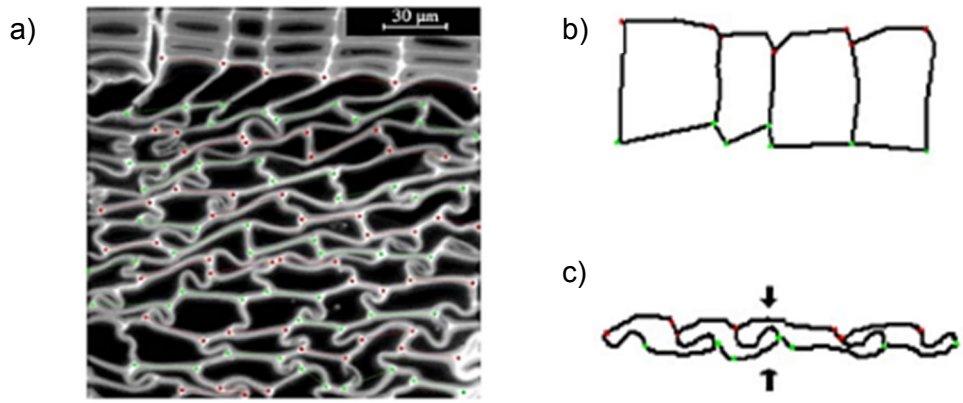

Figure 4-21. a) Cell wall crushing during densification of spruce at 5% within the early wood area. b) Cells before compression. c) S/Z shaped deformation of cells after compression (Sandberg & Navi, 2007).

Brittle fracture of the cell structure of wood can then be avoided through THM modifications. An adequate configuration of pressure, temperature and wood MC will lead to improvements on the mechanical and physical properties of wood (Esteves & Pereira, 2009; Sandberg & Kutnar, 2014; Sandberg & Navi, 2007). For instance, Kutnar *et al.* (2008b) reported no cell wall fracture through a THM densification process titled viscoelastic thermal compression (VTC).

4.5 TM and THM densification and its effects on the physical and mechanical properties of wood and bamboo.

As discussed previously, THM modifications rearrange the microstructure of wood and bamboo and potentially enhance their physical and mechanical properties without causing cell damage. In particular, transverse THM modifications such as TM and THM densification processes are able to increase the cross sectional density of wood and its hardness by transverse compression (along the tangential and radial direction). Furthermore, Sandberg & Kutnar (2014) remark that THM modification techniques applied to wood are key for manufacturing highly engineered timber products (ETP) with reduced environmental impact. For instance, through the increase of the service life of THM modified ETP, carbon can be locked for longer periods of time than with non-engineered wood products; this reduces deforestation and overall, the pressure over wood forests (see Section 2.11).

Depending on the setup of the treatment used, the increase in wood density can lead to either enhanced stiffness and/or strength, whilst the increase in hardness has a significant effect on durability (Esteves & Pereira, 2009; Kutnar & Šernek, 2007; Morsing, 2000; Sandberg & Kutnar, 2014; Sandberg & Navi, 2007). THM densification can be undertaken in open and closed systems. Closed THM densification systems are used mainly for research purposes and are undertaken in small reactors where temperature, pressure and relative humidity can be carefully controlled.

TM and THM densification generally involve four processing stages: a) Plasticisation; b) Transverse compression (radial or tangential, or both); c) Drying set, which includes cooling and drying; and d) Fixation of the densification (post-treatment) (Morsing, 2000). Depending on the setup of the densification process and the desired results, the last two stages can be alternated.

In this study, TM densification will be referred as those treatments that use wood or bamboo below fibre saturation point (FSP) where MC_{fs}~30% (FPL, 2010). This means that no free water is present inside the cell cavities (lumen). Heger *et al.* (2004) recommends wood to be conditioned at 13% MC to avoid cell explosion during TM treatments. On the other hand, treatments that use wood or bamboo at MC>30% or steaming processes to modify their MC will be considered as THM densification treatments.

As will be discussed in Section 4.5.4, TM treatments are undertaken on open systems, whilst THM can be undertaken in both, open and closed systems. Closed treatments are carried

out in sealed chambers that allow variation of moisture content, temperature and pressure of the material throughout the process, whilst open treatments are generally undertaken in hot-presses where MC or RH are not controlled. However, before discussing the effect of TM and THM densification processes on the mechanical properties of wood or bamboo, two concepts that measure the levels of densification and recovery post-densification need to be discussed; these are known as the compression set and compression-set recovery, respectively.

4.5.1 Compression set

Throughout the transverse crushing of the void lumens within the cellular structure of wood or bamboo, TM and THM densification can achieve considerable cross section reductions. The resulting reduction in thickness is defined as the compression set (C_s) illustrated in Figure 4-22 and calculated in Equation 4-1.

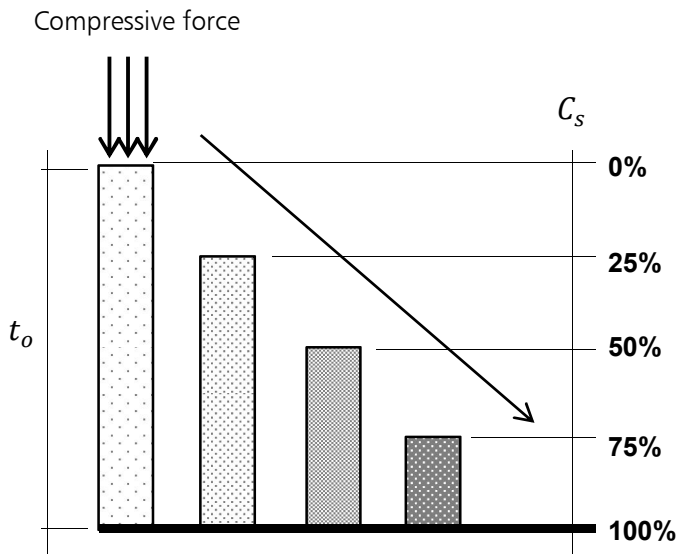

$$C_s = \frac{t_o - t_c}{t_o} \times 100\% \qquad 4\text{-}1$$

where t_o and t_c are the thickness of the samples before and after compression, respectively.

Figure 4-22. Compression set ($\boldsymbol{C_s}$).

4.5.2 Spring-back effect

An important issue facing TH and THM treatment is the spring-back effect post-treatment or hygro-thermal recovery, which is linked to the characteristic viscoelastic behaviour of wood and its tendency to recover from a deformed state (creep). This effect is also known as compression-set recovery (R_s), and is calculated with Equation (4-2).

$$R_s = \frac{t_r - t_c}{t_o - t_c} \times 100\% \qquad 4\text{-}2$$

Where
t_o and t_c are the thickness of the samples before and after compression, respectively
and t_r is the thickness in wet condition after the recovery test.

Inoue *et al.* (1992) (cited in (Morsing, 2000)) studied the recovery of compression-set in soaked wood as a function of temperature (recovery temperature), and established that when the recovery temperature was the same as the temperature used during the densification process the specimens returned to about 90% of their initial thickness (Figure 4-23a). This is in agreement with Sandberg & Navi (2007)'s statement that the deformation produced during wood densification is analogous to the energy stored during the hot-pressing process.

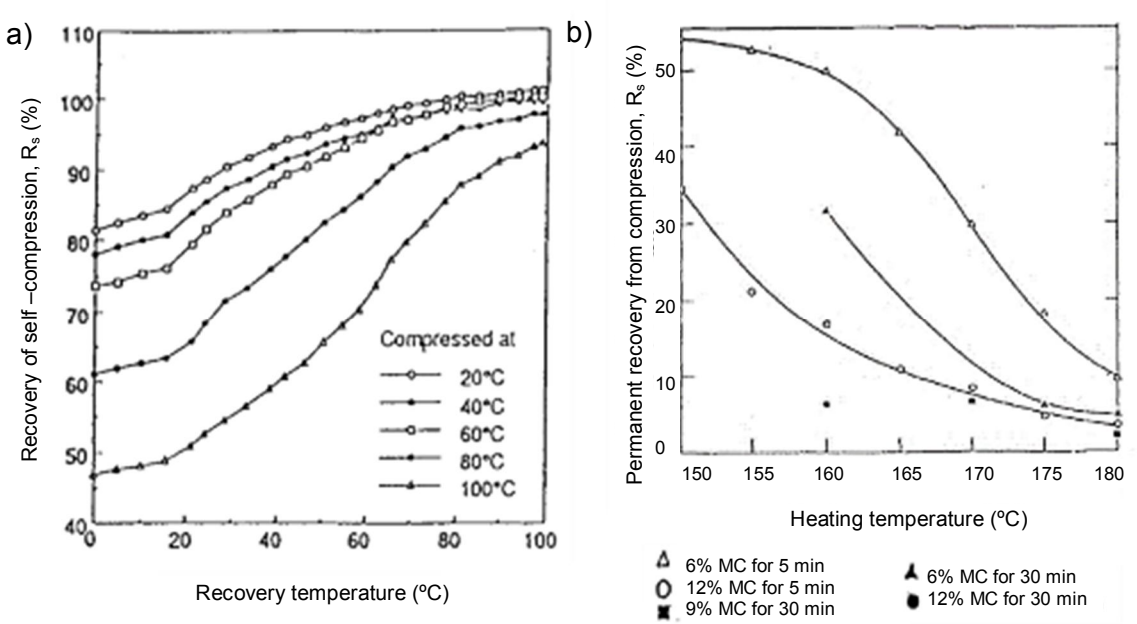

Figure 4-23. a) Recovery of set of wood in saturated condition as a function of the recovery temperature. By Inoue *et al.* (1992) taken from Morsing (2000). b) Recovery as a function of the heating temperature and moisture content of parallel laminated yellow polar. By Seborg *et al.* (1945) taken from (Morsing, 2000). * Approximate temperature values in (ºC), converted from Fahrenheit (ºF).

Seborg *et al.* (1945) (cited in (Morsing, 2000)) found that post densification treatments focussing on the increment of MC, compressing temperature and pressing time, considerably reduced the recovery of set (R_s) of parallel-laminated yellow polar (Figure 4-23b). For conducting these measurements, the authors compressed the specimens for 5 and 30

minutes at ~1.4MPa at 6%, 9% and 12% MC. Inoue *et al.* (1992) cited in (Morsing, 2000), reported similar results for the reduction of the spring-back effect and the recovery time by subjecting the densified specimens to saturated steam at temperatures of 180°C for 8 minutes and 200°C for 2 minutes.

Apart from steam and temperature treatments, spring-back effect has also been avoided in large densified spruce plates when heated in oil (OHT) at temperatures above 200°C (Sandberg & Navi, 2007). Nevertheless, complete recovery is not achievable due to the irre-coverable creep caused by plastic deformation of the wood cells. As previously discussed in Section 4.1.5 (Welzbacher *et al.,* 2007) successfully attained nearly complete dimensional stability of wood through OHT at 200°C (Figure 4-10).

In bamboo, (Parkkeeree *et al.,* 2014) found that by densifying the flattened bamboo boards (modified through OHT) at 240 °C for a minimum of 20 min the spring-back effect was reduced to about 5%.

4.5.3 THM & TM densification in open systems

Sandberg & Navi (2007) remark that previous work by Burmester (1973) with pine wood found a significant resistance to fungus and negligible strength reduction at a temperature of 160°C, pressure of 0.7MPa and moisture contents (MC) between 20% and 30%, through THM densification in an open system. Li *et al.* (1994) increased the density of bamboo species *Bambusa permavillis* by 32% through TM densification treatment in an open system and obtained an improvement in tensile strength and Young's modulus of 31.7% and 44%, respectively. Figure 4-24 illustrates the degree of densification.

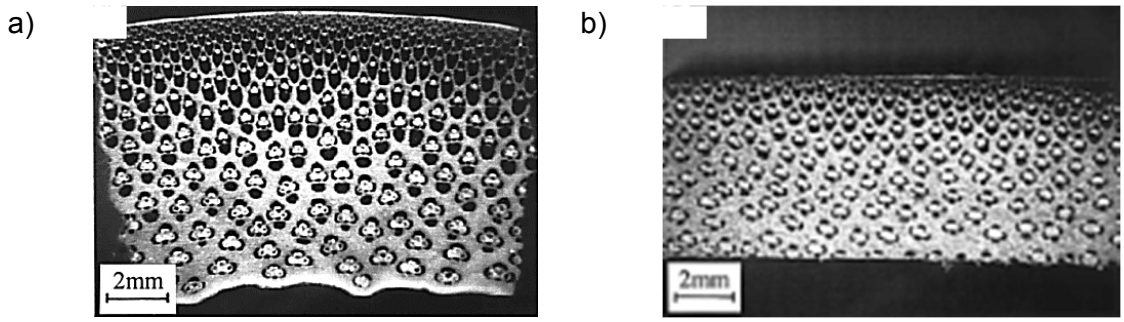

Figure 4-24. Densification of *Bambusa permavillis*. a) Untreated bamboo 'normal' b) Densified 're-formed bamboo' (Li *et al.,* 1994).

Results of the mechanical properties of non-modified bamboo (normal) and densified (reformed) bamboo are presented in Table 4-3.

Table 4-3. Mechanical properties of reformed bamboo and non-modified (normal) bamboo by Li *et al.* (1994).

	Reformed bamboo		Normal bamboo	
	Mean	Dev.	Mean	Dev.
Fibre volume fraction (%)	43.6	13.4	29.2	12.8
Shrinkage coefficient:				
radial	0.252	0.005	0.299	0.020
tangential	0.184	0.057	0.319	0.076
bulk	0.446	0.083	0.663	0.132
Density (10^3 kg m^{-3})	0.87	0.17	0.66	0.07
Tensile strength (MN m^{-2})	271.5	60.6	206.2	24.7
Tensile modulus (GN m^{-2})	29.0	5.6	20.1	3.2
Flexural strength (MN m^{-2})	276.6	22.7	210.3	25.3
Flexural modulus (GN m^{-2})	23.2	4.7	13.1	3.0
Compressive strength (MN m^{-2})	104.7	28.4	78.7	7.6
Shear strength (MN m^{-2})	14.5	2.2	15.1	4.6

Li *et al.* (1994) also noticed a significant correlation between the compressive ratio and the ultimate strength (Figure 4-25a) and Young's modulus (Figure 4-25b). Furthermore, they demonstrated that the compressive ratio or C_s of the *Bambusa* species increased at higher MCs (Figure 4-25c). Using bamboo with MCs of 22.6% and 28.9% (within the range of FSP) compressive ratios superior to 40% were achieved using a pressure of ~20MPa, whilst the same levels of compression in specimens with low MC (8.5%) were achieved using a pressure of ~30MPa.

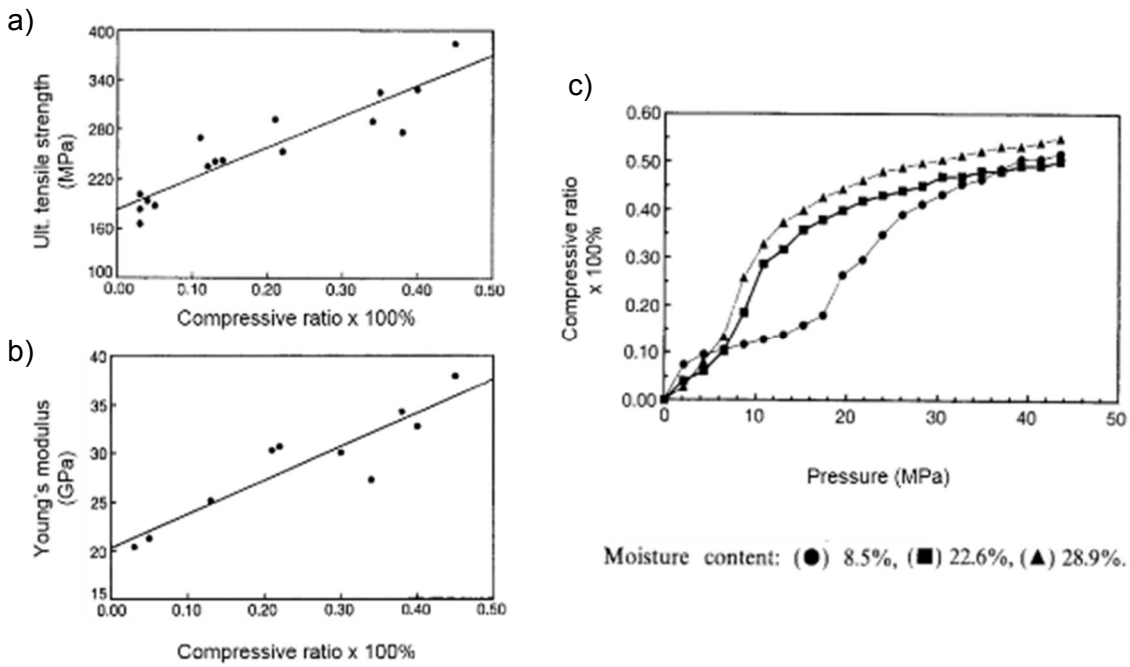

Figure 4-25. Compressive ratio as a function of moisture content of *Bambusa permavillis* bamboo and the applied pressure along the radial direction (Li *et al.,* 1994).

Nugroho & Ando (2000) crushed quarter sections of bamboo (*Pyllostachys pubescens* Mazel) with a roller-press and densified them at a temperature of 160°C and a pressure of 3.5MPa for 15min in a hot-press. Prior to TM densification the roller-pressed sections (zephyr strands) of this variety of Moso bamboo, were air-dried to ~8-12% MC and sprayed with resin. In spite of the use of moderately high temperature and pressure levels, this process could fall into the material reconstitution category within the TH treatments group in Table 4-1. Bamboo-zephyr strands and the resulting densified bamboo zephyr boards (BZB) are depicted in Figure 4-26

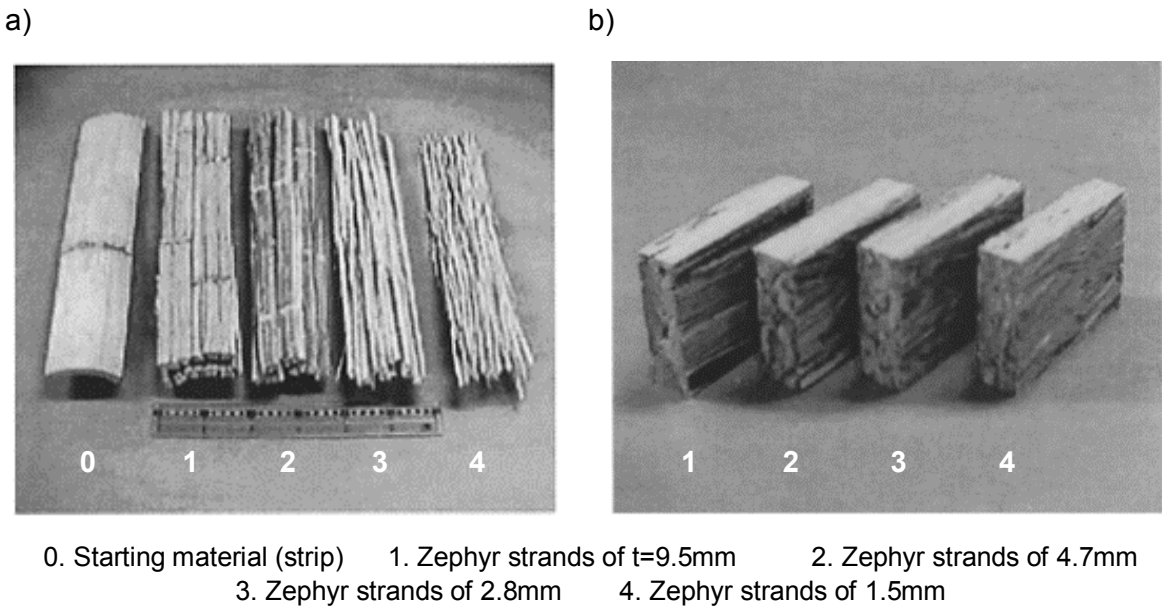

Figure 4-26. Densification of bamboo zephyr into bamboo zephyr boards (BZB). a) Crushing of bamboo into zephyr strands. b) Bamboo zephyr boards (BZB)

In a later study Nugroho & Ando (2001) applied TM densification treatments to strands of bamboo zephyr before lamination with adhesive. Strands of bamboo zephyr of 11mm in thickness in green condition (MC~30%) were densified for 6 minutes at 150°C and a pressure of ~6MPa. The target compression set (C_s) for the process was approximately 46% and the initial density (ρ_o) of 740kg/m^3 was increased by 21% (ρ_f ~900kg/m^3). The authors remark that the densification process was hindered by the dense bamboo cortex, which required slightly longer time than wood to be plasticized. In addition, spring-back tests carried out on densified specimens of bamboo-zephyr at various temperatures indicated that densification temperatures above 150°C are significantly more stable than at lower temperatures. For instance, the recovery set R_s of specimens densified at 100°C after boiling treatment was ~60%, whilst at 150°C it was ~13% (Figure 4-27).

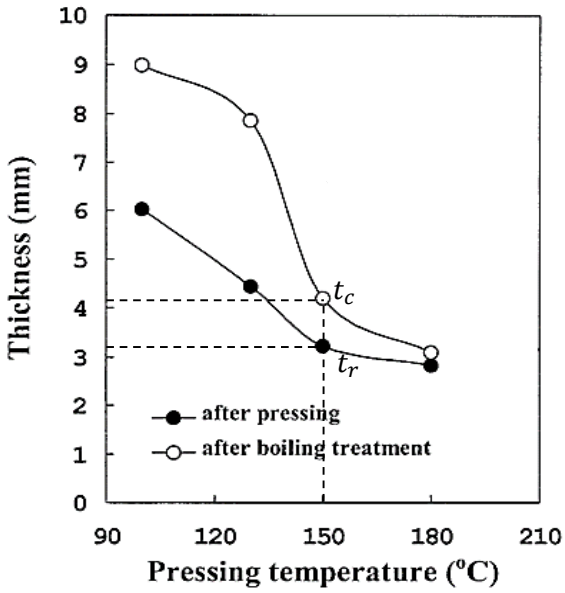

$$R_s = \frac{t_r - t_c}{t_o - t_c} \times 100\%$$

$$t_o = 11mm$$

$$t_c = thickness\ after\ densification$$

$$t_r = thickness\ post - treatment$$

$$R_{s,100°C} \sim 60\%$$

$$R_{s,150°C} \sim 13\%$$

Figure 4-27. Bamboo zephyr mat thickness as a function of densification temperature. After Nugroho & Ando (2001)

After treatment, the thickness of the densified zephyr strands was adjusted to 5mm by mechanical means, prior to unidirectional glue-lamination. The glue spreading rate was 300g/m^2 and the lamination process was undertaken at room temperature under cold pressure of ~2MPa for 12hours. Bamboo Zephyr Board was then subjected to a test programme and results are presented in Table 4-4.

Table 4-4. Mean physical and mechanical properties of four-ply laminated BZB (Nugroho & Ando, 2001).

Type of beam	MOE (×10^{2}kgf/cm^2)		MOR (kgf/cm^2)		IB (kgf/cm^2)	WA (%)		TS (%)		LE (%)	
	H-beam	V-beam	H-beam	V-beam		2h	24h	2h	24h	2h	24h
I	96.2	121.0	639.0	851.0	8.60	12.70	24.10	5.90	12.10	0.19	0.48
	(9.4)	(15.9)	(101)	(87.5)	(2.96)	(3.68)	(7.00)	(1.95)	(3.70)	(0.09)	(0.12)
II	105.0	123.0	707.0	877.0	5.79	13.50	26.10	5.70	12.40	0.18	0.48
	(10.0)	(11.9)	(127.0)	(88.5)	(1.19)	(2.02)	(2.61)	(1.97)	(0.83)	(0.08)	(0.18)
III	107.0	111.0	689.0	755.0	9.10	12.70	24.30	5.60	11.90	0.18	0.48
	(10.7)	(10.0)	(56.9)	(42.9)	(2.98)	(3.64)	(7.03)	(1.77)	(3.71)	(0.08)	(0.17)

Numbers in parentheses are standard deviations from the sample mean
MOE, modulus of elasticity; MOR, modulus of rupture; IB, internal bond strength; WA, water absorption; TS, thickness swelling; LE, linear expansion

These types of densification processes in open systems have been applied to bamboo for the development of commercial products currently available in the market. For instance, SWB (strand woven bamboo) produced by MOSO International B.V. uses a comparable method to the one applied to zephyr bamboo strands by Nugroho & Ando (2001). Conversely, other products, such as flattened bamboo, use high temperature and pressure

during processing to achieve flat surfaces and enhanced density and hardness. Some of the mechanical properties of these engineered bamboo products (EBP) are presented in Table 3-2 (Section 3.3).

Other THM densification processes in open system such as the viscoelastic thermal compression (VTC) devised by Kutnar *et al.* (2008a) use a combination of pressure, steam and heat on a hydraulic press with hot platens that adds venting to the four-stages of the densification process (Figure 4-28).

In the VTC densification process, the venting stage (phase 2) acts as the transition between the steam-plasticisation stage (phase 1) and the densification stage (phase 3). The last stage of the THM densification is the cooling of the specimens.

As stated by the authors, air-venting reduces the internal stresses inside the cells and allows the release of bound water, which in consequence decreases the storage modulus (by mechanosorption) and avoids cell wall breakage (Kutnar & Šernek, 2007).

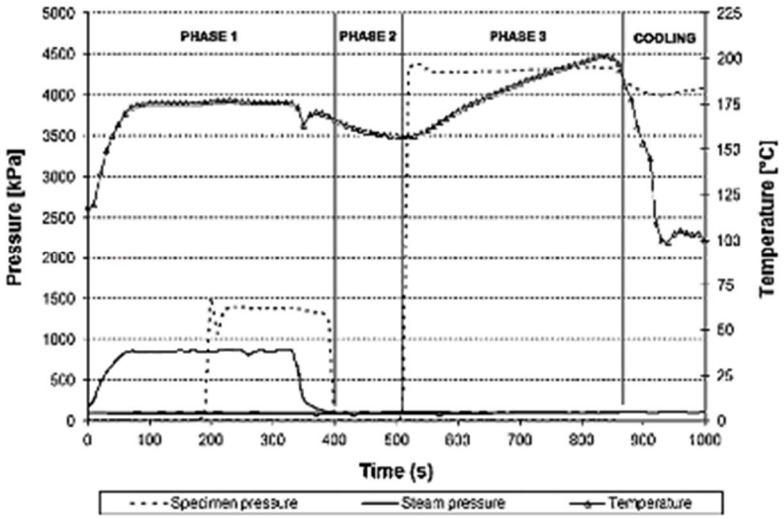

Figure 4-28. Viscoelastic thermal compression (VTC) process applied to low-density hybrid polar (*Populus deltoides x Populus trichocarpa*) (Kutnar *et al.,* 2008a).

Overall, the VTC process in Figure 4-28 has a duration of ~17 minutes and results in a maximum densification of 132% along the radial direction (ratio of the increment in density to the initial density). VTC achieved an approximately two-fold increase in density, strength and stiffness of hybrid polar (*Populus deltoides x Populus trichocarpa*) and provided an appropriate surface for adhesion with phenol formaldehyde adhesives in the development of structural wood composites (Kutnar *et al.,* 2008b).

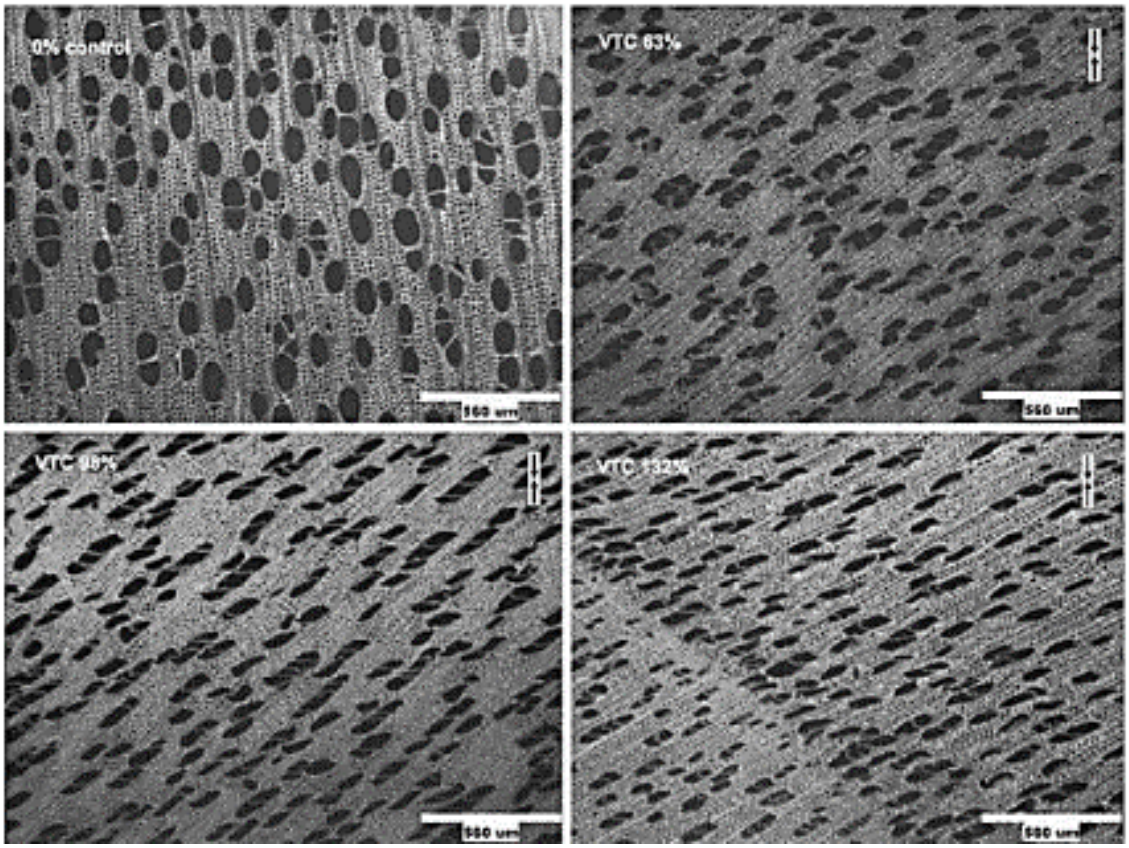

Figure 4-29. Specimens of hybrid polar prior to the VTC process (0% control) and post-densification at different levels (63%, 98% and 132%) by Kutnar *et al.* (2008b), The arrows indicate the direction of the transverse compressive load.

4.5.4 THM densification in closed systems.

As previously discussed, THM densification may be undertaken in sealed chambers (closed system) where temperature, pressure and relative humidity can be adjusted to the required parameters throughout the different stages of the treatment. Closed systems are limited to the modification of small pieces of wood for research purposes and present scale challenges for their industrialisation. Nevertheless, results obtained through this method can help to decide configurations for treatments in open systems. Figure 4-30 illustrates the configuration of a THM reactor for THM densification treatments applied to wood by Heger *et al.* (2004).

Figure 4-30. THM densification in a closed system. a) THM reactor with piston. b) Closed system setup (Sandberg & Navi, 2007).

These authors undertook THM densification and post-treatment of spruce specimens. The specimens were densified from 450kg/m^3 to 1,280 kg/m^3 following the four processing stages of THM densification (Figure 4-31).

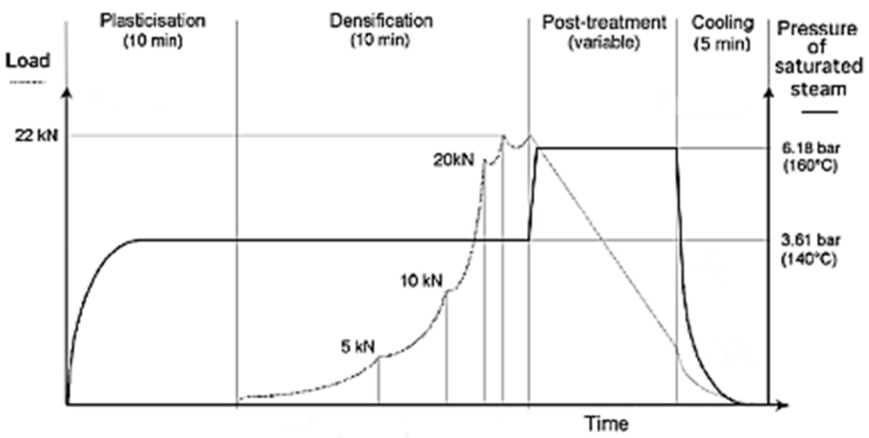

Figure 4-31. Load, steam pressure/temperature vs. time of the THM densification process for spruce specimens in a THM reactor (Heger *et al.,* 2004).

Plasticisation of the specimens was carried out with saturated steam at 140°C for 10 minutes. The densification stage lasted 10 minutes and consisted of a continuous increase in load up to 22kN at the same temperature (140°C). Then, during the post-treatment and to ensure fixation of the densification process undertaken, the temperature of the saturated steam was increased to 180°C for 20 minutes (or 140°C for ~210 minutes), whilst the load was gradually dropped. Finally, cooling lasted for five minutes and pressure was completely removed. As a result of the THM densification process, the authors report a remarkable increase in the average axial shear strength and radial Brinell hardness of the densified spruce specimens of 110.6MPa and 59.8MPa, respectively (Heger *et al.,* 2004).

Concluding remarks

Wood and bamboo have comparable cellular structures and chemical compositions with comparable cellulose, hemicellulose and lignin contents, which make the use of THM modifications feasible for bamboo. As in the case for wood, increasing the moisture content of bamboo specimens is a way forward to avoid cell damage and reduce the T_g and the energy input required for potential THM modifications processes. Appropriate temperature for THM modifications ranges between 85°C (at which lignin starts to degrade) and 160°C (which initiates severe degradation). Adequate combination of MC and processing times will then be key for reducing the energy input for heating the plates of the pressing device. These factors will have a considerable influence in the ultimate environmental impact of the production of THM modified engineered bamboo/Guadua products.

It is also important to remark that although bamboo possesses higher densities than wood, its average cross section is much smaller. Thus, any THM process applied to bamboo might be simpler to undertake. Nevertheless, the effects of the waxy external layer (cortex) and the inner loose membrane in the lacuna (bamboo yellow) on THM modifications need to be considered.

Generally, post-THM densification treatments that use temperatures above 180°C seem to have lower percentages of compression-set recovery; nevertheless, temperatures above 160°C tend to chemically degrade the structure of wood and considerably reduce its stiffness. Post-treatments using oil (OHT) and steam have shown the best effects for reducing spring-back.

In general, insufficient research has been carried out on the chemical and microstructural analysis of the changes occurring during THM modification of bamboo. With regards to Guadua no-research in the field has been conducted.

Overall, these studies have made use of the viscoelastic behaviour of bamboo, facilitating the flow (plasticization) of lignin by increasing the moisture content which leads to the reduction of the glass transition temperature (T_g). This has a positive effect on the modification of bamboo's macrostructure and microstructure when applying elevated temperature and pressure. The modification of the structure of bamboo through THM treatments can lead to the production of engineered materials with enhanced properties and reduced environmental impact.

5. Densification of bamboo and Guadua

Introduction

As for wood, the mechanical properties of bamboo are density dependant. Bamboo's specific modulus is comparable to that of steel, and values of elastic modulus per unit density (specific stiffness) range between 25 and 31 x 10^6 m^2s^{-2} depending on the steel grade and the bamboo species. However, factors such as bamboo's anisotropy and its density variation across and along the culm hinder its use in stiffness-driven applications where steel has been widely used. In its natural state bamboo exhibits variation in its mechanical properties across its wall thickness and also as a function of its height (see Chapter 2, Section 2.6). As previously discussed in Chapter 4, these issues can be potentially tackled through TM and THM densification processes applied to bamboo and Guadua. With the aim of creating a more even distribution of fibres across the section and improving its mechanical properties TM and THM densification processes were applied to bamboo and Guadua.

This Chapter reviews several exploratory THM treatments applied to the bamboo species Moso and Guadua carried out by the author and in conjunction with MEng (Master of Engineering) project students at the University of Bath. With the aim of creating a more even distribution of fibres across the section and improving its mechanical properties TM and THM densification processes were applied to bamboo and Guadua. Ideal conditions were determined for the densification processes applied to Guadua. An initial investigation of the modification of bamboo to manufacture densified nails and strips was made and further experiments optimised the manufacture of THM modified Guadua.

5.1 Densification of bamboo nails

With the aim of producing recyclable bamboo fasteners for timber connections, Betts (2011) TM densified small specimens of Moso bamboo and assessed their mechanical properties (Table 5-1). The ductility, stiffness and strength of the manufactured bamboo nails were compared with those of metal nails in timber connections. Connections with densified bamboo nails (DBN) were 76.5% stronger than non-densified bamboo nails (BN) but, weaker than conventional steel nails. On the other hand, DBN exhibited a brittle failure whilst, BN and steel nails had a more ductile behaviour.

Table 5-1. Results of the TM densification treatment applied to Moso bamboo (Betts, 2011)

Bamboo-nail sample		MC (%)	Initial Density (kg/m³)	Final Density (kg/m³)	Time (Min)	Pressure (MPa)	C_s (%)	Bending MOE (GPa)	MOR (MPa)
Non-densified bamboo (NB)	Mean	-	673.1		0	-	0	**5.17**	**45.0**
	St. Dev.							1.35	7.67
	CoV (%)							26.1	17
Densified bamboo at 150°C	Mean	-	673.1	789.5	90	-	27	**15.81**	**207.1**
	St. Dev.							5.75	78.06
	CoV (%)							36.4	37.7
Densified bamboo at 180°C	Mean	-	673.1	999.0	90	-	47	**16.61**	**190.5**
	St. Dev.							3.93	41.47
	CoV (%)							23.7	21.8
Densified bamboo at 200°C	Mean	-	673.1	1150.5	60	-	54	**14.83**	**172.6**
	St. Dev.							1.71	30.81
	CoV (%)							11.6	17.9

For the THM densification, specimens were taken from the middle section of the bamboo culm-wall and three treatments were undertaken at 150, 180 and 200°C for 90, 90 and 60 minutes, respectively. For these treatments the final density was 17, 48 and 71% higher than the initial density (673.1kg/m³). The moisture content (MC) of the specimens was not measured and was assumed to be below the FSP (at ~13% MC); variable pressure was applied radially with a manual hot-press machine (MOORE Birmingham hot-press) with 200 x 200mm plates. Figure 5-1a illustrates the different types of nails treatments.

Three point bending tests were undertaken on control and densified specimens using an Instron test machine with a 100kN load cell at a 0.2mmm/min loading rate. A total of six

specimens per sample were tested (NB, 150, 180 and 200°C) and the typical size of the specimens was 70mm long, 20mm wide and 4mm thick. Specimens were not conditioned prior to testing. Bending modulus of elasticity (MOE) was evaluated (Figure 5-1b) and values of modulus of rupture (MOR) are reported in Table 5-1.

a)

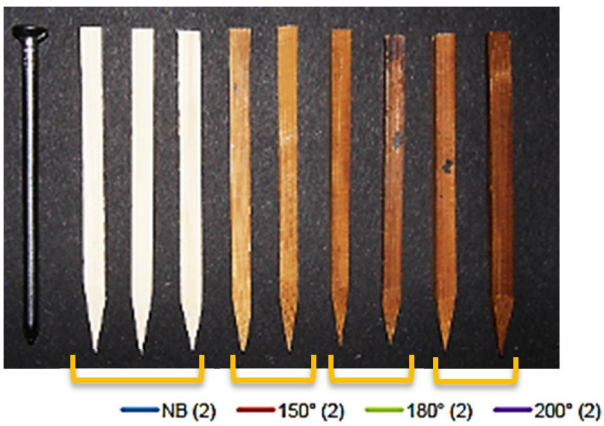

b)

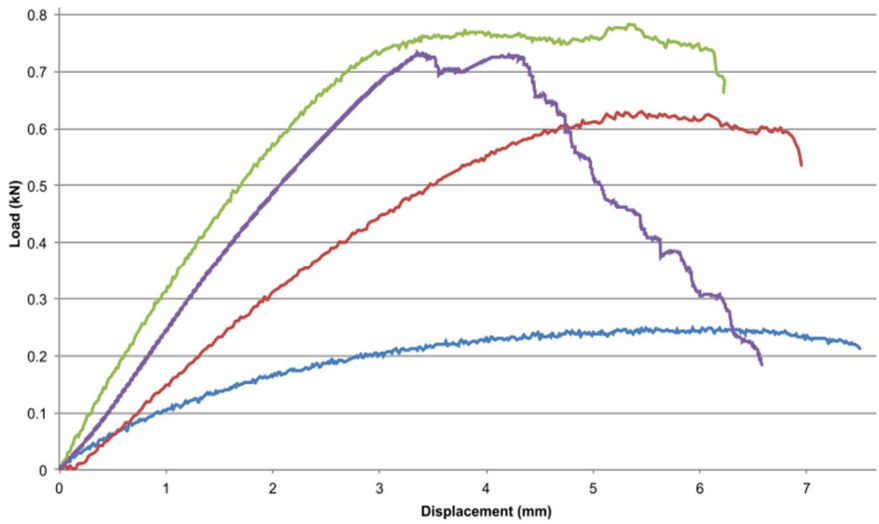

Figure 5-1. a) Metal, non-densified (NB) and TM densified bamboo nails. b) Load-displacement graph for specimen No. 2 (2) during three point bending test (Betts, 2011).

Discussion & results

The mechanical properties of Moso bamboo were enhanced through TM densification at 150°C resulting in significantly higher MOE and strength values than the non-densified (control) sample. Furthermore, the treatments applied at 180°C and 200°C resulted in slightly inferior mechanical properties. The MOE and MOR values of the densified sample at 150°C were approximately 3 to 5 times higher than the values of the non-densified sample. In fact, the densified material became more brittle and experienced no gain in stiffness when the TM temperatures was set above 150°C.

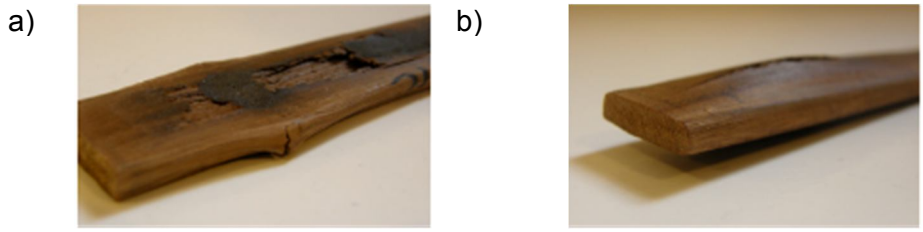

Figure 5-2. a) Burnt external layer of Moso bamboo after densification. b) Material swelling

Finally, Betts (2011) experienced problems with the outer and inner skins of Moso during TM densification. The external layer burnt (Figure 5-2a), whilst the internal surface exploded and/or buckled (Figure 5-2b) mainly during preliminary experimentation tests at 200°C. The first phenomenon occurs due to the high lignification and waxy nature of the external layer, which presents a physical barrier for the transference of heat towards the inside of the specimen. The second phenomenon might be due to an abrupt increase in the applied pressure that increases the steam pressure inside the cell cavities generating high internal stresses that are suddenly released through the weakest cellular interface (internal layer tissues).

5.2 Improving the ductility of densified bamboo

Unlike the work undertaken by Betts (2011), Cura (2012) plasticised the specimens of Moso prior to densification by steaming and boiling them in water. Experimentation without the inner and outer layers was also carried out (Figure 5-3). The specimens were steamed for 20, 40 and 60 minutes at 80, 100 and 120°C. The same temperatures were used for soaking in water, but the exposure time was set at 60 minutes. Subsequently, THM densification was undertaken for 15 minutes at 150°C up to a maximum C_s of 67%. Mechanical properties were assessed in three point bending test and MOE and MOR values were calculated.

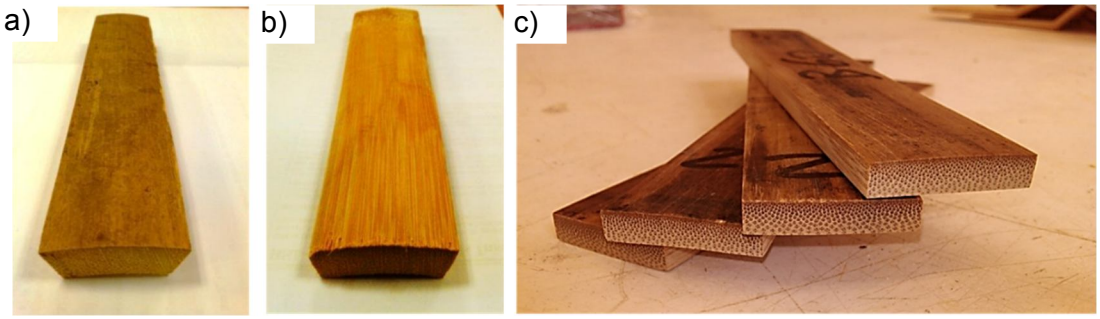

Figure 5-3. a) Non-densified Moso-bamboo specimen with internal and external skins. b) Non-densified Moso-bamboo specimen without internal and external skins. c) Densified Moso-bamboo specimen (Cura, 2012).

Three point bending tests were undertaken using a 100kN Dartec Universal on three specimens per treatment. The specimen's length, width and thicknesses were 140mm, 25mm and 5mm, respectively, and the span between the rollers was 120mm.

Discussion & results

Cura (2012) remarks that the highest values of MOE (16.5GPa) and MOR (201MPa) were obtained through steaming the specimens at 120°C before THM densification. These results are comparable to the results reported by Betts (2011) for TM densified bamboo at 180°C. Cracks were reported specially in the specimens steamed at 100°C and 120°C for 60 minutes, which induced early bending failure and reduced strength in mechanical tests. Nevertheless, specimens with cracks did not experience immediate spring-back recovery after densification, as seen in boiled and steamed specimens without cracks. This might be due to the release of internal stresses through the formation of cracks.

5.3 Assessment of the hardness of Guadua after densification

With the aim of producing laminated Guadua boards (Wills, 2012), studied the manufacture of flattened Guadua sheets employing different mechanical, thermal and softening processes. The manufacture of the Guadua boards involved three stages: splitting of Guadua; hot-pressing; and glue lamination using an epoxy-resin.

For splitting Guadua (Wills, 2012) experimented with several devices; amongst them were Stanley knife blades, chisels, rotating blades and a drill hammer, which were used for scoring the outer surface of Guadua. Eventually, the best method was chosen and the splitting process was carried out as follows: round sections of Guadua were soaked for 24 hours in cold water and then, opened flat through several cuttings around the external layer using a Stanley blade (Figure 5-4a,b & c).

The split sections of Guadua were subsequently TM densified in a hot-press for 30minutes at 180°C and 10MPa. Then, the internal layer of the densified sections of Guadua was sanded-off before bonding with an epoxy-resin (Sicomin Wood Epoxy Resin SR5550 with SR5505 hardener). Specimens were clamped for 24 hours and cured for another 24 hours in an oven at 30°C (Figure 5-4d, e & f). Further curing for five days was allowed before assessing the physical and mechanical properties of the laminated Guadua boards through hardness Rockwell and three point bending tests.

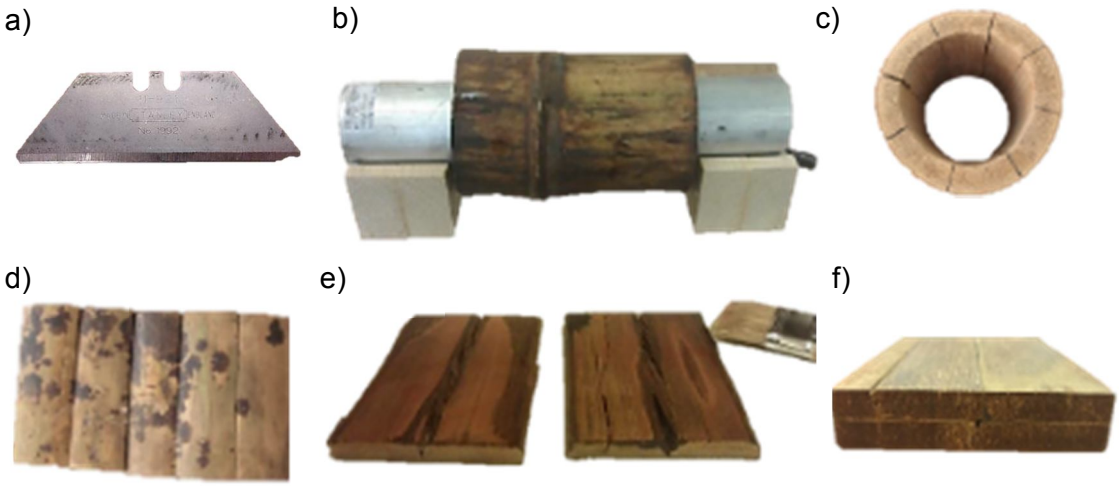

Figure 5-4. Manufacturing processes for Guadua boards. a) Stanley blade. b) Specimen mounted on aluminium rod. c) Culm split in eight. d) Opened flat sections of Guadua. e) Densification and glue lamination of split Guadua. f) Final product (Wills, 2012).

Discussion & results

The research project compared Rockwell hardness test results for normal, cold and hot-pressed, boiled, steamed and soaked Guadua. Prior to testing, Guadua was either boiled for 30 minutes at 100°C; steamed for 30 minutes at temperatures above 100°C; cold pressed to ~41.4MPa; hot pressed for 30minutes at 120°C and 10MPa; or, soaked in cold water for three hours. Results of the test are presented in Figure 5-5 (HRM refers to the Rockwell hardness M scale value).

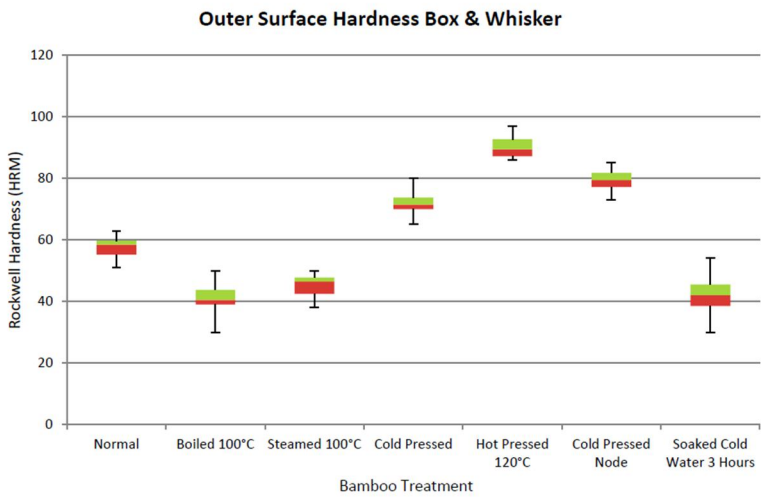

Figure 5-5. Box & whisker plots of the outer surface Rockwell hardness of Guadua as a function of the treatment applied (Wills, 2012).

As observed in Figure 5-5 the highest Rockwell hardness values for the outer surface of

Guadua were obtained by cold and hot pressing the material. The hardness of cold-pressed specimens tested in the nodes was slightly higher than the hardness of cold-pressed specimens tested in the internodes: ~HRM70 and HRM80, respectively. Nevertheless, unlike hot-pressed specimens, a rapid spring-back recovery occurred after cold pressing. Experimentation by Wills (2012) also showed that through steaming, boiling and soaking, the hardness of the outer surface of Guadua was reduced from HRM57.6 (normal) to approximately HRM45 when steamed, HRM41 when boiled and HRM42.5 when soaked. These treatments increased the MC of the material and were key for plasticising the material before densification.

Finally, three point bending test of the epoxy-resin bonded boards resulted in a bending MOE of 19.44GPa. Brief experimentation by the author using a drilling resistance measurement system (DRMS) showed that compressed specimens presented a higher resistance to drilling.

5.4 Further experimentation

Table 5-2 presents the results of experimentation on processing techniques for modifying Guadua through pressure, temperature and heat, which was carried out by the author. These results influenced the selection of the most appropriate technique for transforming Guadua into flat densified sheets for cross-laminated panels.

Table 5-2. Experimental results of different flattening, densification and gluing processes.

Type of process	Picture		Comments
	Cold pressing		
Cold rolling			Severe tissue damage.
	TM Densification		
With skins riven Guadua at 150°C			Immediate spring-back recovery

Without skins Staggered at 150°C		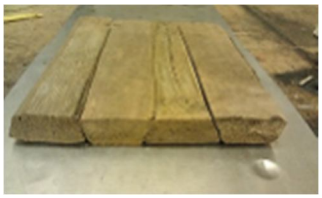	Improved shape stability
THM Densification			
Soaked without skins at 150°C		 Radial cross-section  Longitudinal cross-section	No immediate spring-back & flat surface
Welding			
Inner to Inner faces at 200°C for 2hours			No glue required, but high temperature & pressure for a long time
Gluing / Laminating			
Unidirectional lamination	X-Lam riven Guadua	X-Lam Guadua strips	X-Lam staggered G. strips
	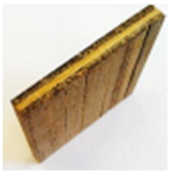		

5.5 Densification process

An open system was utilized for the densification of Guadua specimens. Radial compression was applied by a 200mm x 200mm MOORE manual press with heated plates mounted on four vertical columns. The press was equipped with analogue gauges for pressure measurement, a digital temperature control and a 40 tonne capacity manual jack. The compression set (C_s) value for samples B and C changed due to the natural variability in thickness of the material; however the target value was about 45%. C_s and density values in Table 5-3 are the mean values of all the specimens prepared for testing (see Section 7.1) with average initial thickness (t_o) before densification of ~10mm. The temperature of top and bottom of the hot-press plates was set at 150°C.

As seen in Table 5-3, the densification treatment was applied to samples of Guadua B and C (without skins), which had different pre-treatments (dry and soaked, respectively). A control sample (A) from the same region (middle part) was used to compare the results of mechanical testing.

Table 5-3. Densification treatments applied to Guadua

Bamboo species: *Guadua angustifolia* Kunth		Section: Middle (in height)		Age: Mature (3-5 years old)
		Samples A Raw un-pro-cessed	Samples B TM densified	Samples C Pre-soaked+Hot pressed+Dried
Time		0	20 min	20 min
Pressure		0	5.8 MPa	5.8 MPa
Temperature		0	150°C	150°C
Compression set (C_s) (Mean)		0	46.08%	42.51%
Oven dried density	Mean	543.3 kg/m^3	814.6 kg/m^3	890.9 kg/m^3
	St. dev.	11.60	63.09	91.79
	CoV	2.14%	7.75%	10.30%

Figure 5-6 shows the diagram of the densification treatment (a) and a sequence of the densification process (b-d). Sample C was pre-soaked in water for 24 hours prior to the THM densification. The process started with a 10-minute period to allow the plasticisation of the specimen where both pressure and temperature increase to about 6MPa and 150°C, respectively. The temperature and pressure were maintained for 10 minutes during the densification stage followed by cooling with a steady drop in pressure. As a result of the densification, the surface roughness of Guadua samples B and C was lower than that of non-densified Guadua samples (A).

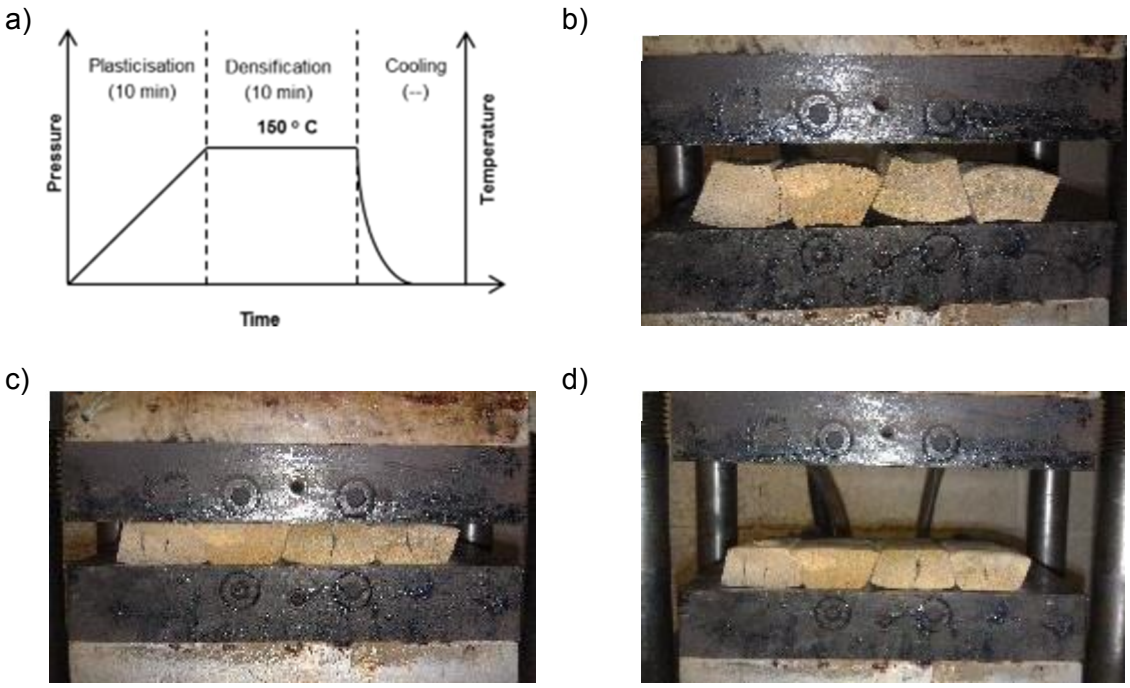

Figure 5-6. a) Pressure versus time for the THM treatment, b, c & d) Specimens in the press during THM treatment.

Concluding remarks

Although the research findings of the MEng final year students were not completely rigorous, the experimentation undertaken during these projects provided a better understanding of alternative methods for plasticising, densifying and in general processing bamboos Moso and Guadua. Several flaws with these studies were found; amongst them were: the low number of specimens tested and the lack of basic information regarding the treatments undertaken and testing conditions (*eg*. hot-press pressure applied and specimens conditioning or MC).

Own experimentation contributed to define an adequate set of temperature, pressure and heat values for the TM and THM densification of Guadua. Water soaking was applied for initiating the softening of the microstructure of Guadua prior to densification. Removal of external and internal skins of Guadua was beneficial for allowing the transfer of heat across the section to be densified. The combination of these factors resulted in an increase in density and a stable flat surface, after densification.

6. Microstructural analysis of Guadua and TM and THM modified Guadua.

Introduction

With the aim of identifying the microstructure of the bamboo species: *Guadua angustifolia* Kunth (Guadua), specimens of this plant were observed using a Scanning Electron Microscope (SEM) and a Focused Ion Beam (FIB) microscope. Optical microscopes were used to image the changes to the microstructure of Guadua produced by the thermo-mechanical (TM) and thermos-hydro-mechanical (THM) densification processes. Microscopy images produced with a stereo microscope were used for comparing the proportion of vascular bundles in sections across densified and non-densified samples.

Additionally, analysis of the elemental composition of Guadua was carried out on small specimens using Energy Dispersive X-ray Spectroscopy (EDXS). The main interest in using this elemental mapping technique was to track the presence of silicon across the section of Guadua culms. Silicon is the cause of high wear in cutting tools used during manufacture of bamboo products, which is an important consideration in the development of any engineered product.

Unidirectionally laminated specimens of densified Guadua that were subjected to shear block test were also imaged using a stereo microscope. This observation helped to better understand the factors affecting the adhesion between Guadua and epoxy resin.

6.1 SEM Imaging

The SEM images specimens under vacuum with a high-energy electron beam that scans the surface. Electrons hit the specimen interacting with its atoms gathering information such as topography, crystallography, composition and electrical conductivity. Specialized detectors are placed inside the microscope chamber to receive the secondary electrons emitted and the image is digitally produced (Figure 6-1). Some depth of field in the specimen is achieved as a result of the short wavelength of the finely focused electron beam used by SEM. Useful magnification lies in the range between 10-10,000x.

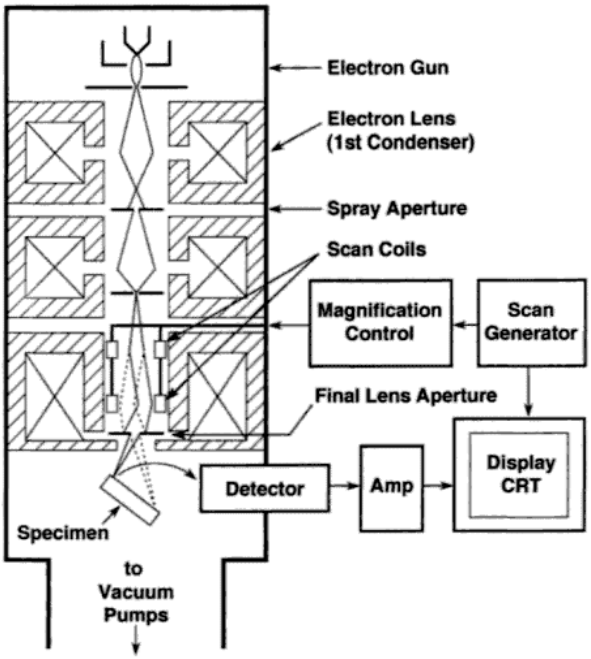

Figure 6-1. SEM diagram showing the electron gun, lenses, deflection system and electron detector (Goldstein, 2003).

6.1.1 Imaging of Guadua by SEM

Small pieces cut from different sections along the height and across the wall thickness from mature and young specimens of Guadua were prepared for SEM imaging. 5mm cubes were boiled for five minutes and subsequently cut by hand with single-edge stainless steel blades. Sections were attached to specimen mounts using double-sided carbon conductive tape. Silver paint at one side of the specimen was used to conduct electrons to earth. Subsequently the cubes were left in a vacuum for a week and when dry, sputter coated with gold before observation. A JEOL JSM6480LV (Jeol Ltd., Tokyo, Japan) SEM installed at the MAS

(Microscopy and Analysis Suite) facilities of the University of Bath was used.

The ground tissue of bamboos in general is composed of 52% parenchyma cells, 40% of fibres and 8% of conductive tissue (Liese, 1998). Figure 6-2 shows the microstructural arrangement of a vascular bundle incorporating metaxylem vessels and phloem whose main functions are the transport of water and nutrients. These are part of the conductive tissue together with the protoxylem which also transports water, but during the early stages of growth (Liese, 1998).

Vascular bundles vary in shape depending on their position along height and across the wall. Their size increases and number decreases towards the lacuna (inner part of bamboo). Figure 6-3 illustrates how the main conductive tissue is surrounded by fibre sheaths on a pair of vascular bundles from the middle part of a culm wall and there are parenchyma cells separating these vascular bundles. Figure 6-4 and Figure 6-5 illustrate parenchyma cells with pit openings in the cell wall that allow cellular interconnection.

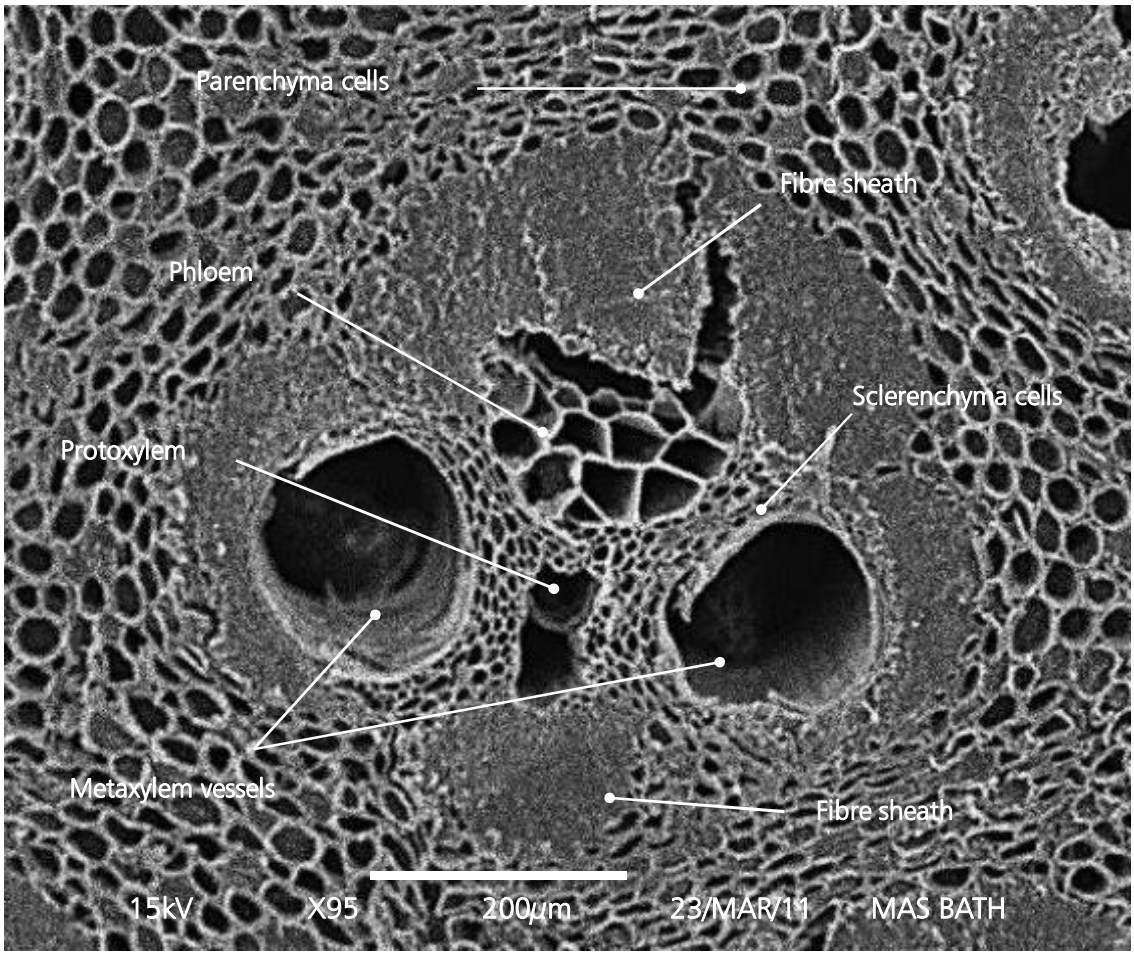

Figure 6-2. Detail of a vascular bundle in *Guadua angustifolia* Kunth. MAS SEM / Amplification 95x.

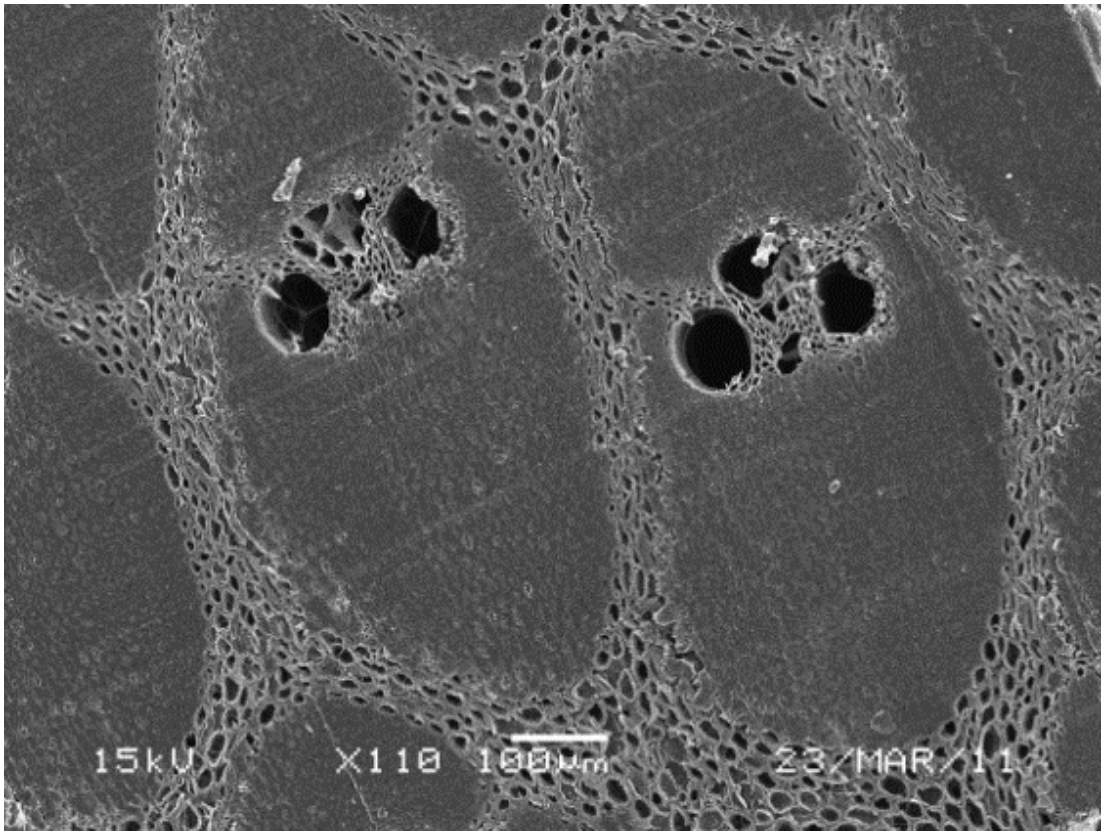

Figure 6-3. Pair of vascular bundles from the middle part of the wall thickness of a *Guadua angustifolia* Kunth specimen. MAS SEM / Amplification 110x.

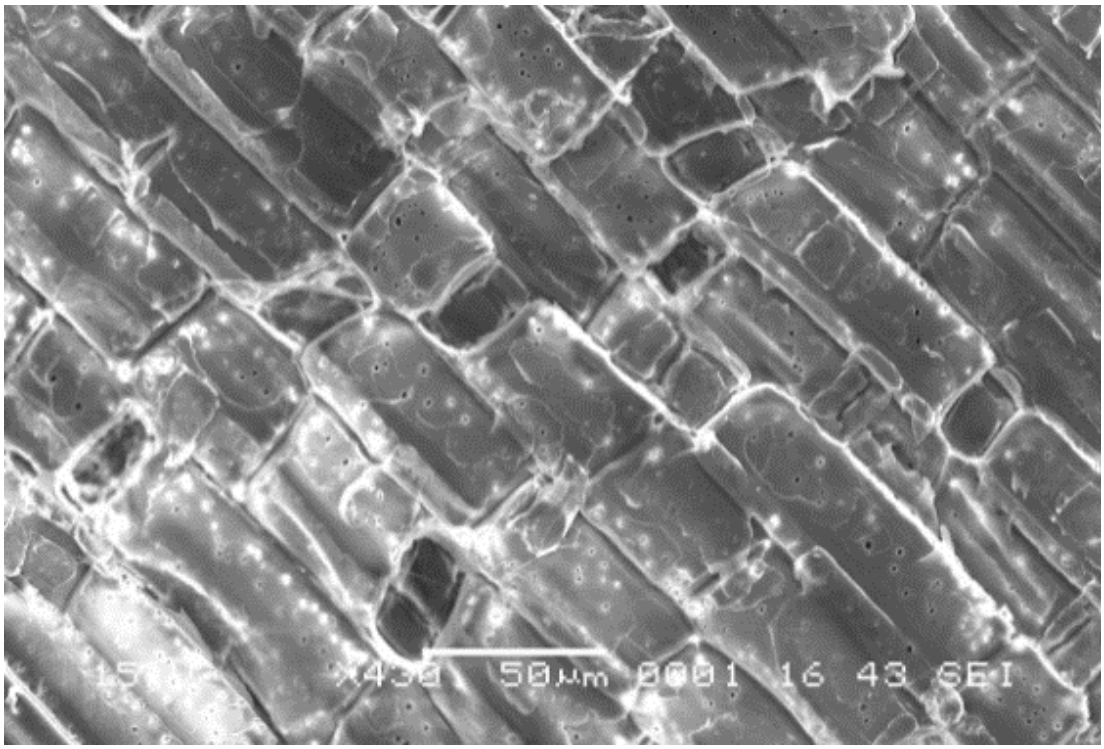

Figure 6-4. Shorter and longer cells of parenchyma with pit openings *Guadua angustifolia* Kunth. MAS SEM / Amplification 430x.

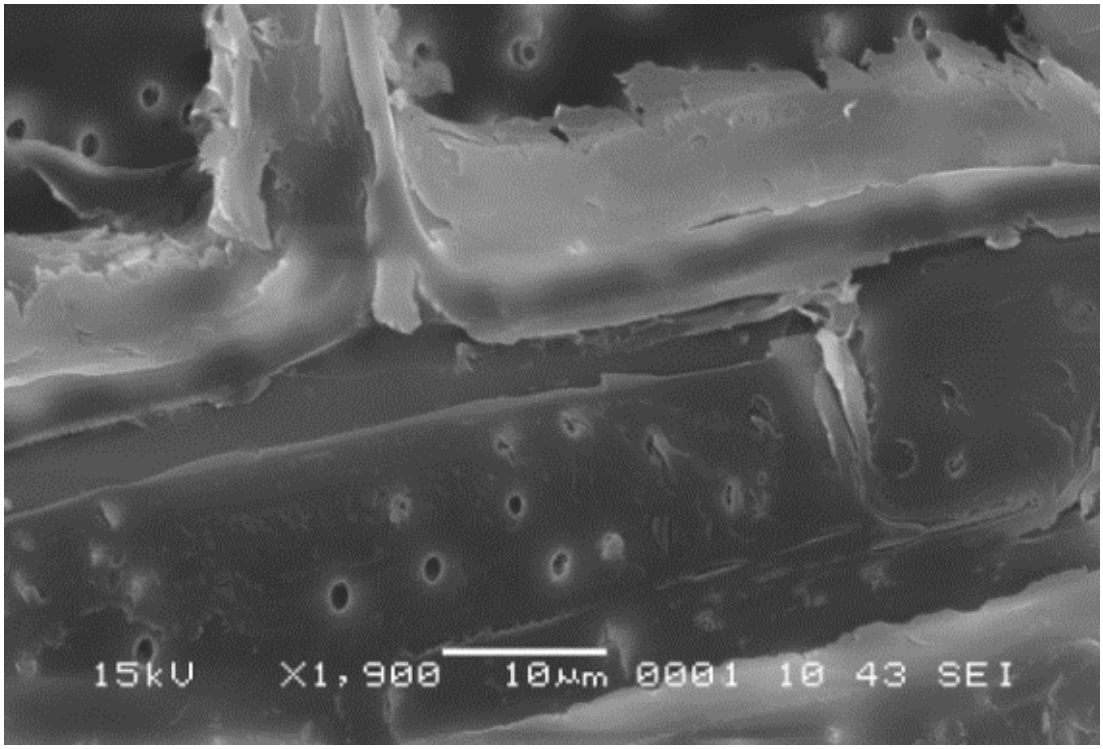

Figure 6-5. Inner side of a parenchyma cell with pit openings in *Guadua angustifolia* Kunth. MAS SEM / Amplification 1,900x.

6.2 FIB Imaging

Specimens of *Guadua angustifolia* Kunth were imaged at the Interface Analysis Centre (IAC) of the University of Bristol with a FEI FIB201 gallium Focused Ion Beam (FIB) instrument. High-resolution images of Guadua specimens obtained under the FIB assisted the identification of some microstructural features of the material within the ground tissue.

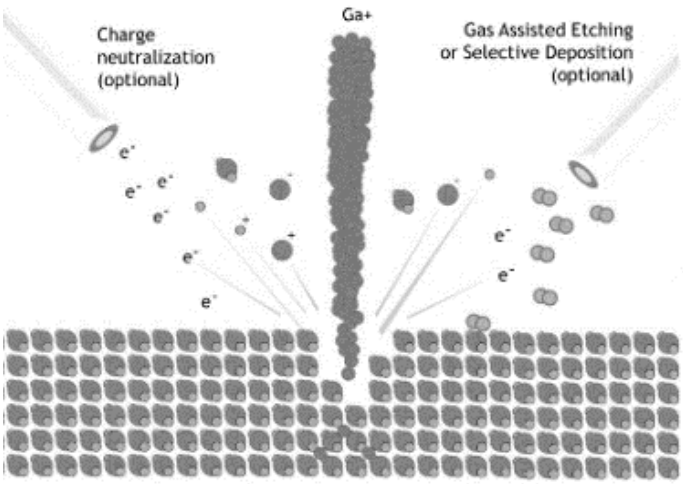

Figure 6-6. Diagram of a focused Ion Beam (http://www.fibics.com/).

FIB microscopy uses an ion beam to sputter or mill the surface of specimens. The image is produced by the detection of sputtered ions and secondary electrons emitted from the specimen (Figure 6-6). The FIB at Bristol uses a gallium (Ga+) ion source. Low beam currents are used for imaging the specimen and high beam currents for sputtering and milling the specimen. Atoms from the substrate are removed by the ion beams in a controlled and precise way allowing the removal of material at nanometre scale. The main differences with SEM are the possibility of obtaining high-resolution images and the possibility of carving the surface to analyse specific features; however, the high current used by the beam significantly damages the specimen.

6.2.1 Imaging of Guadua by FIB

The preparation of the specimens followed the same parameters as those for SEM; boiled specimens were cut with razor blades, vacuumed for a week and sputter coated with gold before observation was made.

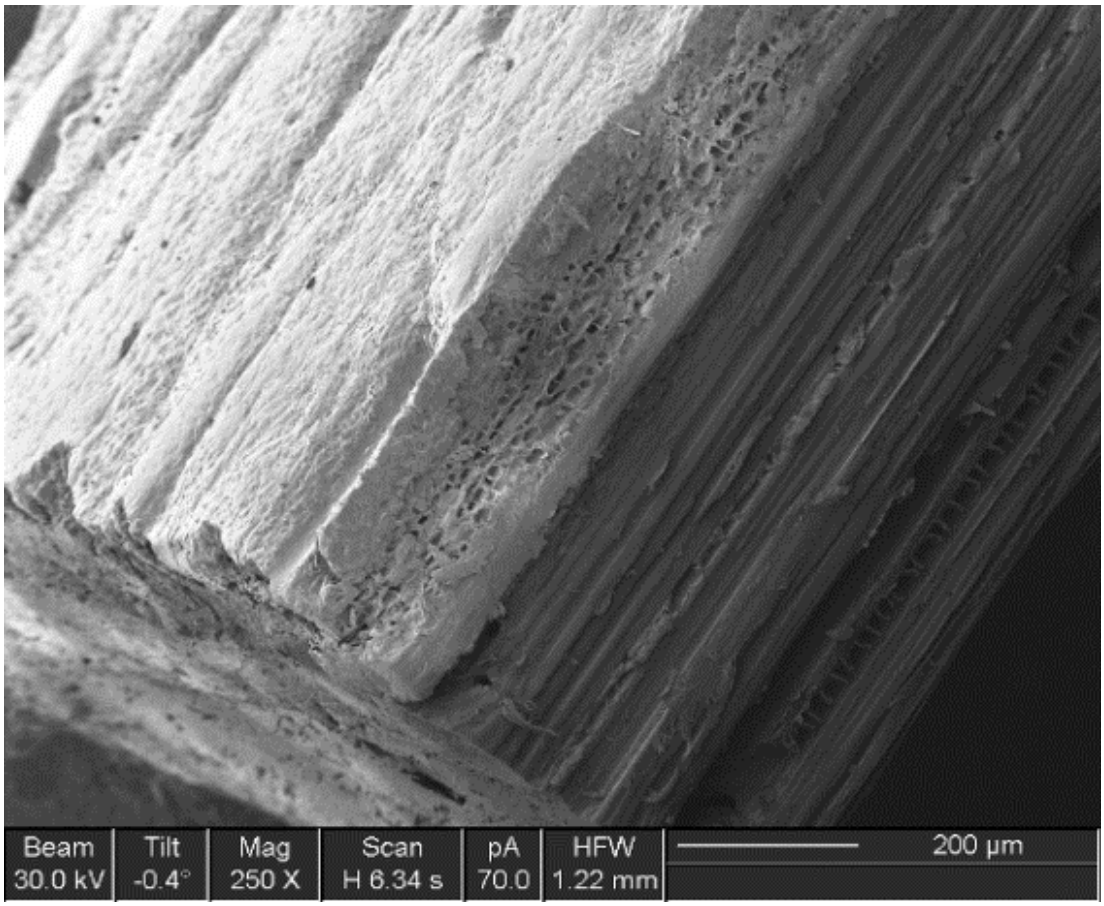

Figure 6-7. FIB image of the cortex and a section through a Guadua specimen.

A view of the cortex and section through a Guadua specimen is depicted in Figure 6-7. Variation in the density and composition of the material can be observed in this FIB image. The outermost part (brighter in the image) is composed of a cutinized cellulose and pectin layer which is covered by a wax coating (Liese, 1998) which together provide protection to the tissue and a barrier to water and insects. Cork cells containing silica as well as the stomata are located in this epidermal tissue underneath the cutinized layer.

Sputtering of the surface of the specimens permitted the observation of different features at high magnifications with a voltage of 30kV. The interior of parenchyma cells evidencing the cell wall lamellation can be observed in Figure 6-8 and ring thickening of protoxylem lacuna in Figure 6-9.

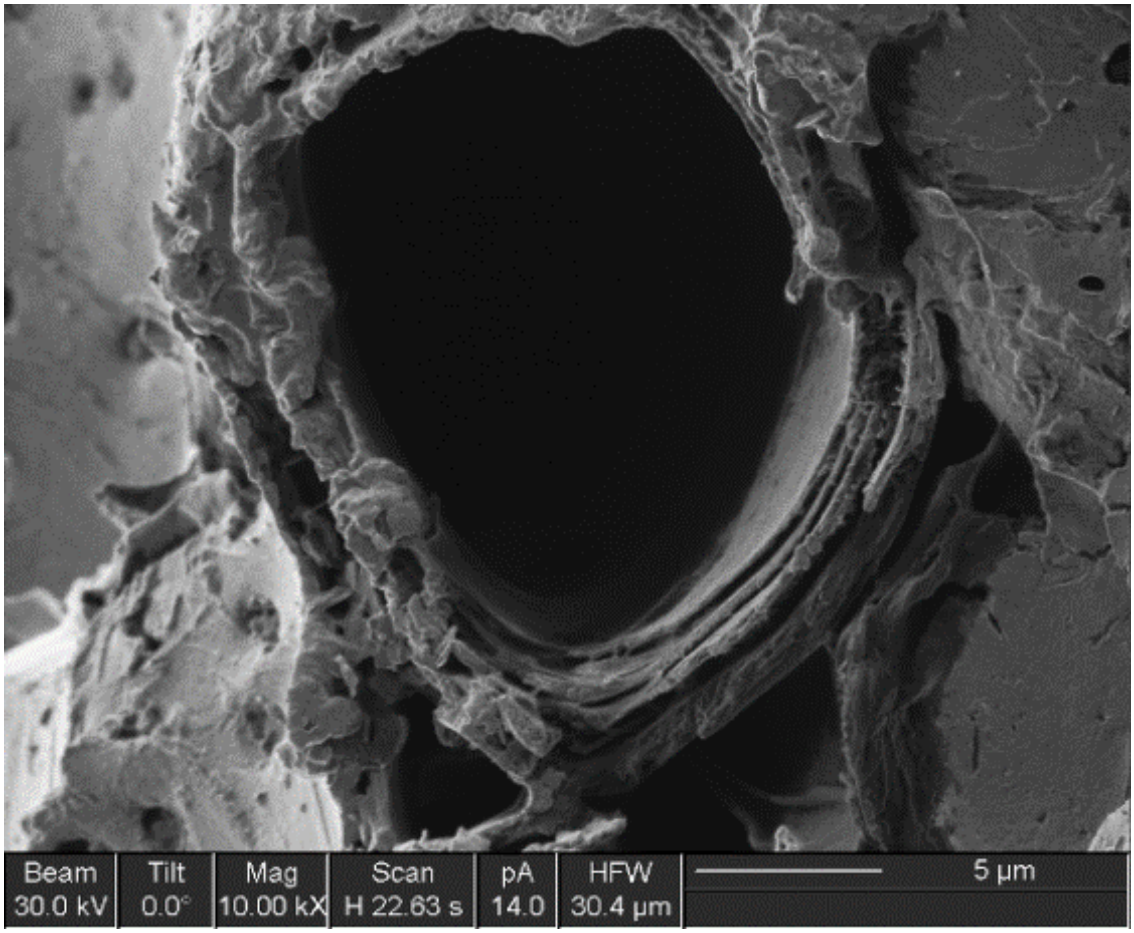

Figure 6-8. Interior of a parenchyma cell of *Guadua angustifolia* Kunth.

A hole 40μm long, 20μm wide and approximately 20μm deep was carved on the surface of a specimen of Guadua by the ion beam and the cell wall structure was exposed. Darker zones on the polylamellate cell walls were observed, which suggested the fixation of an inorganic material on these layers (Figure 6-10).

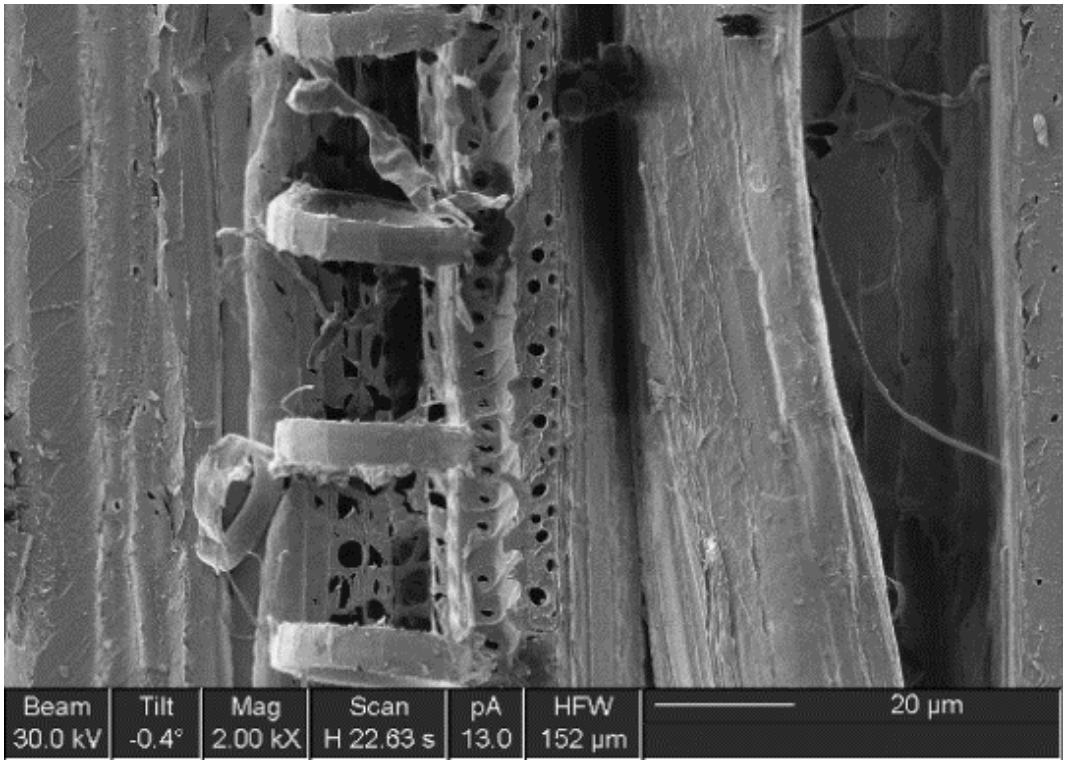

Figure 6-9. Protoxylem lacuna with individual ring thickenings.

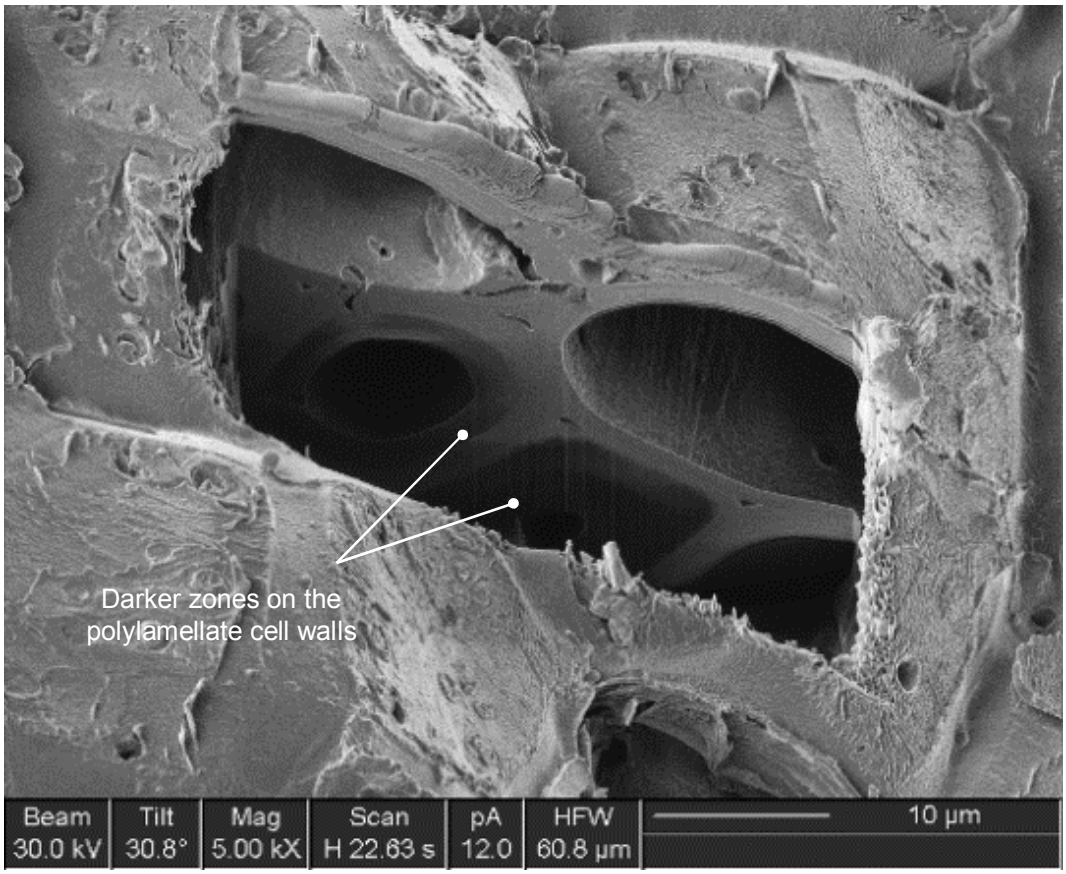

Figure 6-10. FIB imaging of Guadua specimens by sputtering into its cell structure.

6.3 Optical microscopy

Samples A, B and C (as defined in Section 5.5) were imaged with a Leica DM ILM inverted microscope and a Leica M 205C stereomicroscope. Both microscopes were fitted with digital cameras connected to a computer. The former provided a magnification range from 50x to 500x over small sections of the specimen and the latter captures higher depth of field images over a larger area producing high quality images. The zoom range of the stereo microscope was between 7.8x and 160x on a fixed 1.5x objective. Small features at cellular level of the densified and non-densified samples were imaged using the inverted microscope. Microscopic images produced with the stereo microscope were used for measuring the fibre surface area across the sections of densified and non-densified samples.

a)

b)

Figure 6-11. a) Leica DM ILM inverted microscope. b) Leica M 205C stereomicroscope.

The majority of the specimens used for optical microscopy were embedded in low-viscosity resin by vacuum impregnation prior to observation. The face imaged was polished in order

to improve the quality of the surface. Gradually finer silicon carbide papers to a 1200 grit size were used before polishing with, 6, 3 and 1 mm diamond paste.

a)

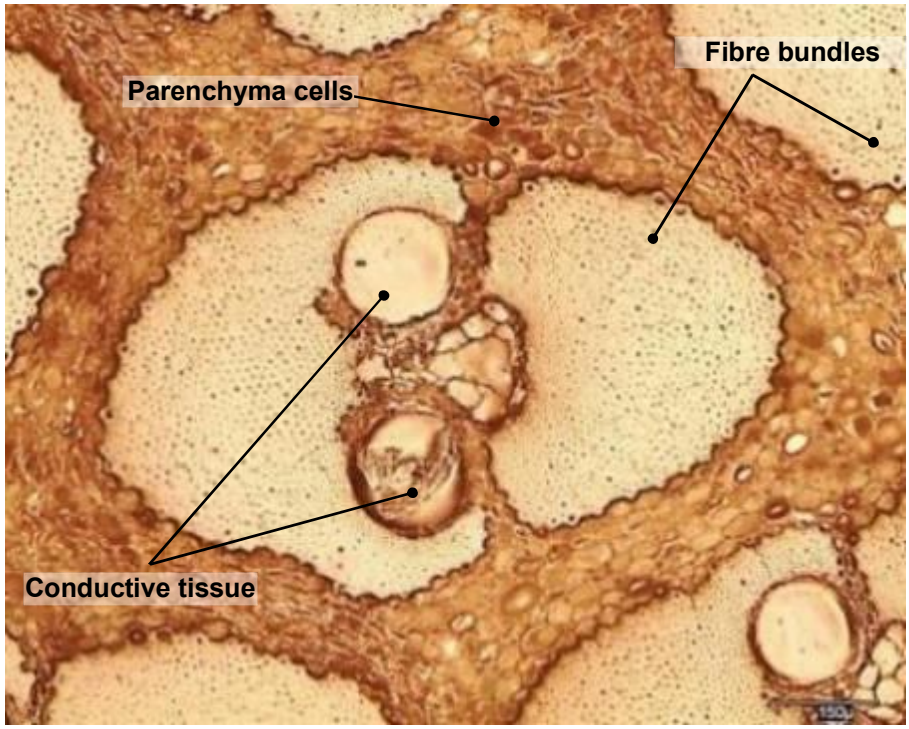

b)

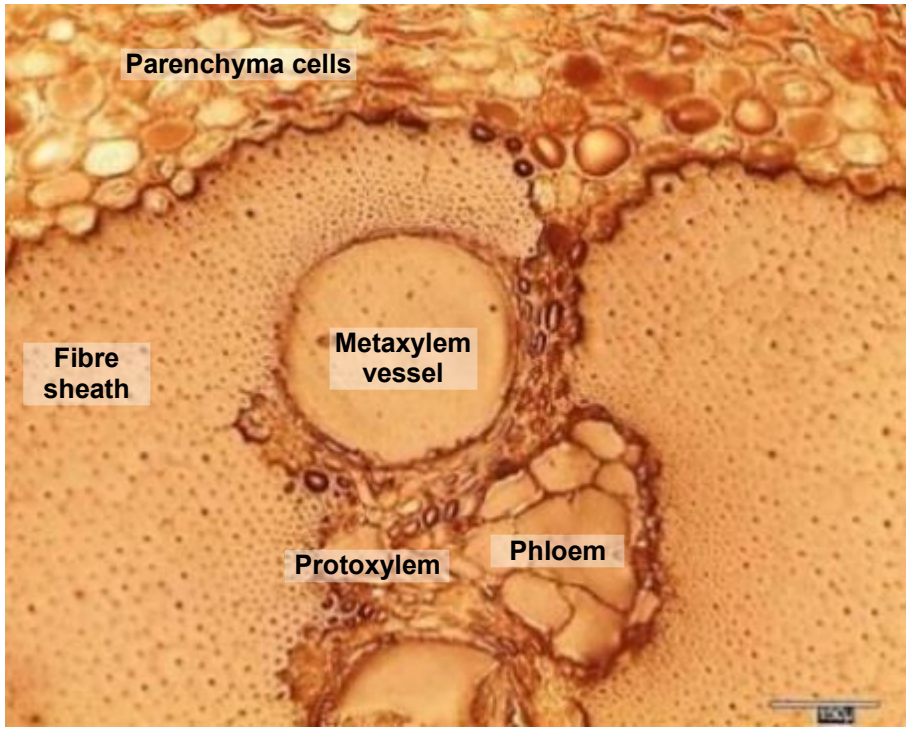

Figure 6-12. Inverted microscope images of a Guadua specimen embedded in resin. a) Vascular bundle with surrounding parenchyma cells and conductive tissue prior to densification (Sample A). b) Detail of the same vascular bundle prior to densification (Sample A) illustrating the conductive tissue inside and parenchyma cells above.

Figure 6-12a illustrates the normal shape and size of conductive vessels (phloem, metaxylem and protoxylem within a vascular bundle) and parenchyma cells surrounding a section of a vascular bundle of Guadua prior to densification. Figure 6-12b details these conductive tissue in a section of the same vascular bundle. Phloem, a metaxylem vessel, sclenrenchyma and parenchyma cells are clearly imaged. Two fibre sheaths surround the conductive tissues inside the vascular bundle. A detail of a fibre sheath is imaged on Figure 6-13. The average length and width of Guadua fibres as reported by Liese (1998) is 1.60mm and 11µm, respectively. As can be observed their size decreases towards the metaxylem and phloem side (conductive tissue) and increases towards the outside of the vascular bundle where they meet with parenchyma cells (see also Figure 6-15b).

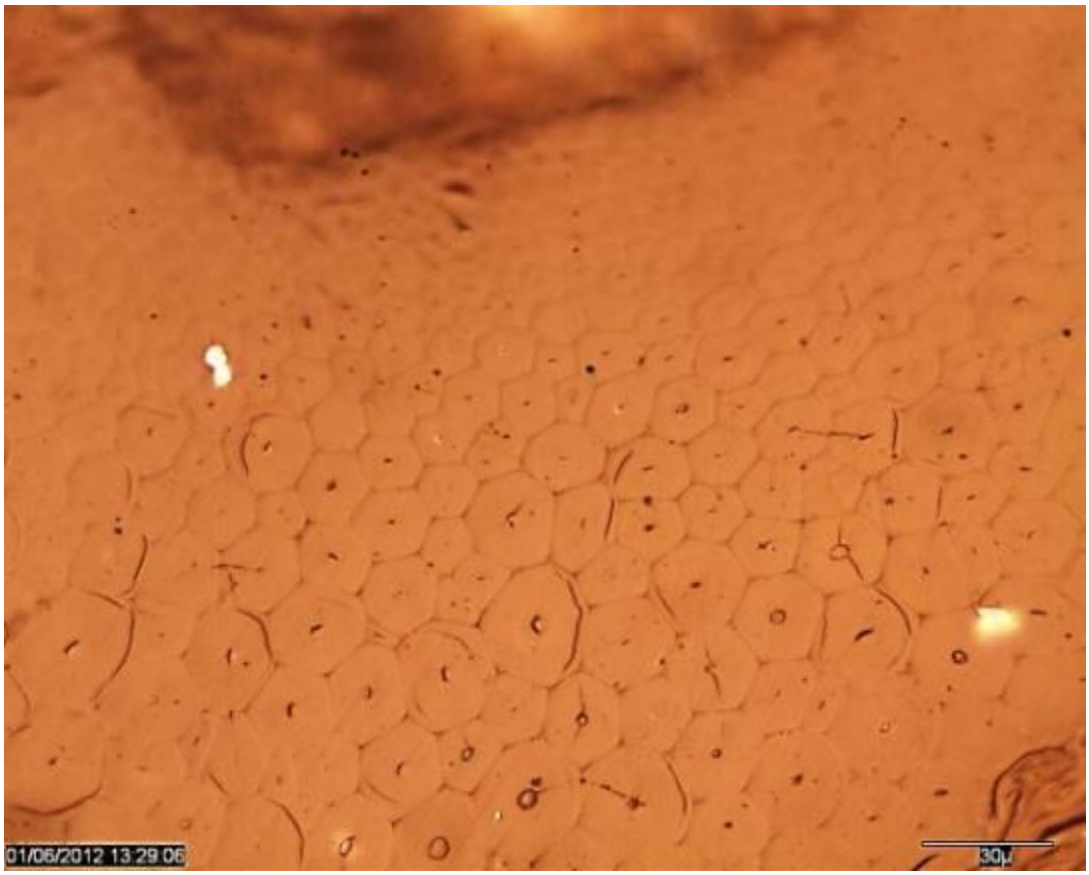

Figure 6-13. Inverted microscope images of a fibre bundle or fibre sheath taken with a Leica DM ILM at 50x magnification.

Figure 6-14a and Figure 6-14b illustrate the collapse of conductive vessels and parenchyma cells after the densification process C (described in Section5.5) in specimens of Guadua from different parts of the culm. Figure 6-15 details the collapse of these void tissues (parenchyma cells and conductive vessels) on a vascular bundle which occurred during densification.

a)

b)

Figure 6-14. Inverted microscope images of a specimen of sample C at 10x magnification. a) Vascular bundles with surrounding parenchyma cells and conductive after densification of a specimen close to the cortex. b) Vascular bundle following densification of a specimen from the middle part of the culm.

Figure 6-15. Inverted microscope image of a vascular bundle following densification (sample C). Taken with a Leica DM ILM at 10x magnification.

A sequence of microscopy images across the thickness of a densified specimen (sample C) is presented in Figure 6-16. This image depicts the variation in size and number of vascular bundles in the cross section of Guadua, as well as the higher surface area of parenchyma cells towards the lacuna (innermost layer of a bamboo culm).

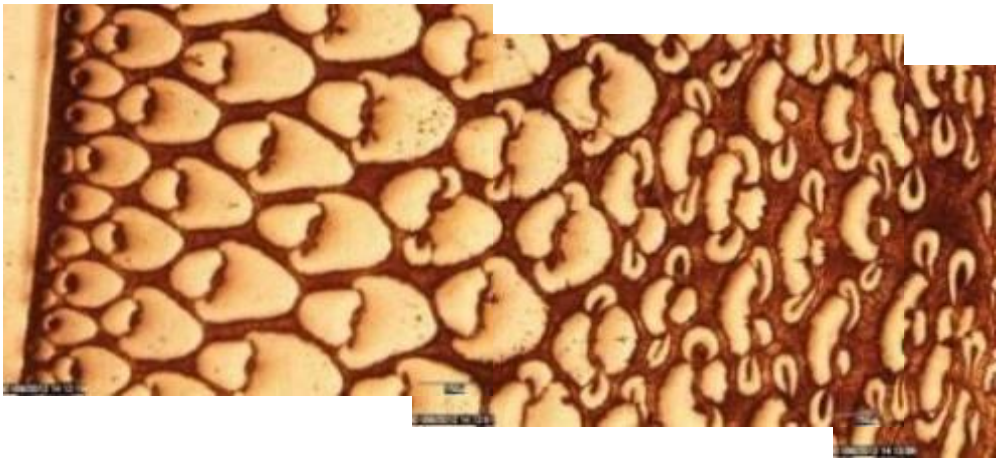

Figure 6-16. Sequence of inverted microscope images of a cross section of densified Guadua (sample C) illustrating the fibre surface variation across the thickness. Taken with a Leica DM ILM at 50x magnification.

Figure 6-17a illustrates the initial state (natural) of parenchyma cells without TM or THM modification, whilst Figure 6-17b shows their collapse after applying a THM treatment (sample C).

a)

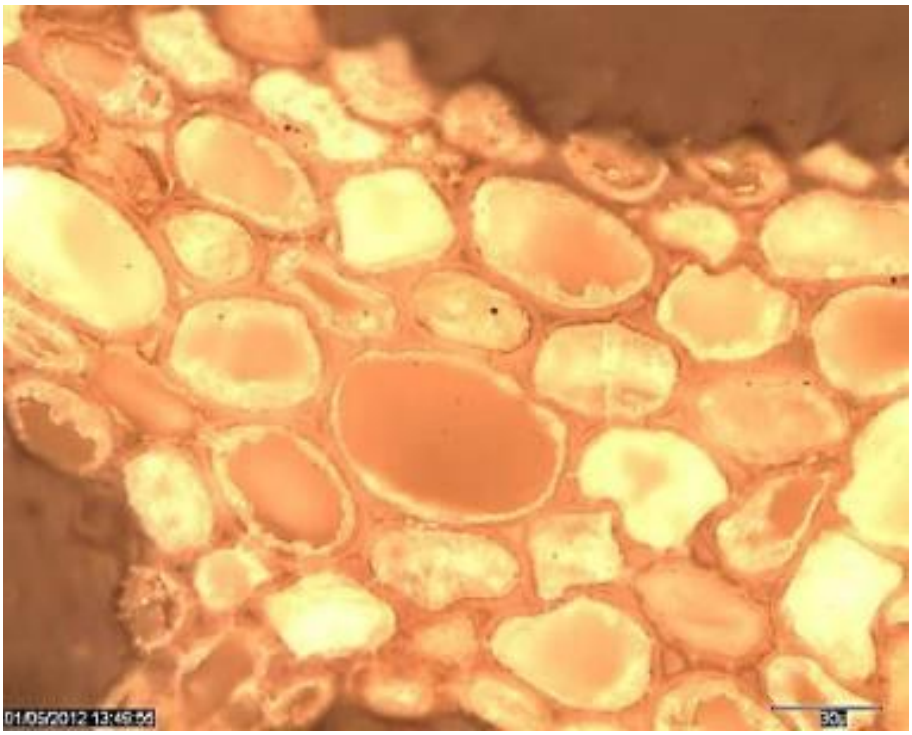

b)

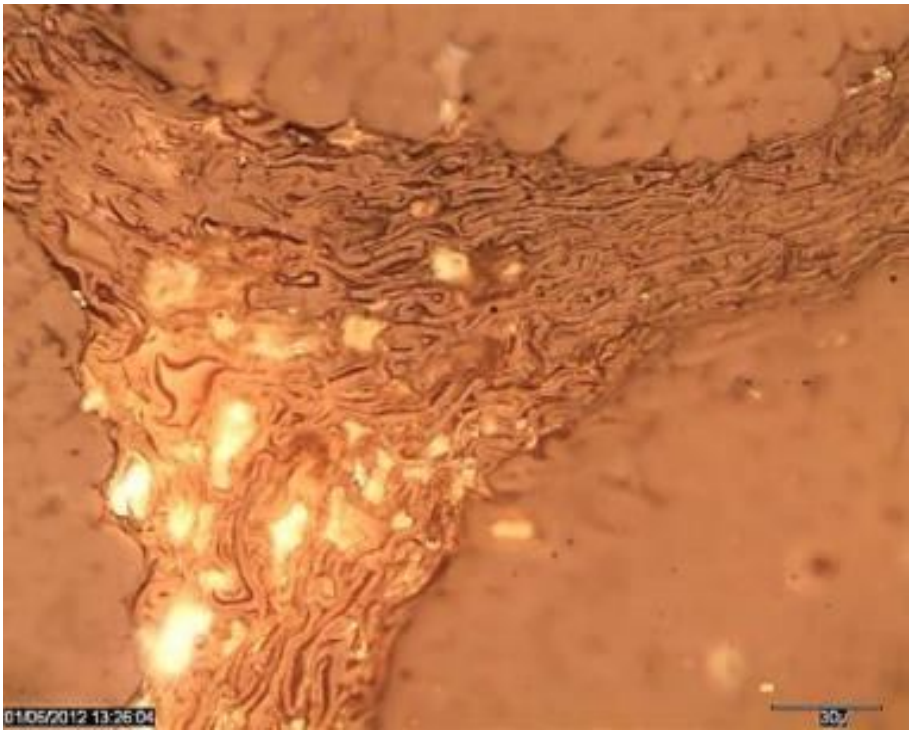

Figure 6-17. Parenchyma cells pre (a) and post-densification (b) taken with a Leica DM ILM inverted microscope at 50x magnification.

Figure 6-18 compares the densification process of a specimen of Guadua (a) with the densification process of a specimen of Spruce (b). In the Spruce specimen (Sandberg & Navi, 2007) the radial compression starts with the earlywood and the latewood follows (see Section 4.3, Figure 4-20 and Figure 4-21). This is similar to what occurs during the densification of Guadua, where the low density material at the inner side of the culm collapses before the dense material at the outer side (cortex).

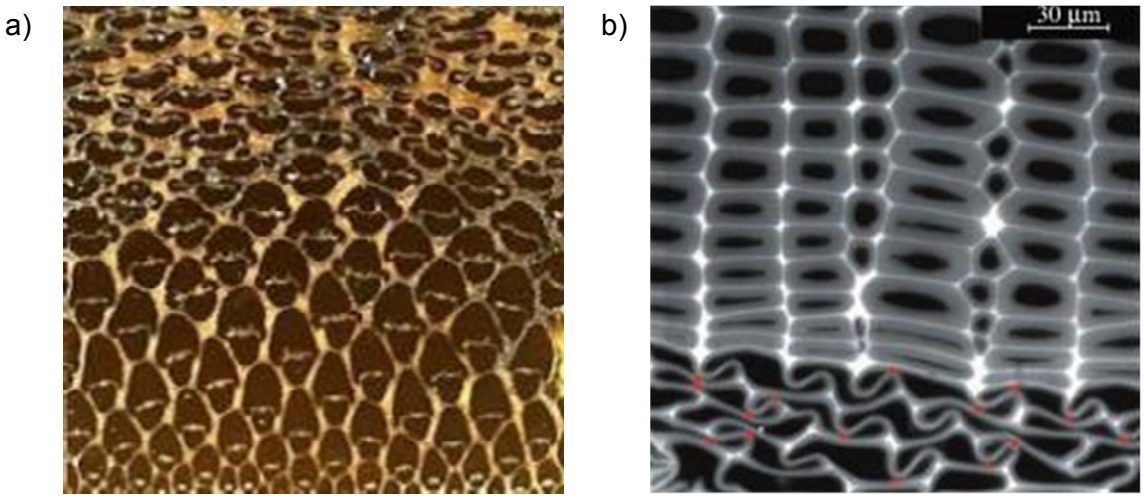

Figure 6-18. a). Microscopy image taken with a Leica M205C stereo microscope showing the variation on fibre surface from inner (top) to outer (bottom) layer of a densified cross section of Guadua. b) Confocal microscopy image of a densified specimen of spruce in the radial direction (Sandberg & Navi, 2007).

Figure 6-19 compares the fibre content within two sections of Samples A and C of the same area. Figure 6-18 and 6-19 were taken with the Leica M205C stereomicroscope.

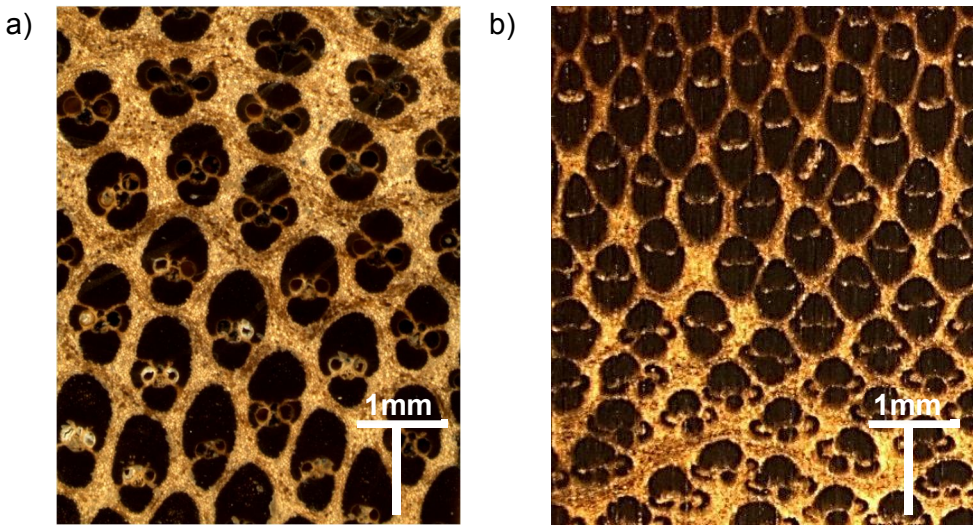

Figure 6-19. a) Non-modified cross section of Guadua and b) Thermo-hydro-mechanically modified cross section of Guadua.

TM densified specimens of Guadua (sample B) laminated unidirectionally and glued with epoxy resin were also imaged using the Leica M205C stereo microscope (Figure 6-20, Figure 6-21 and Figure 6-22). These specimens were subjected to a shear block test with the aim of assessing the shear strength of the interface. These images illustrate a characteristic failure of the low density material (parenchyma cells) that is torn apart by the applied shear force, while the high density material (fibres) remain attached to the adhesive.

a)

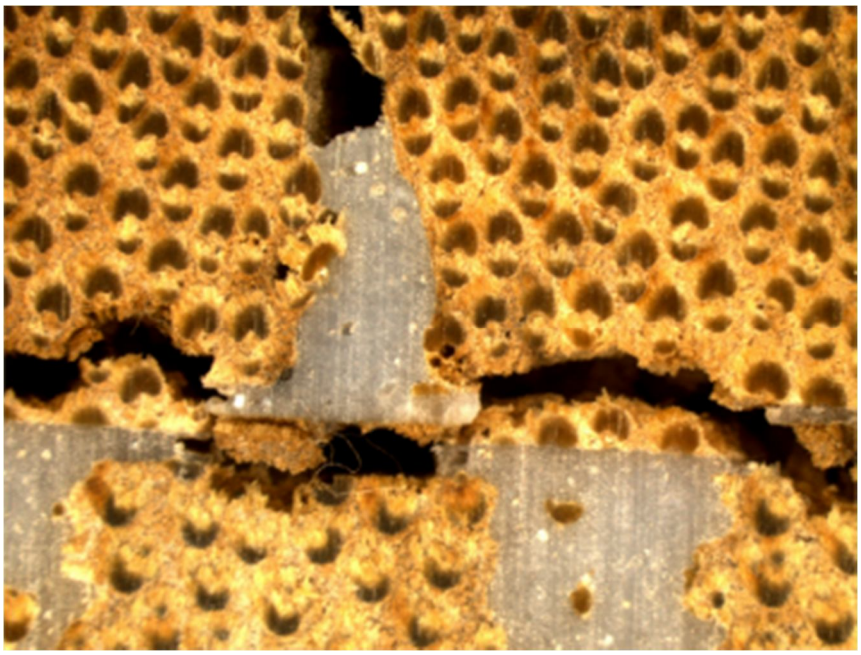

b)

Figure 6-20. A laminated specimen of densified Guadua (sample B) subjected to a shear block test.

Figure 6-21 illustrates the shear failure of a fibre sheath in the glue line. This occurs by

buckling of fibre cell walls (Navi, 2010) and showcases the higher strength of these high density cells when compared to parenchyma cells with lower density (Figure 6-22).

Figure 6-21. Shear failure of a Guadua fibre sheath from a laminated specimen of densified Guadua (sample B) subjected to a shear block test.

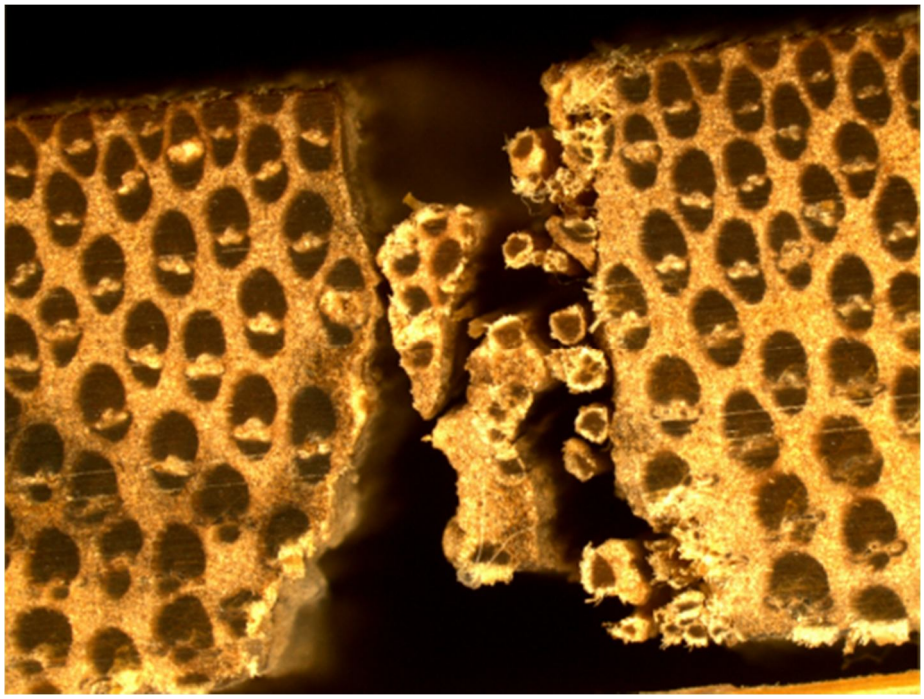

Figure 6-22. Failure of low density tissues surrounding the vascular bundle of a specimen of densified Guadua (sample B) subjected to shear block test.

6.4 Image analysis

Optical microscopy images were analysed using the open source image processing software: ImageJ with the aim of measuring the changes in surface area across the section of Guadua samples after the application of heat and pressure treatments.

6.4.1 Fibre surface area analysis

Three optical microscopy images of Guadua samples A, B and C (Figure 6-23) were chosen to measure fibre surface area with ImageJ. For each image, the area for the analysis was cropped and the scale set.

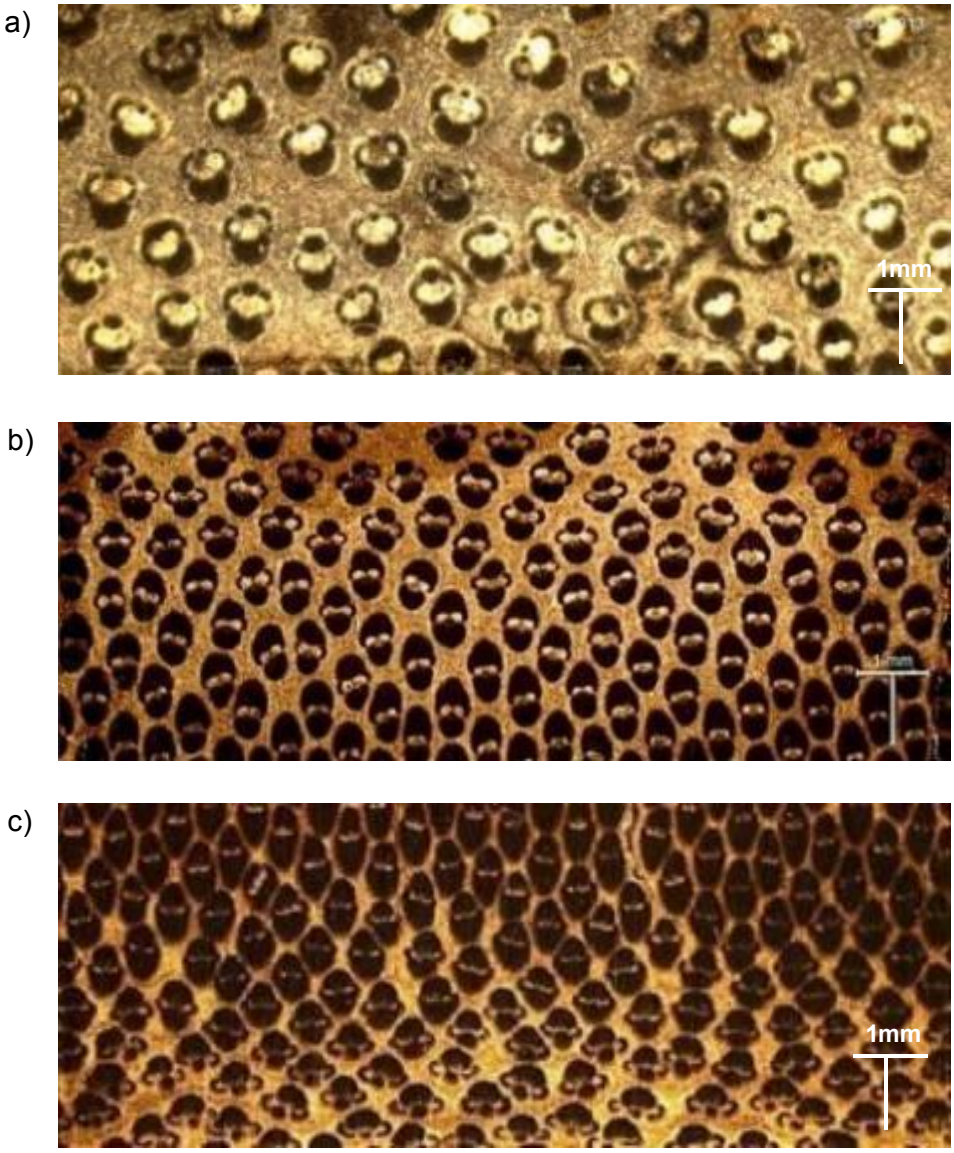

Figure 6-23. Microscopy images of samples A (a), B (b) and C (c) taken with a Leica M205C stereo microscope.

The area consisting of conductive tissue and parenchyma cells was filtered out and the fibre surface area of samples A, B and C was measured (Figure 6-24, 5-25 and 5-26). The fibre surface area of A, B and C samples accounted for 25.33%, 45.47% and 47.78% of the imaged cross sections.

Figure 6-24. Image analysis of a sample A specimen with Image J (Total area=13.6mm^2, Fibre surface=25.53%).

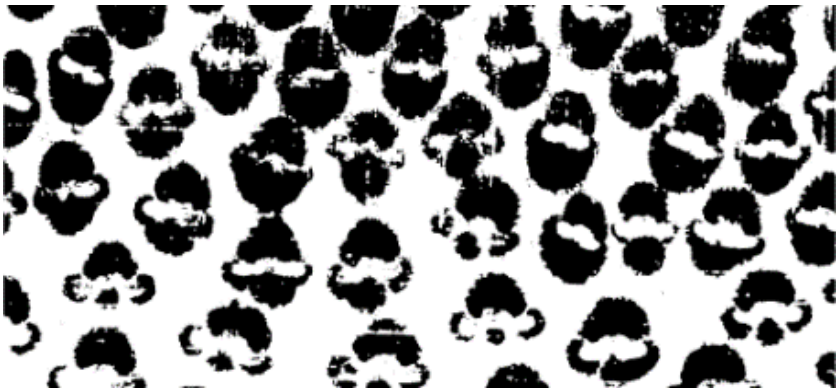

Figure 6-25. Image analysis of a sample B specimen with Image J (Total area=19.42mm^2, Fibre surface=45.47%).

Figure 6-26. Image analysis of a sample C specimen with Image J (Total area=23.08mm^2, Fibre surface=47.78%).

6.5 SEM/EDXS elemental analysis

The presence of silica in bamboos has been reported by several authors (Ding *et al.,* 2008; Herrera-Giraldo *et al.,* 2009; Janssen, 2000; Li *et al.,* 2006; Liese, 1998; Lux *et al.,* 2003). Liese (1998) highlights the structural support that is given to bamboos by the occurrence of short silica-containing cells along with cork cells and the stomata in the epidermal layer of culms. An amorphous form of hydrated silica ($SiO_2.nH_20$) is fixed in plants through absorption by roots and a chemical process that polymerizes monocilic acid ($Si(OH)_4$) from the soil (Dayanandan *et al.,* 1983). Bamboos show a high quantity of silica in the epidermis 1.5% (*Bambusa vulgaris*) and 6.4% (*Schizostachyum lumampao*) strengthening the epidermal layer (Liese, 1998). Liese defines silica cells as "epidermal, short cell filled by a single silica body". Silica polymerizes in the cell lumen and forms part of the chemical composition of the cell. Silica is present in wood (FPL, 2010) and its presence in plants, its shape and function have also been extensively studied by (Bonnett, 1972; Dayanandan *et al.,* 1983; Lanning *et al.,* 1958; Mehra & Sharma, 1965).

The amorphous silica content increases towards the top of bamboos along the periphery of the culm, whereas in the radial direction towards the lacuna (inner part) it is almost zero (Liese, 1998). Lux *et al.* (2003) evaluated the accumulation of silicon in leaves and roots of bamboo *Phyllostachys heterocycla* Mitf where its presence protects the plant against damage and insects, and assists the rhizomes in spreading underground in difficult soil conditions (Lux *et al.,* 2003). The presence of silica within bamboo also hinders cutting in manufacturing processes. Due to intense saw wear, the use of diamond saw blades is necessary in bamboo species such as Guadua. Furthermore, silica behaves as a pozzolanic material that improves the cementitious qualities of Portland cement by increasing the amount of calcium silicate hydrate (C-S-H) through reaction with lime (Dwivedi *et al.,* 2006). This effect is desirable when using cement plasters on the surface of Guadua panels for construction applications. Thus, the presence of silicon across the section of Guadua specimens was mapped out using Energy Dispersive X-ray Spectroscopy (EDXS).

6.5.1 Mapping of silica using SEM/EDXS

Some of the specimens prepared for the SEM imaging of the microstructure of Guadua were subject to X-ray analysis using EDXS installed on the JEOL JSM6480LV at the University of Bath. Oxford INCA x-ray analyser software was used for the quantitative analysis of the components. The distribution of silicon content from the outer to the inner part of the culm has been imaged. As observed in Figure 6-27, there is a high concentration of silicon in the

cortex of bamboo, together with carbon and oxygen, which confirms the results of previous research in the same topic (Hunter & Junqi, 2002; Z. Li *et al.,* 2006; Lybeer *et al.,* 2006). The inner layer of the Guadua wall has a more scattered distribution of silicon as seen in Figure 6-28.

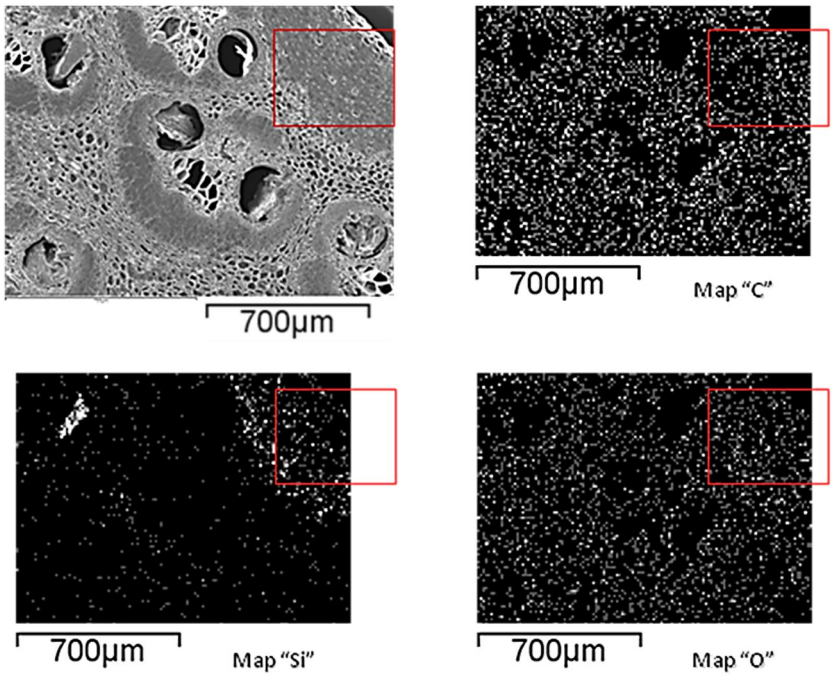

Figure 6-27. Elemental composition analysis of a section of the outer part of Guadua.

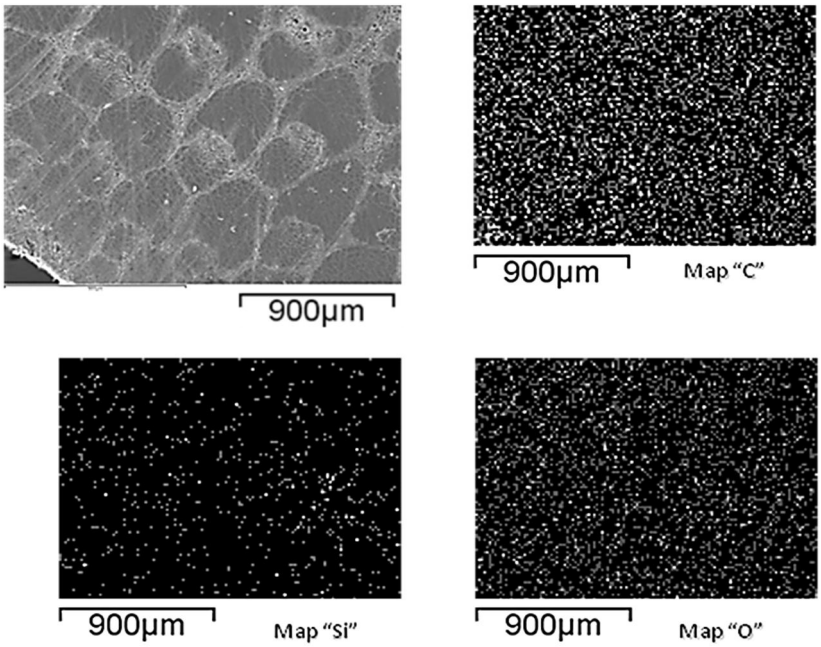

Figure 6-28. Elemental composition analysis of a section of the inner part of Guadua.

Concluding remarks.

Techniques for the preparation of Guadua specimens for microscopy could be improved. Several problems were experienced during the preparation of the specimens. The preparation of clean, polished surfaces has been an issue with Guadua specimens due to the hardness of the material resulting from the high content of silica in the outermost layer. The boiling of the specimens contributed to softening the tissues and improved the quality of sections; however, some specimens suffered from micro-cracking evidenced by the detachment of the vascular bundles from the surrounding low density tissue. The quality of surfaces was not significantly improved by using glass knifes on a rotary manual microtome, nor by polishing them with diamond and alumina powder on rotary discs which contaminated the specimen. Embedment of Guadua specimens in resin before sectioning might be a way of improving the quality of section for SEM imaging. Specimens for optical microscopy were embedded in resin and their faces polished.

Through SEM and optical microscopy, imaging of the densification profile of the THM modified samples (B and C) was possible. Densification of the cross section occurred by collapse of the low density material within the Guadua microstructure: void parenchyma cells and conductive tissues (metaxylem vessels, protoxylem and floem). The reduction in cross-sectional area of the foam-like structure formed by this low density material allowed for fibres to get closer, thus increasing the fibre-surface area across the section from 25.53% to 45.47 in sample B and 47.78% in sample C.

Imaging of laminated specimens tested using the shear block method was undertaken with the aim of better understanding the factors affecting the adhesion between Guadua and epoxy resin. Shear failure on these blocks ocurred in the low density material whilst fibres in the glue line remained well bonded to the adhesive.

The presence of silica at cellular level was observed. Preliminary experimentation of the interaction of the silica contained in the cell walls of Guadua and lime (Limeboo) was undertaken to measure levels of adhesion, but the bonding between both materials was extremely weak. The potential interaction between lime and silica for inducing a pozzolanic reaction will require thorough research. Silica cells need to be broken in order to fix lime mortars to the surface.

7. Small scale testing.

Introduction

An experimental plan was devised with the aim of assessing the mechanical properties of small specimens of Guadua before and after thermo hydro mechanical treatments (THM). The elastic parameters of Guadua in the longitudinal (X_1), tangential (X_2) and radial (X_3) directions were evaluated through various testing methods. In some tests, passive strains were recorded and Poisson's ratios in the three directions were evaluated. A total of four elastic moduli (E_1, E_2, E_3 and G_{12}) and four Poisson's ratios (υ_{12}, υ_{21}, υ_{32}, and υ_{13}) were measured. With the exception of the assessment of modulus of rupture (MOR) in bending, strength values were not measured in this study. Longitudinal tensile tests, compression tests, Iosipescu shear tests and three point bending tests were carried out following testing protocols from international standards for wood and bamboo (ISO, ASTM, BS-EN and NTC). Alternative test methods were employed where there were difficulties associated with the production of small clear specimens of Guadua according to the standards specifications. The same challenges are faced with bamboos in general due to their small wall thicknesses, curvature and variation in cross sectional density. Samples were classified as class A, B or C, depending on the treatment undertaken. Sample A was the untreated control material. Sample B was thermo-mechanically (TM) treated from the dry state and Sample C was thermo-hydro mechanically (THM) treated from the pre-soaked condition in an open system. A description of the experimental methods and tests results are presented in this section. Results obtained in this part of the research will be used for the prediction of the mechanical properties of G-XLam Guadua panels and their simulation with finite element models.

7.1 Specimen preparation

Selection and preparation of the material for all the tests followed the same procedure defined by the ISO standard 22157-1 (ISO, 2004a). Mature and dried *Guadua angustifolia* Kunth (Guadua) strips from the middle region of the plant were cut and machined to the required shapes and dimensions as seen in Figure 7-1.

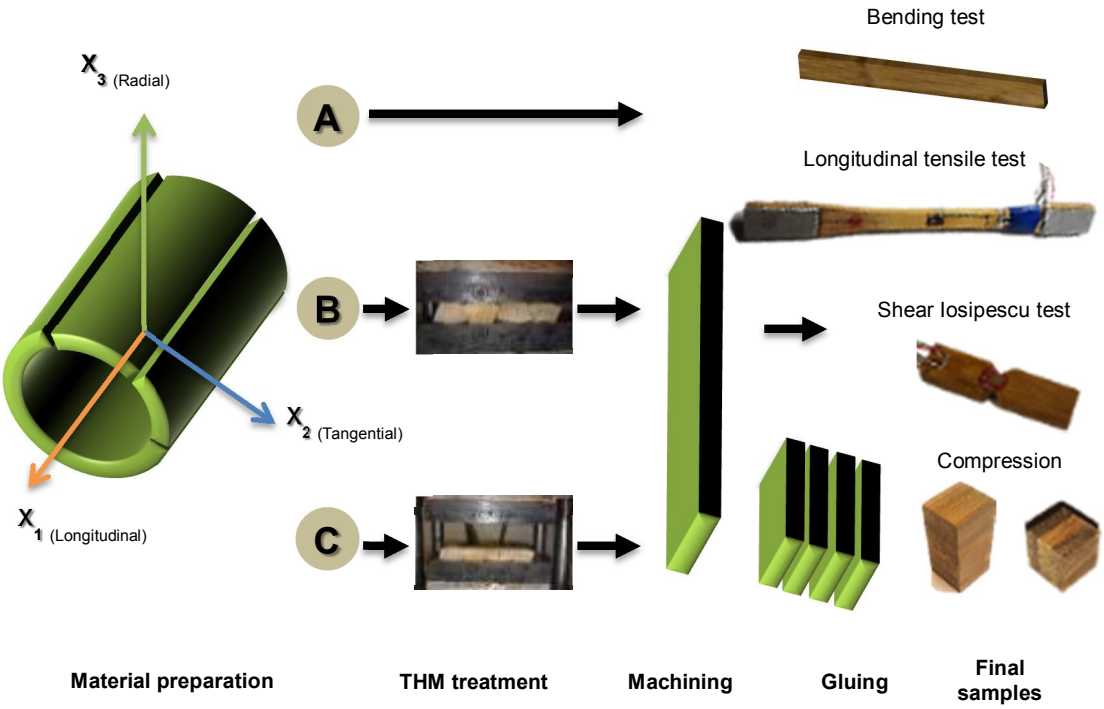

Figure 7-1. Specimens selection and preparation for mechanical testing.

Sample A was untreated and used as control for the different testing procedures. Sample B and C were subjected to the THM treatments previously described in Section 5.5.

Following preparation, all the specimens of Guadua were oven-dried at 105°C and subsequently stored at a controlled temperature (27°C ± 2°C) and relative humidity (70±5 %) in a conditioning room, enabling them to reach equilibrium at 12% moisture content. In order to calculate their average density, dimensions and weight of each specimen were checked prior to testing with digital callipers and scales, respectively. Table 7-1 summarizes the treatments and resulting oven dried densities for each sample. For the shear-Iosipescu and compression tests, rectangular sections of Guadua were glued together using an epoxy resin (Sicomin SR 5550) with the aim of achieving adequate sections for the application of loads along the tangential (X_2) and radial (X_3) axes.

Table 7-1. Specification of the Guadua samples used for the tensile, compression, shear and bending tests.

Bamboo species: *Guadua angustifolia* Kunth		Section: Middle (in height)		Age: Mature (3-5 years old)
		Samples A Raw un-processed	Samples B TM densified	Samples C THM densified
Time		0	20 min	20 min
Pressure		0	5.8 MPa	5.8 MPa
Temperature		0	150°C	150°C
Compression set (C_s) (Mean)		0	46.08%	42.51%
Oven dried density	Mean	543.3 kg/m³	814.6 kg/m³	890.9 kg/m³
	St. dev.	11.60	63.09	91.79
	CoV	2.14%	7.75%	10.30%

7.2 Longitudinal Tensile test.

A longitudinal tensile test was carried out along the X_1, L (longitudinal) direction and strain measured in this direction. As seen in Figure 7-2 during the same test, passive strains in the X_2 and X_3 directions (radial and tangential, respectively) were also recorded. Young's modulus and Poisson's ratio (υ) were calculated from the experimental data.

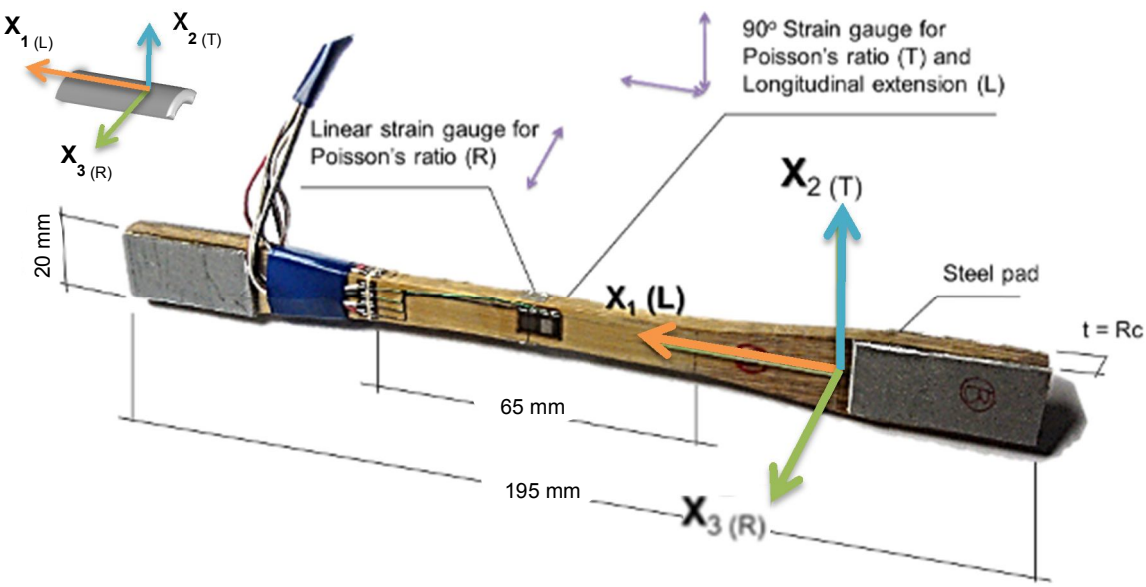

Figure 7-2. Longitudinal tensile test specimen with dimensions and orthotropic and geometric axes.

7.2.1 Materials and methods

TM and THM treated (B & C) and non-treated (A) samples of small clear specimens of Guadua were prepared following ISO (2004b). The longitudinal tensile test procedure and determination of Young's modulus followed standards for testing small clear specimens of

wood from BS 373 (BSI, 1957) and BS EN 408 (BSI, 2010). The average cross sectional area at the middle of the specimen for all the samples was 66.82±3.63mm^2 with a CoV of 5.44%. Micro-strain gauges, with a grid resistance of 350.0±0.2% ohms, were attached to both faces and sides of the specimens for measuring the deformation (Figure 7-2 & 7-3 a, b); and the electrical signal was recorded continuously during loading. In materials with high specific heat capacity such as wood and bamboo, these gauges are preferred to 120 ohms gauges, because heat generation is reduced by three fold for the same voltage applied thanks to their high resistance (Micro-Measurements, 2014). Their use is also recommended by ASTM (1998).

Three specimens of samples A, B and C were used for the test and five loading repetitions below the proportional elastic limit were carried out (a control specimen from sample A was tested to failure to determine the maximum load and the proportional limit). Individual specimens were numbered from one to three (e.g. A1, A2, A3 and B1, B2, etc.). The effect of the presence of internodes was neglected as the material for the proposed Cross-Laminated Guadua (G-XLam) panels is considered to be an orthotropic continuum flat sheet with symmetry axes identified (Bodig & Jayne, 1982); thus, the presence of defects and nodes is dispersed and is assumed to have a negligible effect when laminated.

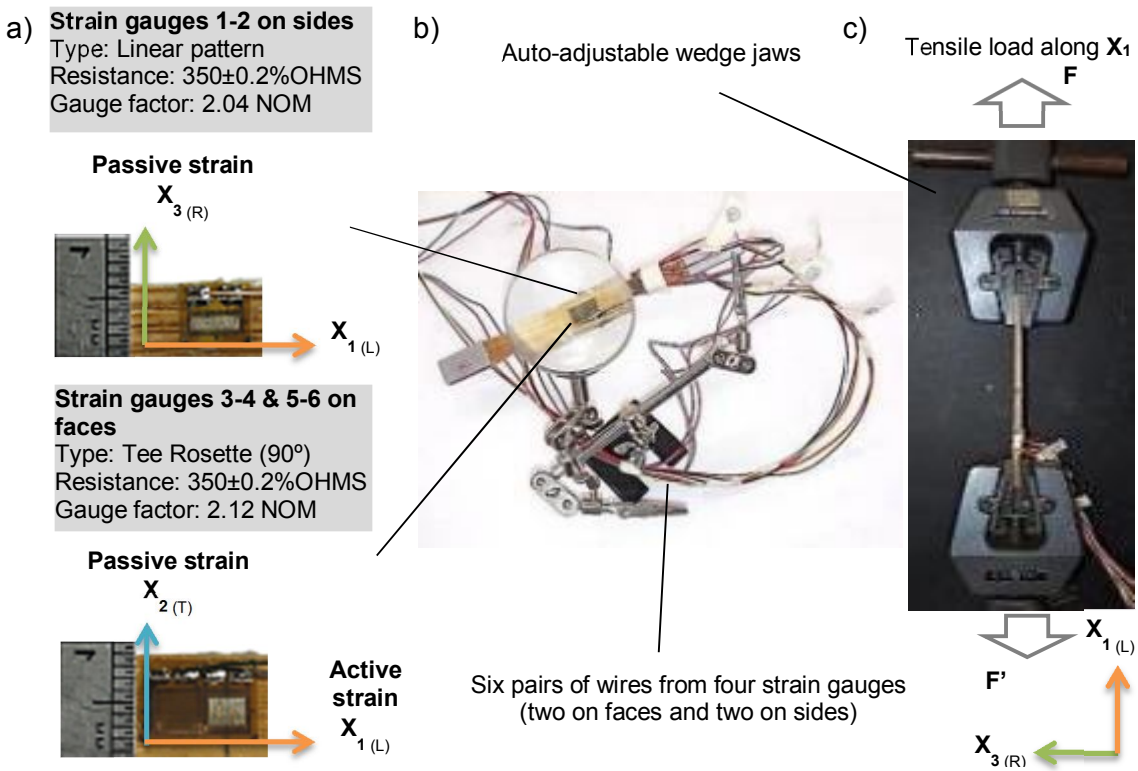

Figure 7-3. a) Strain gauges attached to the test specimen and used for strain measurement. b) Test specimen wired and ready for testing. c) Final test set up on the testing machine.

An INSTRON 5585H floor model testing machine with a 200kN load cell (Figure 7-3c) was used for the tensile tests and a Vishay System 6000 (Model 6100) Data Logger was used to record the data from the micro-strain gauges. The rate used for the test was 0.5mm/min, which complied with the standard's requirement of reaching maximum load within 300±120s, and avoided creep. Steel pads were glued to the ends of the specimen to improve the grip in the self-tightening wedge jaws.

For the determination of Young's modulus and Poisson's ratio of samples A, B and C, the load-deformation response was plotted and a section between 0.3kN and 3.0kN was used for linear regression analyses. This portion of the graph corresponded to the section between 10% and 40% the maximum load ($\boldsymbol{F}_{\max}$) of the control sample and was used for all the samples (Figure 7-4).

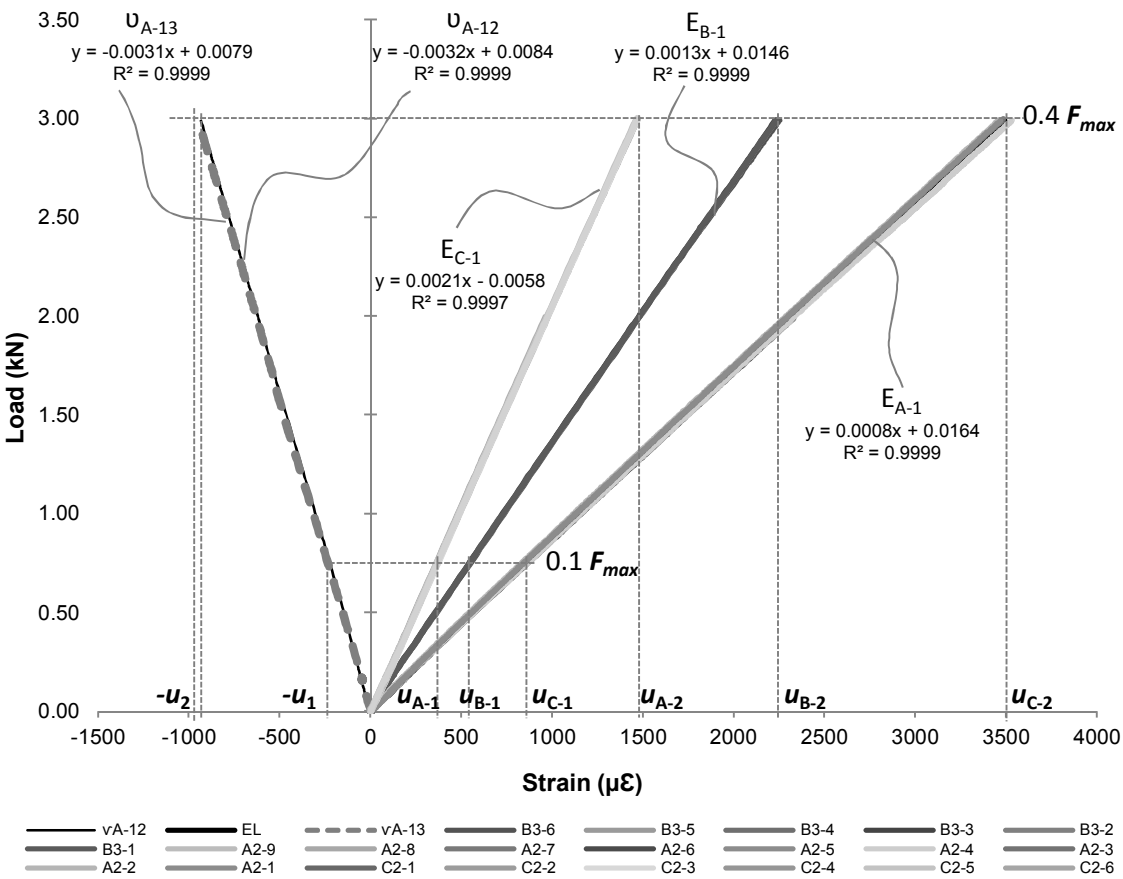

Figure 7-4. Typical initial load-strain graph for samples A, B and C under longitudinal tensile test. The portion of the graph between 0.1 $\boldsymbol{F}_{\max}$ and 0.4 $\boldsymbol{F}_{\max}$ was used for the linear regression analyses and values within this portion and a correlation coefficient $R^2 \geq 0.99$ were used for calculating υ_{13}, E_{12} and υ_{12} for all samples.

From the load-strain graph in Figure 7-4, a steady linear behaviour (gradient) with a correlation coefficient $R^2 \geq 0.99$ was obtained for samples A, B and. Equation 7-1 was then employed for calculating the Young's modulus from the resulting stress and strain values:

$$E_t = \frac{(F_2 - F_1)}{(u_2 - u_1) \cdot A} \qquad 7\text{-}1$$

where
$(F_2 - F_1)$ is the increase of load between 0.1 $\boldsymbol{F}_{\max}$ and 0.4 $\boldsymbol{F}_{\max}$
and $(u_2 - u_1)$ is the increase of deformation corresponding to $(F_2 - F_1)$ using the linear regression line.

Poisson's ratio (υ) is defined as the ratio of passive strain to active strain. Thus, υ_{12} was obtained from the ratio of passive strain along the tangential direction (X_2) to active strain along the longitudinal direction (X_1). Similarly, υ_{13} was calculated as the ratio of passive strain along the radial direction (X_3) to active strain along X_1. These are denoted by:

$$\upsilon_{12} = -\frac{\varepsilon_2}{\varepsilon_1} \qquad 7\text{-}2$$

Poisson's ratio in the 1-2 plane caused by a load applied along X_1.

$$\upsilon_{13} = -\frac{\varepsilon_3}{\varepsilon_1} \qquad 7\text{-}3$$

Poisson's ratio in the 1-3 plane caused by a load applied along X_1.

As can be seen, the first figure subscript indicates the direction of the applied stress and the second figure the direction of the resulting deformation. The same notation system is used along this document.

7.2.2 Results and discussion

Determination of E_1, υ_{12} and υ_{13} by tensile testing along X_1.

As in the case for timber, issues regarding the natural variability of bamboo and its anisotropy complicate characterization of its mechanical properties. Bamboo also shows viscoelastic behaviour (Obataya *et al.,* 2007) and behaves semi-plastically at high strain. However, none of the Guadua samples A, B and C under test experienced high strain, as the elastic limit of the material was not exceeded. Overall, the initial stress-strain gradient for all

the samples was constant and permanent deformation was avoided. The variation of Young's modulus and Poisson's ratio by unit of density for samples A, B and C are shown in Figure 7-5a & b. The higher volume fraction of the densified samples B and C resulted in much higher values of tensile elastic moduli for these TH and THM treated samples of Guadua.

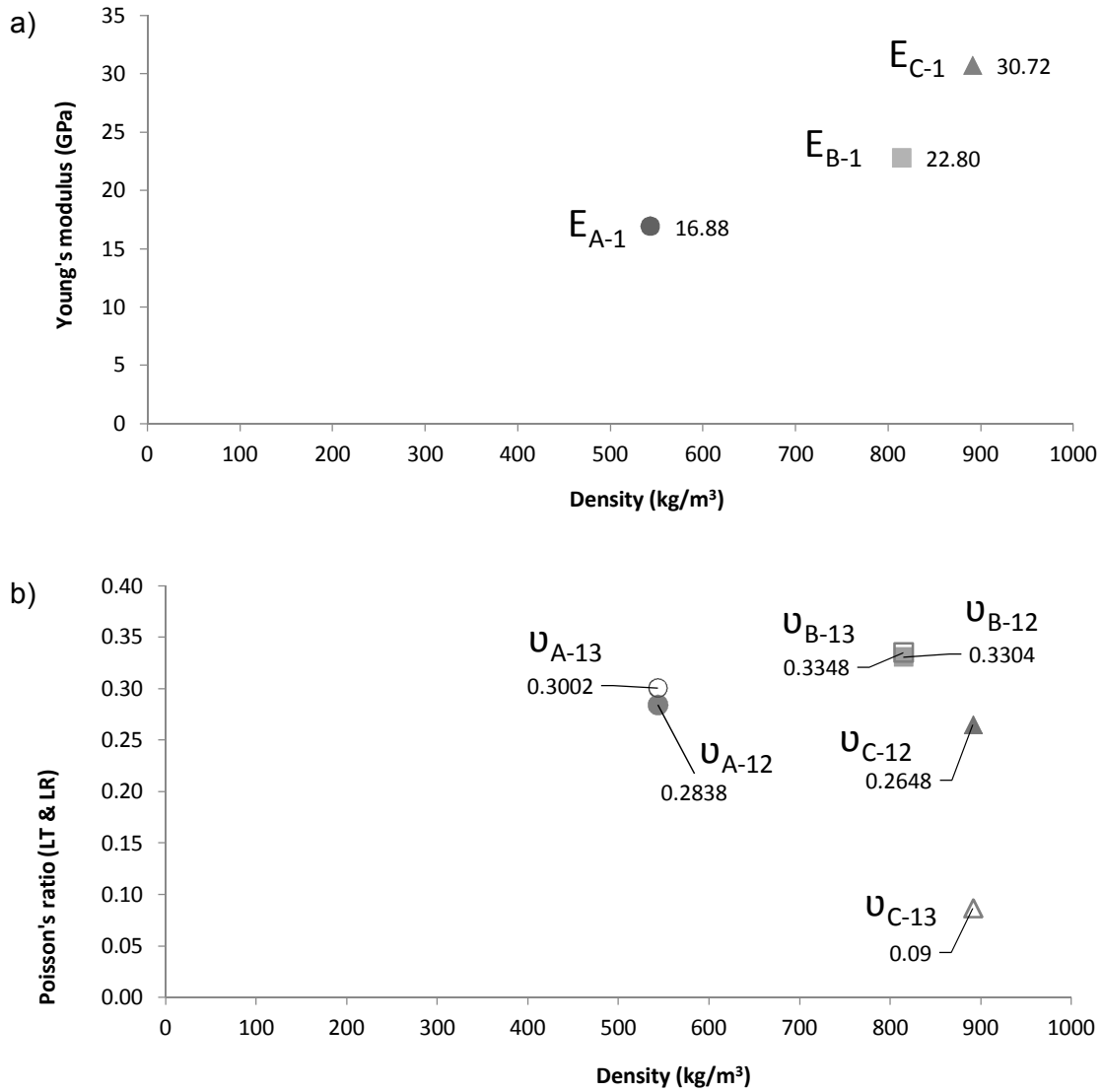

Figure 7-5. Elastic results from longitudinal tensile test. a) Young's modulus versus density for samples A, B and C. b) Poisson's ratio versus density for samples A, B and C.

Results for Young's modulus longitudinal to the direction of the fibres (E_1) for sample C showed an increase of almost two fold compared to the value of the control sample (A). Despite the small difference in the average density between samples B and C, a significant increase in the Young's modulus values for sample C indicates effective plasticization of

Guadua resulting in a densified profile with improved mechanical properties. Thus, the specific stiffness for THM treated Guadua has also increased. Table 7-2, 7-3 and 7-4 present the resulting values E_1, υ_{12} and υ_{13}, respectively, including mean values, standard deviation (st. dev) and CoV values. These figures are the result of the five loading cycles to which the three specimens on each sample (A, B and C) were subjected. Whilst Figure 7-6 and 7-7a and 7-7b present the same values including means, maximums and minimums in box & whisker plots.

Table 7-2. Result for elastic modulus in tension (Young's modulus) of samples A, B and C.

$E_t = \frac{(F_2 - F_1)}{(u_2 - u_1)A}$		No.	E_t (GPa)	St. dev.		No.	E_t GPa)	St. dev.		No.	E_t (GPa)	St. dev.
E_1 Tens	E_{A1}	A1	15.95	1.33E-04	E_{B1}	B1	24.26	0.70	E_{C1}	C1	34.09	7.24E-04
		A2	13.19	0.46		B2	21.34	0.69		C2	30.98	0.74
		A3	21.49	0.35		B3	22.80	0.79		C3	27.10	0.00
Mean			**16.88**				**22.80**				**30.72**	
St. dev.			0.33				0.73				0.43	
CoV			2%				3.2%				1. 4%	
Density (ρ)	(mean)		**543.3 kg/m³**				**814.6 kg/m³**				**890.9 kg/m³**	
	St. dev.		11.60				63.09				91.79	
	CoV		2.14%				7.75%				10.30%	
Spec. Stiffness			**31.06 m²/s²**				**27.99 m²/s²**				**34.49 m²/s²**	

Table 7-3. Poisson's ratio results for samples A, B and C.

$\upsilon_{12} = -\frac{\varepsilon_2}{\varepsilon_1}$		No.	υ_{12}	St. dev.		No.	υ_{12}	St. dev.		No.	υ_{12}	St. dev.
υ_{12}	υ_{A12}	A1	0.26	3.03E-05	υ_{B12}	B1	0.29	0.01	υ_{C12}	C1	0.31	3.14E-03
		A2	0.28	0.02		B2	0.38	0.01		C2	0.25	5.43E-03
		A3	0.31	4.26E-03		B3	0.33	0.01		C3	0.24	3.70E-03
Mean (μ)			**0.28**				**0.33**				**0.26**	
St. dev.			0.01				0.01				4.20E-03	
CoV			3%				4%				2%	

Table 7-4. Poisson's ratio results for samples A, B and C.

$\upsilon_{13} = -\frac{\varepsilon_3}{\varepsilon_1}$		No.	υ_{13}	St. dev.		No.	υ_{13}	St. dev.		No.	υ_{13}	St. dev.
υ_{13}	υ_{A13}	A1	0.30	0.01	υ_{B13}	B1	0.26	0.01	υ_{C13}	C1	0.28	0.01
		A2	0.30	0.02		B2	0.43	0.02		C2	-0.04	0.02
		A3	0.31	0.02		B3	0.32	0.01		C3	0.01	4.55E-03
Mean (μ)			**0.30**				**0.33**				**0.09**	**0.28***
St. dev.			0.02				0.02				0.02	0.01*
CoV			5%				5%				18%	3.39%*

* Results for specimen C1.

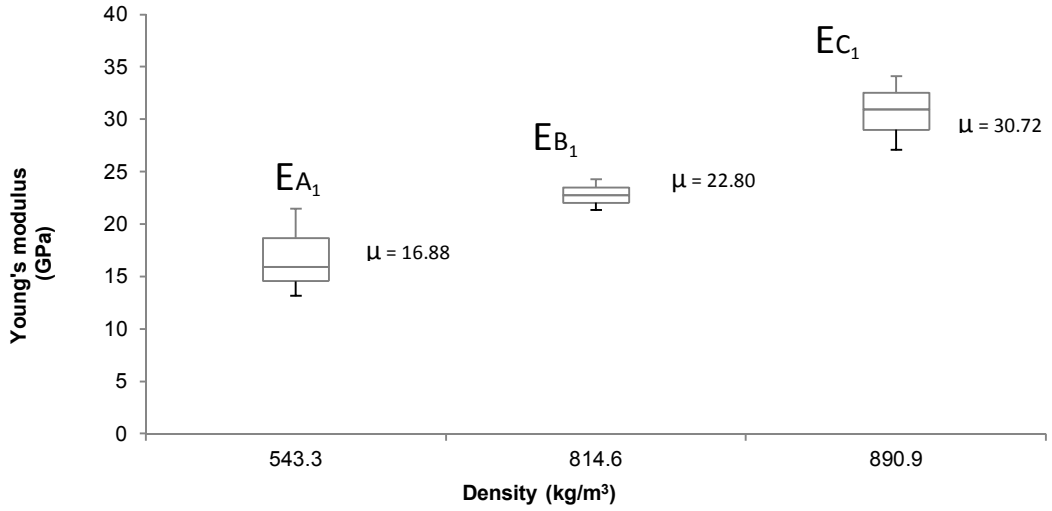

Figure 7-6. Box plot of the Young's modulus longitudinal to the direction of the fibres ($\boldsymbol{E_1}$) of samples A, B and C.

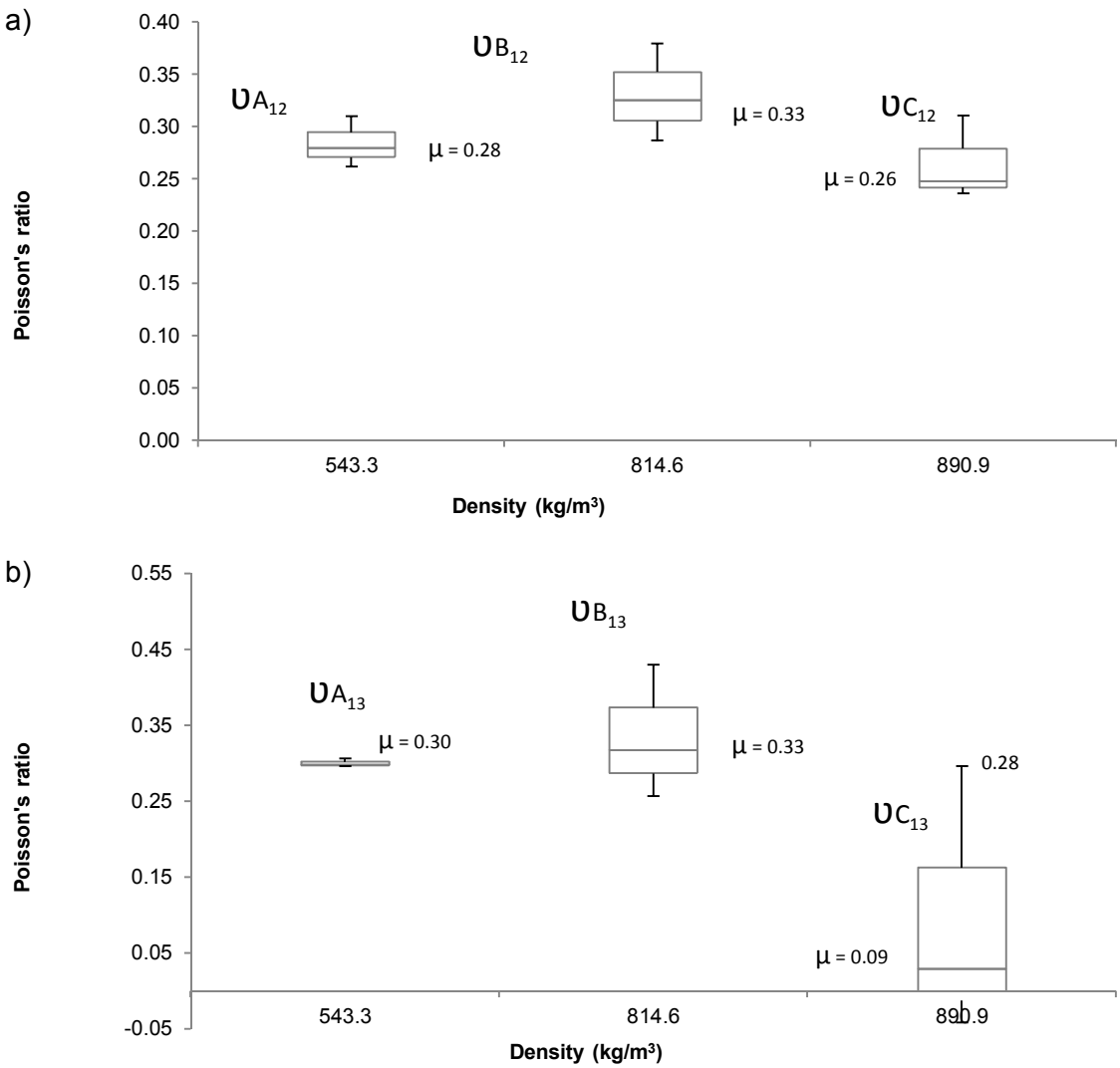

Figure 7-7. Box plots of the Poisson's ratios υ_{12} (a) and υ_{13} (b) of samples A, B and C.

Overall, Poisson's ratios υ_{12} and υ_{13} presented similar values. Despite a significantly low mean υ_{13} value for sample C, no significant effect of the densification process in the Poisson's ratio was observed for sample B (A is the control).

As can be seen in Table 7-4 Poisson's ratios for specimens C2 and C3 are extremely low, which might be due either to flaws on the coupling of the strain gauges to the specimen's surface or data recording. High dispersion of υ_{13} results for specimens C2 and C3 was found during the analysis of the individual cycles (CoV = 60% and 26%, respectively), which evidences test-procedure issues. In contrast, specimen C1 presented a low CoV ~ 4% (figures with asterisk in Table 7-4).

Although in statistical terms the sample size used for this test was very low, the value of radial Poisson's ratio (υ_{13}=0.28) obtained for specimen C1 is more representative of the actual response of the material and will be used for further analysis. Furthermore, values for the tangential (υ_{13}) and radial Poisson's ratio of samples A, B and C were similar to those reported in the literature (Ghavami & Marinho, 2005; Osorio-Saraz *et al.,* 2007) for non-densified Guadua samples.

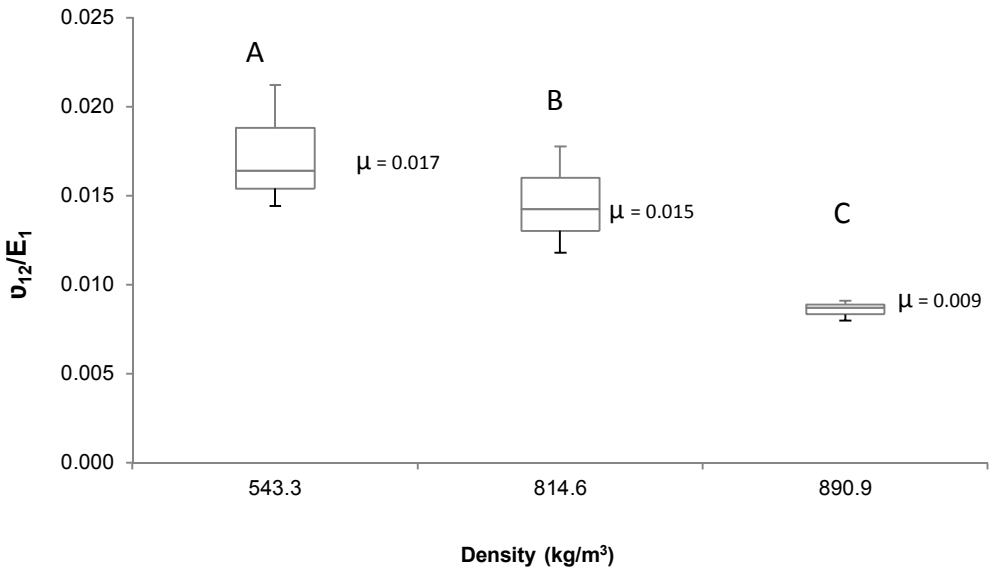

Figure 7-8. Box plot of the ratio of Poisson's ratio to Young's modulus

The ratio of Poisson's ratio to Young's modulus (υ_{12}/E_1), which is used in the comparison of the elastic properties of orthotropic materials decreased with the increase in density. This densification is dependent on the TH or THM treatment applied to the material. Figures of υ_{12}/E_1 for samples A, B and C were 0.017, 0.015 and 0.009, respectively (Figure 7-8).

7.3 Compression test

Elastic parameters E_2 & E_3 of densified (B & C) and non-treated (A) samples of Guadua along the tangential (X_2) and radial directions (X_3) were assessed by compression tests. Passive and active strains were recorded and Poisson's ratios along the longitudinal and the tangential axes resulting from the compressive stresses applied along X_2 and X_3, respectively (υ_{12} and υ_{32}) were calculated.

7.3.1 Materials and methods

Material preparation followed the process described in Section 7.1. Rectangular strips of samples A, B and C were sanded to an average thickness of 5±0.5 mm and bonded using a high performance epoxy resin for wood (Sicomin SR 5550). Radial specimens consisted of five strips, whilst tangential were comprised of three strips which resulted in a shorter specimen height. This counteracted the effects of the natural curvature of the material and ensured a near-to-natural cross-section, particularly for samples A. Thin rigid glue lines were obtained by fastening the strips using manual clamps. Once the resin was set (after 24 hours), the specimens were machined to 17.5±0.5mm regular thicknesses (t) and left to cure in a conditioning room at a temperature of 27°±2°C and relative humidity of 70±5% for a period of 20 days before testing. Care was taken to allow for the upper and lower surfaces to be plane and parallel. Preparation of test specimens and analysis of results followed the standards for wood: BS EN 789 (BSI, 2004) and BS EN 408 (BSI, 2010).

Load was applied along the X_2 and X_3 axes at a rate of 0.5mm/min with an INSTRON 5585H floor model testing machine fitted with a 200kN load cell for the tangential and radial compression tests, respectively. The resulting strains from the attached micro-strain gauges were recorded with a Vishay System 6000 (Model 6100) Data Logger. A total of 18 specimens (three specimens for each condition A, B, and C) were used for both tests and five repetitions below the elastic limit were recorded.

Figure 7-9 illustrates the typical specimen size and the test procedure for the compression test along the radial direction (X_3). The three pairs of wires observed in this figure are connected to the three micro-strain gauges with a grid resistance of 350.0±0.2% ohms attached to the specimens. One of them recorded the active strain along X_3 (ε_3) and had a gauge length equivalent to 1/3 the height of the specimen (h/3). This measurement was taken with the aim of averaging the radial deformation across the thickness of two strips and to account for the variation in cross sectional fibre content. The other two strain gauges

registered the passive strain along X_2 (ε_2) and their values were averaged for the calculation of the resulting Poisson's ratio along the tangential direction caused by the stress applied along X_3 (υ_{32}). Details of the compression test along the tangential direction (X_2) are presented in Figure 7-10.

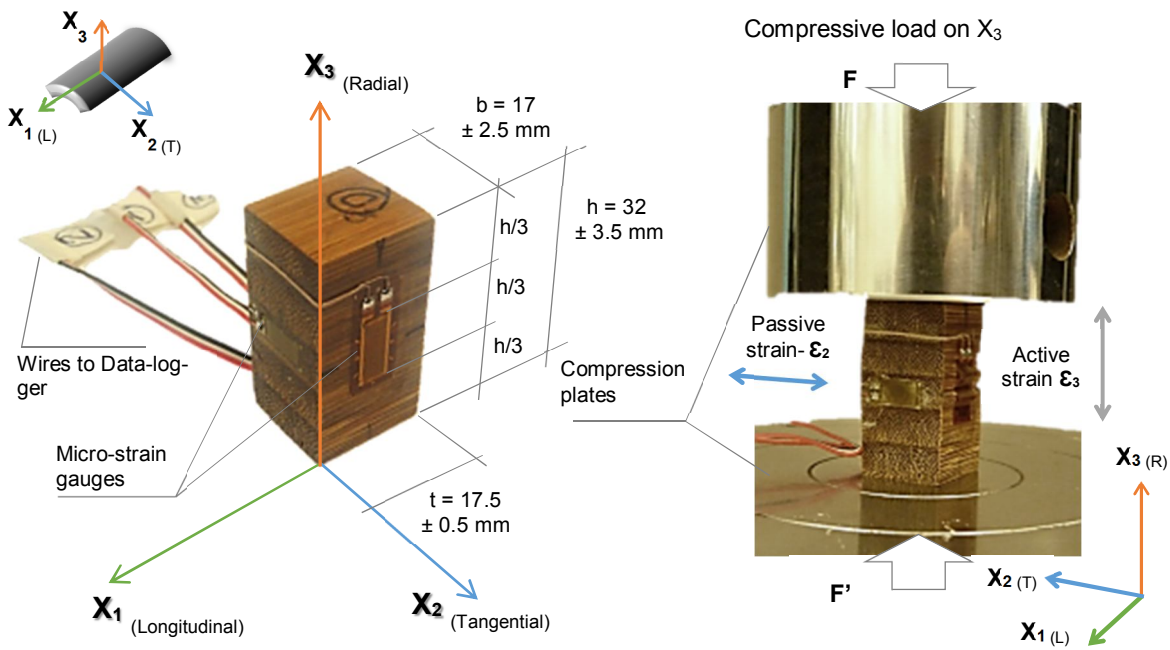

Figure 7-9. Typical specimen size and compression test set up for load applied along the radial direction.

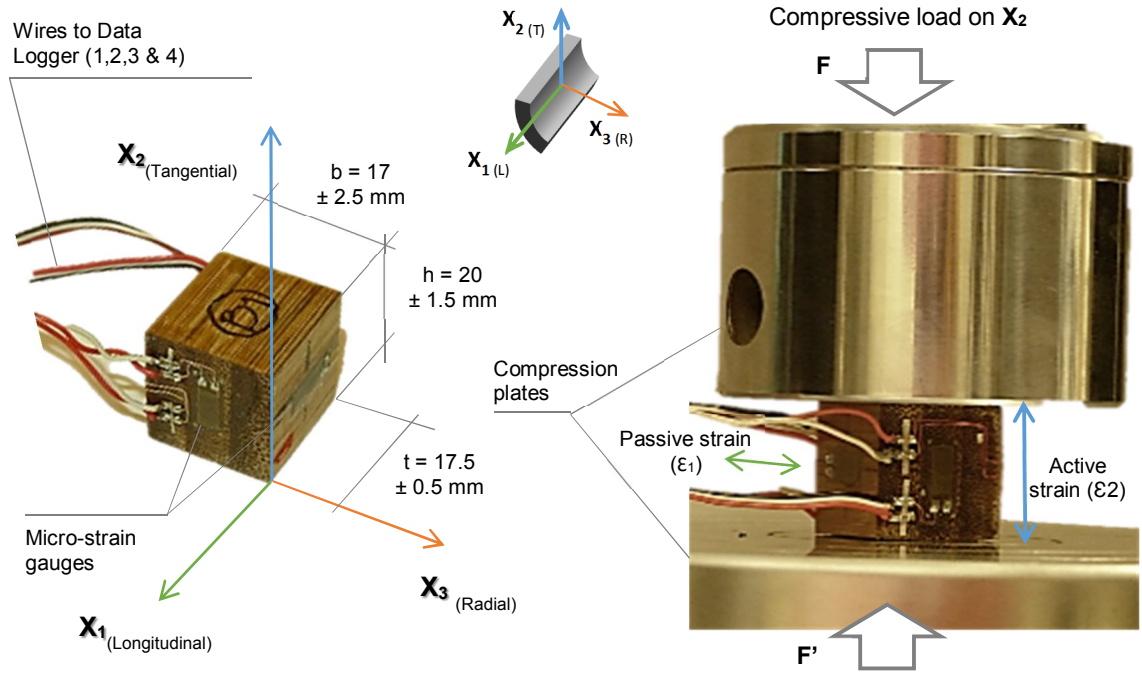

Figure 7-10. Typical specimen size and compression test set up for load applied along the tangential direction.

Four strain gauges were attached to the specimen; two recorded active strain (ε_2) along X_2 and two passive strain (ε_1) along X_1. Strain values were averaged for the calculation of the tangential modulus of elasticity (E_2) and the Poisson's ratio (υ_{12}) resulting along X_1.

For both tests (tangential and radial compression) active and passive strains results were plotted against stress and graphs such as the one in Figure 7-11 were produced after each test.

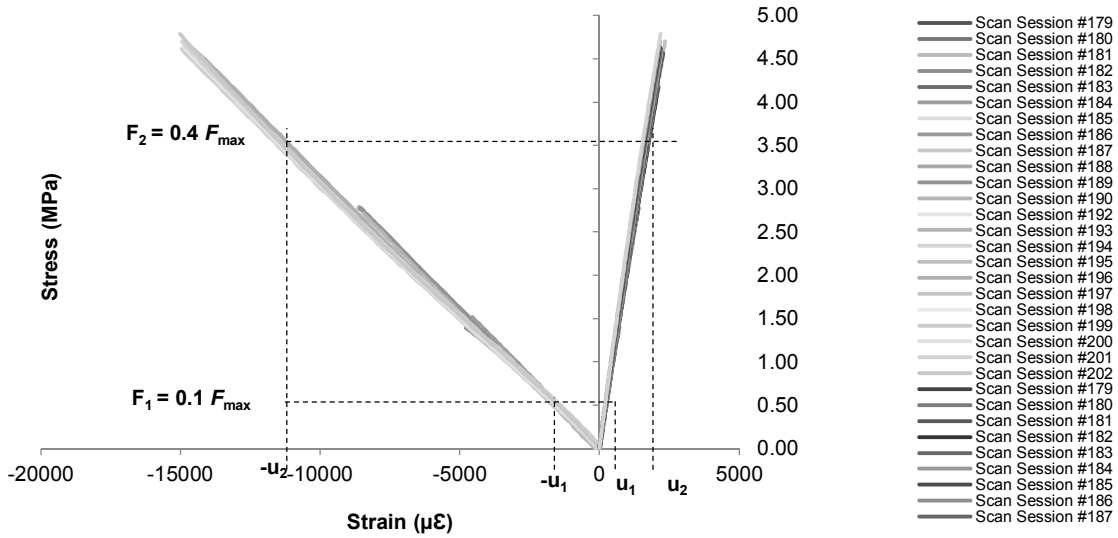

Figure 7-11. Typical strain-stress graph plotted from the results of a radial compression test on specimens of sample C (scan sessions represent the repetitions undertaken).

Elastic values and Poisson's ratios of samples A, B and C were calculated using the strain values $(u_2 - u_1)$ on the linear regression line between $0.1\boldsymbol{F}_{\max}$ and $0.4\boldsymbol{F}_{\max}$. Calculation of the compression modulus of elasticity ($\boldsymbol{E_c}$) followed the formula:

$$E_c = \frac{(F_2 - F_1)}{(u_2 - u_1) \cdot A} \qquad \text{7-4}$$

where
$(F_2 - F_1)$ is the increase of load between $0.1\boldsymbol{F}_{\max}$ and $0.4\boldsymbol{F}_{\max}$
and $(u_2 - u_1)$ is the increase of deformation corresponding to $(F_2 - F_1)$ using the linear regression line.

υ_{21} and υ_{32} resulting from the load applied along the tangential and radial axes, respectively, were also calculated. υ_{21} was defined as the ratio of passive strain along X_1 (ε_1) to active strain along X_2 (ε_2) and υ_{32} as the ratio of passive strain along X_2 (ε_2) to active strain along X_3 (ε_3). Calculations followed typical Equations 7-2 and 7-3 for Poisson's ratio.

7.3.2 Results and discussion

Determination of E_2 and υ_{21} by compression testing along X_2.

Mean results for Poisson's ratio (υ_{21}) and tangential modulus of elasticity in compression (E_2) are compiled in Table 7-5 and 7-6 and illustrated in Figure 7-12 and 7-13.

Table 7-5. MOE results for the compression test of samples A, B and C orientated on the tangential direction (X_2).

		No.	MOE (GPa)	St. dev.		No.	MOE (GPa)	St. dev.		No.	MOE (GPa)	St. dev.
E_2 Comp	E_{A_2}	A1	0.33	9.7E-07	E_{B_2}	B1	1.83	5.4 E-02	E_{C_2}	C1	0.84	7.7 E-06
		A2	0.53	0.17		B2	1.04	3.3 E-06		C2	0.83	2.4 E-06
		A3	0.79	3.5 E-06		B3	1.06	7.9 E-06		C3	0.85	1.1 E-06
Mean (μ)			0.55				1.31				0.84	
St. dev.			0.10				1.34 E-01				1.94 E-03	
CoV			18%				2.5%				5.62E-06%	
Density (ρ)		(mean)	543.3 kg/m³				814.6 kg/m³				890.9 kg/m³	
		St. dev.	11.60				63.09				91.79	
		CoV	2.14%				7.75%				10.30%	
Spec. Stiffness			1.02 m²/s²				1.61 m²/s²				0.94 m²/s²	

Table 7-6. Poisson's ratio results for the compression test of samples A, B and C orientated on the tangential direction (X_2).

$\upsilon_{21} = -\varepsilon_2/\varepsilon_1$		No.	υ_{21}	St. dev.		No.	υ_{21}	St. dev.		No.	υ_{21}	St. dev.
υ_{21}	υ_{A21}	A1	0.01	2.2E-04	υ_{B21}	B1	0.03	1.2E-03	υ_{C21}	C1	0.007	2.7E-04
		A2	0.02	9.7E-03		B2	0.01	1.5E-03		C2	0.013	1.1E-03
		A3	0.03	4.9E-03		B3	0.02	2.9E-03		C3	0.001	3.1E-04
Mean (μ)			0.02				0.02				0.01	
St. dev.			6.27E-03				1.99E-03				6.84E-04	
CoV			32%				13%				10%	

In average E_2 of modified TM and THM samples (B and C, respectively) increased by almost a factor of two with the increase on density when compared to the non-modified sample (A); however, this increase was not proportional. Mean values of E_2 and specific stiffness for sample B with a density of 814.6kg/m^3 were 56% and 70% higher than those of sample C, respectively, which had a slightly higher density: 890.9 kg/m^3.

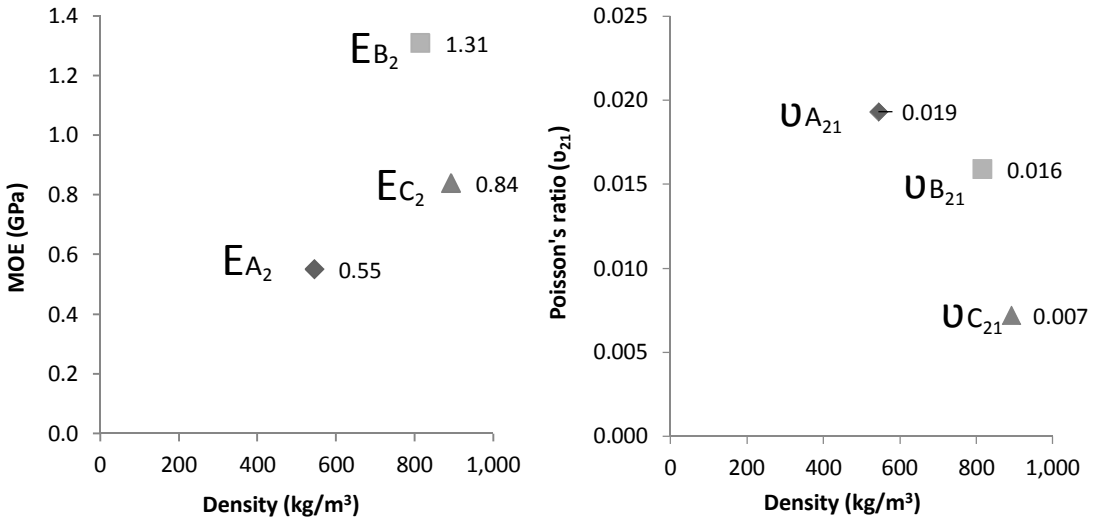

Figure 7-12. Characteristic values of E_2 and υ_{21} versus density for samples A, B and C.

Furthermore, results for E_2 and υ_{21} of samples A and B showed significant variability (CoV ranged from 2% to 18% for the former and 13% to 32% for the latter), whilst these two properties (E_2 and υ_{21}) in sample C exhibited a more stable behaviour (Figure 7-13) with negligible to moderate variability, (5.62E-06% and 10%, respectively).

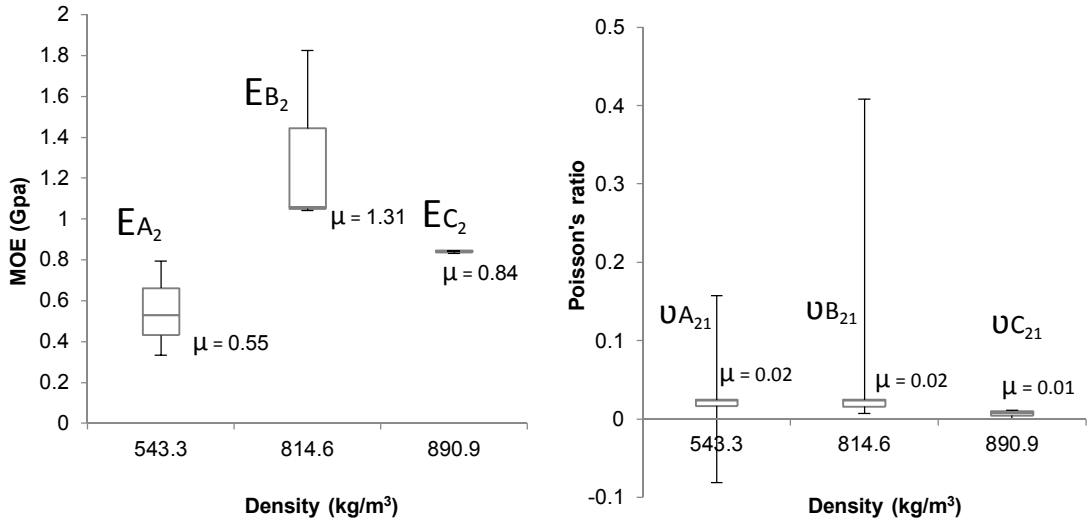

Figure 7-13. Box-plots of E_2 and υ_{21} for samples A, B and C versus density.

Values for the ratio of Poisson's ratio to modulus of elasticity (υ_{21}/E_2) showed a significant decrease with the increase in density (Figure 7-14); ratios υ_{21}/E_2 for samples A, B and C with densities of 543.3kg/m^3, 814.6kg/m^3 and 890.9kg/m^3 were 0.035, 0.015 and 0.009, respectively. The ratio modulus of elasticity along the tangential direction to density, namely specific stiffness (E_2/ρ) of samples A and C presented comparable results (1.02 and 0.94,

respectively), despite an increase of about two fold on the mean elastic properties of sample C. Sample B presented an increase on the specific stiffness of about 70%.

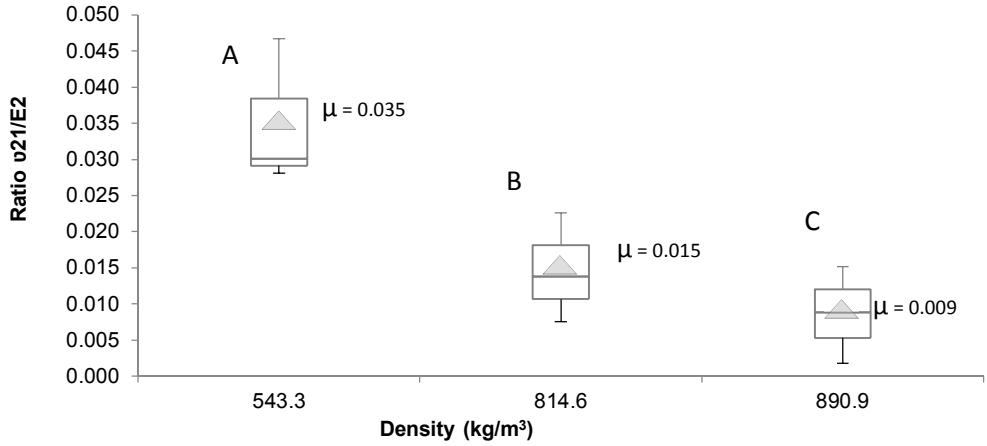

Figure 7-14. Box plot of the ratio of Poisson's ratio to modulus of elasticity (υ_{21}/E_2) and density.

- Determination of E_3, and υ_{32} by compression testing along X_3.

In contrast to the elastic values along the tangential direction (E_2), the elastic modulus of samples along the radial direction (E_3) and Poisson's ratio along the tangential direction as a result of the radial load applied (υ_{32}) decreased with increased density (Figure 7-15). Values for specific stiffness also decreased (Table 6-7). Poisson's ratio υ_{32} of the control sample (A) was about 42 times higher than sample B, which was negative (-0.0035) and almost three fold the value of the Poisson's ratio of sample C (Table 7-8).

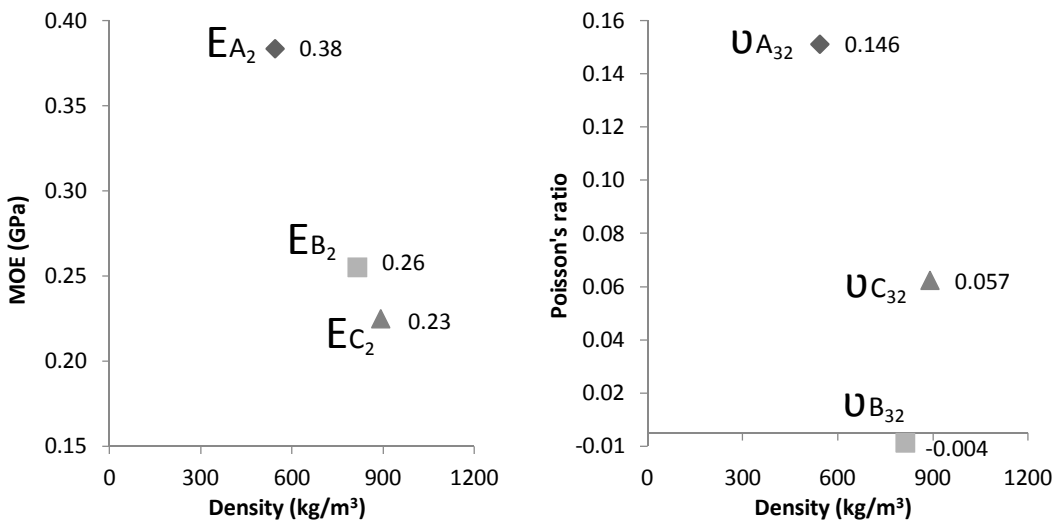

Figure 7-15. Characteristic values of E_3 and υ_{32} versus density for samples A, B and C.

Table 7-7. MOE results for the compression test of samples A, B and C orientated on the radial direction (X_2).

		No	MOE (GPa)	St. dev.		No.	MOE (GPa)	St. dev.		No.	MOE (GPa)	St. dev.
$E_{3\,Comp}$	E_{A_3}	A1	0.62	5.8E-06	E_{B_3}	B1	0.23	1.4E-02	E_{C_3}	C1	0.28	4.0E-07
		A2	0.22	1.1E-02		B2	0.25	1.7E-06		C2	0.24	1.4E-02
		A3	0.31	1.8E-06		B3	0.28	7.4E-07		C3	0.16	1.2E-02
Mean (μ)			0.38				0.26				0.23	
St. dev.			6.2E-03				8.1E-03				1.1E-02	
CoV			1.6%				3.2%				4.61%	
Density (ρ)	(mean)		543.3 kg/m³				814.6 kg/m³				890.9 kg/m³	
	St. dev.		11.60				63.09				91.79	
	CoV		2.14%				7.75%				10.30%	
Spec. Stiffness			0.71 m²/s²				0.31 m²/s²				0.25 m²/s²	

Table 7-8. Poisson's ratio results for the compression test of samples A, B and C orientated on the radial direction (X_2).

$\upsilon_{32} = -\varepsilon_3/\varepsilon_2$		No	MOE (GPa)	St. dev.		No.	MOE (GPa)	St. dev.		No.	MOE (GPa)	St. dev.
υ_{32}	υ_{A32}	A1	0.25	2.1 E-06	υ_{B32}	B1	-0.01	1.9E-03	υ_{C32}	C1	0.14	9.0E-03
		A2	0.10	4.9E-03		B2	-0.01	2.6E-03		C2	0.05	7.0E-03
		A3	0.09	1.4 E-06		B3	0.009	2.3E-03		C3	-0.01	7.0E-03
Mean (μ)			0.15				-0.0035				0.057	
St. dev.			2.8E-03				2.3E-03				7.7E-03	
CoV			2%				65.5%				13.5%	

Data for the modulus of elasticity in the radial direction (E_3) had an adequate fit to the linear regression analyses undertaken for each specimen across all the samples (A, B and C); coefficients of determination obtained were above 0.99 ($r^2 \geq 0.99$). The same tendency was obtained for the measured values of Poisson's ratio υ_{32} of samples A and C; however, for sample B the data acquired in some of the test specimens were more disperse and did not have a consistent fit to the regression line ($0.23 \leq r^2 \geq 0.99$). This significant statistical variation is remarked by the significantly high CoV of sample B (65.5%), reflecting inconsistency of results among the specimens tested. Hence, υ_{32} values of samples B do not provide enough confidence for further comparison.

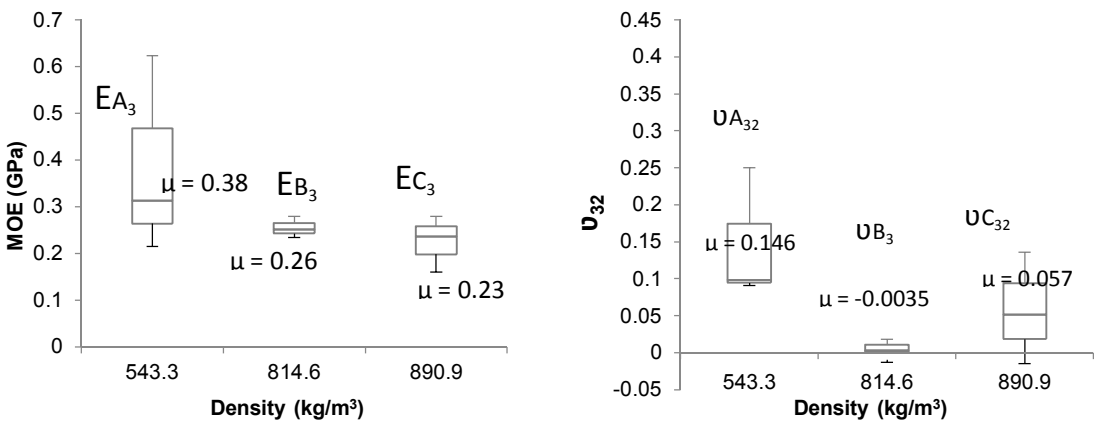

Figure 7-16. Box-plots of E_3 and υ_{32} for samples A, B and C versus density.

The decrease in elastic properties along the radial direction can be be explained by the densification process that pre-stresses the material along the radial direction and rearranges the microstructure of Guadua across the section. It must also be said that unlike wood, radial cells are not present in bamboo and a weaker response to stresses perpendicular to the grain might be expected.

In a state of plane stress were directions X_1 and X_2 are the principal axis for the analysis, the effects of a weak response along X_3 can be safely neglected (Bodig & Jayne, 1982). Elastic properties along the radial axis will be important if the system is subjected to out of plane stress.

The ratio of Poisson's ratio to modulus of elasticity (υ_{21}/E_2) decreased with the increase in density (Figure 7-17); ratios υ_{21}/E_2 for samples A, B and C with densities of 543.3kg/m^3, 814.6kg/m^3 and 890.9kg/m^3 were 0.38, -0.016 and 0.204, respectively. Results for sample B are biased by the inconsistent values of υ_{32}.

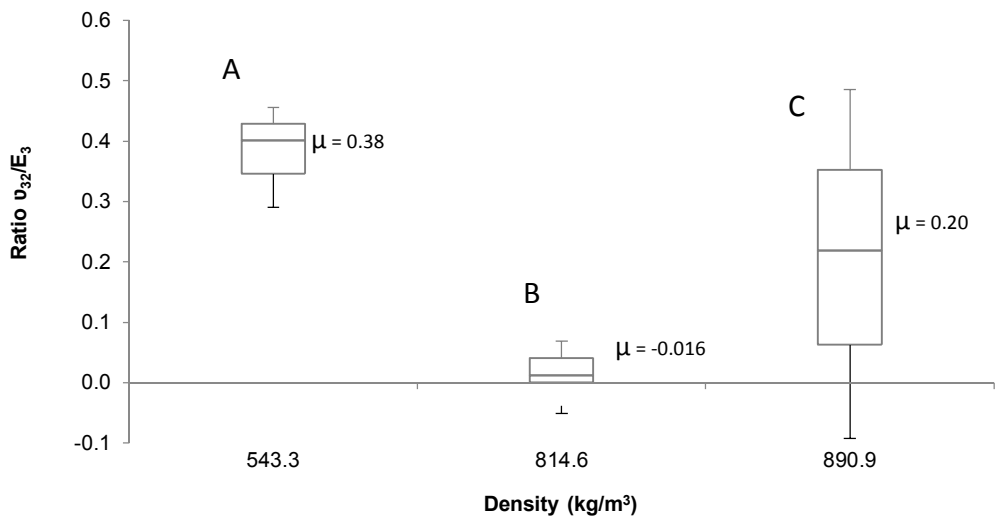

Figure 7-17. Box plot of the ratio of Poisson's ratio to modulus of elasticity (υ_{32}/E_3) and density.

7.4 Iosipescu-shear test

With the aim of assessing the in-plane shear modulus of Guadua samples A, B and C, an Iosipescu-shear test method was selected. Although this test method was originally developed for metals and ceramics, it has been widely used for evaluating the in-plane shear properties of composite materials (ASTM, 1998; Gédiac *et al.,* 1994; Pierron & Vautrin, 1994) and wood (Kubojima *et al.,* 2000; Xavier *et al.,* 2004; Yoshihara *et al.,* 1999), which usually possess anisotropic properties. The Iosipescu-shear test method uses a special test

fixture and assumes a uniform distribution of pure shear stress between two V-notches at mid-length of the specimen. This is due to the action of two opposite loads of equal magnitude applied to the specimen that counteract the resulting moments producing a constant shear force at the specimen's middle section. The shear and bending moment diagrams in Figure 7-18 illustrate this response.

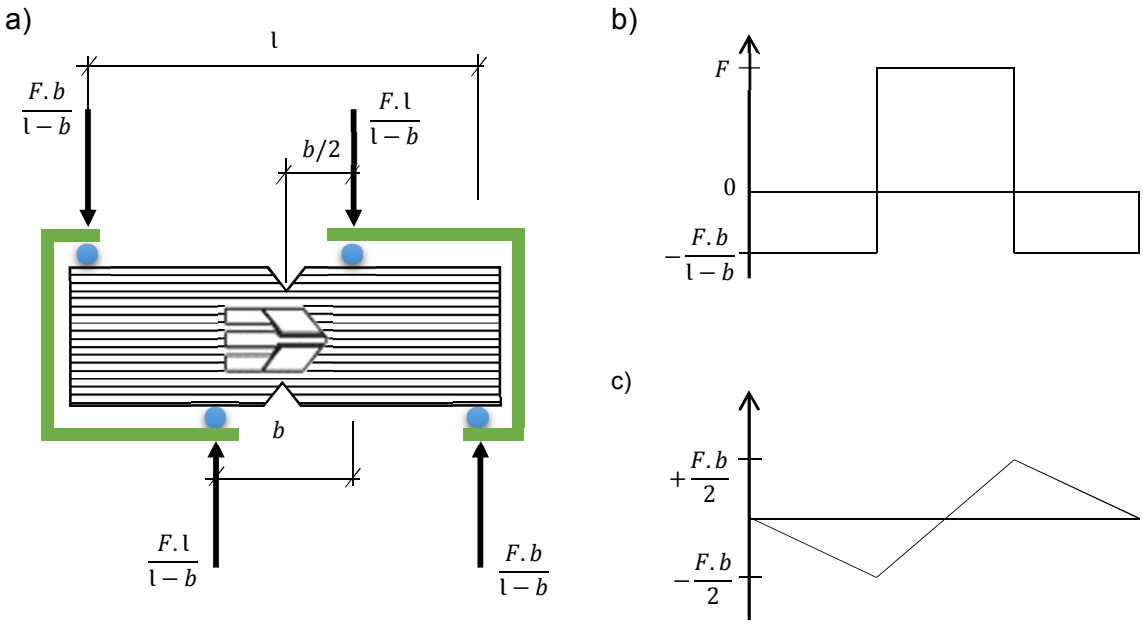

Figure 7-18. Iosipescu-shear test: a) Force diagram, b) Shear diagram and c) Moment diagram.

The cross sectional area under uniform shear stress is defined as the thickness of the specimen multiplied by the distance between the two 90° angle v-notches. Shear strain is measured between these notches by biaxial strain gauges placed on each face of the specimen at mid-length. The shear modulus is then calculated as the ratio of shear strain to shear stress.

The ASTM D5379 (ASTM, 1998) standard states that elastic modulus measurements using the Iosipescu method are overestimated by about 10% in unidirectional fibre reinforced carbon/epoxy composites when tested in the 1-2 plane using specimens with main fibre direction at 0° (along the X_1 axis). Thus, this standard recommends the use of specimens with fibre direction 0°/90° for the determination of in-plane shear modulus of unidirectional materials, which give the most accurate measurement.

Errors in measurements can be introduced due to misalignment of the test fixture, twisting of the specimen and poor specimen preparation (Hodgkinson, 2000). These will affect the uniform distribution of shear stress and introduce transverse tensile stresses at the notch

edge. In order to account for these uncertainties correction factors can be introduced to determine the true shear moduli (Pierron & Vautrin, 1994). However, studies by Xavier *et al.* (2004) and Yoshihara *et al.* (1999) on timber specimens have reported low statistical differences between apparent and true shear modulus. Other studies conducted by Chiang & He (2002) and Hawong *et al.* (2004) have proved through experimental and analytical models that a fairly uniform distribution of shear stress is produced in the central region of the cross-section; which is the area between the 90° angle notches. These results neglect the use of correction factors and provide confidence in the use of the Iosipescu test for determining the shear moduli of anisotropic materials such as wood and bamboo. In addition, the ASTM D 5379 (ASTM, 1998) standard accepts the validity of results when strain values obtained from rosette-type strain gauges located on both sides of the specimens are averaged.

Commonly, the assessment of the shear properties of Guadua is challenging and little research on the subject has been undertaken. Takeuchi-Tam (2004), Ghavami & Marinho (2005) and García *et al.* (2012) have reported shear moduli values that range between 0.58 and 0.644GPa using round culm sections. Shear properties of bamboo using the Iosipescu-shear test fixture have never been reported (including the species Guadua). This is due to the curved geometry of bamboo and small wall thickness; however, in-plane shear modulus of specimens along the direction of the grain can be assessed using the Iosipescu-shear method.

Based on the characteristics of the test procedure and the specimen requirements, the V-notched shear fixture was used to evaluate the shear modulus in the 1-2 plane (G_{12}) were 1-direction denotes the orientation of the fibres and the 2-direction in which the load is applied to the Guadua specimens.

7.4.1 Materials and methods

Iosipescu shear test was undertaken on samples A, B and C of *Guadua angustifolia* Kunth. For the preparation of the specimens, two rectangular strips of A, B and C material were cut and glued longitudinally face to face using an epoxy resin (see Figure 7-1). The faces of the specimens were aligned and manually clamped to guarantee a thin rigid glue line. Following a resin setting time of 24 hours, the specimens were machined to a length and height of ι=72mm and h=17mm, respectively. Subsequently, two 90° angle notches were machined in each specimen to a depth of about 20% of their height (±4 mm). The faces and sides of the specimens were sanded to the dimensions shown in Figure 7-19. This process removed

undesirable impurities to ensure good adhesion of the strain gauges.

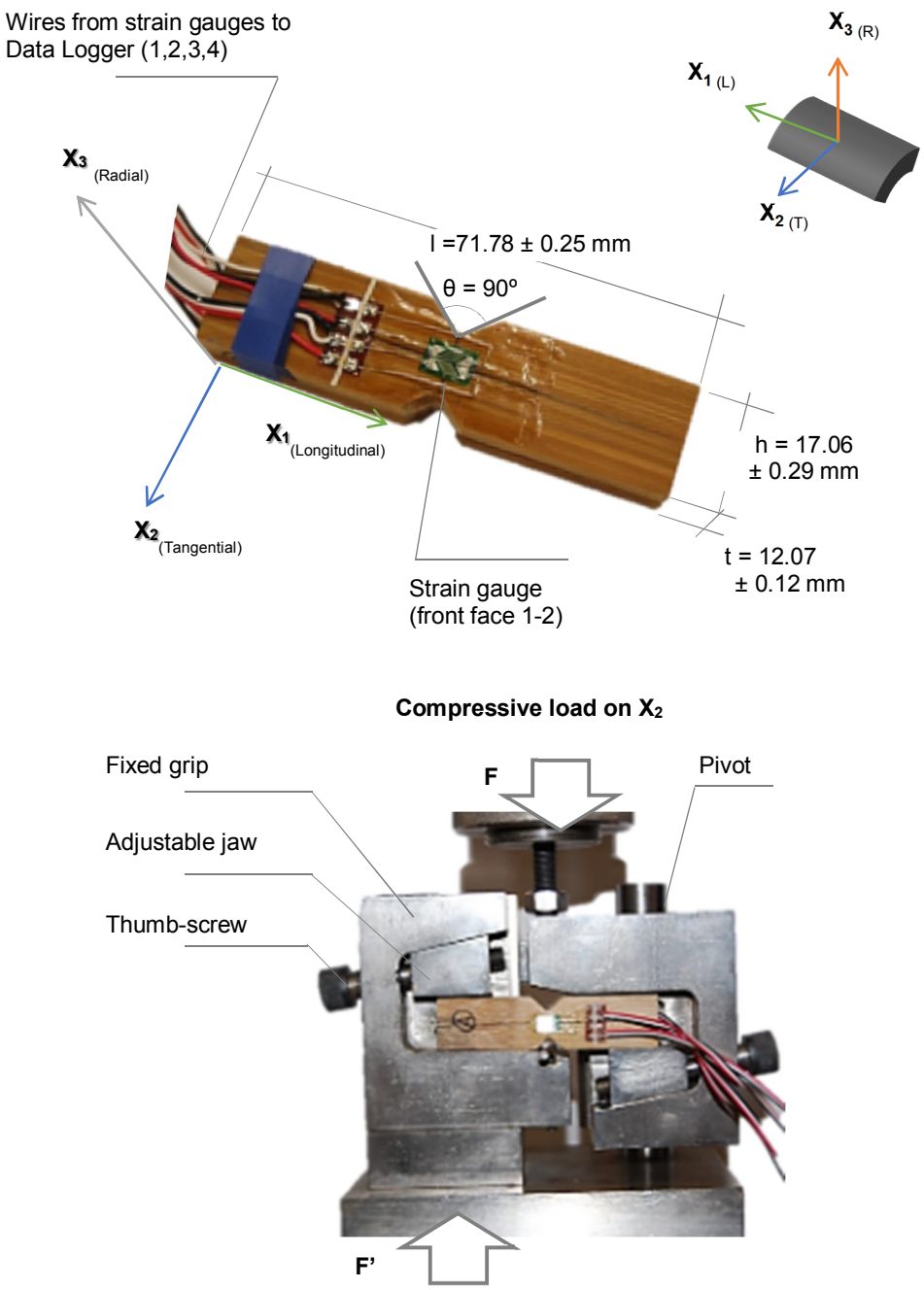

Figure 7-19. Specimens for Iosipescu test (left) and Iosipescu test fixture (right).

Two-element micro-strain gauges with grids at 45° and -45° to the main axis (rosettes) were attached to both faces of the specimens and wired to the data logger. Extreme care was taken to place the gauges at the exact centre (mid-length/mid-height) of the specimens. All the specimens were kept under controlled temperature and humidity before testing in a conditioning room at 27°±2°C and relative humidity of 70±5% for a period of 20 days. In

total four specimens per sample of Guadua (A, B and C) were prepared and strain-gauged; additional trial specimens were used to calibrate the system and set the elastic limit. The final shape of the test specimens and setup of the test using the Iosipescu fixture can be observed in Figure 7-19 and Figure 7-20a. Alignment of the V-notch fixture was controlled to avoid twisting of the specimen and avoid error in the shear strain measurements. Also the specimen thickness (t) was increased to account for any twisting and to avoid the use of bonded tabs or additional aligning procedures.

Strains from the rosette-type strain gauges were recorded separately for front and back faces and +45° and -45° orientations (Figure 7-20b) using a Vishay System 6000 (Model 6100) Data Logger. A total of four pairs of wires were attached to the specimen and the information was recorded on independent channels. Load was applied at a rate of 0.5 mm/min with an INSTRON 5585H floor model testing machine with a 200kN load cell acting along the X_2 axis (Figure 7-20a) and kept below the elastic limit of the material. Several cycles were then run without inducing failure. After each load cycle, the specimens were taken out of the Iosipescu fixture, turned around and loaded again to offset the effects of boundary conditions.

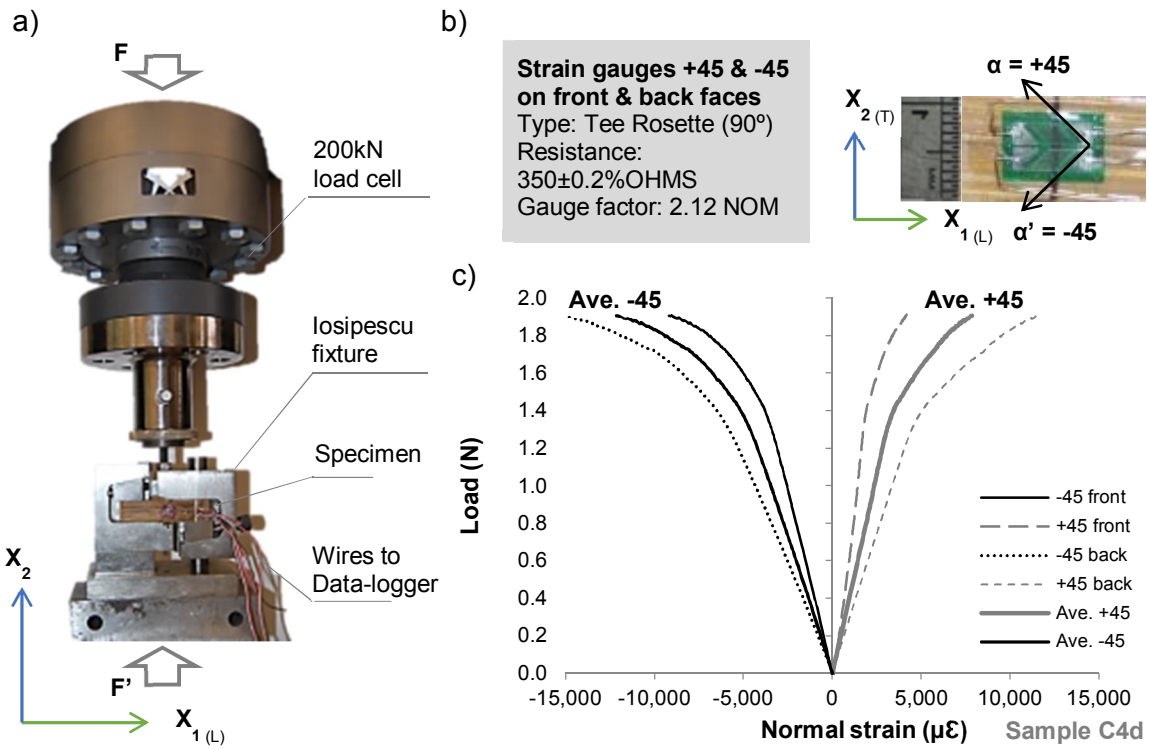

Figure 7-20. a) Iosipescu shear test set-up on INSTRON. b) Specifications of the strain gauge used. c) Typical load-strain graph for +45 and -45 strain gauges readings on front and back faces and their average for both orientations (+45 and -45).

Pairs of strain signals (+45° and -45°) recorded during testing for both faces were plotted against load (Figure 7-20c). Positive and negative normal strain values were averaged to minimise any effects of out-of-plane movement or twisting (Hodgkinson, 2000; Xavier *et al.,* 2004) and shear strain (ϒ) was obtained from the sum of their absolute values (|με 45| + |με -45|). Subsequently, shear strain was plotted against shear stress (τ) (Figure 7-21).

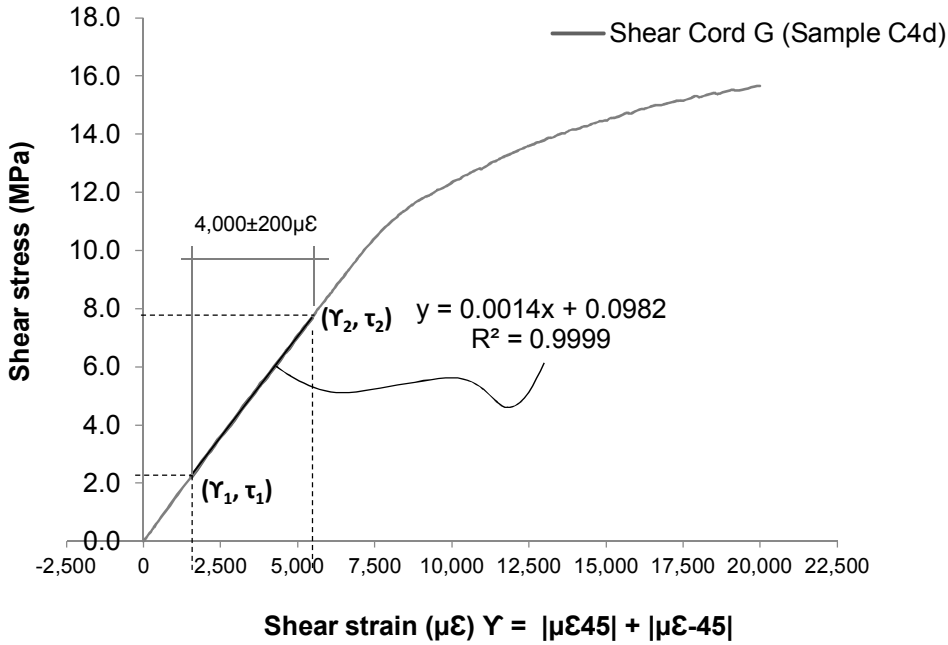

Figure 7-21. Typical strain-stress graph illustrating the section used for the determination of the shear chord modulus of elasticity between 1,500 με and 5,500με.

A linear regression was performed and the linear portion of the strain-stress graph between 1,500με (γ_1) and 5,500με (γ_2) with a correlation coefficient ≥ 0.99 was used to determine the apparent shear modulus (G_{12}^{app}) and the shear chord modulus of elasticity (G_{12}^{chord}) as defined by ASTM D5379 (ASTM, 1998). Then, values complying with this condition were on the portion of the graph between 0.15% and 0.55% shear strain and below 5% strain to avoid failure as recommended by (ASTM, 1998).

Pierron & Vautrin (1994) suggest the use of 0.2% as the maximum strain level for the determination of the linear elastic region of materials tested using the Iosipescu shear fixture and the application of stress (C') and strain (S') correction factors. These factors account for shear stress and strain non-uniformities between the notches and over the area of the gauge grid, respectively, and are calculated by finite element analysis ($C \cdot S = 0.912$). However, the same authors concluded that averaging the strain results recorded from both faces of a

specimen for each orientation (+45 and -45) results on small scattering due to testing conditions (specimen geometric non-linearity and test boundary conditions) in specimens with main fibre direction at 0°. Therefore, the linear elastic region used for the determination of the shear modulus was the section suggested by ASTM (between 1,500$\mu\varepsilon$ and 5,500$\mu\varepsilon$) and strain values recorded by the rosette gauges at +45° and -45° from front and back were averaged.

The apparent shear modulus is then defined as the ratio of average shear stress to shear strain as expressed in Equation 7-5.

$$G_{12}^{app} = \frac{\tau^{av}}{\Upsilon^{av}} \qquad 7\text{-}5$$

And the ratio of the difference in applied shear stress and resulting shear strain ($\Delta\tau / \Delta\Upsilon$) is the shear chord modulus of elasticity (G^{chord}) as expressed in Equation 7-6.

$$G_{12}^{chord} = \frac{(\Delta\tau)}{(\Delta\Upsilon)} \qquad 7\text{-}6$$

where
$\Delta\tau$ is the difference of shear stress between τ_2 and τ_1
and $\Delta\Upsilon$ is the difference of shear strain between Υ_2 and Υ_1.

Validation of the accuracy of the ASTM (ASTM, 1998) and Pierron (Pierron & Vautrin, 1994) methods for the determination of shear moduli (G_{12}^{app} and G_{12}^{chord}) was undertaken through statistical analysis of the strain-stress data collated for 0% to 0.2% and 0.15% to 0.55% strain ranges. It was found that although both sections of the test displayed a linear fit with correlation coefficients≥0.99 (which could be considered as the linear elastic region of samples A, B and C under Iosipescu test) the second section (between 1,500$\mu\varepsilon$ and 5,500$\mu\varepsilon$) had the lowest statistical variation of G_{12}^{app} and G_{12}^{chord} values (CoV≤10% and standard deviation≤0.1GPa). Calculation of the same values using the first section and the correction factor ($C \cdot S$) suggested by Pierron & Vautrin (1994) presented CoV values of 16%, 22% and 8% and standard deviations of 0.11GPa, 0.23GPa and 0.12GPa for samples A, B and C, respectively. Furthermore, the percentage of twist of the specimens during Iosipescu shear

test decreased at higher strain levels and was fairly stable between 0.15% to 0.55% strain ranges. This percentage was assessed for both situations using Equation 7-7 –as defined by ASTM (1998).

$$\left|\frac{(G_a - G_b)}{(G_a + G_b)}\right| \cdot 100 \qquad 7\text{-}7$$

where
G_a is the shear modulus of the sample's side (a)
and G_b is the shear modulus of the sample's side (b)

7.4.2 Results and discussion

Determination of G_{12} by Iosipescu shear testing.

Values for the apparent shear modulus (G_{12}^{app}) of four specimens per sample are presented in Table 7-9 and plotted in Figure 7-22. Mean results per specimen (e.g. A1, A2, etc.) correspond to the average of five load cycles undertaken during testing. Errors and coefficients of variation (CoV) obtained from the analysis of the results for all the specimens are reported in both Table 7-9 and Figure 7-22.

The variability of results for G_{12}^{app} across all Guadua samples is comparable to the widely reported variability of mechanical properties of wood (Bodig & Jayne, 1982; FPL, 2010; Wood, 1960) where the CoV fluctuates between 10% and 30%.

Table 7-9. Apparent shear moduli values for samples A, B and C.

Specimen	*Average* (GPa)*	*Max (GPa)*	*Min (GPa)*	*Stand dev.*	*CoV (%)*	*Error (+)*		*Error (-)*	
A1	0.57	0.66	0.50	0.04	7.72%	0.09	15%	0.07	12%
A2	0.49	0.56	0.45	0.03	5.97%	0.07	15%	0.04	7%
A3	0.54	0.64	0.44	0.07	12.15%	0.10	18%	0.10	18%
A4	0.58	0.74	0.50	0.07	11.44%	0.16	28%	0.08	15%
Mean (μ)	0.54			0.05	9.3%				
B1	0.96	1.11	0.84	0.08	8.68%	0.15	15%	0.12	13%
B2	0.89	1.05	0.78	0.08	8.94%	0.16	17%	0.12	13%
B3	0.79	0.89	0.70	0.06	8.05%	0.10	12%	0.10	12%
B4	0.84	0.95	0.76	0.06	6.61%	0.11	13%	0.08	10%
Mean (μ)	0.87			0.07	8.1%				
C1	1.41	1.53	1.28	0.08	5.37%	0.12	8%	0.13	9%
C2	1.40	1.55	1.30	0.08	5.53%	0.15	11%	0.10	7%
C3	1.41	1.56	1.31	0.07	5.18%	0.15	11%	0.10	7%
C4	1.42	1.45	1.40	0.02	1.06%	0.03	2%	0.02	1%
Mean (μ)	1.41			0.06	4.3%				

* Average of five cycles

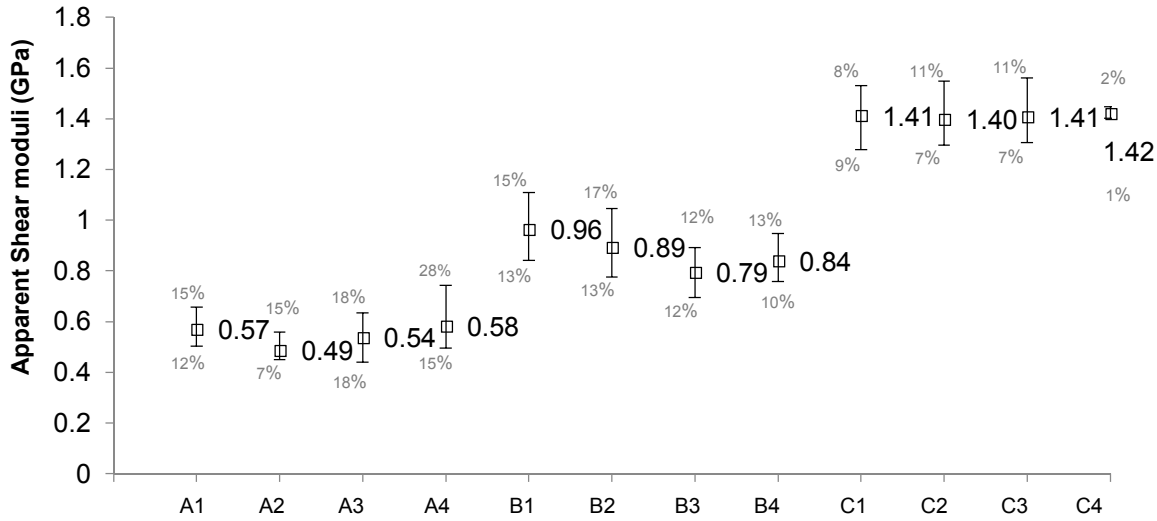

Figure 7-22. Apparent shear moduli values for samples A, B and C.

Papers by Pierron & Vautrin (1994) and Xavier *et al.* (2004) have reported a similar fluctuation of mean G_{12}^{app} results (up to 18%) for different non-modified wood species assessed by the Iosipescu shear method. Average CoV for samples A, B and C were 9.3%, 8.1% and 4.3%, respectively, which shows reduced dispersion of results about the mean with the higher degree of densification. A non-linear elastic response is clearly appreciated in Figure 7-23 for samples A and B. Sample C behaved linear elastically, while A and B behaved non-linear because of their viscoelastic response. Sample B behaved more elastically than sample A due to their TM modification. The section of the slope used for the determination of the shear chord modulus (G_{12}^{chord}) is shown in Figure 7-23.

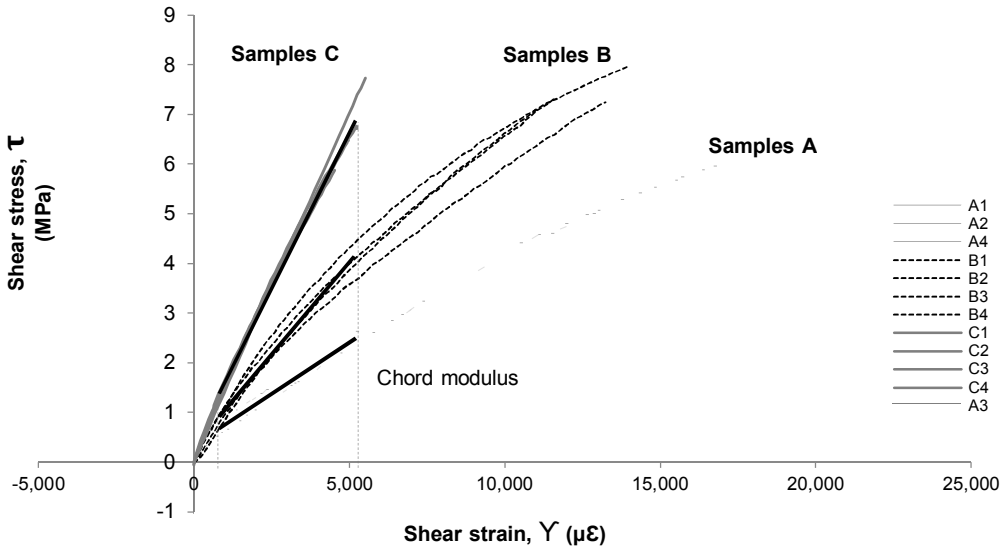

Figure 7-23. Typical Iosipescu-shear stress versus shear strain graph of samples A, B and C.

Table 7-10 shows the results for the shear chord modulus of samples A, B and C assessed by the Iosipescu-shear test method and calculated using Equation 7-6. The shear properties of the material on the TL plane (G_{12}^{chord}) increased from A to C; this increase in shear modulus can be also explained by the treatment applied to the different samples and their higher density (543.3, 814.6 and 890.9kg/m^3 for samples A, B and C, respectively).

Table 7-10. Shear chord moduli of rigidity G_{12}^{chord} by Iosipescu shear test.

	No.	G (GPa)	G_a (GPa)	G_b (GPa)	Twist (%)		No.	G (GPa)	G_a (GPa)	G_b (GPa)	Twist (%)		No.	G (GPa)	G_a (GPa)	G_b (GPa)	Twist (%)
$G_{A_{21}}$	A1	0.45	0.44	0.46	2%	$G_{B_{21}}$	B1	0.71	0.83	0.63	12%	$G_{C_{21}}$	C1	1.26	1.89	0.94	31%
	A2	0.42	0.36	0.49	15%		B2	0.68	0.70	0.66	2%		C2	1.28	1.68	1.04	21%
	A3	0.36	0.34	0.39	8%		B3	0.67	0.71	0.63	14%		C3	1.33	2.06	0.99	38%
	A4	0.40	0.34	0.49	17%		B4	0.69	0.76	0.64	15%		C4	1.40	2.10	1.05	34%
Mean		**0.41**	0.37	0.46	10%			**0.69**	0.75	0.64	8%			**1.32**	1.94	1.01	32%
Density (ρ)			**543.3 kg/m³**						**814.6 kg/m³**						**890.9 kg/m³**		
St. dev.		0.03	11.60					0.03	63.09					0.08	91.79		
CoV		8.58%	2.14%					4.47%	7.75%					5.97%	10.30%		

Similarly to the results reported for the apparent shear modulus (G_{21}^{app}), values of coefficient of variation (CoV) of the distribution of shear chord moduli (G_{21}^{chord}) obtained from four specimens per test sample (A, B and C) were below 10%. Figure 7-24 illustrates the range of variation of the results (lower quartile, median and upper quartile within the boxes), the maximum and minimum values (whiskers) and the mean (μ) values for all the samples.

The twist percentage as defined by ASTM for the Iosipescu-shear test and discussed in the previous Section (7.4.1) has to be carefully considered when testing bamboo specimens due to their significant variation in cross sectional fibre content, which increases towards the outermost layer. Whilst the coefficient of variation (CoV) in Table 7-10 can explain the scatter due to boundary conditions and geometric non-linearity of the specimens, twist values in the same table are more representative of the variation in rigidity between the shear chord modulus values obtained from outermost and the innermost layers of Guadua samples A, B, and C (G_a and G_b, respectively).

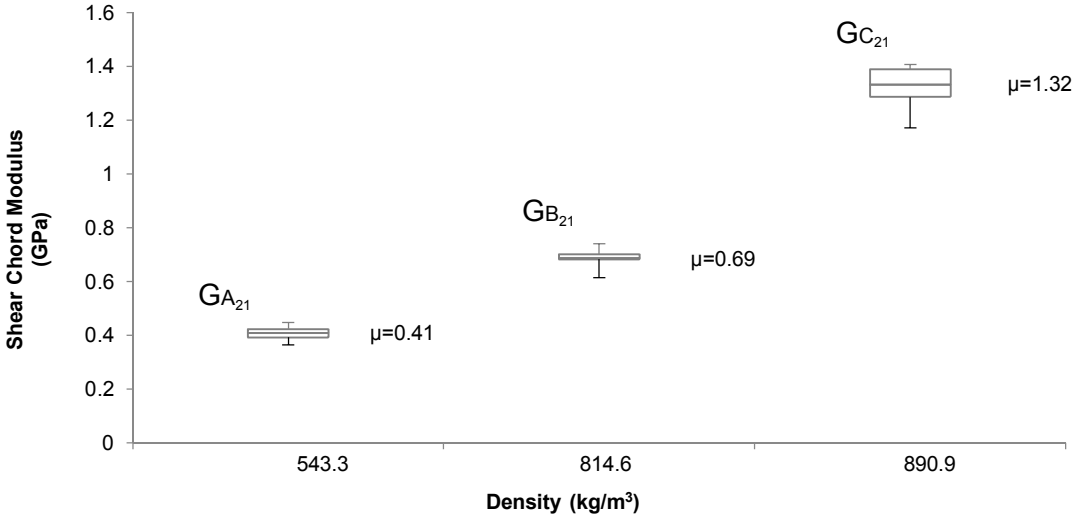

Figure 7-24. Box and whisker plots for shear chord results of samples A, B and C.

Differences on the G_{12}^{chord} values of the material encountered between the face to face results (G_a, G_b) evidences the density dependence of the material's elastic properties. Front and back faces of the specimens corresponded to the outermost (G_a) and innermost (G_b) sides (across the radial direction) of the raw (A) and densified material (B and C) to which the strain gauges were attached. Samples A and B exhibited the lowest percentage of twist (between 2% and 15%) obtained from the strain recorded on the inner and outer faces of the specimens (Figure 7-25 and 7-26), whilst sample C showed the highest percentage of twist (up to 38%) between (G_a) and (G_b) faces (Figure 7-27).

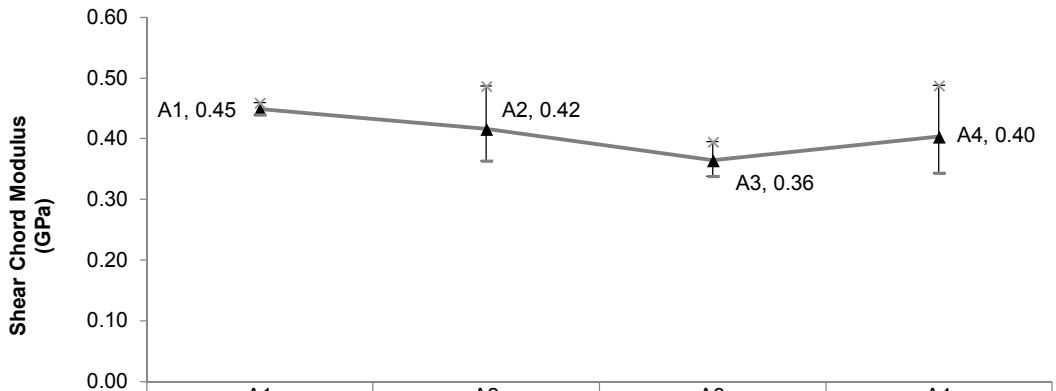

	A1	A2	A3	A4
A (G average)	0.45	0.42	0.36	0.40
A (Ga outer)	0.44	0.36	0.34	0.34
A (Gb inner)	0.46	0.49	0.39	0.49

Figure 7-25. Average, G_a (outer) and G_b (inner) shear chord moduli values for sample A.

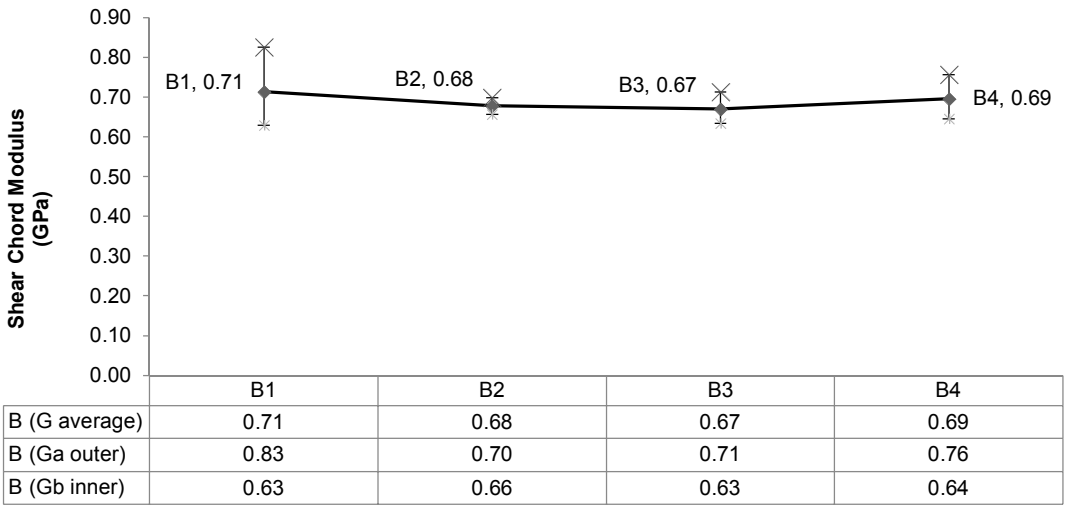

Figure 7-26. Average, G_a (outer) and G_b (inner) shear chord moduli values for sample B.

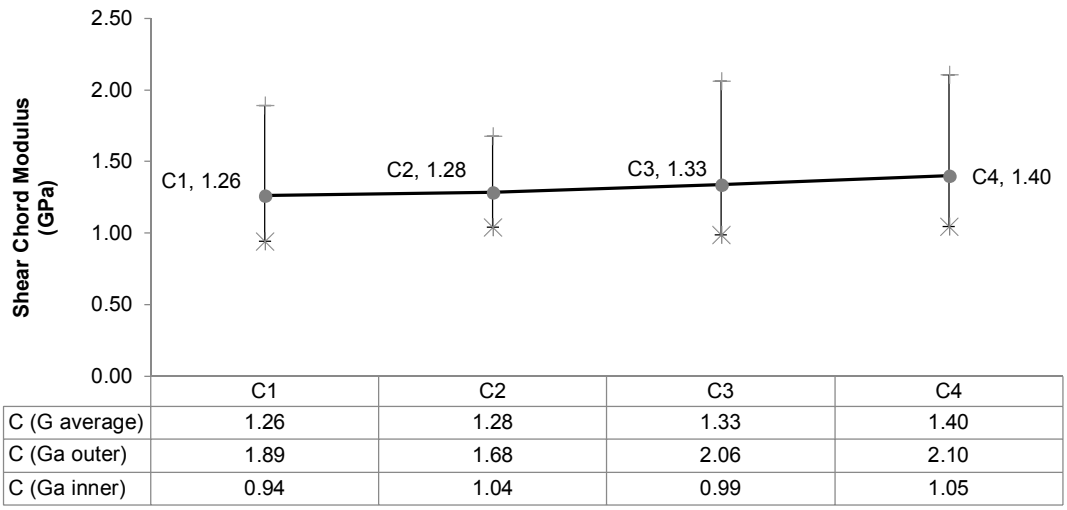

Figure 7-27. Average, G_a (outer) and G_b (inner) shear chord moduli values for sample C.

Higher values of G_{12}^{chord} at the G_a faces of sample C are the result of the higher degree of densification occurring at the outer layer of Guadua subjected to the THM treatment.

On separate calculations, results for the apparent shear moduli (G_{12}^{app}) of Guadua samples A, B and C were obtained using the strain ratio from 0% to 0.10% suggested by (Pierron & Vautrin, 1994). These values were 0.69GPa, 1.03GPa and 1.56GPa with CoV of 16%, 22% and 8%, for samples A, B and C, respectively; and resulted on values 27%, 18% and 10% higher than the G_{12}^{app} results obtained in this study using the 0.15% to 0.55% strain range. Furthermore, when compared to the G_{12}^{chord} results the variation is significantly higher (68%, 49% and 18% for A, B and C). Percentage of twist was high within the 0.1% strain range

and stabilized as the load increased; local crushing of fibres along the X_2 axis (tangentially) was also observed on the specimens at the initial stages of the test (Figure 7-28).

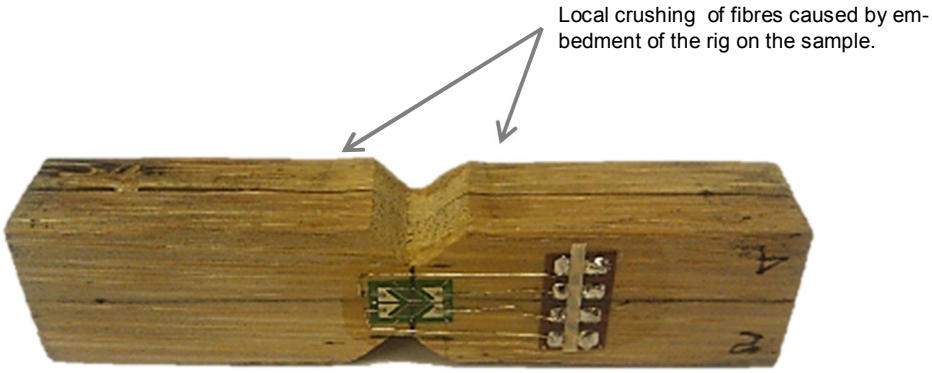

Figure 7-28. Specimen post Iosipescu-shear test showing local crushing of fibres due to embedment of the test fixture.

7.5 Three point bending test

THM modified and non-modified small clear specimens of Guadua (samples C and A, respectively) were subjected to static three point bending tests to determine their modulus of elasticity in bending and bending strength. Additionally the effect of fibre content was studied by undertaking several bending tests on A and C samples with their inner and outer positions (less dense and more dense) facing the tension side of the test.

As discussed in Chapter 2 (see Figure 2-8) fibre and parenchyma percentages are inversely proportional to their position across the thickness, whilst the first decreases towards the lacuna (inner part of the culm), the second decreases towards the cortex (outermost layer). During THM the percentage of fibres by unit area is increased, thus a positive effect on the mechanical properties of the material is expected. This improvement in the elastic properties of the bulk material was demonstrated by the testing results previously presented in Sections 7.2 to 7.4. Furthermore, shear-Iosipescu test showed differences on the shear moduli results from opposite faces of the specimens with different densities. However, the influence of variable cross sectional fibre content on the mechanical properties of densified and non-densified Guadua was not studied. Therefore, bending tests were undertaken to analyse this effect and assess the degree of homogeneity obtained by THM modification.

7.5.1 Materials and methods

Five rectangular specimens of Guadua A and C samples were cut to length and widths of about 110mm and 28 mm, respectively. Subsequently, these specimens were stored in a conditioning room under controlled temperature and relative humidity (27ºC±2ºC and 70±5% RH, respectively) prior to test. Dimensions and weight were also checked before the test with digital callipers and scales in order to calculate density; values obtained are reported in Table 7-11.

Table 7-11. Specimens for static bending tests.

	Number of Specimens	span (l) (mm)	width (b) (mm)	thickness (h) (mm)	density (kg/m^3)
Sample A (inner)	5	110	28.06	5.92	
Sample A (outer)	5	110	28.12	5.84	
Mean		**110**	**28.09**	**5.88**	**543.3**
St. dev.		-	0.13	0.09	11.60
CoV			0.46%	1.51%	2.14%
Sample C (inner)	5	110	27.10	6.29	
Sample C (outer)	5	110	27.26	6.31	
Mean		**110**	**27.18**	**6.3**	**890.9**
St. dev.		-	0.17	0.1	91.79
CoV			0.62%	1.54%	10.30%

* Mean oven dried density of rectangular specimens of Guadua and average values of width and thickness.

A number of previous studies (Correal & Arbeláez, 2010; Osorio-Serna *et al.,* 2010; Takeuchi-Tam & González, 2007) and different standards (BS 373 and ISO 22157) from timber and bamboo were used to design the experiment, as the majority of bamboo standards give guidelines for round culms only. The British standard BS 373 for small clear specimens of wood (BSI, 1957) was however, the main reference source. Specimens were prepared with a ratio of span (l) to thickness (h) of $l \geq 18$h, and for each sample (A and C) five specimens were prepared (Figure 7-29).

Static bending tests were performed in three point bending with an INSTRON 5585H floor model testing machine with a 200kN load cell acting along the X_3 axis, using Bluehill control software; the load was applied at a rate of 2mm/min and the temperature during the test was in the range of 27ºC±2ºC. A linear variable differential transformer (LVDT) connected to a Vishay System 6000 (Model 6100) Data Logger, was used to measure the deflection occurring at the midpoint of the specimen. Figure 7-29 illustrates the dimensions of the specimens and the test setup.

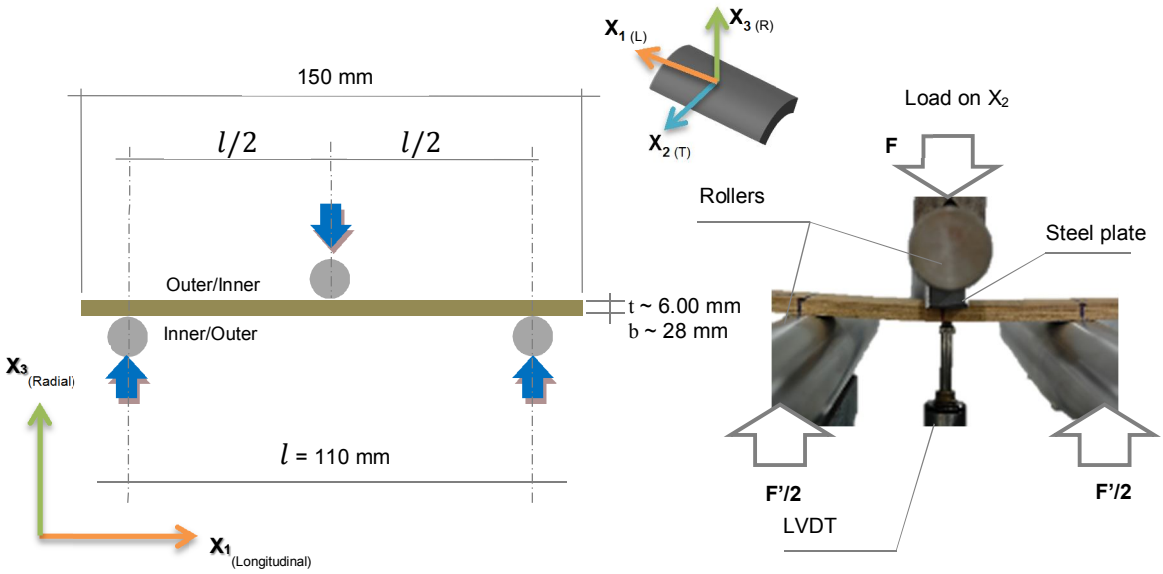

Figure 7-29. Dimensions of specimen for bending test and detail of the test setup.

For the determination of local modulus of elasticity in bending (E_b), the graph load/deformation was plotted and a regression analysis of the graph section between 0,1F_{max} (F_1) and 0.4F_{max} (F_2) was analised. The longest portion of those sections with a correlation coefficient ≥ 0,99 were used to calculate E_b.

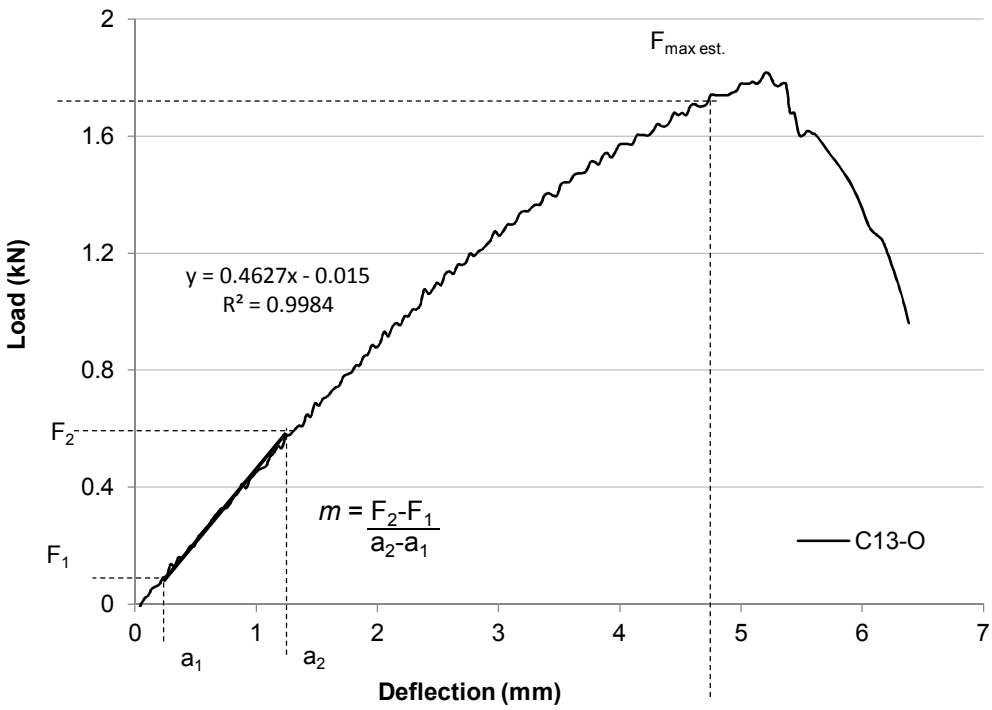

Figure 7-30. Typical load- deflection graph for a static bending test (Specimen C13-O) showing the range of elastic deformation used for the calculation of the MOE, and the maximum load considered for the calculation of MOR.

The expression used to calculate the modulus of elasticity in bending was:

$$E_b = \frac{l^3\, m}{4bh^3} \qquad 7\text{-}8$$

where
l is the span, m is the slope or $(F_2 - F_1)\,/(a_2 - a_1)$
b is the width and h is the thickness of the specimen (depth)

This equation is the same given by DIN 52 186 for MOE of wood specimens in bending (González *et al.,* 2007). Figure 7-30 shows a load-deflection graph with the range of elastic deformation for a specimen of sample C (C-13 O), the values considered for the calculations and the equation from the regression analysis.

Modulus of rupture in bending (MOR_b) was also calculated for all the samples and followed the expression:

$$MOR_b = \frac{3\,P\,l}{2\mathrm{bh}^2} \qquad 7\text{-}9$$

where
P is the maximum estimated load ($F_{\max}$)
l is the span, b is the width and h is the thickness of the specimen (depth)

7.5.2 Results and discussion

Determination of elastic modulus (E_b) and strength (MOR_b) values by static three point bending test.

Results for the modulus of elasticity E_b and MOR_b calculated using Equation 7-8 and 7-9, respectively, for inner and outer positions facing the tension side of the static bending test are presented in Table 7-12 for sample A, and Table 7-13 for sample C. Mean values for each test batch (I-inner & O-outer) and sample type (A & C) are also presented in these tables. The resulting load-deflection graphs for all the specimens in both samples were plotted and can be found in Figure 7-31. Less scattering of the slope results for sample C subjected to THM modification can be observed in Figure 7-31b.

Table 7-12. Modulus of elasticity and modulus of rupture in bending for tested specimens of sample A for Outer and Inner positions facing the tension side.

	Specimen No.	$E_{b,A,Out}$ (GPa)	F_{max} (kN)	$MOR_{b,A,Out.}$ (MPa)		Specimen No.	$E_{b,A,Inn}$ (GPa)	F_{max} (kN)	$MOR_{b,A,Out.}$ (MPa)
Outer	A11-O	18.93	1.18	199.73	Inner	A2-I	16.28	0.847	143.57
	A12-O	20.36	1.08	186.60		A1-I	15.20	0.771	132.26
	A13-O	15.47	1.05	179.73		A5-I	14.20	0.832	135.22
	A14-O	9.71	0.49	88.57		A4-I	12.87	0.694	116.45
	A15-O	17.13	1.11	182.13		A3-I	10.63	0.610	101.31
	Mean	16.32	0.98	167.35		Mean	13.83	0.751	125.76
	SD	4.13	0.28	44.72		SD	2.19	0.10	16.83
	CoV (%)	25.30%	28.5%	26.72%		CoV (%)	15.83%	13.17%	13.38%
	$E_{b,A}$	15.08±3.38 GPa		CoV 22.42 %		$MOR_{b,A}$	146.56±38.67 MPa		CoV 26.38 %

Table 7-13. Modulus of elasticity and modulus of rupture in bending for tested specimens of sample C for Outer and Inner positions facing the tension side.

	Specimen No.	$E_{b,C,Out}$ (GPa)	F_{max} (kN)	$MOR_{b,C,Out.}$ (MPa)		Specimen No.	$E_{b,C,Inn}$ (GPa)	F_{max} (kN)	$MOR_{b,C,Out.}$ (MPa)
Outer	C13-O	22.41	1.816	275.70	Inner	C2-I	24.60	1.152	187.74
	C15-O	23.44	1.442	223.65		C5-I	19.99	1.122	167.82
	C14-O	21.13	1.351	207.72		C1-I	18.07	0.733	109.75
	C11-O	19.29	1.244	195.58		C4-I	16.83	0.870	131.76
	C12-O	17.91	1.488	217.83		C3-I	18.78	1.236	186.20
	Mean	20.84	1.468	224.10		Mean	19.65	1.022	156.65
	SD	2.25	0.22	30.76		SD	2.99	0.21	34.58
	CoV (%)	10.80%	14.70%	13.72%		CoV (%)	15.22%	20.73%	22.08%
	$E_{b,C}$	20.25 ± 2.57 GPa		CoV 12.71 %		$MOR_{b,A}$	190.38 ±47.07 MPa		CoV 24.72 %

Overall, mean results for MOR and E_b in bending of sample C are about one third higher than those obtained for sample A, with a relatively high coefficient of variation (CoV) for all the values except for the averaged values (outer & inner) of $E_{b,C}$ (CoV=12.71%). Samples A and C display a moderate dispersion of results, which is consistent with the characteristic mechanical properties variation of other cellulosic materials such as wood (Bodig & Jayne, 1982; FPL, 2010; Wood, 1960).

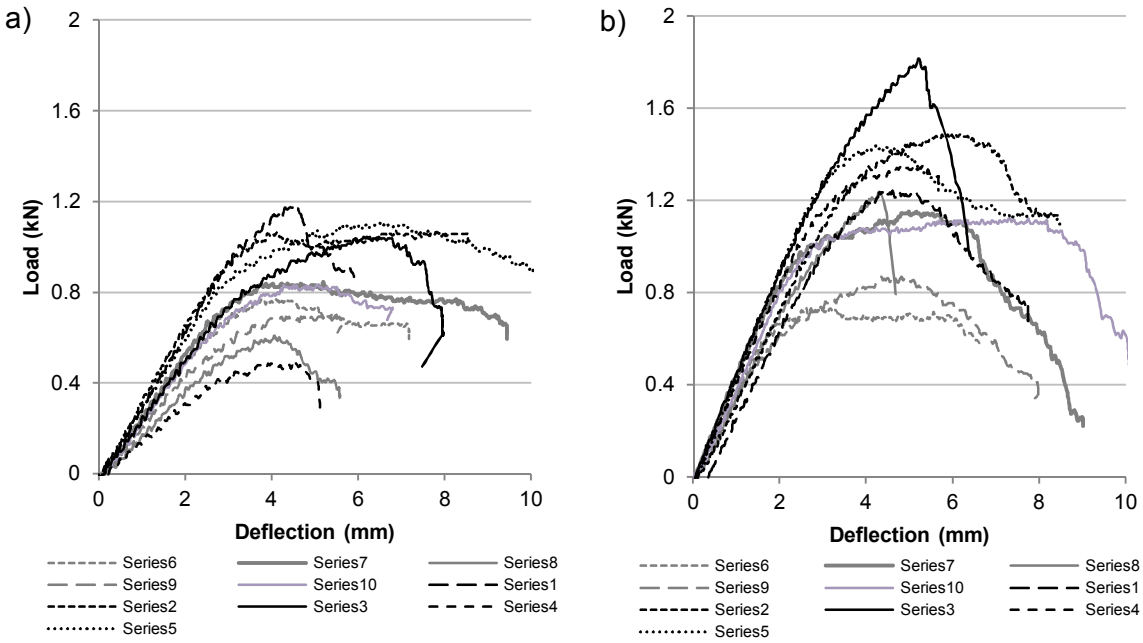

Figure 7-31. Load-deflection graphs in static three point bending test for a) A sample and b) C sample.

With the aim of finding the statistical significance of the E_b results for both inner (I) and outer (O) positions on samples A and C, two independent two-sample t-tests with 95% interval of confidence were undertaken. For both samples (A & C), no-significant difference between the results of inner and outer E_b was encountered; as expressed by the P-values (p=0.28 for sample A and p=0.5 for sample C which are ≥ 0.05=α). This might be due to the relatively high CoV and the small number of specimens tested. For the MOR_b results, the same type of t-test was undertaken to find the statistical significance of inner and outer position facing the tension side during test. As a result, statistically significant difference with an interval of confidence of 95% was found for sample C, but not for sample A. For the former p=0.01 ≤ α=0.05 and for the latter p=0.11 which is ≥ 0.05=α. In addition, two independent t-tests analyses using the mean results (inner and outer) obtained for the elastic modulus in bending (E_b) and the bending strength (MOR_b) of samples A and C showed a statistically significant difference. P-values (p) obtained for the E_b of samples A and C and the MOR_b of samples A and C were p=0.0013 ≤0.05=α & p=0.0362 ≤0.05=α, respectively.

In summary, the THM treatment has had a positive effect on the overall elastic and plastic properties of the modified sample. Although, mean figures of E_b and MOR_b for samples with the inner and outer side facing the tension zone of the bending show a numeric difference, no statistically significant difference was found.

Concluding remarks

Mechanical testing of TM and THM modified (B & C) and non-modified (A) Guadua samples were conducted with the aim of characterising their elastic properties. Four elastic values ($E_{1,t,b}$, $E_{2,c}$, $E_{3,c}$, and G_{12}), four Poisson's ratios (υ_{12}, υ_{21}, υ_{32}, and υ_{13}) and one strength value (MOR_b) have been obtained. These values will allow the prediction of the mechanical properties of cross laminated Guadua (G-XLam) panels, insight with the results of panel testing and a finite element model (FEM) simulation of their response to set load conditions (Table 7-14).

Table 7-14. Assessment of the mechanical properties of non-modified, TM and THM densified Guadua samples.

Guadua angustifolia Kunth		Mature 3-5 years old		Section: Middle part of the culm
		Sample A Control (non-modified)	Sample B TM + Dried	Sample C THM + Dried
	Time	0	20 min	20 min
	Pressure	0	6 MPa	6 MPa
	Temperature	0	150° C	150° C
	Compress. Set (C)	0	46.08%	42.51%
	Oven dried density*	543.3 kg/m³	814.6 kg/m³	890.9 kg/m³
			Testing values	
$\boldsymbol{E_{1,t}}$	Mean (GPa)	16.88 ± 0.33	22.80 ± 0.73	30.72 ± 0.43
	CoV	2%	3.20%	1.4%
	Spec. Stiffness	31.06 m²/s²	27.99 m²/s²	34.49 m²/s²
$\boldsymbol{E_{1,b}}$	Mean (GPa)	15.08 ± 3.38	-	20.25 ± 2.57
	CoV	22.42%	-	12.71%
	Spec. Stiffness		-	
$\boldsymbol{E_{2,c}}$	Mean (GPa)	0.55 ± 0.10	1.31 ± 0.13	0.84 ± 0.002
	CoV	18%	2.5%	5.62E-06%
	Spec. Stiffness	1.02 m²/s²	1.61 m²/s²	0.94 m²/s²
$\boldsymbol{E_{3,c}}$	Mean (GPa)	0.38 ± 0.006	0.26 ± 0.008	0.23 ± 0.011
	CoV	1.6%	3.2%	4.61%
	Spec. Stiffness	0.71 m²/s²	0.32 m²/s²	0.25 m²/s²
$\boldsymbol{G_{12,Ios}}$	Mean (GPa)	0.41 ± 0.03	0.69 ± 0.03	1.32 ± 0.08
(G_{12}^{chord})	CoV	8.58%	4.47%	5.97%
	Spec. Stiffness			
MOR_b	Mean (MPa)	146.56 ± 38.67	-	190.38 ± 47.07
	CoV	26.38 %	-	24.72 %
υ_{12}	Mean (GPa)	0.28 ± 0.01	0.33 ± 0.01	0.26 ± 4.20E-03
	CoV	3%	4%	2%
υ_{13}	Mean (GPa)	0.30 ± 0.02	0.33 ± 0.02	0.09 ± 0.02
	CoV	5%	5%	18%
υ_{21}	Mean (GPa)	0.02 ± 0.0062	0.02 ± 0.002	0.01 ± 0.00069
	CoV	32%	13%	10%
υ_{32}	Mean (GPa)	0.15 ± 0.003	-0.0035 ± 0.002	0.057 ± 0.007
	CoV	1.66%	65.5%	13.5%

Elastic values

Values for the Young's modulus $E_{1,t} = 30.72 \pm 0.33$ have been modified to account for the 30% overestimation of the tensile modulus along the fibres stated by (ISO, 2004b) when using bamboo specimens without an internode in the middle part of the test specimen. Then, $E_{1,t} = 21.74 \pm 0.33$; this will allow for more accurate predictions and FE simulations of the G-XLam panel properties.

Normally, Young's moduli values in wood are expected to be higher than bending by about 10%, which can explain the disparity of results in Guadua. These differences are illustrated in Table 7-16 for different species of wood and for samples of Guadua A (non-modified) and C (THM densified). The values of specific stiffness of these Guadua samples is comparable to those of hardwoods and some softwoods such as Douglas fir.

Table 7-15. Characteristic values for wood at 12% MC and mean values for non-modified (A) and THM densified (C) samples of Guadua.

	Hardwood				Softwood		Bamboo	
	Meranti[2] (*Shorea spp.*)	Oak red, Pin [2]	Basswood [a]	Sugar Maple [a]	Douglas fir (UK) [3]	Sitka Spruce [b]	Guadua non-mod. (A)	Guadua THM (C)
Density (kg/m^3)	680	630	370[2]	630[2]	450	400[2]	543.3	890.9
$E_{1,b}$ (GPa)	18	11.9	12.97	13.07	11.12	13.9	15.88	20.84
$E_{1,c}$ (GPa)	-	-	9.65	11.42	-	11.6	-	-
$E_{1,t}$ (GPa)	14.5	-	18.25	14.60	14.5	-	16.88	30.72
G_{12} (GPa)	-	-	0.42	0.68	0.83	-	0.41	1.32
MOR_b (MPa)	129.6	97	60	109[2]	52	70[2]	146.56	190.38
υ_{12}	-	0.448	0.406[2]	0.476[2]	-	0.467[2]	0.28	0.26
Specific stiffness (m^2/s^2)	21	19	49	23	32	26	31.06	34.49

[a] Elastic values at 12% MC (Schneider & Phillips, 1991); [b] Elastic values of round timber specimens (Ranta-Maunus, 2000); [2] (FPL, 2010) and (Bodig & Jayne, 1982).
Meranti in table is from *baulau* group, some species of *Shorea* are known as Philippine mahogany

As can be seen in Table 7-16, the values of mechanical properties of non-treated samples of Guadua (Sample A) obtained from the testing programme (Table 7-14) are in accord with those reported in the literature for round and small clear specimens of Guadua and other bamboo species (García *et al.,* 2012; Ghavami & Marinho, 2005; Rusinque & Takeuchi-Tam, 2007; Takeuchi-Tam & González, 2007). Furthermore, the coefficient of variation (CoV) for the obtained results is in the range of variation for the mechanical properties of clear wood; as defined by FPL (2010) CoV for the modulus of elasticity measured in bending, compression perpendicular and tension parallel to the grain are 22%, 28% and 25%, respectively.

Table 7-16. Elastic values and Poisson's ratios obtained by other authors for non-modified samples of Guadua.

Property	Reference	Value	Details
$E_{1,\ Tens}$	(Ghavami & Marinho, 2005)	14.60 GPa	Guadua middle part (average without > with node)
$E_{1,\ Comp}$		12.20 GPa	
$E_{1,\ Comp}$	(Takeuchi-Tam & González, 2007)	17.85 GPa	Compressive strength is not affected by nodes
$E_{1,\ Bend}$	(Obataya *et al.,* 2007)	15 -16 GPa	Middle part of 5 years old *Phyllostachys pubescens* (Moso)
E_1	CES EduPack *	15-20 GPa	Moso bamboo
$E_{1,\ Comp}$	(Chung & Yu, 200)	9.30 GPa	For round culms of *Bambusa pervariabilis (Kao Jue),* at MC=5-20%
$E_{1,\ Bend}$		18.50 GPa	
$E_{1,\ Comp}$		7.80 GPa	For round culms of *Phyllostachys pubescens* (Mao Jue), at MC=5-20%
$E_{1,\ Bend}$		11.40 GPa	
$E_{1,\ Bend}$	(Rusinque & Takeuchi-Tam, 2007)	16.53 GPa	For round culms of Guadua
$E_{1,\ Bend}$	(Correal & Arbeláez, 2010)	17 GPa	For round culms of Guadua middle part (average with and without node)
$G_{TL,\ Tens}$	(García *et al.,* 2012)	0.58	Found through rings method
υ_{12}	(García *et al.,* 2012)	0.40	Found through rings method
υ_{12}	(Ghavami & Marinho, 2005)	0.25 (tens)	Guadua middle part (average with and without node)
υ_{12}		0.36 (comp)	
υ_{13}	CES EduPack *	0.32 - 0.46	Moso bamboo

* CES EduPack version 2012 is a commercial materials education software developed by M. Ashby and others at the University of Cambridge (Granta Design Limited, 2013)

Elastic properties of wood decrease depending on the orientation following the pattern $E_L>E_R>E_T$ (Bodig & Jayne, 1982; FPL, 2010); however, a different trend was found for the elastic properties of the non-modified Guadua sample: $E_L>E_T>E_R$. This could be easily explained by the absence of radial rays in bamboo, which weakens its structural response to stresses perpendicular to the grain. Ghavami & Marinho (2005) found a similar behaviour

but, there is not general consensus on this regard; few research has been undertaken on the determination of the mechanical properties of bamboo in the three main planes X_1 (L), X_2 (T) and X_3 (R). As experienced during the experimental work, difficulties with the preparation of small clear specimens of bamboo and lack of testing standards affect the holistic analysis of the mechanical properties of bamboo.

Poisson's ratio

υ_{21} and υ_{31} are very small and less precisely determined due to their high scattering of results; research conducted by Ling *et al.* (2009) on the determination of the Poison's ratios of wood in compression found similar issues.

Although an auxetic behaviour of the compressed material (samples B and C) cannot be stated, the results obtained for Poisson's ratio of the samples C and B subjected to radial and tangential compression test showed exceptionally small and negative values. Neelakantan *et al.* (2014) states that negative values can be expected after modification of certain materials with particular molecular structure (austenitic stainless steel fibre). Nevertheless, information about this type of behaviour in wood is limited and in the case of bamboo, no mention of this response was found. Parenchyma cells and vessels (conductive tissue) might present an auxetic behaviour. These void cells collapse during TM or THM densification and can suffer hardening under further compressive stress, as explained by Sandberg & Navi (2007) (Figure 4-18). This is a remarkable feature of Guadua and bamboos in general that can be exploited in the manufacture of smart composite materials, but that requires extensive research. Digital image correlation (DIC) and the virtual fields method (Gédiac *et al.,* 1994) could be used to track and analysis this behaviour in small specimens of bamboo/Guadua.

Iosipescu

The main interest for undertaking the shear-Iosipescu test was the determination of a shear moduli value that could be used for the prediction of the panel values and input on the FE model. This method provided consistent values for the shear moduli of Guadua along the grain direction. The same method will not be feasible for determining shear values in the transverse directions due to the curved and reduced section of bamboo and Guadua. With the aim of standardising this type of test for bamboo, research on the different results in shear moduli between front and back or inner and outer surfaces of the specimens is required.

8. Manufacture of Cross Laminated Guadua G-XLam panels

Introduction

Guadua angustifolia Kunth (Guadua) has been widely used for structural applications in small and large-scale buildings, bridges and temporary structures in South and Central America; however, Guadua remains a material for vernacular construction associated with high levels of manual labour and structural unpredictability. Engineered Guadua products are scarce and require complex manufacturing processes. For instance, fabrication of laminated Guadua products results in an energy intensive process due to the machining of round culms into rectangular strips that produces high amounts of waste (de Flander & Rovers, 2009; Vogtländer *et al.,* 2010). Therefore, the development of engineered Guadua products needs to exploit its remarkable features, tackle the issues regarding manufacture and improve issues regarding durability. The positive effects of thermo hydro mechanical (THM) treatment 'C' on the elastic properties and specific stiffness of Guadua samples (about two fold and 11%, respectively) were reported in the previous Chapter (Chapter 7). Dimensionally stable densified flat Guadua sheets (FGS) were manufactured into engineered panels that could make use of these qualities. FGS were densified at the BioComposites Centre, Bangor University, then three and five lamellae were arranged in a cross laminated fashion, glued using a high performance epoxy resin and cold-pressed to manufacture cross laminated Guadua (G-XLam) panels. In total four panels of different configurations and sizes were manufactured with the aim of assessing the viability of the process and producing large panel specimens for mechanical testing. The present Chapter reports on this experience. Overall, the G-XLam panels were manufactured using straightforward densification and assembly methods that could be easily applied industrially.

8.1 Preparation of the material

Dried round culms of Guadua were cut to 1000mm and 700mm lengths and their outermost layers were removed using a Metabo GSI14CE professional burnisher fitted with a 100 mm x 289 mm x 40 grit Zirconium cloth belt as can be seen in Figure 8-1. This highly abrasive belt was used to remove between 100μm and 1 mm of the tough cutinized layer that covers the cortex of Guadua. Subsequently the peeled lengths of cylindrical Guadua were radially cut into six to eight strips (depending on the diameter) and the inner pith cavity membrane was also removed using the burnisher.

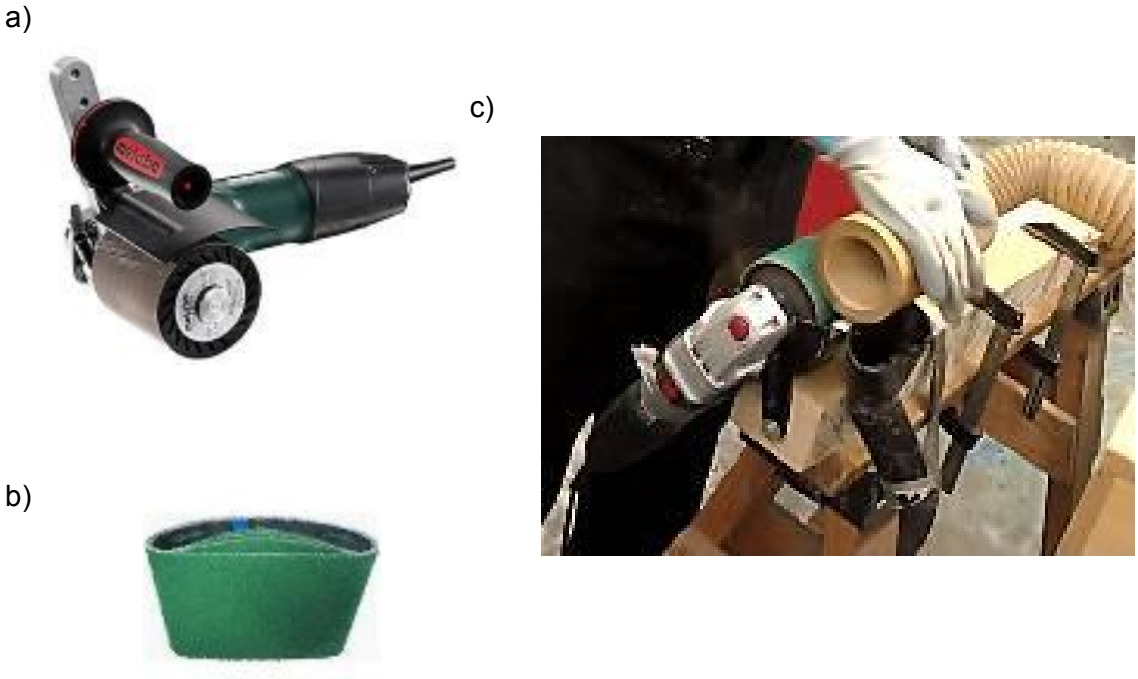

Figure 8-1. a) Metabo GSI14CE professional burnisher (image from https://www.rsis.co.uk). b) Grit 40 Zirconium cloth belt (image from http://www.ussander.com). c) Peeling off process of the outermost layer of Guadua culms.

Figure 8-2 illustrates the process undertaken and compares the weighted wastage produced by conventional manufacturing of rectangular strips through machining - about 50% (de Flander & Rovers, 2009), with a reduction of 27% in wasted material achieved by abrading the outer and innermost layers of Guadua culms.

Once these layers were removed, the strips were stored under controlled temperature (27°C ± 2°C) and relative humidity (70 ± 5%) in a conditioning room, enabling them to reach equilibrium at 12% moisture content (MC).

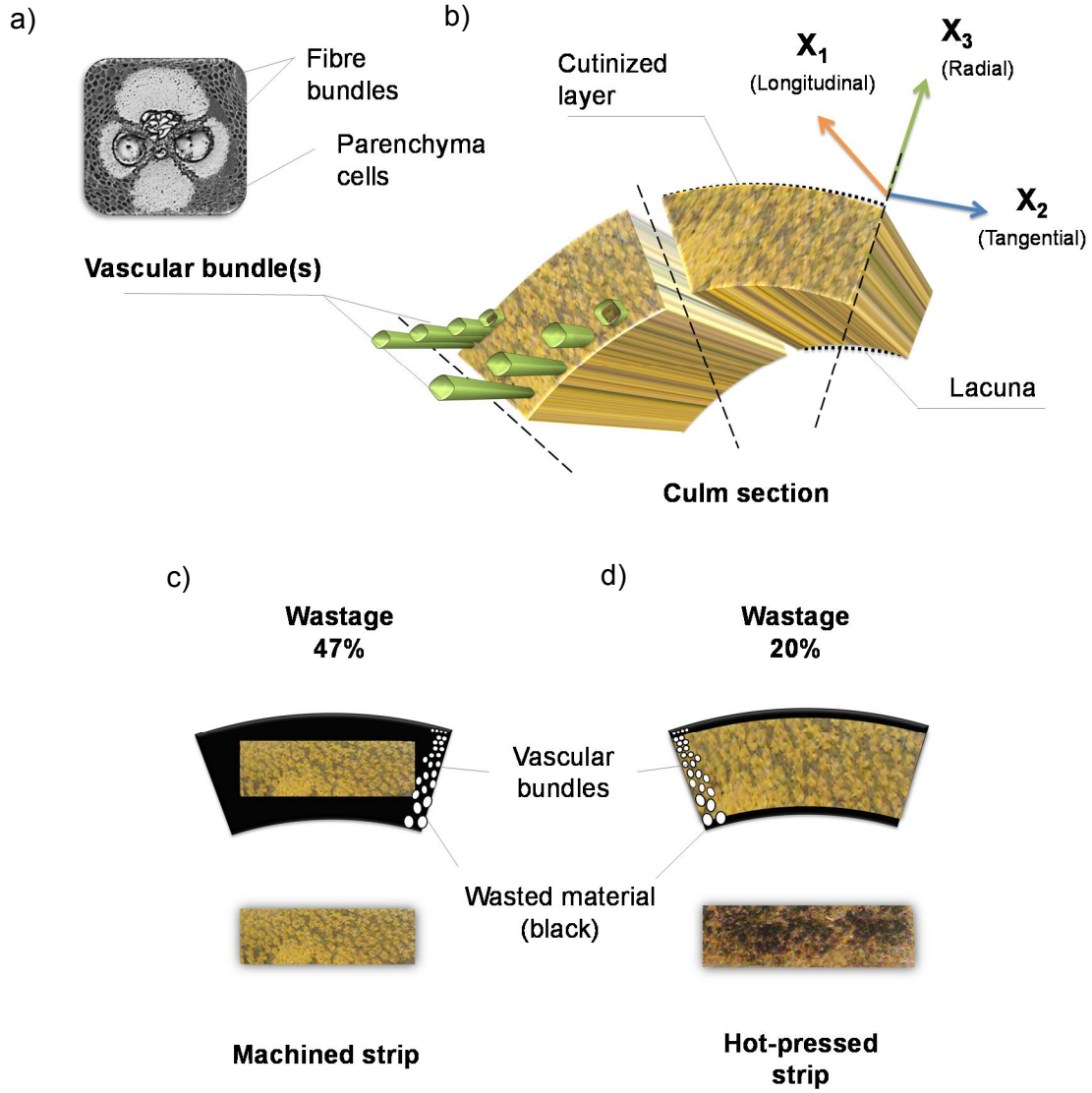

Figure 8-2. a) SEM image of a Guadua vascular bundle. b) Section of bamboo divided into strips showing the increase in size and the reduction in number of vascular bundles from the cutinized layer (cortex) to the lacuna. c) In black the material wasted by conventional processing. d) In black the material discarded using the burnisher method.

8.2 Densification process

THM treatment C was applied to the peeled strips of Guadua (see Section 5.5) at the facilities of the BioComposites Centre, Bangor University in North Wales. This produced densified flat Guadua sheets (FGS) measuring 700 mm and 1000 mm in length, 30±5 mm in width with thicknesses below 6.0 mm.

Following immersion in water for 24 hours, the strips were hot pressed for 20 minutes using a daylight opening hot press with 1000 mm^2 oil heated platens. The strips were arranged

in an "inside-outside" alternating arrangement (Figure 8-3). Pressure on the hydraulic press was computer controlled using PressMAN software and applied across the radial direction. Maximum pressure, temperature and compression set (C_s) were fixed at 4.9 MPa, 150°C and 45%, respectively.

As illustrated in Figure 8-3a, THM modification occurred in three stages; the first was a plasticisation stage where temperature and pressure on the strips of Guadua was increased for 10 minutes. In the second densification stage, maximum pressure and temperature were maintained for 10 minutes. Finally, temperature and pressure were dropped and no post-treatment was undertaken on the densified specimens.

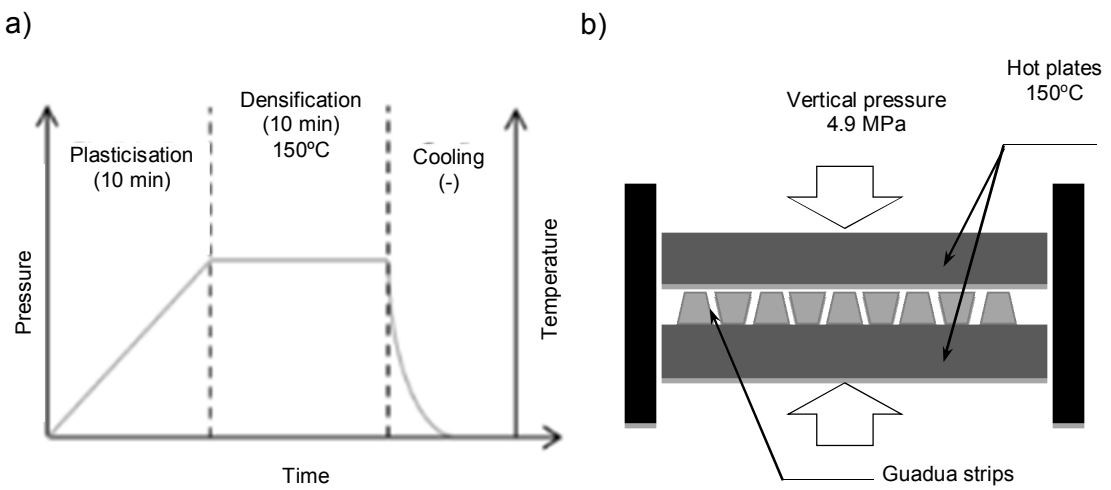

Figure 8-3. (a) THM diagram. (b) Diagram of the platen press showing "inside-outside" arrangement of strips.

This densification process provided densified FGS with improved mechanical properties (Chapter 7). Figure 8-4 shows the steps followed during the densification process.

Dry and wet weight were recorded (pre and post-THM) using digital scales; control strips were oven dried for 24 hours at 105°C and their weight was also recorded. After immersion in water for 24 hours the strips gained 20% of their initial weight. Post-THM treatment, a slight reduction of approximately 0.5% in the dry weight of the strips was recorded compared to the initial weight.

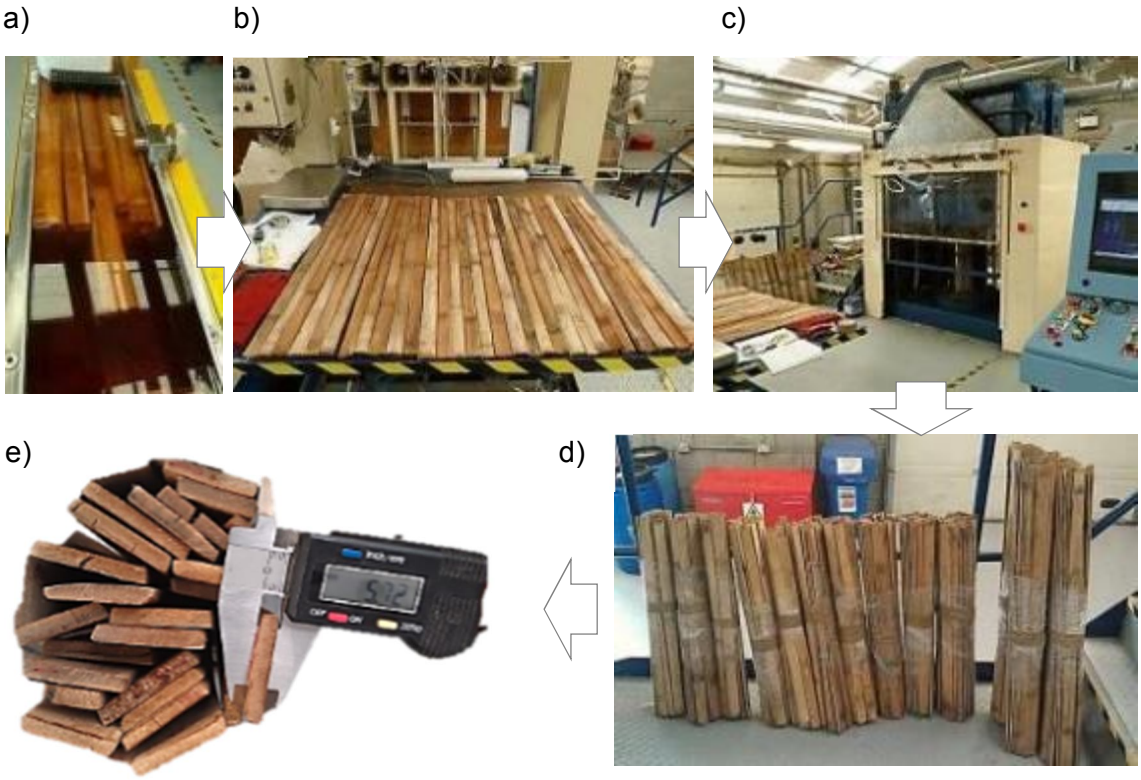

Figure 8-4. a) Strips immersed in water prior to THM treatment. b) Alternating arrangement of strips inside-outside before densification. c) Daylight opening hot press used for the densification. d) Strips of Guadua after densification (FGS). e) Measuring the thickness of FGS.

8.3 Cross-lamination

A laminate is a stack of bonded lamellas/plies that can be orientated unidirectionally or in different directions (multidirectionally). Stiffness and strength in a laminate will therefore be dependent on the orientation of the individual layers. Lamination processes can minimize swelling, shrinkage and splitting in the board plane. These are characteristic features of timber products such as plywood and cross-laminated-timber (CLT), where multi-layered veneers and planks can provide high in-plane load-bearing capacity. CLT panels are normally an arrangement of softwood planks glued together at 0° and 90° orientations, while plywood panels are formed from unidirectional or cross-laminated thin wood veneers. Both products are commonly manufactured with an odd number of plies. Particularly in CLT, acceptable out of plane capacity is achievable (thanks to its higher thickness), as well as a two-way slab action comparable to a reinforced concrete slab.

With the aim of exploiting these characteristics, individual lamellas of FGS were arranged in consecutive layers at 0° and 90° angles to form three and five layer (G-XLam-3 & G-XLam-

5) cross-laminated Guadua panels. The face position of FGS (inside-outside) forming a lamella was alternated during densification (Figure 8-3b and 8-4b) and lamination with the aim of counteracting the effects of side irregularity and compensating for slight variations of cross sectional density post-THM treatment. These lamellae were glued with a mix of wood epoxy resin (Sicomin SR 5550) and wood gap filler (Woodfill 250), which also increased the viscosity of the mix. The content of resin by total weight of the composite was ~4% and the spreading rate was 215g/m^2. Cold pressure of about 3.43 MPa was applied to the panels until the resin was set and then the panel was left to cure in a conditioning room at controlled temperature (27°C ± 2°C) and relative humidity (70 ± 5 %) for about 20 days before machining. Figure 8-5 illustrates the different stages of the lamination process and details of the resulting panels.

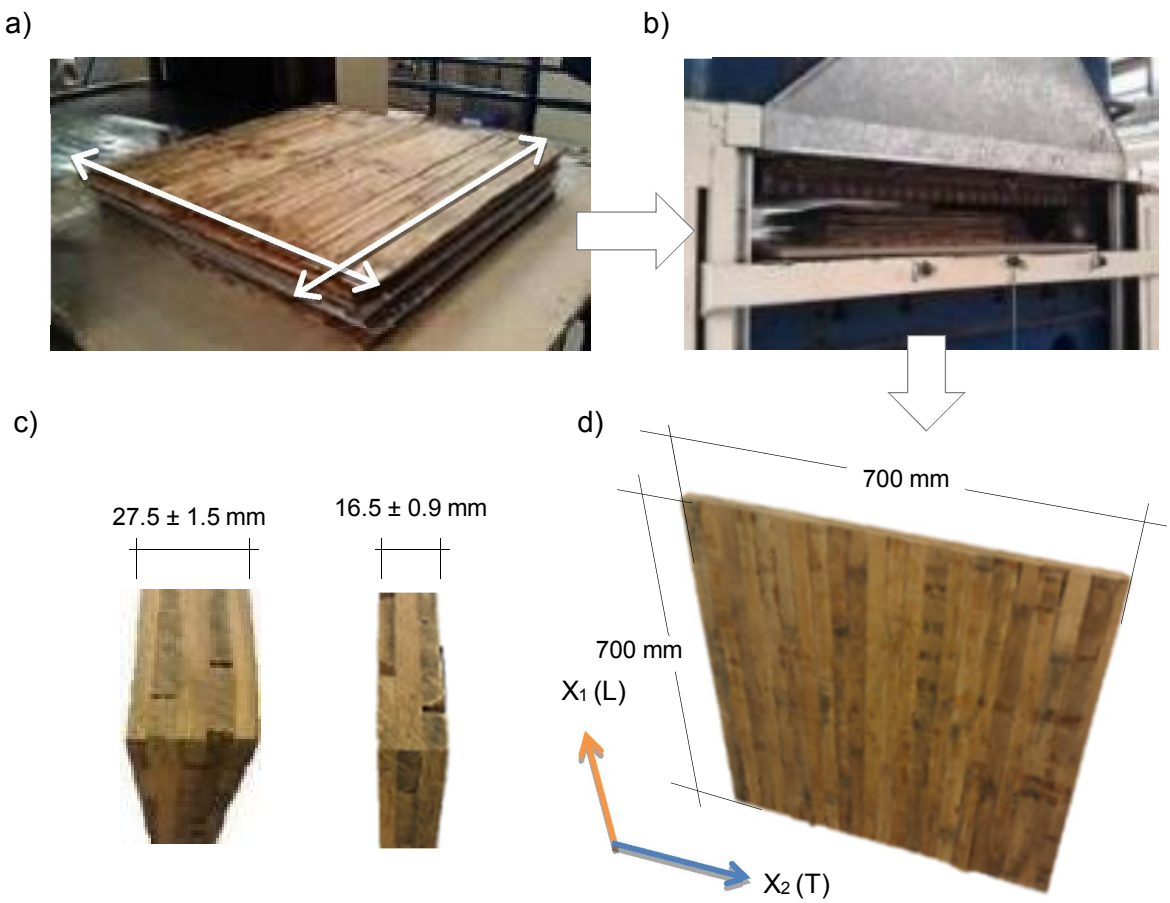

Figure 8-5. a) Cross lamination of FGS to form G-XLam panels of three and five layers. b) Daylight opening hot press used for densification of Guadua strips and cold pressing of panels. c) Guadua strips after densification (FGS). d) Average thickness and size of the G-XLam panels manufactured for testing.

Although epoxy resin is neither the cheapest or the most commercially used glue for this type of laminates, its choice was influenced by the following reasons:

- Its high mechanical properties that offered a strong interface between the cross laminated layers. Furthermore, the concern of this research was primarily the thermo hydro mechanical modification (THM) of Guadua and its use as a structural material.

- Its sets and cures at ambient temperature and has a low cure shrinkage.

- In general, epoxy resins also offer high water and temperature resistance.

The chosen epoxy resin system Sicomin SR 5550 allowed the use of the wood gap filler Woodfill 250, as thixotropic agent to account for the irregularities within the lamellae and to avoid losing resin in the gaps within individual strips of THM modified Guadua.

The laminate panel comprised an odd number of lamellae (three and five) with alternating layers disposed at 0° and 90°. Each layer possessed fairly regular thicknesses of 5.5±0.3mm. For structural analysis the G-XLam3 and G-XLam5 panels are considered as shell elements under plane stress conditions that require the evaluation of their orthotropic elastic properties (MOE, shear modulus and Poisson's ratio).

The longitudinal orientation of the G-XLam panels corresponds to its load bearing direction and is defined by the orientation of Guadua fibres in the outer layers. Hence, the highest number of layers are orientated in the X_1 direction with a ratio 2 out of 3 for G-XLam3 and 3 out of 5 for G-XLam5.

Concluding remarks

This Chapter described the manufacture of engineered Guadua products in a THM process. Flat cross-laminated (G-XLam) panels were manufactured from Guadua strips using a simplified process that largely eliminated the wastage produced from conventional machining processes for bamboo strips by approximately 27%. It is a novel method that has not been implemented in Colombia. This process differs from industrial technologies applied to Moso in China on several aspects, amongst them: a) Non-use of bamboo strands, but strips (thanks to Guadua's thicker walls); b) Peeling of the bamboo's skin instead of mechanical shaping; c) No-pre-treatment or dipping in resins but, softening in water; and d) Less use of adhesive from about 30% to 3%.

Four G-XLam panels were produced with the aim of assessing the technical challenges associated with their manufacture and their mechanical properties when subjected to different load conditions. The effect of the densification process of individual Guadua strips into FGS on the bulk mechanical properties of G-XLam panels will also be assessed in Chapter 10.

Recorded values for MC prior and post THM modification suggest that no post-THM drying of the Guadua strips is required. Water bound inside the cells of Guadua is released during the THM treatment and the same equilibrium moisture content (EMC) as the EMC before soaking is achieved after densification. This is why the two stages of the THM process (plasticisation and densification) are key to reach a stable state; if heat and pressure were applied suddenly, the water contained inside the cells would be forced to leave very quickly and steam explosion would occur.

Dimensions of panels were limited by the press to one square metre ($1m^2$). However, at an industrial scale, a simple mechanism could be devised to apply THM process to longer sections of Guadua strips. The regularity of the panels could be improved by applying lateral pressure to the strips during pressing to eliminate gaps between strips.

9. Analytical and numerical models of G-XLam panels

Introduction

The mechanical properties of cross-laminated Guadua (G-XLam) panels are dependent on the direction of applied stress, the arrangement of the individual layers that form the panel and the specific mechanical properties of the constituent material. For structural analysis G-XLam panels have been considered as multi-layered systems composed of contiguous lamellas with orthotropic axes orientated at 0° and 90°. A thermoset epoxy resin was used and assumption of a perfectly rigid connection between these layers was made (as explained in Chapter 8); thus the effect of glue bonds is neglected for the analysis of the elastic properties of G-XLam panels (Bodig & Jayne, 1982). This cross-laminated composition is typical of plywood and CLT (cross-laminated timber) panels, hence analytical design methods developed for these systems have been applied to G-XLam panels in this study. Usually the lay-up of CLT and plywood is symmetrical, hence calculation of their mechanical properties is based on a mechanically symmetrical composition of alternated cross layers (an imaginary plane is drawn across the middle layer in uneven arrangement of layers). G-XLam panels are composed of densified flat Guadua sheets (FGS) arranged orthogonally and glued together forming a three and five layer symmetrical composition (G-XLam3 & G-XLam5). Timber engineering methods normalized by European standards are used in this study for the prediction of the mechanical properties of G-XLam panel. Bending stiffness properties of these panels were predicted using the transformed cross section method to find the modulus of elasticity of the beam from the moduli of elasticity of the individual layers. As the elastic properties of the laminate system depend on the elastic properties of the individual layers, the elastic parameters for small clear specimens obtained previously (Chapter 7) were used for the numerical analysis and finite element (FE) analysis of G-XLam panels. Compression stiffness and shear stiffness of the cross-laminated panels were also calculated and a FE model of G-XLam panels simulated the response of the panels to axial compressive load in the longitudinal and transversal directions.

9.1 Analytical design methods for G-XLam panels.

The structural response under load of cross-laminated Guadua panels (G-XLam) depends on the mechanical properties of the material used to form the layers of the panel and the arrangement of layers to form the panel structure. In timber engineering, several methods have been used to analyse the mechanical response of multi-layered materials such as plywood and CLT (Bodig & Jayne, 1982; BSI, 2010, 2011, 2014; Ceccotti, 2008; Gagnon & Pirvu, 2011). The structural design of CLT is dictated by European standards (BSI, 2010, 2011, 2014; TRADA, 2009). Two of the calculation methods used for the determination of CLT design values for floor plates and wall panels in Eurocode 5 (BSI, 2014) are the theory of mechanically jointed beams and the composite theory method (TRADA, 2009). The former, also referred to as the Gamma method considers layers acting only in the load direction, connected by imaginary fasteners and with no shear deformations for span to width ratios of 30 (Gagnon & Pirvu, 2011). The composite theory or 'k-method' based on plywood analysis theory, assumes that the longitudinal modulus of elasticity E_0 is thirty times the transverse modulus E_{90}. Both theories neglect shear deformation for span to width ratios $\geq$ 30.

As an alternative, BS EN 14272 (BSI, 2011) derives the mechanical properties of plywood panels in bending, compression and tension from the independent properties of rigidly connected layers and their transformed cross section. Thus, composite theory of laminated systems and equivalent section area are used for the prediction of the stiffness and strength values. This is in agreement with the method given by (Bodig & Jayne, 1982) for the analysis of multilayered orthotropic wood laminates. A similar approach known as the shear analogy was developed by Kreuzinger (Blass *et al.,* 1995) for calculating the stiffness and strength values of solid panels with cross-laminated layers in bending including those with span to width ratios $<$30. The BS EN 14272 procedure is widely accepted for the analysis of cross-laminated timber systems (Blass & Fellmoser, 2004; Ceccotti, 2008; Gagnon & Pirvu, 2011; Okabe *et al.,* 2013) and is used in this study for the prediction of the elastic properties of G-XLam panels in bending, compression and shear.

9.1.1 Determination of modulus of elasticity of the panels in bending ($\boldsymbol{Ep_m}$).

For the determination of the G-XLam panel's modulus of elasticity in bending (Ep_m) the second moment of area of the transformed cross section (I) was calculated using Equation 9-1.

$$I = I_o + \mathrm{A} \cdot z^2$$

9-1

where
I_o is the second moment of area of the cross section about its neutral plane,
A is the cross sectional area and
z_i is the distance between the centre point of each layer and the central axis.

This equation uses Huygens-Steiner's theorem (parallel axis theorem) for the determination of the second moment of area (I) about the parallel axis crossing the centre point of each individual layer and the distance between both axes (z_i). I_o is the second moment of area of the whole panel cross section ($A = b \cdot h$) about its the neutral axis (N). As the panel is composed of a (n) number of layers the resulting equation describing the full transformed cross section is:

$$\mathrm{I} = \sum_{i=1}^{i=n} \frac{b \cdot h_i^3}{12} + \sum_{i=1}^{i=n} b \cdot h_i \cdot z_i^2 \qquad 9\text{-}2$$

Then, bending stiffness of the panel as defined by BS EN 14272 is obtained by the sum of the stiffness of each individual lamella (Equation 9-3) assuming that the width (b) is equal to one unit ($A_i = h_i \cdot 1$). This equation is in agreement with (Bodig & Jayne, 1982).

$$Ep_m \cdot \mathrm{I} = Ep_m \cdot \frac{h_i^3}{12} = \sum_{i=1}^{n} E_i \cdot h_i \cdot z_i^2 + \sum_{i=1}^{n} E_i \cdot \frac{h_i^3}{12} \qquad 9\text{-}3$$

The resulting equation to determine Ep_m (9-4) is also used in BS EN 14272 (BSI, 2011).

$$Ep_m = \frac{12 \cdot \sum_{i=1}^{n} E_i \cdot h_i \cdot z_i^2 + \sum_{i=1}^{n} E_i \cdot h_i^3}{(\sum_{i=1}^{n} h_i)^3} \qquad 9\text{-}4$$

Figure 9-1 illustrates the neutral axis of the panel and the individual axes of each layer composing a five layer cross-laminated panel with variable modulus of elasticity (E_i).

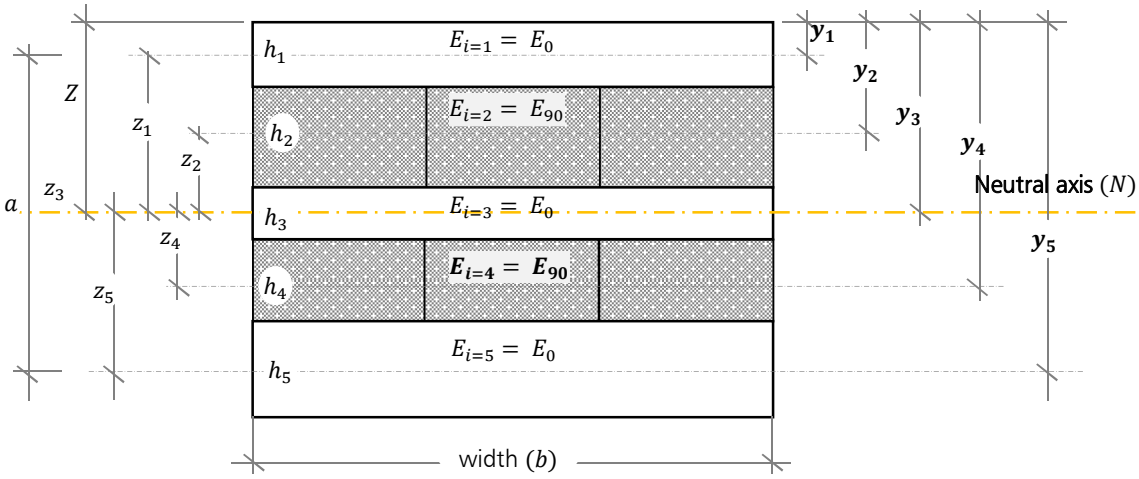

Figure 9-1. Typical cross section of a five layer cross-laminated panel using the shear analogy method.

BS EN 338 (BSI, 2009) and BS EN 14272 (BSI, 2011) assume that the modulus of elasticity in bending of the longitudinal layers ($E_{0,m}$) is 30 times higher than the moduli of elasticity in bending of the cross layers ($E_{90,m,t,c}$). This applies for softwoods (Equation 9-5), whilst Equation 9-6 applies for hardwoods.

$$E_{90,m,t,c} = \frac{E_{0,m}}{30} \qquad 9\text{-}5$$

$$E_{90,m,t,c} = \frac{E_{0,m}}{15} \qquad 9\text{-}6$$

Additionally, bending strength (fp_m) was calculated using Equation 9-8 given by BS EN 14272 (BSI, 2011).

$$fp_m = \frac{12 \cdot \sum_{i=1}^{n} MOR_i \cdot h_i \cdot z_i^2 + \sum_{i=1}^{n} MOR_i \cdot h_i^3}{(\sum_{i=1}^{n} h_i)^3} \cdot \frac{\sum_{i=1}^{n} h_i}{2 \cdot \mathrm{Z}} \qquad 9\text{-}7$$

where
h_i is the thickness of each individual layer and
Z corresponds to half the total thickness of the panel or ($\sum_{i=1}^{n} h_i$ /2) for a symmetrical panel composition.

9.1.2 Determination of the panel shear modulus (G_v).

In timber engineering, the shear modulus parallel to the grain (G_0) for softwood CLT panels

is generally considered to range between 1/12 and 1/20 of the longitudinal modulus of elasticity of the panel (E_0) and conservatively assumed to be 1/16 of E_0. Furthermore, the shear modulus perpendicular to grain known also as the rolling shear modulus (G_R) is assumed to be 1/10 of G_0 (Gagnon & Pirvu, 2011) (Figure 9-2).

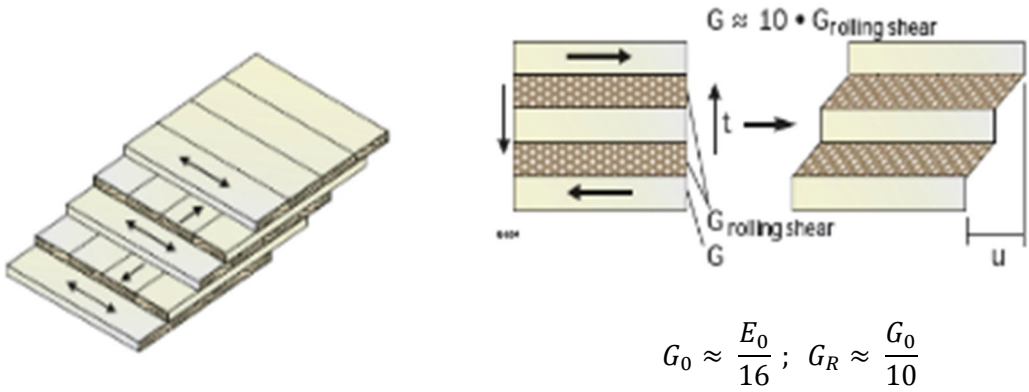

Figure 9-2. Shear modulus parallel (G_0) and perpendicular to grain (G_R) of a cross laminated panel. Image by (Gagnon & Pirvu, 2011)

BS EN 14272 (BSI, 2011) defines the panel shear modulus (G_v) as the summation of the individual shear moduli of the constituting layers (Equation 9-8).

$$G_v = \frac{\sum_{i=1}^{n-1} G_{vi} \cdot h_i}{\sum_{i=1}^{n-1} h_i} \qquad 9\text{-}8$$

where
h_i is the thickness of each individual layer

9.1.3 Determination of the modulus of elasticity in compression and tension of cross-laminated panels.

The MOE of cross laminated panels in compression and tension ($Ep_{t,c}$) can be calculated according to BS EN 14272 (BSI, 2011) using Equation 9-9. $Ep_{t,c}$ is equal to the summation of the elastic properties of the compound layers in the panel.

$$Ep_{t,c} = \frac{\sum_{i=1}^{n-1} E_{i\ t,c} \cdot h_i}{\sum_{i=1}^{n-1} h_i} \qquad 9\text{-}9$$

Assumption of one unit of width is also made in Equation 9-9.

Prediction of the elastic properties of G-XLam panels using stiffness values from their individual constituting layers (FGS).

Calculation of the mean elastic properties of three and five layer cross-laminated Guadua (G-XLam3 & G-XLam5) panels in compression (Ep_c), shear (G_v) and bending (Ep_m) was undertaken using Equations 9-9, 9-8 and 9-4, respectively. From Table 9-1 to Table 9-18, calculation of these elastic properties of the panels is illustrated.

In these tables, panel's moduli of elasticity in bending parallel ($Ep_{m,0}$) and perpendicular ($Ep_{m,90}$) to the direction of outer skins (considered as the main direction) are calculated. Furthermore, moduli of elasticity in compression along the longitudinal ($Ep_{c,0}$) and transverse ($Ep_{c,90}$) axes, and in-plane shear are calculated. Values obtained previously for E_0, E_{90} and G_o (G_{12}) through testing of small clear specimens (Table 7-14 in Chapter 7) were used as the characteristic properties of the individual layers in the three and five layers cross laminated panels (G-XLam3 and G-XLam5).

Bending strength of the panels (fp_m) was calculated as the sum of the mean strength values of the individual layers (Equation 9-8) using results of MOR_b obtained from small clear specimens testing in Chapter 7. For this calculation, cross layers (E_{90}) were not taken into account and a symmetrical composition of the cross laminated (G-XLam) panel was assumed.

In the following tables, mostly the notation system from BS EN 14272 (BSI, 2011) has been adopted and related to the Equations 9-9, 9-8 and 9-4 used for calculating the elastic properties of the G-XLam panels as explained below:

$A_i = h_i \cdot b_i \cdot E_i$; where $b = 1$;

$I_i = A_i \cdot \frac{h_i^2}{12} = \sum_{i=1}^{n} E_i \cdot \frac{h_i^3}{12}$ and $J_i = A_i \cdot C_i = \sum_{i=1}^{n} E_i \cdot \frac{h_i^3}{12} \cdot z^2$ in (kN.mm^2); where $C_i = z_i^2$ in mm^2; $Ep_m \cdot \mathrm{I} = Ep_m \cdot \frac{h_i^3}{12} = 12 \cdot \frac{\sum_{i=1}^{n} I_i + J_i}{\sum_{i=1}^{n} h_i^3}$; where $\mathrm{I} = \frac{b \cdot h_i^3}{12}$

and finally, for the panel shear modulus (G_v), $N_i = h_i \cdot G_{vi}$; where G_{vi} refers to the shear modulus of the individual layers.

z_{ax} (kN.mm^2) in symmetrical panel compositions is $T/2$ (half the total thickness of the panel); z_i is the distance between the centre point of each layer and the central axis and Y_i is the distance between the external face and the central axis of each layer in (mm), as illustrated in Figure 9-1.

Table 9-1. Calculation of the bending modulus of elasticity (Ep_m) of a G-XLam3 panel with main fibre-direction along its length (E_0) based on the elastic properties of all its compounding layers (2L, E_0 + 1T, E_{90}) and on a unit of width.

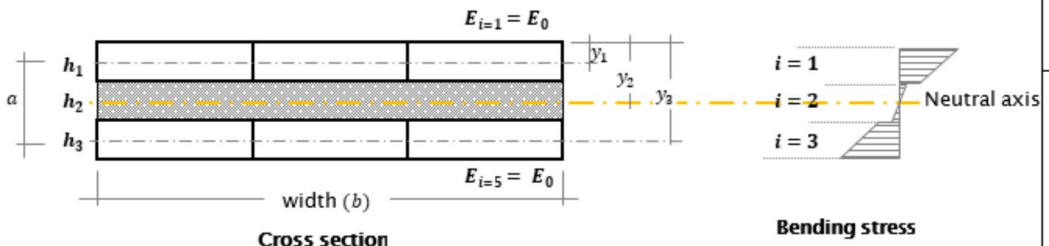

Type of panel: G-XLam5

2 L + 1 T layers THM modified Guadua
Calculation including cross layers

$$Ep_m = \frac{12 \cdot \sum_{i=1}^{n} E_i \cdot h_i \cdot z_i^2 + \sum_{i=1}^{n} E_i \cdot h_i^3}{(\sum_{i=1}^{n} h_i)^3}$$

$Ep_{m,0-\text{G-XLam3 (2L + 1T)}}$

$E_0 = 21.74\ kN/mm^2$

$E_{90} = 1.02\ kN/mm^2$

$G_0 = 1.32\ kN/mm^2$

G-XLam3		thickness	Property	A_i	T_i	Y_i	B_i	z_i	C_i	I_i	J_i
		h_i	E_i	$h_i * b_i * E_i$	$t_{i-1}+T_{i-1}$	$T_i + t_i/2$	$A_i * Y_i$	$\lvert Z_{ax} - Y_i \rvert$	z_i^2	$A_i * h_i^2/12$	$A_i * C_i$
Layers	Grain	(mm)	(kN/mm²)	(kN)	(mm)	(mm)	(kN*mm)	(mm)	(mm)²	(kN.mm²)	(kN.mm²)
h_1	L, (0°)	5.70	21.74	123.87	0.00	2.85	352.85	5.70	32.46	335.05	4,020.58
h_2	T, (90°)	5.70	1.02	5.81	5.70	8.55	49.66	0.00	0.00	15.72	0.00
h_3	L, (0°)	5.70	21.74	123.87	11.39	14.24	1,764.27	5.70	32.46	335.05	4,020.58
$\sum_{i=1}^{n} =$		**17.09**		**253.55**			**2,166.79**			**685.81**	**8,041.16**

$z_{ax} = \frac{\sum_{i=1}^{n} B_i}{\sum_{i=1}^{n} A_i}$	**8.55 mm** ($z_{ax} = 17.09/2$)	$I =$ **415.95 mm⁴**	$Ep_m \cdot I =$ **8,726.97 kN.mm²**	Ep_m **= 20.97 kN/mm²**

Table 9-2. Calculation of the bending modulus of elasticity (Ep_m) of a G-XLam3 panel with main fibre-direction along its length (E_0) based on the elastic properties of the two longitudinally orientated layers only (2L, E_0) and on a unit of width.

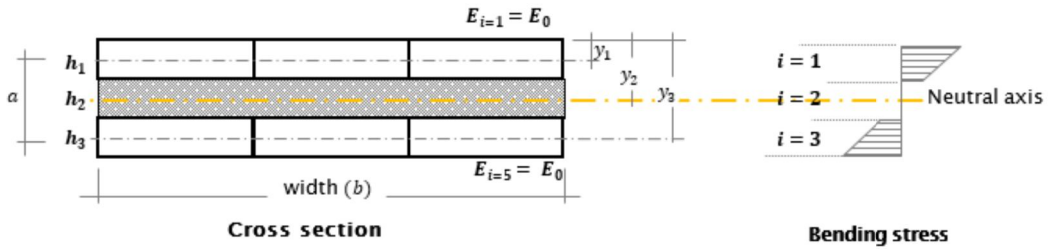

Type of panel: G-XLam5

2 (L) + 1 (T) layers THM modified Guadua
Calculation including cross layers

$$Ep_m = \frac{12 \cdot \sum_{i=1}^{n} E_i \cdot h_i \cdot z_i^2 + \sum_{i=1}^{n} E_i \cdot h_i^3}{\left(\sum_{i=1}^{n} h_i\right)^3}$$

$Ep_{m,0-\ G-XLam3\ (2L)}$

$E_0 = 21.74\ kN/mm^2$

$E_{90} = 0.00\ kN/mm^2$

$G_0 = 1.32\ kN/mm^2$

G-XLam3		thickness	Property	A_i	T_i	Y_i	B_i	z_i	C_i	I_i	J_i
		h_i	E_i	$h_i * b_i * E_i$	$t_{i-1}+T_{i-1}$	$T_i + t_i/2$	$A_i * Y_i$	$\lvert Z_{ax} - Y_i \rvert$	z_i^2	$A_i * h_i^2/12$	$A_i * C_i$
Layers	Grain	(mm)	(kN/mm²)	(kN)	(mm)	(mm)	(kN*mm)	(mm)	(mm²)	(kN.mm²)	(kN.mm²)
h_1	L, (0°)	5.70	21.74	123.87	0.00	2.85	352.85	5.70	32.46	335.05	4,020.58
h_2	T, (90°)	5.70	0.00		5.70						
h_3	L, (0°)	5.70	21.74	123.87	11.39	14.24	1,764.27	5.70	32.46	335.05	4,020.58
$\sum_{i=1}^{n} =$		**17.09**		**247.74**			**2,117.13**			**670.10**	**8,041.16**

$z_{ax} = \frac{\sum_{i=1}^{n} B_i}{\sum_{i=1}^{n} A_i}$	**8.55 mm** ($z_{ax} = 17.09/2$)	$I =$ **415.95 mm⁴**	$Ep_m \cdot I =$ **8,711.25 kN.mm²**	$Ep_m =$ **20.94 kN/mm²**

$MOR_i = 190.38\ N/mm^2$	$Z = \frac{\sum_{i=1}^{n} h_i}{2} = 8.55$ mm	$fp_m = \frac{12 \cdot \sum_{i=1}^{n} MOR_i \cdot h_i \cdot z_i^2 + \sum_{i=1}^{n} MOR_i \cdot h_i^3}{\left(\sum_{i=1}^{n} h_i\right)^3} \cdot \frac{\sum_{i=1}^{n} h_i}{2 \cdot Z}$	$fp_m =$ **183.33 N/mm²**

Table 9-3. Calculation of the bending modulus of elasticity (Ep_m) of a G-XLam3 panel with main fibre-direction along the transverse axis (E_{90}) based on the elastic properties of the two transversally and one longitudinally orientated layers (2T, E_{90} + 1L, E_0) and on a unit of width.

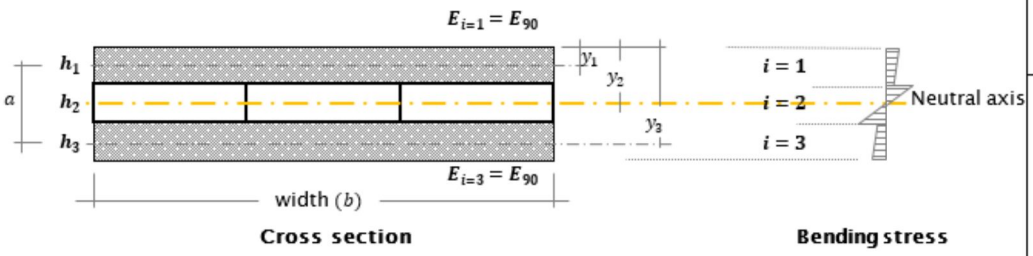

Type of panel: G-XLam5
2 (T) + 1 (L) layers THM modified Guadua
Calculation including cross layers

$$Ep_m = \frac{12 \cdot \sum_{i=1}^{n} E_i \cdot h_i \cdot z_i^2 + \sum_{i=1}^{n} E_i \cdot h_i^3}{\left(\sum_{i=1}^{n} h_i\right)^3}$$

$Ep_{m,90-\ G-XLam3\ (2T+1L)}$

$E_0 = 21.74\ kN/mm^2$

$E_{90} = 1.02\ kN/mm^2$

$G_0 = 1.32\ kN/mm^2$

G-XLam3		thickness	Property	A_i	T_i	Y_i	B_i	z_i	C_i	I_i	J_i
		h_i	E_i	$h_i * b_i * E_i$	$t_{i-1}+T_{i-1}$	$T_i + t_i/2$	$A_i * Y_i$	$\lvert Z_{ax} - Y_i \rvert$	z_i^2	$A_i * h_i^2/12$	$A_i * C_i$
Layers	Grain	(mm)	(kN/mm²)	(kN)	(mm)	(mm)	(kN*mm)	(mm)	(mm)²	(kN.mm²)	(kN.mm²)
h_1	T, (90°)	5.70	1.02	123.87	0.00	2.85	16.55	5.70	32.46	15.72	188.62
h_2	L, (0°)	5.70	21.74	5.81	5.70	8.55	1058.56	0.00	0.00	335.05	0.00
h_3	T, (90°)	5.70	1.02	123.87	11.39	14.24	82.77	5.70	32.46	15.72	188.62
$\sum_{i=1}^{n} =$		**17.09**		**135.49**			**1,157.89**			**366.48**	**377.24**

$z_{ax} = \frac{\sum_{i=1}^{n} B_i}{\sum_{i=1}^{n} A_i}$	**8.55 mm** ($z_{ax} = 17.09/2$)	$I =$ **415.95 mm⁴**	$Ep_m \cdot I$ **= 743.73 kN.mm²**	$Ep_m =$ **1.79 kN/mm²**

Table 9-4. Calculation of the bending modulus of elasticity (Ep_m) of a G-XLam3 panel with main fibre-direction along the transverse axis (E_{90}) based on the elastic properties of the two transversally orientated layers only (2T, E_{90}) and on a unit of width.

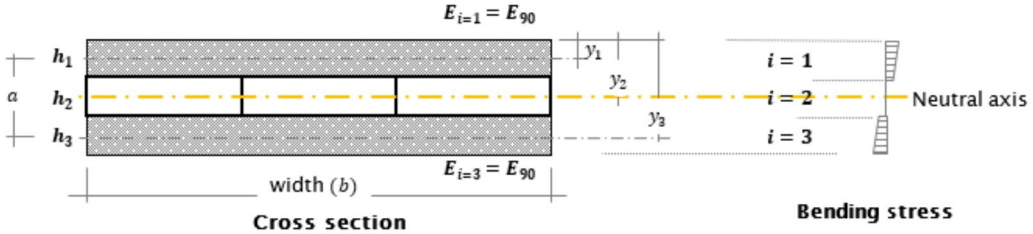

Type of panel: G-XLam5
2 (T) layers THM modified Guadua
Calculation including cross layers

$$Ep_m = \frac{12 \cdot \sum_{i=1}^{n} E_i \cdot h_i \cdot z_i^2 + \sum_{i=1}^{n} E_i \cdot h_i^3}{\left(\sum_{i=1}^{n} h_i\right)^3}$$

$Ep_{m,90-\ G-XLam3\ (2T)}$

$E_0 = 21.74\ kN/mm^2$

$E_{90} = 0.00\ kN/mm^2$

$G_0 = 1.32\ kN/mm^2$

G-XLam3		thickness	Property	A_i	T_i	Y_i	B_i	z_i	C_i	I_i	J_i
		h_i	E_i	h_i* b_i* E_i	$t_{i-1}+T_{i-1}$	$T_i + t_i/2$	A_i * Y_i	$\lvert Z_{ax} - Y_i \rvert$	z_i^2	A_i * $h_i^2/12$	A_i * C_i
Layers	Grain	(mm)	(kN/mm²)	(kN)	(mm)	(mm)	(kN*mm)	(mm)	(mm²)	(kN.mm²)	(kN.mm²)
h_1	T, (90°)	5.70	1.02	5.81	0.00	2.85	16.55	5.70	32.46	15.72	188.62
h_2	L, (0°)	5.70	0.00		5.70						
h_3	T, (90°)	5.70	1.02	5.81	11.39	14.24	82.77	5.70	32.46	15.72	188.62
$\sum_{i=1}^{n} =$		**17.09**		**11.62**			**99.32**			**31.44**	**377.24**

$z_{ax} = \frac{\sum_{i=1}^{n} B_i}{\sum_{i=1}^{n} A_i}$	**8.55 mm** ($z_{ax} = 17.09/2$)	$I =$ **415.95 mm⁴**	$Ep_m \cdot I =$ **408.68 kN.mm²**	Ep_m **= 0.98 kN/mm²**

Table 9-5. Calculation of the bending modulus of elasticity (Ep_m) of a G-XLam5 panel with main fibre-direction along its length (E_0) based on the elastic properties of all its compounding layers (3L, E_0 + 2T, E_{90}) and on a unit of width.

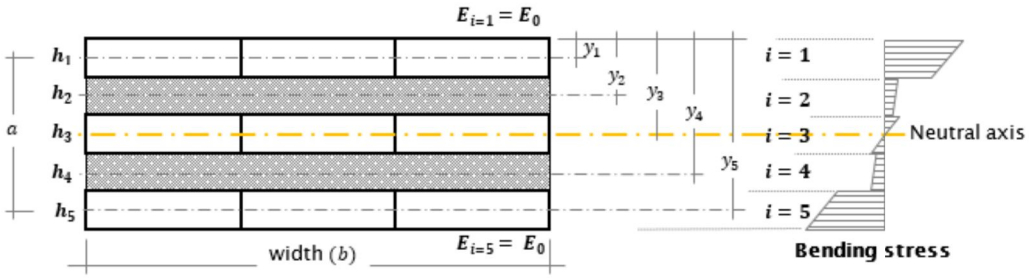

Type of panel: G-XLam5
3 (L) + 2 (T) layers THM modified Guadua
Calculation including cross layers

$$Ep_m = \frac{12 \cdot \sum_{i=1}^{n} E_i \cdot h_i \cdot z_i^2 + \sum_{i=1}^{n} E_i \cdot h_i^3}{\left(\sum_{i=1}^{n} h_i\right)^3}$$

$Ep_{m,0-\ G-XLam5\ (3L+2T)}$

$E_0 = 21.74\ kN/mm^2$

$E_{90} = 1.02\ kN/mm^2$

$G_0 = 1.32\ kN/mm^2$

G-XLam5		thickness	Property	A_i	T_i	Y_i	B_i	z_i	C_i	I_i	J_i
		h_i	E_i	h_i* b_i* E_i	$t_{i-1}+T_{i-1}$	$T_i + t_i/2$	A_i * Y_i	$\lvert Z_{ax} - Y_i \rvert$	z_i^2	A_i* $h_i^2/12$	A_i* C_i
Layers	Grain	(mm)	(kN/mm²)	(kN)	(mm)	(mm)	(kN*mm)	(mm)	(mm)²	(kN.mm²)	(kN.mm²)
h_1	L, (0°)	5.25	21.74	114.15	0.00	2.63	299.63	10.50	110.25	262.18	12,584.54
h_2	T, (90°)	5.25	1.02	5.36	5.25	7.88	42.17	5.25	27.56	12.30	147.60
h_3	L, (0°)	5.25	21.74	114.15	10.50	13.13	1,498.16	0.00	0.00	262.18	0.00
h_4	T, (90°)	5.25	1.02	5.36	15.75	18.38	98.40	5.25	27.56	12.30	147.60
h_5	L, (0°)	5.25	21.74	114.15	21.00	23.63	2,696.69	10.50	110.25	262.18	12,584.54
$\sum_{i=1}^{n} =$		**26.25**		**353.15**			**4635.05**			**811.13**	**25,464.28**

$z_{ax} = \frac{\sum_{i=1}^{n} B_i}{\sum_{i=1}^{n} A_i}$	**13.13 mm** ($z_{ax} = 26.25/2$)	$I =$ **1,507.48 mm⁴**	$Ep_m \cdot I =$ **26,275.41 kN.mm²**	Ep_m **= 17.43 kN/mm²**

Table 9-6. Calculation of the bending modulus of elasticity (Ep_m) of a G-XLam5 panel with main fibre-direction along its length (E_0) based on the elastic properties of the three longitudinally orientated layers only (3L, E_0) and on a unit of width.

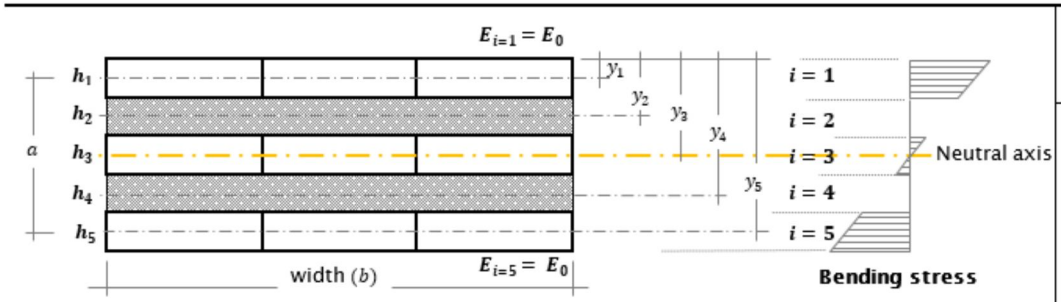

Type of panel: G-XLam5
3 (L) layers THM modified Guadua
Calculation without cross layers

$$Ep_m = \frac{12 \cdot \sum_{i=1}^{n} E_i \cdot h_i \cdot z_i^2 + \sum_{i=1}^{n} E_i \cdot h_i^3}{\left(\sum_{i=1}^{n} h_i\right)^3}$$

$Ep_{m,0-\text{G-XLam5 (3L)}}$

$E_0 = 21.74\ kN/mm^2$

$E_{90} = 0\ kN/mm^2$

$G_0 = 1.32\ kN/mm^2$

G-XLam5		thickness	Property	A_i	T_i	Y_i	B_i	z_i	C_i	I_i	J_i
		h_i	E_i	$h_i * b_i * E_i$	$t_{i-1}+T_{i-1}$	$T_i + t_i/2$	$A_i * Y_i$	$\lvert Z_{ax} - Y_i \rvert$	z_i^2	$A_i * h_i^2/12$	$A_i * C_i$
Layers	Grain	(mm)	(kN/mm²)	(kN)	(mm)	(mm)	(kN*mm)	(mm)	(mm)²	(kN.mm²)	(kN.mm²)
h_1	L, (0°)	5.25	21.74	114.15	0.00	2.63	299.63	10.50	110.25	262.18	12,584.54
h_2	T, (90°)	5.25	0.00		5.25						
h_3	L, (0°)	5.25	21.74	114.15	10.50	13.13	1,498.16	0.00	0.00	262.18	0.00
h_4	T, (90°)	5.25	0.00		15.75						
h_5	L, (0°)	5.25	21.74	114.15	21.00	23.63	2,696.69	10.50	110.25	262.18	12,584.54
$\sum_{i=1}^{n} =$		**26.25**		**342.44**			**4,494.48**			**786.53**	**25,169.08**

$z_{ax} = \frac{\sum_{i=1}^{n} B_i}{\sum_{i=1}^{n} A_i}$	**13.13 mm** ($z_{ax} = 26.25/2$)	$I =$ **1,507.48 mm⁴**	$Ep_m \cdot I =$ **25,955.62 kN.mm²**	$Ep_m =$ **17.22 kN/mm²**
$MOR_i = 190.38\ N/mm^2$	$Z = \frac{\sum_{i=1}^{n} h_i}{2} =$ 13.13 mm	$fp_m = \frac{12 \cdot \sum_{i=1}^{n} MOR_i \cdot h_i \cdot z_i^2 + \sum_{i=1}^{n} MOR_i \cdot h_i^3}{\left(\sum_{i=1}^{n} h_i\right)^3} \cdot \frac{\sum_{i=1}^{n} h_i}{2 \cdot Z}$	$fp_m =$ **150.78 N/mm²**

Table 9-7. Calculation of the bending modulus of elasticity (Ep_m) of a G-XLam5 panel with main fibre-direction along the transverse axis (E_{90}) based on the elastic properties of all its compounding layers (3T, E_{90} + 2L, E_0) and on a unit of width.

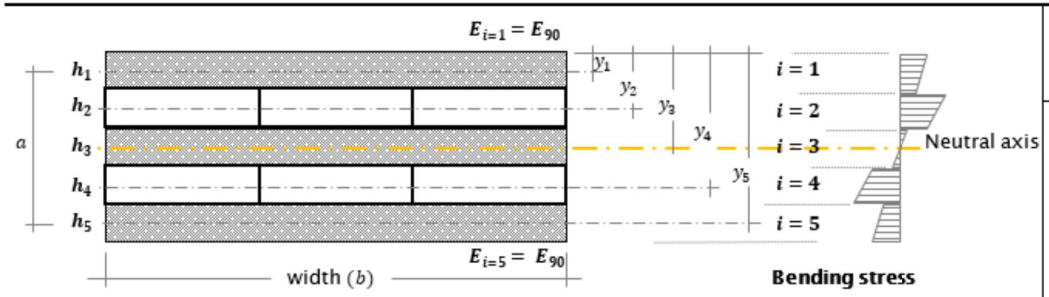

Type of panel: G-XLam5
3 (T) + 2 (L) layers THM modified Guadua
Calculation including cross layers

$$Ep_m = \frac{12 \cdot \sum_{i=1}^{n} E_i \cdot h_i \cdot z_i^2 + \sum_{i=1}^{n} E_i \cdot h_i^3}{\left(\sum_{i=1}^{n} h_i\right)^3}$$

$Ep_{m,90-\ G-XLam5\ (3T+2L)}$

$E_0 = 21.74\ kN/mm^2$

$E_{90} = 1.02\ kN/mm^2$

$G_0 = 1.32\ kN/mm^2$

G-XLam5		thickness	Property	A_i	T_i	Y_i	B_i	z_i	C_i	I_i	J_i
		h_i	E_i	$h_i * b_i * E_i$	$t_{i-1}+T_{i-1}$	$T_i + t_i/2$	$A_i * Y_i$	$\lvert Z_{ax} - Y_i \rvert$	z_i^2	$A_i * h_i^2/12$	$A_i * C_i$
Layers	Grain	(mm)	(kN/mm²)	(kN)	(mm)	(mm)	(kN*mm)	(mm)	(mm)²	(kN.mm²)	(kN.mm²)
h_1	T, (90°)	5.25	1.02	5.36	0.00	2.63	14.06	10.50	110.25	12.30	590.39
h_2	L, (0°)	5.25	21.74	114.15	5.25	7.88	898.90	5.25	27.56	262.18	3146.14
h_3	T, (90°)	5.25	1.02	5.36	10.50	13.13	70.28	0.00	0.00	12.30	0.00
h_4	L, (0°)	5.25	21.74	114.15	15.75	18.38	2097.42	5.25	27.56	262.18	3146.14
h_5	T, (90°)	5.25	1.02	5.36	21.00	23.63	126.51	10.50	110.25	12.30	590.39
$\sum_{i=1}^{n} =$		**26.25**		**244.36**			**320.17**			**561.26**	**7,473.05**

$z_{ax} = \frac{\sum_{i=1}^{n} B_i}{\sum_{i=1}^{n} A_i}$	**13.13 mm** ($z_{ax} = 26.25/2$)	$I =$ **1,507.48 mm⁴**	$Ep_m \cdot I =$ **8,034.30 kN.mm²**	$Ep_m =$ **5.33 kN/mm²**

Table 9-8. Calculation of the bending modulus of elasticity (Ep_m) of a G-XLam5 panel with main fibre-direction along the transverse axis (E_{90}) based on the elastic properties of the transversally orientated g layers only (3T, E_{90}) and on a unit of width.

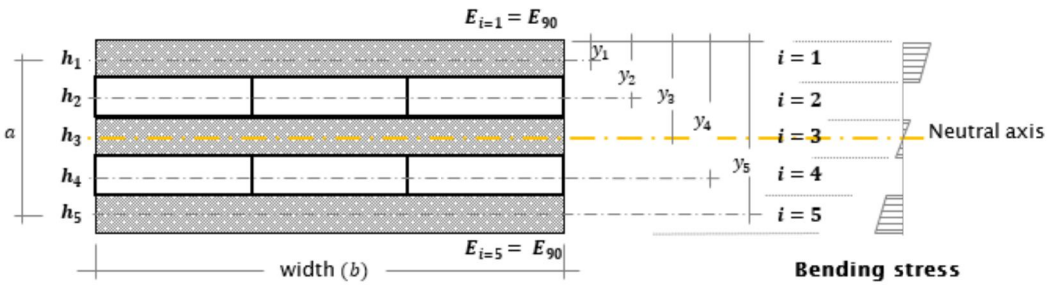

Type of panel: G-XLam5
3 (T) + 2 (L) layers THM modified Guadua
Calculation without including cross layers

$$Ep_m = \frac{12 \cdot \sum_{i=1}^{n} E_i \cdot h_i \cdot z_i^2 + \sum_{i=1}^{n} E_i \cdot h_i^3}{\left(\sum_{i=1}^{n} h_i\right)^3}$$

$Ep_{m,90-\,G-XLam5\,(3T)}$

$E_0 = 21.74\ kN/mm^2$

$E_{90} = 0\ kN/mm^2$

$G_0 = 1.32\ kN/mm^2$

G-XLam5		thickness	Property	A_i	T_i	Y_i	B_i	z_i	C_i	I_i	J_i
		h_i	E_i	$h_i * b_i * E_i$	$t_{i-1}+T_{i-1}$	$T_i + t_i/2$	$A_i * Y_i$	$\lvert Z_{ax} - Y_i \rvert$	z_i^2	$A_i * h_i^2/12$	$A_i * C_i$
Layers	Grain	(mm)	(kN/mm²)	(kN)	(mm)	(mm)	(kN*mm)	(mm)	(mm)²	(kN.mm²)	(kN.mm²)
h_1	T, (90°)	5.25	1.02	5.36	0.00	2.63	14.06	10.50	110.25	12.30	590.39
h_2	L, (0°)	5.25	0.00		5.25						
h_3	T, (90°)	5.25	1.02	5.36	10.50	13.13	70.28	0.00	0.00	12.30	0.00
h_4	L, (0°)	5.25	0.00		15.75						
h_5	T, (90°)	5.25	1.02	5.36	21.00	23.63	126.51	10.50	110.25	12.30	590.39
$\sum_{i=1}^{n} =$		**26.25**		**16.07**			**210.85**			**36.90**	**1,180.78**

$z_{ax} = \frac{\sum_{i=1}^{n} B_i}{\sum_{i=1}^{n} A_i}$	**13.13 mm** ($z_{ax} = 26.25/2$)	$I =$ **1,507.48 mm⁴**	$Ep_m \cdot I =$ **1,217.68 kN.mm²**	$Ep_m =$ **0.81 kN/mm²**

Table 9-9. Calculation of the compression modulus of elasticity of a G-XLam3 panel with main fibre-direction along its length (Ep_{c-L}) including the elastic properties of all its compounding layers (2L, E_0 + 1T, E_{90}) and based on a unit of width.

G-XLam3 panel	2 (L) + 1 (T) layers THM modified Guadua			$Ep_{c,0\ \ G-XLam3\ (2L+1T)}$
Axial load		thickness	Layer Property	A_i
		h_i	E_i	h_i* b_i*E_i
$E_{i=1}, E_{i=3} = E_0$	Layers	Grain	(mm)	(kN/mm²)	(kN)
	h_1	L, (0°)	5.70	21.74	123.87
	h_2	T, (90°)	5.70	1.02	5.81
	h_3	L, (0°)	5.70	21.74	123.87
width (b)	$\sum_{i=1}^{n} =$		17.09		253.5
h_1 h_2 h_3	$Ep_{t,c} = \frac{\sum_{i=1}^{n} E_i \cdot h_i}{\sum_{i=1}^{n} h_i}$			$Ep_{C,0}$ = 14.83 kN/mm²	

Table 9-10. Calculation of the compression modulus of elasticity of a G-XLam3 panel with main fibre-direction along its length (Ep_{c-L}) neglecting the elastic properties of the transversally orientated layer (2L, E_0) and based on a unit of width.

G-XLam3 panel	2 (L) layers THM modified Guadua			$Ep_{c,0\ \ G-XLam3\ (2L)}$
Axial load		thickness	Layer Property	A_i
		h_i	E_i	h_i* b_i*E_i
$E_{i=1}, E_{i=3} = E_0$	Layers	Grain	(mm)	(kN/mm²)	(kN)
	h_1	L, (0°)	5.70	21.74	123.87
	h_2	T, (90°)	5.70	0	
	h_3	L, (0°)	5.70	21.74	123.87
width (b)	$\sum_{i=1}^{n} =$		17.09		247.74
h_1 h_2 h_3	$Ep_{t,c} = \frac{\sum_{i=1}^{n} E_i \cdot h_i}{\sum_{i=1}^{n} h_i}$			$Ep_{C,0}$ = 14.49 kN/mm²	

Table 9-11. Calculation of the compression modulus of elasticity of a G-XLam3 panel with main fibre-direction oriented transversally (Ep_{c-T}) including the elastic properties of all its compounding layers (2T, E_{90} +1L, E_0) and based on a unit of width.

G-XLam3 panel	2 (T) + 1 (L) layers THM modified Guadua			$Ep_{c,90\ G-XLam3\ (2T+1L)}$	
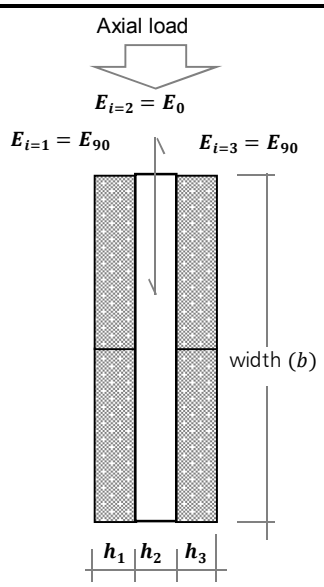			thickness	Layer Property	A_i
			h_i	E_i	h_i* b_i*E_i
	Layers	Grain	(mm)	(kN/mm²)	(kN)
	h_1	T, (90°)	5.70	1.02	5.81
	h_2	L, (0°)	5.70	21.74	123.87
	h_3	T, (90°)	5.70	1.02	5.81
	$\sum_{i=1}^{n} =$		17.09		135.49
	$Ep_{t,c} = \frac{\sum_{i=1}^{n} E_i \cdot h_i}{\sum_{i=1}^{n} h_i}$			$Ep_{C,90} = 7.93$ kN/mm²	

Table 9-12. Calculation of the compression modulus of elasticity of a G-XLam3 panel with main fibre-direction oriented transversally (Ep_{c-T}) neglecting the elastic properties of the longitudinally orientated layer (2T, E_{90}) and based on a unit of width.

G-XLam3 panel	2 (T) layers THM modified Guadua			$Ep_{c,90\ G-XLam3\ (2T)}$	
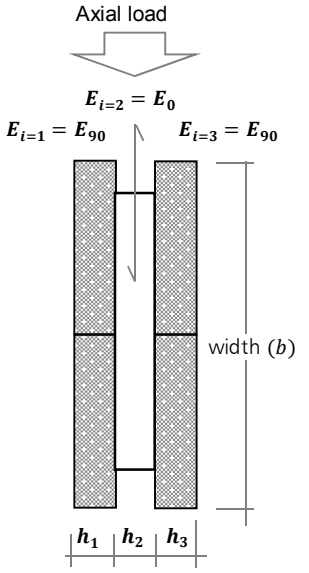			thickness	Layer Property	A_i
			h_i	E_i	h_i* b_i*E_i
	Layers	Grain	(mm)	(kN/mm²)	(kN)
	h_1	T, (90°)	5.70	1.02	5.81
	h_2	L, (0°)	5.70	0.00	
	h_3	T, (90°)	5.70	1.02	5.81
	$\sum_{i=1}^{n} =$		17.09		11.62
	$Ep_{t,c} = \frac{\sum_{i=1}^{n} E_i \cdot h_i}{\sum_{i=1}^{n} h_i}$			$Ep_{C,90} =$ 0.68 kN/mm²	

Table 9-13. Calculation of the compression modulus of elasticity of a G-XLam5 panel with main fibre-direction along its length (Ep_{c-L}) including the elastic properties of all its compounding layers (3L, E_0 + 2T, E_{90}) and based on a unit of width.

G-XLam5 panel	3 (L) + 2 (T) layers THM modified Guadua			$Ep_{c,0\ G-XLam5\ (3L+2T)}$
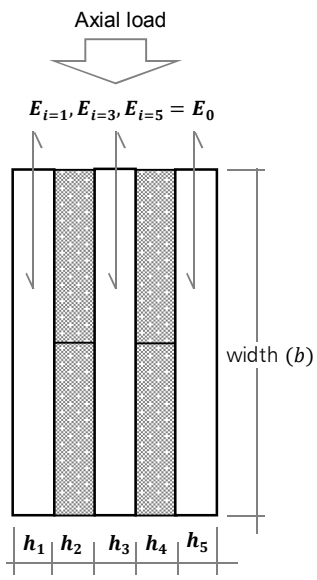		thickness	Layer Property	A_i
		h_i	E_i	h_i* b_i*E_i
	Layers	Grain	(mm)	(kN/mm²)	(kN)
	h_1	L, (0°)	5.25	21.74	114.15
	h_2	T, (90°)	5.25	1.02	5.36
	h_3	L, (0°)	5.25	21.74	114.15
	h_4	T, (90°)	5.25	1.02	5.36
	h_5	L, (0°)	5.25	21.74	114.15
	$\sum_{i=1}^{n} =$		26.25		353.15
	$Ep_{t,c} = \frac{\sum_{i=1}^{n} E_i \cdot h_i}{\sum_{i=1}^{n} h_i}$			$Ep_{C,0} = 13.45$ kN/mm²	

Table 9-14. Calculation of the compression modulus of elasticity of a G-XLam5 panel with main fibre-direction along its length (Ep_{c-L}) neglecting the elastic properties of the transversally orientated layer (3L, E_0) and based on a unit of width.

G-XLam5 panel	3 (L) + 2 (T) layers THM modified Guadua			$Ep_{c,0\ G-XLam5\ (3L)}$
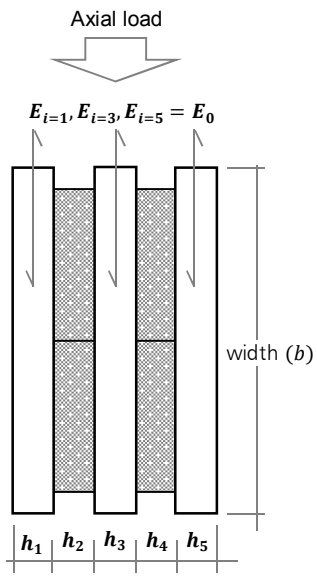		thickness	Layer Property	A_i
		h_i	E_i	h_i* b_i*E_i
	Layers	Grain	(mm)	(kN/mm²)	(kN)
	h_1	L, (0°)	5.25	21.74	114.15
	h_2	T, (90°)	5.25	0.00	
	h_3	L, (0°)	5.25	21.74	114.15
	h_4	T, (90°)	5.25	0.00	
	h_5	L, (0°)	5.25	21.74	114.15
	$\sum_{i=1}^{n} =$		26.25		342.44
	$Ep_{t,c} = \frac{\sum_{i=1}^{n} E_i \cdot h_i}{\sum_{i=1}^{n} h_i}$			$Ep_{C,0} = 13.05$ kN/mm²	

Table 9-15. Calculation of the compression modulus of elasticity of a G-XLam5 panel with main fibre-direction transversally (Ep_{c-T}) including the elastic properties of all its compounding layers (3T, E_{90} + 2L, E_0) and based on a unit of width.

G-XLam5 panel	3 (T) + 2 (L) layers THM modified Guadua.			$Ep_{c,90\ G-XLam5\ (3T+2L)}$
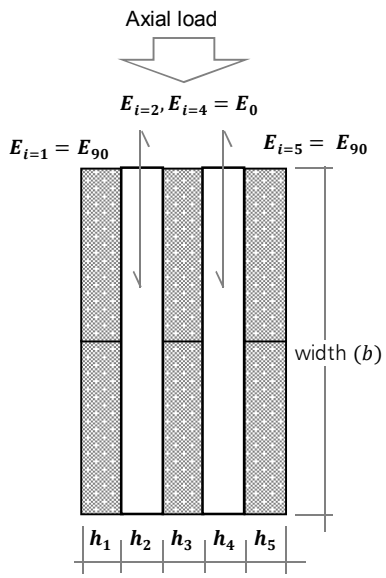		thickness	Layer Property	A_i
		h_i	E_i	h_i* b_i*E_i
	Layers	Grain	(mm)	(kN/mm²)	(kN)
	h_1	T, (90°)	5.25	21.74	114.15
	h_2	L, (0°)	5.25	1.02	5.36
	h_3	T, (90°)	5.25	21.74	114.15
	h_4	L, (0°)	5.25	1.02	5.36
	h_5	T, (90°)	5.25	21.74	114.15
	$\sum_{i=1}^{n} =$		26.25		244.36
	$Ep_{t,c} = \frac{\sum_{i=1}^{n} E_i \cdot h_i}{\sum_{i=1}^{n} h_i}$			$Ep_{C,90} =$ 9.31 kN/mm²	

Table 9-16. Calculation of the compression modulus of elasticity of a G-XLam5 panel with main fibre-direction oriented transversally (Ep_{c-T}) neglecting the elastic properties of the longitudinally orientated layers (3T, E_{90}) and based on a unit of width.

G-XLam5 panel	3 (T) + 2 (L) layers THM modified Guadua.			$Ep_{c,90\ G-XLam5\ (3T)}$
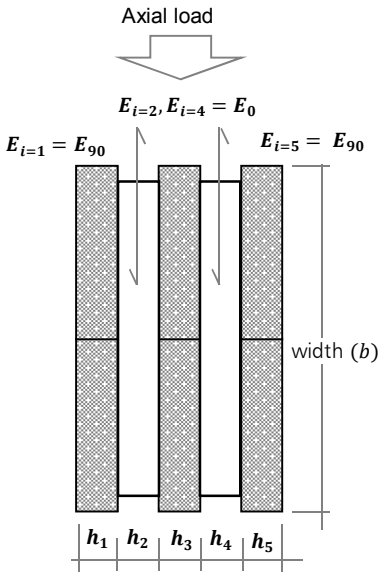		thickness	Layer Property	A_i
		h_i	E_i	h_i* b_i*E_i
	Layers	Grain	(mm)	(kN/mm²)	(kN)
	h_1	T, (90°)	5.25	1.02	5.36
	h_2	L, (0°)	5.25	0.00	
	h_3	T, (90°)	5.25	1.02	5.36
	h_4	L, (0°)	5.25	0.00	
	h_5	T, (90°)	5.25	1.02	5.36
	$\sum_{i=1}^{n} =$		26.25		16.07
	$Ep_{t,c} = \frac{\sum_{i=1}^{n} E_i \cdot h_i}{\sum_{i=1}^{n} h_i}$			$Ep_{C,90} =$ 0.61 kN/mm²	

Table 9-17. Calculation of the panel shear rigidity (G_v) of a G-XLam3 panel including the shear moduli of all its compounding layers ($2G_0 + 1G_R$) and based on a unit of width.

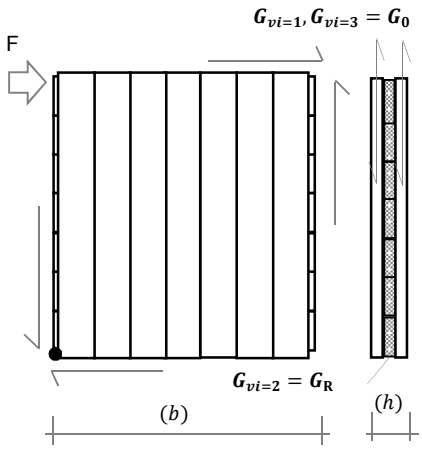

	G-XLam3 panel		$G_{v,\ \mathrm{G-XLam3}}$	
		thickness	Layer Property	N
		h_i	G_{vi}	$N_i = h_i \cdot b_i \cdot G_{vi}$
Layers	Grain	(mm)	(kN/mm²)	(kN)
h_1	G_0	5.70	1.32	6.93
h_2	G_R	5.70	0.13	0.69
h_3	G_0	5.70	1.32	6.93
$\sum_{i=1}^{n} =$		17.09		**15.79**

$$G_v = \frac{\sum_{i=1}^{n-1} G_{vi} \cdot h_i}{\sum_{i=1}^{n-1} h_i} \qquad G_v = 0.92 \text{ kN/mm}^2$$

Table 9-18. Calculation of the panel shear rigidity (G_v) of a G-XLam5 panel including the shear moduli of all its compounding layers ($3G_0 + 2G_R$) and based on a unit of width.

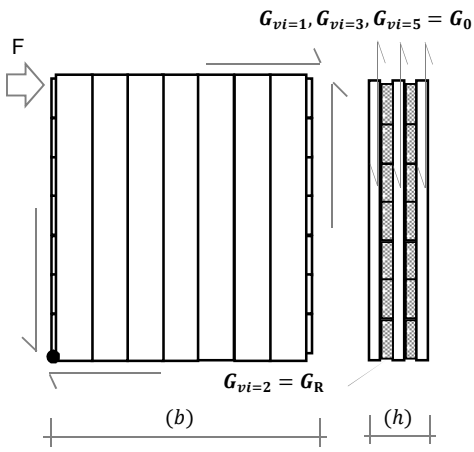

	G-XLam5 panel		$G_{v,\ \mathrm{G-XLam5}}$	
		thickness	Property	N
		h_i	G_{vi}	$N_i = h_i \cdot b_i \cdot G_{vi}$
Layers	Grain	(mm)	(kN/mm²)	(kN)
h_1	G_0	5.25	1.32	6.93
h_2	G_R	5.25	0.13	0.69
h_3	G_0	5.25	1.32	6.93
h_4	G_R	5.25	0.13	0.69
h_5	G_0	5.25	1.32	6.93
$\sum_{i=1}^{n} =$		26.25		**16.07**

$$G_v = \frac{\sum_{i=1}^{n-1} G_{vi} \cdot h_i}{\sum_{i=1}^{n-1} h_i} \qquad G_v = 0.84 \text{ kN/mm}^2$$

9.1.4 Analytical results

A summary of all the predicted elastic values for G-XLam panels in bending (Ep_m), compression (Ep_c) and shear (G_v) obtained in Table 9-1 to Table 9-18 is presented in Table 9-19. As can be seen, no-significant contribution to the stiffness of the panels is given by the cross layers (those transversally orientated or at 90° to the main direction of the panel). A very small influence of the rolling shear (G_R) on the mean panel modulus of rigidity (G_v) is also observed. Overall, G_v calculations including G_R presented an improvement in stiffness between 5% and 6%, while stiffness values in the longitudinal direction of G-XLam panels in bending are about 35% higher than those in compression. Similar behaviour for structural and non-structural wood panels is reported by BSI (2008) and Marcroft (2012). This reduction in the elastic properties in compression can be explained by the effects of shear and buckling during in-plane loading.

Table 9-19. Predicted elastic values for G-XLam panels in bending, compression and shear.

Property	Main direction of layers	Symbol	G-XLam 3		G-XLam 5	
			2L+1T	2L	3L+2T	3L
Bending	Longitudinal (L)	$Ep_{m,0}$	20.97 GPa	20.94 GPa	17.43 GPa	17.22 GPa
	Transverse (T)	$Ep_{m,90}$	1.79 GPa	0.98 GPa	5.33 GPa	0.81 GPa
Bending strength	Longitudinal (L)	fp_m	-	183.33 MPa	-	150.78 MPa
Compression	Longitudinal (L)	$Ep_{c,0}$	14.83 GPa	14.49 GPa	13.45 GPa	13.05 GPa
	Transverse (T)	$Ep_{c,90}$	7.93 GPa	0.68 GPa	9.31 GPa	0.61 GPa
Shear	-	G_v	0.92 GPa	0.88 GPa	0.84 GPa	0.79 GPa

L = main load direction (longitudinal)
T = 90° to the main load direction (transverse

Bending strength (fp_m) values predicted for G-XLam3 and G-XLam5 panels were 183.33MPa and 150.78MPa, respectively. These results are within the range of MOR values obtained by three point bending tests for the individual layer (sample C); where $MOR_{b,C} = 190.38 \pm 47.07\ MPa$ was used for the calculation of fp_m. On the other hand, elastic values in bending, compression and shear calculated for G-XLam panels are generally higher than the mean values of conventional structural and non-structural wood products (Table 9-20).

Table 9-20. Mean elastic values of structural and non-structural wood panels.

Property	Main layer direction (external)	Symbol	Multi-layer solid wood panels [a] (20 to 30mm)	Particle boards [b] (20 to 25mm)	Birch plywood [b] (8.5 to 25mm)	OSB/4 [b] (18 to 25mm)	CLT 3	G-XLam3 17.09 mm	CLT 5	G-XLam5 26.25 mm
Bending Modulus (GPa)	0° (L)	Ep_m	8.2	3.0	9.7	6.78	11.6 [c]	20.97	-	17.43
	90° (T)	$Ep_{m,90}$	0.55	-	6.1	2.68	0.37 [c]	1.79	-	5.33
Compression modulus (GPa)	0° (L)	$Ep_{c,0}$	3.5	1.8	9.0	4.3	**7.42**	14.83	**6.74**	13.45
	90° (T)	$Ep_{c,90}$	2.9	-	7.9	3.2	**3.91**	7.93	**4.62**	9.31
Shear Modulus (GPa)	-	G_v	0.47	0.86	-	1.09	0.65 [c]	0.92	-	0.84

[a] (BSI, 2008); [b] (Marcroft, 2012); [c] CLT M1 BSP (C24) crossplan (Kaufmann, 2009).

9.2 Finite Element Model (FEM)

As a minor part of this study, FEMs of G-XLam3 and G-XLam5 panels were developed using ABAQUS/CAE 6.10-2 to simulate the elastic behaviour of panels under in-plane compression. Orthogonal behaviour was assumed for the model. Elastic properties presented in Table 9-21 and a rolling shear ($\boldsymbol{G_R}$) value of 0.581 MPa reported by García *et al.* (2012) were used for the analysis.

Table 9-21. Characteristic elastic values and Poisson's ratio of flat Guadua sheets (FGS) pre and post THM modification.

Property	Pre-THM (control sample)	Post-THM (modified FGS)
$E_{1,t}$	16.88 GPa	21.74 GPa
$E_{2,c}$	0.55 GPa	0.84 GPa
υ_{12}	0.28	0.26
υ_{13}	0.30	0.09
Compression set (C)	0 %	42.51 %
Density (ρ)	540 kg/m^3	890 kg/m^3
Specific stiffness (average)	31.06 m^{2}s^{-2}	34.49 m^{2}s^{-2}

In addition, finite element analyses were undertaken to study the influence of the gaps. FEMs were developed for 3-layered and 5-layered panels (G-XLam3 and G-XLam5) and

loaded in both in-plane directions (X_1 and X_2). For the FEMs, the total height and width of the panel is 600 mm and all configurations were modelled with and without gaps. The widths of the individual strips (FGS) modelled are 30 mm for the models with gaps and 33 mm for the gapless models, respectively. The thickness of each layer is 5.5 mm and the width of the gaps is 3 mm.

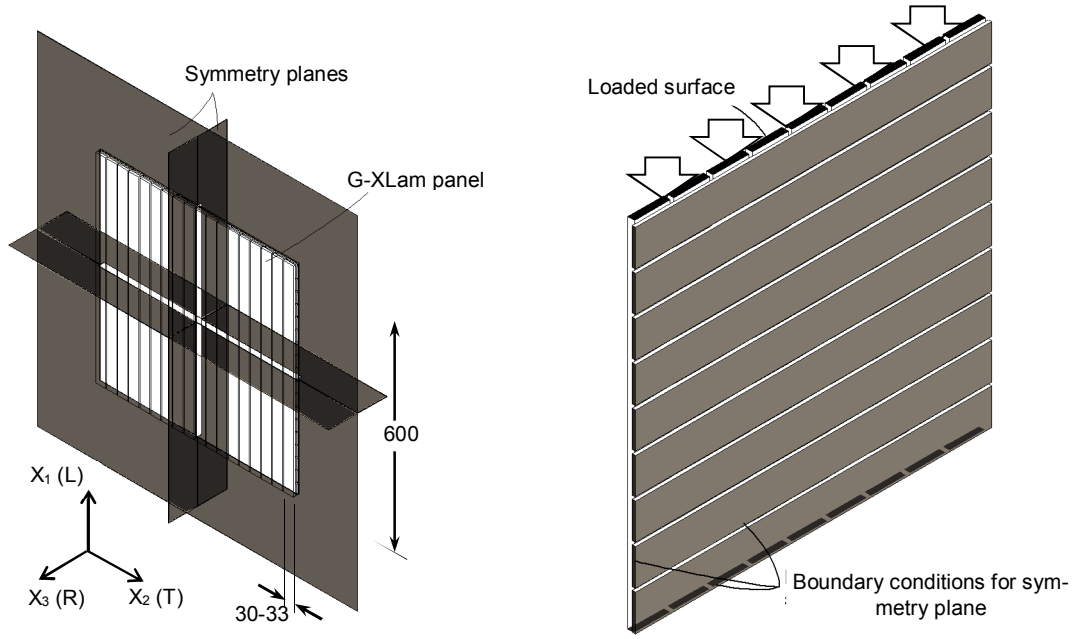

Figure 9-3. a) Symmetry planes of the tested G-XLam panel. b) Location of boundary conditions in FEM.

It can be observed in Figure 9-3a that the panel has three symmetry planes, thus only 1/8 of the actual panel is modelled. The parts that are not modelled can be simulated by boundary conditions. To replicate a symmetry plane, all out of plane translations and rotations have to be restrained. The geometry of the 1/8 model can be seen in Figure 9-3b. Grey surfaces indicate the boundary conditions, whilst black surfaces on the top of the panel indicate that load is only applied to the lamellae with the grain direction parallel to the load (L).

The elements used for the analysis were 3 dimensional linear 8-node elements with reduced integration. Each element has only one integration point which is located in the centre of the element. This element type is prone to *hourglassing*, which occurs when the element is bent. The strain in the centre of the element is then zero which leads to zero energy modes and an overestimation of deflections. The enhanced *hourglass* control function of ABAQUS was applied to avoid this hourglassing. The mesh was composed of four elements in the thickness direction of the lamellae (X_3) to be able to simulate shear deformations. In the

other two directions the element size was kept at 3 mm which is equal to the gap size. By doing this, the nodes of the lamellae that were in contact coincided. Normal hard contact described the behaviour of two lamellae parallel to each other. In this contact a master and slave surface are chosen, where the slave nodes cannot penetrate the master surface. Since the mesh and material properties of both lamellae were similar, the master and slave surfaces could be randomly chosen. The glued connection between two crossing lamellas was simulated with tie constraints. The nearest nodes of both members were tied together and could not move relatively to each other. As the surface nodes of contacting members coincided in the model, the coinciding nodes behaved as one.

9.2.1 Results FEM

Table 9-22 contains the values of MOE in compression for G-XLam3 and G-XLam5 panel configurations along the longitudinal (Ep_{c-L}) and transverse (Ep_{c-T}) orientations obtained through numerical and the FE analysis using the properties of all their constituting layers.

Table 9-22. Modulus of elasticity in compression longitudinal (E0) and transverse (E90) directions of the G-XLam panels determined by FE analysis

MOE Values	G-XLam3		G-XLam5	
	$Ep_{C,0}$ (2L+1T)	$Ep_{C,90}$ (2T+1L)	$Ep_{C,0}$ (3L+2T)	$Ep_{C,90}$ (3T+2L)
FEM (gapless)	14.95 GPa	8.05 GPa	13.52 GPa	9.36 GPa
Analytical prediction	14.83 GPa	7.93GPa	13.45GPa	9.31 GPa
FEM (with gaps)	12.75 GPa	7.56 GPa	12.94 GPa	8.42 GPa

No significant variation is observed between the predicted results and the values obtained through the FE analysis, which validates the accuracy of the FEM. G-XLam3 and G-XLam5 panels longitudinally oriented presented a load capacity considerably higher than their transverse orientation in both predicted and FEM results. Results from the FEM for panels with gaps show the influence that gaps can have on the overall compressive stiffness of the G-XLam panels, which was reduced by about 10%. This percentage can be used to adjust the analytically predicted mechanical properties of G-XLam3 and G-XLam5 panels to the actual conditions of the panels manufactured in this study. Confirmation or rejection of this hypothesis will be possible through the assessment of the elastic properties of the panels by mechanical testing (see following Chapter).

Concluding remarks

Given the mechanical properties of the individual components (layers) of the panelised system G-XLam, its bulk mechanical behaviour could be predicted through different mathematical expressions that consider the variation of number of layers, orientation, thickness and mechanical properties of the individual layers. These formulae are based on analytical design methods for plywood and CLT that are accepted by European standards.

Stiffness values obtained provide design values for structural design, nevertheless these values will need to be compared to mechanical test results.

10. Characterization of the elastic properties of G-XLam panels by mechanical testing

Introduction

Large cross-laminated Guadua (G-XLam) panels comprised of three and five layers (G-XLam3 and G-XLam5) were tested in compression, shear and bending. In-plane compression tests were performed in both X_1 (L, longitudinal) and X_2 (T, transverse) directions and LVDT transducers were used to follow in-plane deformation in the elastic region. Both G-XLam3 and G-XLam5 panels were also tested using the digital image correlation (DIC) method to measure strain variations in the X_1 X_2 plane and out of plane in the X_3 direction, again in the elastic zone. A shear picture frame method was used to measure the shear moduli (G_v) of the panels. Four point bending tests were also performed along the longitudinal axis to determine elastic properties in flexure and ultimately to measure flexural strength by testing to failure.

Data from several applications of load were analysed for each test configuration and compression moduli of elasticity of the panels in both directions L ($Ep_{C,0}$) and T ($Ep_{C,9\ 0}$) were determined. Shear tests used LVDT and DIC techniques simultaneously, while four point bending tests only used LVDTs. Results and details of the mechanical testing programme undertaken on G-XLam3 and G-XLam5 panels are presented in this Chapter. These results enabled the complete assessment of the panel's overall response to different load conditions and determine the factors affecting panel quality including voids and spacing between individual flat Guadua sheets or gluing defects. Furthermore, these experimental results will confirm the mathematical and finite element analyses implemented in the previous Chapter (Chapter 9) which used the elastic properties of the individual layer components determined in Chapter 7.

10.1 Testing programme

G-XLam3 and G-XLam5 panels with dimensions of 600x600mm and 700x700mm were subjected to mechanical testing. These sizes are considered to be representative volume elements (RVE) of potentially larger commercial size panels. The testing programme included in-plane compression tests in the X_1 (longitudinal) and X_2 (transverse) directions, four point bending test and in-plane shear test (Figure 10-1).

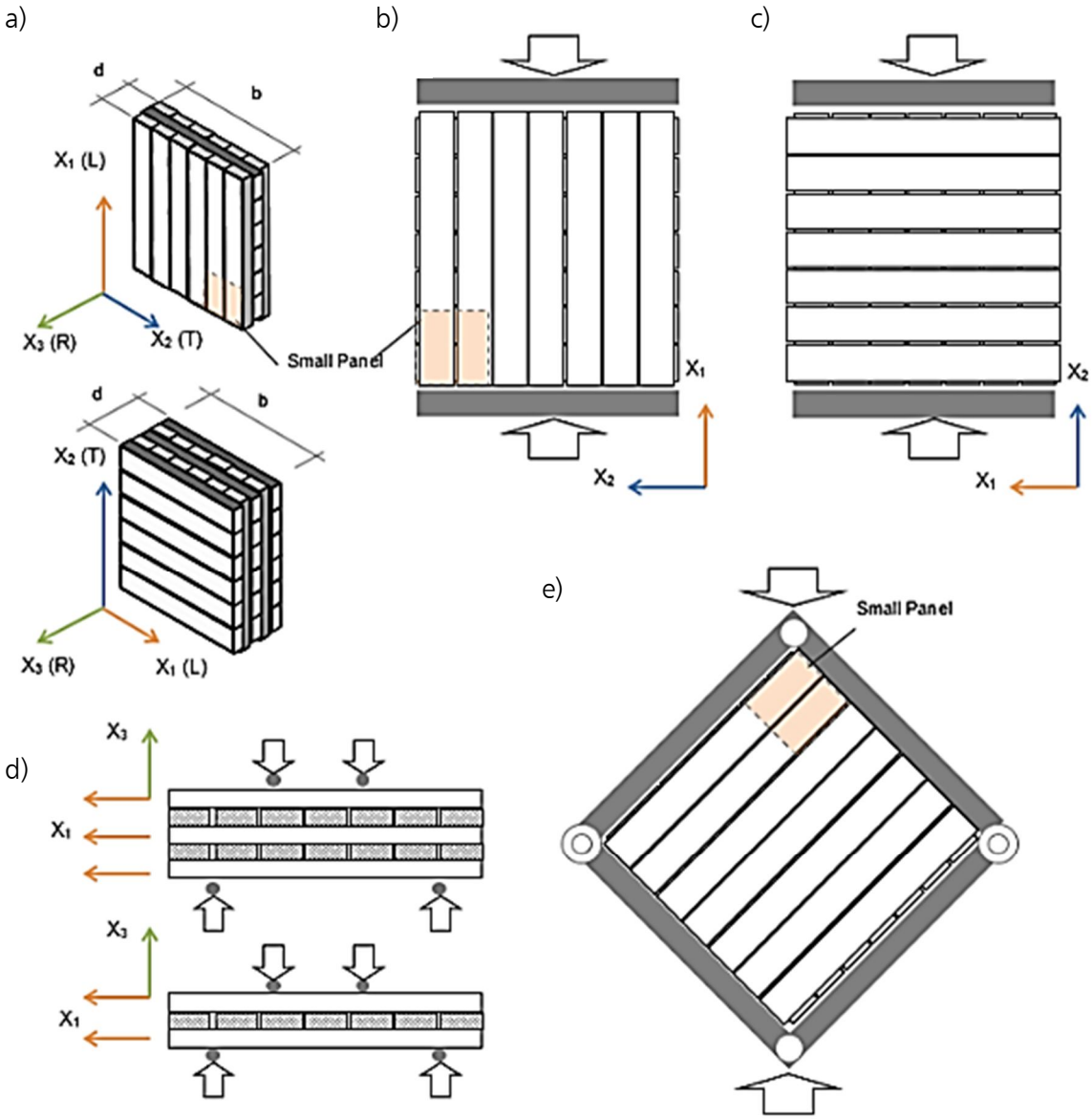

Figure 10-1. a) Geometric (X_1, X_2, X_3) axes of G-XLam3 and G-XLam5 panels. b) Diagram of the compression test in the longitudinal direction of the panel. c) Diagram of the compression test in the transverse direction of the panel. d) Diagram illustrating 4-point bending test setup for G-XLam3 and G-XLam5 panels. e) Diagram of the picture frame panel shear test.

Due to limited number of panels available (only three large panels were manufactured), the general aim of these tests was to determine the in-plane elastic properties (shear and elastic moduli) of G-XLam panels by using different test configurations and measurement techniques on the same panel specimens.

Non-contact and physical measurement methods were used to track deformation during testing. Digital image correlation (DIC) and linear variable differential transformer (LVDT) transducers were used separately or in combination depending on the constraints of the test setup. DIC was not used for bending tests. During shear and compression tests, large panel specimens were subjected to multiple test repetitions below the elastic limit using different measurement systems under the same boundary conditions. Figure 10-2 illustrates the control panel specimens of 170mm square tested in compression and shear prior to large scale testing. The orientation of these small panels, in comparison with the larger panels, is shown in Figure 10-1.

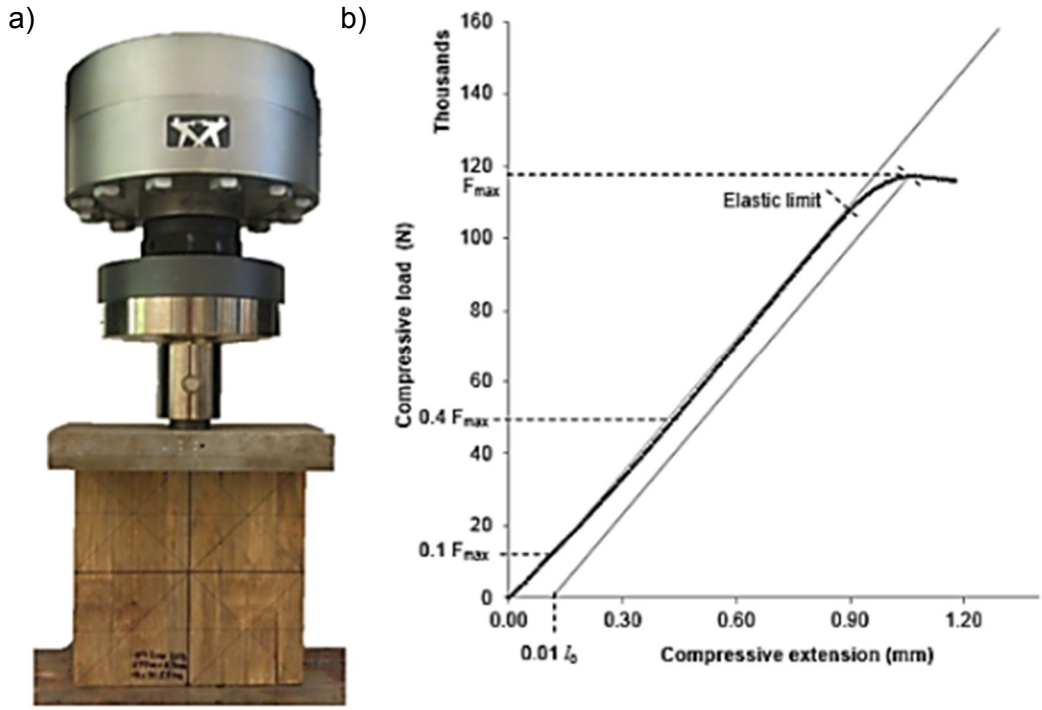

Figure 10-2. Preliminary compression test of a small panel (control specimen). a) Specimen on the test machine. b) Load-deformation graph used to determine the elastic limit and maximum load applied to the specimen (F_{max}).

A small –control- panel instrumented with triaxial strain gauges and mounted on a picture frame fixture was tested in shear and images were recorded using the DIC method (Figure 10-3). This allowed normalisation of the test procedure and determination of the elastic limit for further testing.

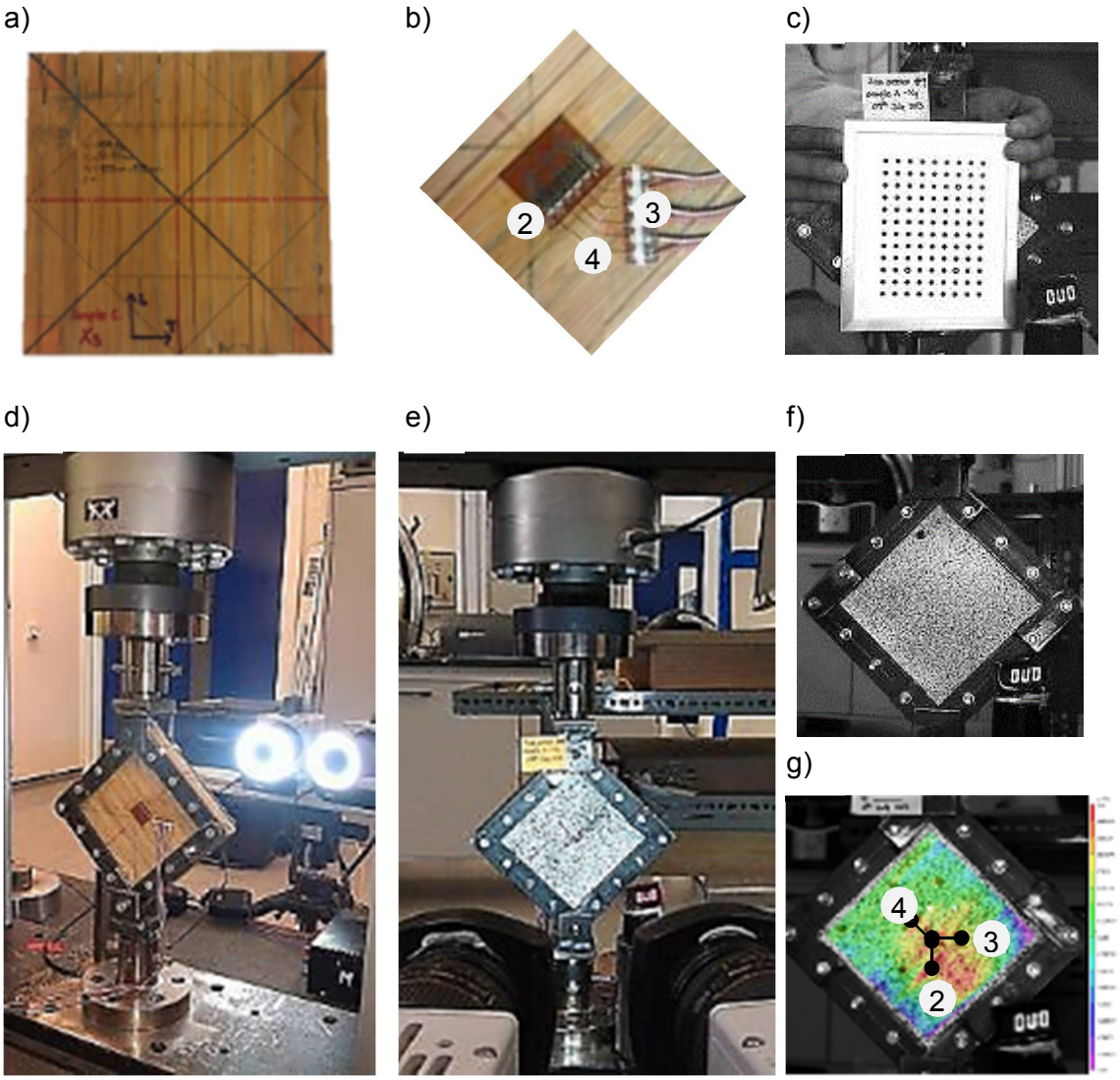

Figure 10-3. Diagram of the picture frame shear test procedure of a control specimen using DIC and triaxial strain gauges for measuring deformation. a) Small panel (control specimen). b) Triaxial strain gauge attached to the surface of the panel. c) Calibration of the DIC system. d) Test setup (panel front face). e) Test setup (panel back face) with speckle pattern. f) Reference image. g) DIC analysis using virtual extensometers.

Two series of in-plane compression tests of large G-XLam panels were undertaken, one series with and another series without buckling restraints. These restraints were required for panel sizes with a slenderness ratio (λ) over 11 (Bodig & Jayne, 1982), as illustrated in Table 10-1. For the restrained test series, buckling supports presented an obstacle, which prevented the capture of full field images of the panel surfaces, thus DIC was not utilized and deformation was measured using LVDTs. For the unrestrained series, deformation was recorded using the DIC technique (explained in Section 10.2) and buckling failure was avoided. λ was calculated as expressed in Equation 10-1.

$$\lambda = \frac{l}{R_g} \qquad 10\text{-}1$$

where:
l is the length of the column and
R_g is the two dimensional radius of gyration and is defined as the square root of the ratio of second moment of inertia (I) to the cross sectional area (A).

Table 10-1. Slenderness ratio of the G-XLam panels tested.

	G-XLam3 (700mm x 700mm)	G-XLam5 (700mm x 700mm)	G-XLam3 (600mm x 600mm)	G-XLam5 (600mm x 600mm)
b (mm)	700	700	600	600
d (mm)	16.5	27.5	16.5	27.5
I (mm^4)	262,040.25	1,213,151.04	224,606.25	1,039,843.75
A (mm^2)	11,550	19,550	9,900	16,500
R_g (mm)	4.76	7.87	4.76	7.93
λ	147	89	126	75

Table 10-1 compares the slenderness ratio of the G-XLam3 600x600mm and 700x700mm panels. The distribution of cross sectional area (A) around the G-XLam3 panel's centroid axis or radius of gyration (R_g) was almost the same for both panel sizes. Likewise R_g is almost the same for the 600x600mm and 700x700mm size G-XLam5 panels. The slenderness ratio exceeded 11 in all cases so restraints were necessary. For the shear test, the panels were fitted with a special fixture (picture frame) around the edges to induce in-plane shear; therefore, no out-of-plane restraints were necessary and both DIC and LVDT measurement systems were used.

G-XLam specimens for four point bending test were the only ones taken to failure. The BS EN 789 (BSI, 2004) standard for structural timber elements provided guidelines for testing the G-XLam panels in bending and in-plane compression, while ASTM E5 19-02 (ASTM, 2002) was consulted for testing in shear.

10.2 Compression tests using DIC method.

DIC was used to produce an overall picture of deformation of G-XLam3 and G-XLam5 large panels and carry out strain measurements on their surface when subjected to in-plane compression load. No buckling restraints could be used for these tests. Two monochrome high

speed cameras (Fast Cam SA3, items 2 and 3 in Figure 10-4) fitted with Nikon 24-85mm lenses (AF-D Nikkor f/2.8-4) recorded simultaneous images of the painted speckle pattern surface (item 1 in Figure 10-4 and 10-5b) at a rate of one frame per second. Both cameras were mounted on a tripod rail that was parallel to the panel and positioned at a stereo angle below 60º (item 7 and 11 in Figure 10-4). Adjustable LED ring lamps fixed to the lenses provided additional illumination (item 11 in Figure 10-4). Sharp focus, adequate illumination and correct brightness were controlled on screen with the aid of the recording software Photron FASTCAM. A monitor displaying load and stroke readings (item 4 in Figure 10-4) from the test machine was positioned on one of the camera's field of view.

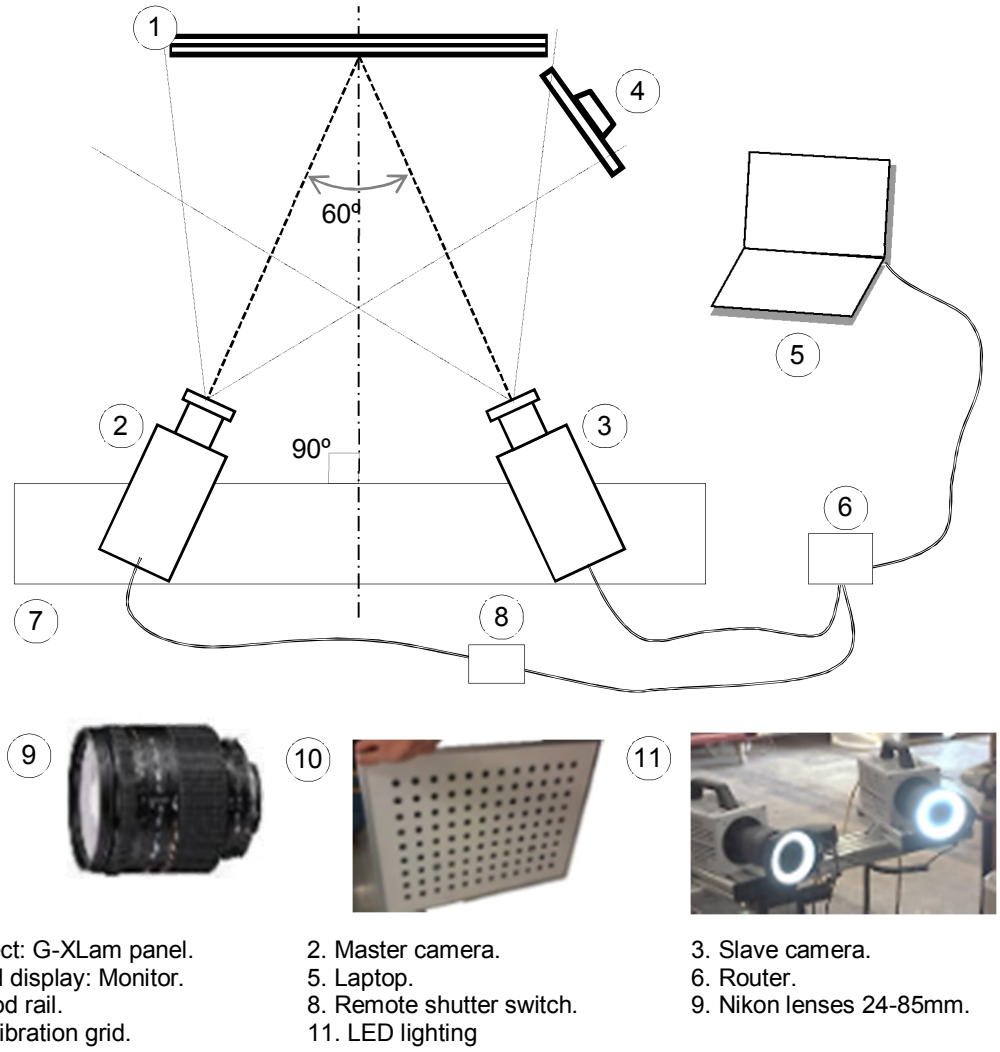

Figure 10-4 DIC test configuration and instrumentation.

Prior to test, a calibration grid with 12mm dots spaced at 34.93mm (item 10 in Figure 10-4) that covered the full field of view was gently moved in front of the panel and sets of approximately 60 images were recorded. Rotation about all three axes permitted the

calibration of the stereo-vision system. These images were then analysed using the calibration tool of the VIC3D-2009 software and a low overall error (standard deviation of residuals) for all views (e≤0.015 –given by the software (Correlated Solutions, 2010)) was ensured before running the test. Both recording and analysing software was installed on a laptop (item 5) with sufficient processing and storage capacity. A reference image was taken once the calibration was performed and before the application of load.

10.2.1 Materials and methods

Following curing of the manufactured G-XLam panels as explained in Chapter 8, two G-XLam3 and one G-XLam5 were cut to 700x700mm squares and one of their faces was painted with a non-repetitive speckle pattern (low contrast speckle pattern: LC-Sp in Figure 10-5).

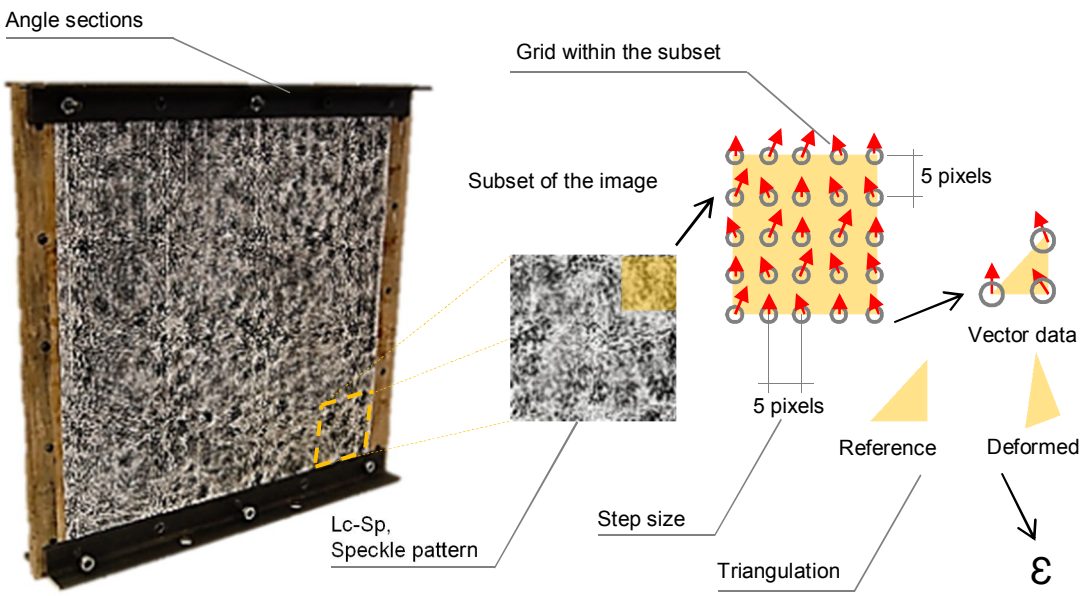

Figure 10-5. G-XLam with special fixtures on top and bottom and detail of the speckle pattern used together with the subset image chosen (21) and the step size (5 pixels)

Subsequently, two mild steel angle sections were bolted to the top and bottom of the panels to provide vertical alignment and anchorage to the 200kN Mayes universal test machine (Figure 10-6). Then, an evenly distributed in-plane compressive load was applied by the test machine at a rate of 0.5mm/min. The panels were loaded five times below the elastic limit and buckling failure was avoided. During testing, master and slave cameras captured consecutive images of the full field of view, the increase in load from a monitor (Item 7 in Figure 10-6) placed to one side, and the corresponding deformations in the X, Y (in-plane) and Z (out of plane) axes of the panel.

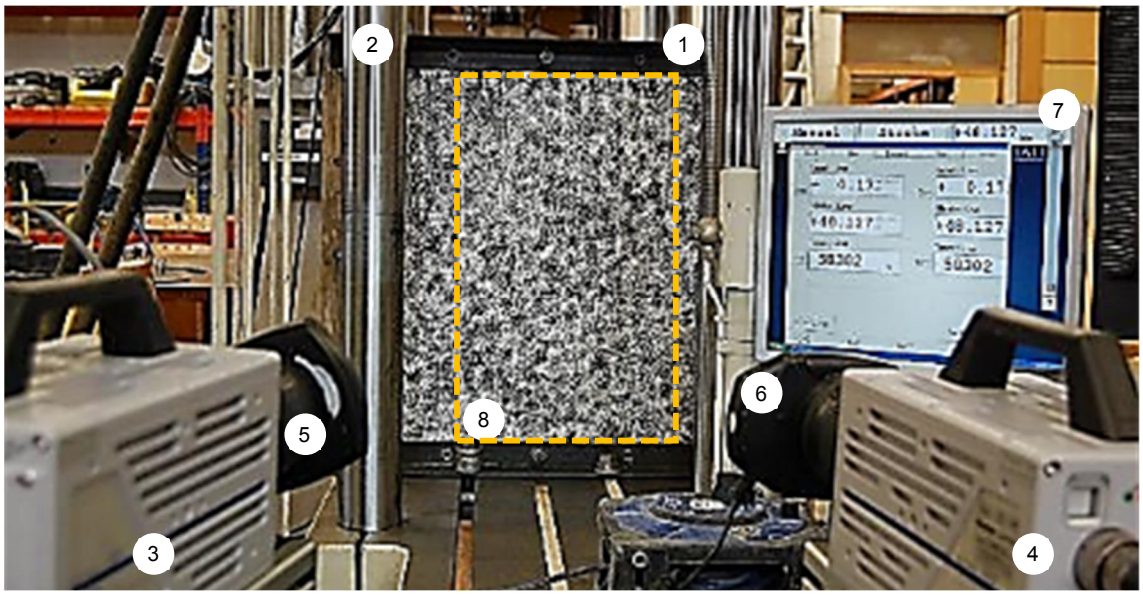

1. Object: G-XLam panel. 2. Mayes 20kN test machine. 3. Master camera. 4. Slave camera.
5. Nikon lenses 24-85mm. 6. LED lighting. 7. Load display: Monitor. 8. Area of interest.

Figure 10-6. Setup for the compression test of G-XLam panels using the DIC method.

It was then possible to track both load and strain for each pair of images at a rate of one image per second. These sets of paired images were analysed using VIC3D-2009 software and 2D and 3D strain maps (Figure 10-7 & 10-8) of the pre-defined area of interest (AOI, item 8 in Figure 10-6) were produced. Regions with spikes or noise were avoided and a subset value of 21 (size of the tracking grid of points) and step size of five pixels (distance between the points tracked by the software) was chosen for the DIC analysis (Figure 10-5). The software calculated the resulting strain by triangulation of the points in the grid.

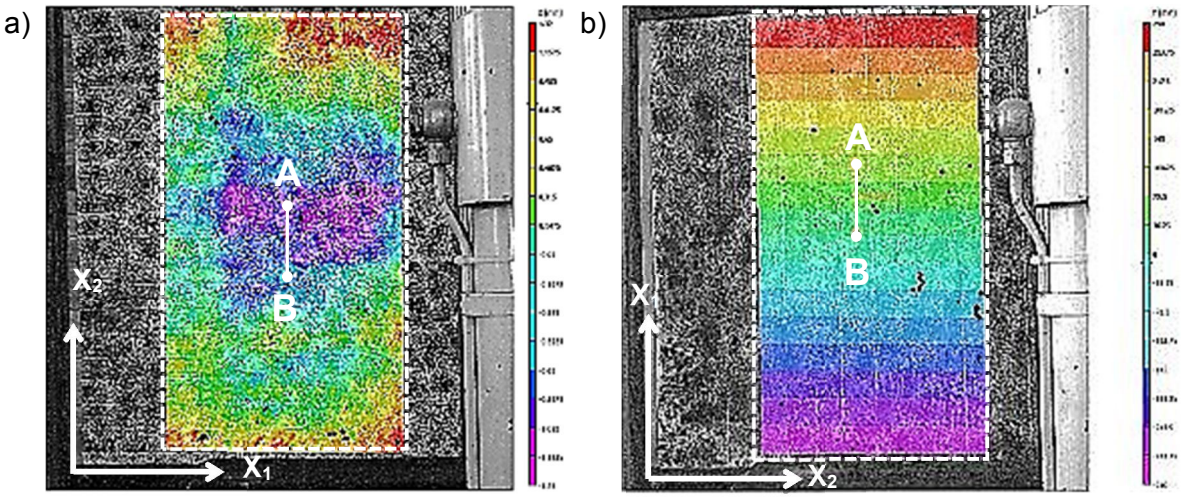

Figure 10-7. a) Strain map in X_3 (radial) direction of a G-XLam panel tested in compression along X_2 (transverse) axis. b) Strain map resulting in X_1 of a G-XLam panel tested in compression along X_1 (longitudinal) axis.

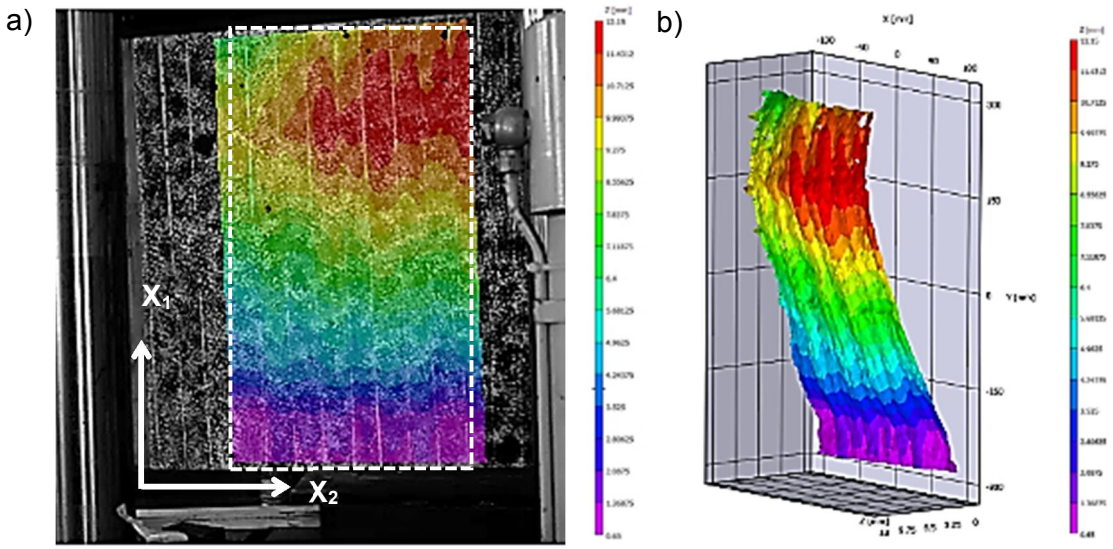

Figure 10-8. a) Front view of the 3D strain map of the deformation in z (X_3) of a G-XLam panel tested in compression E_0 (this panel was discarded due to fabrication defects that produced severe buckling). b) Axonometric view of the 3D strain map of the deformation in z (X_3) of the G-XLam -3 panel tested in compression E_0 (*scale on the 3D strain map is exaggerated*).

Using VIC3D-2009 software a virtual extensometer (A-B) was placed at mid-point and mid-height of the reference image of each G-XLam panel and the axial strain variation for all the captured images was calculated. Figure 10-9 shows a typical graph of the raw data obtained from the strain analysis using the DIC technique.

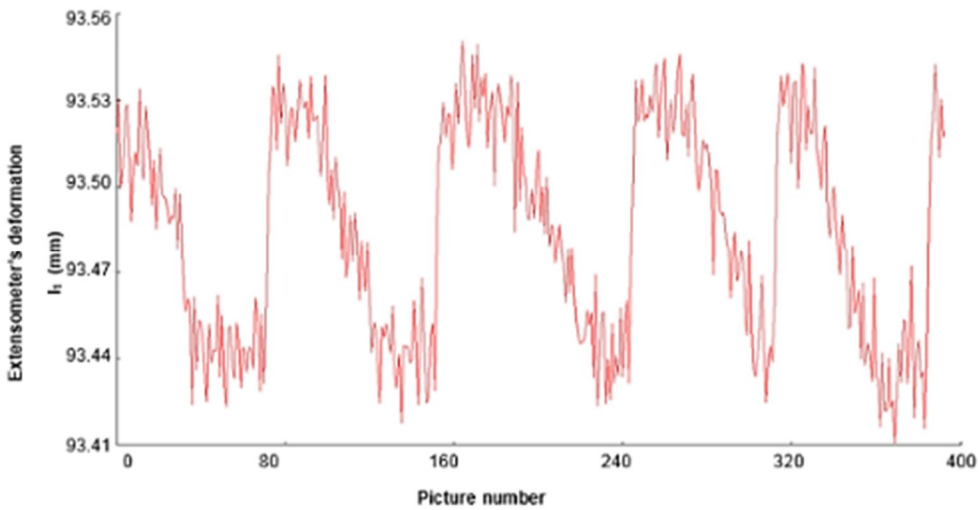

Figure 10-9. Typical graph of calculated deformation from virtual extensometer during five loading cycles.

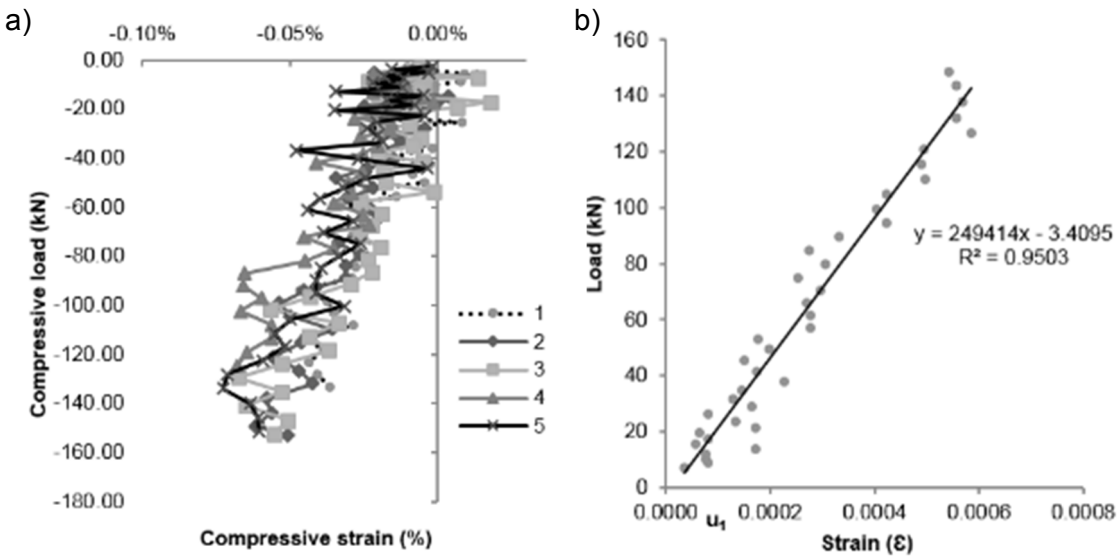

Figure 10-10. a) Typical graph of compressive strain vs. compressive load obtained from the in-plane compression test of G-XLam panels. b) Typical strain-stress graph (both correspond to a G-XLam5 panel tested along the longitudinal, X_1 axis).

Engineering strain (ε) was then calculated as the change in length ΔL per unit of original length L, as expressed in Equation 10-2.

$$\varepsilon = \frac{(\Delta L)}{(L)} = \frac{(l_1 - l_0)}{(l_0)} \qquad 10\text{-}2$$

where
l_0 is the initial length of the extensometer and l_1 its final length.

Load-strain responses from the five load cycles were obtained from the compression test of two G-XLam panels of three and five layers. The normal stress-strain response of each panel was plotted, and a linear regression analysis was performed. Values for stress and strain obtained from the longest linear portion of the graph between $0.1F_{max}$ and $0.4F_{max}$ were input into Equation (10-3) to determine the compression moduli of elasticity (MOE) of the panels in the longitudinal ($Ep_{C,0}$) and transverse ($Ep_{C,90}$) direction. The maximum permitted load (F_{max}) and elastic limit were previously determined from the preliminary compression test with a small panel (control specimen in Figure 10-2).

$$Ep_{C,0,90} = \frac{(F_2 - F_1)l}{(u_2 - u_1)A} \qquad 10\text{-}3$$

where

$F_2 - F_1$ is the increment of load between $0.1F_{max}$ and $0.4F_{max}$
$u_2 - u_1$ is the increment of engineering strain corresponding to $F_2 - F_1$
l is the gauge length (A-B length of the virtual extensometer), and
A is the cross sectional area of the panel.

10.2.2 Results and discussion

Determination of E_0 and E_{90} of G-XLam3 and G-XLam5 panels by compression test using DIC.

Engineering strain values obtained from the virtual extensometer placed (A-B) on G-XLam3 and G-XLam5 panels (Figure 10-11) were used for the calculation of modulus of elasticity in compression in both transverse (X_2) and longitudinal (X_1) orientations ($Ep_{C,90}$ and $Ep_{C,0}$, respectively) where 'Ss' refers to the scan session.

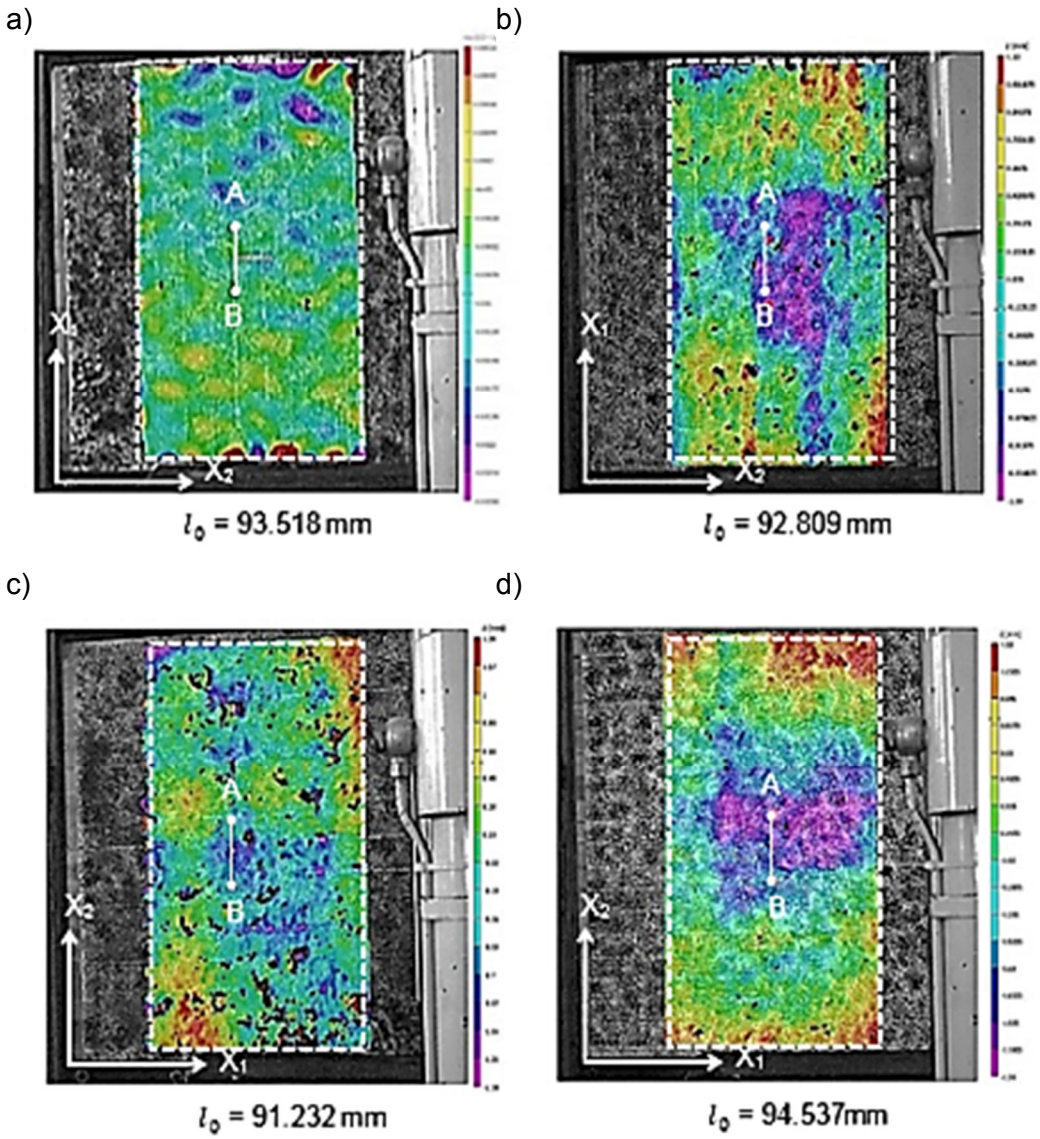

Figure 10-11. 2D strain maps of the in-plane compression test using DIC method for: a) G-XLam3 (L) Ss 17. b) G-XLam5 (L) Ss 21. c) G-XLam3 (T) Ss 18 d) G-XLam5 (T) Ss 22

Typical stress-strain response were plotted for both panels and orientations, and a linear regression analysis was performed for each configuration (Figure 10-12 and 10-13).

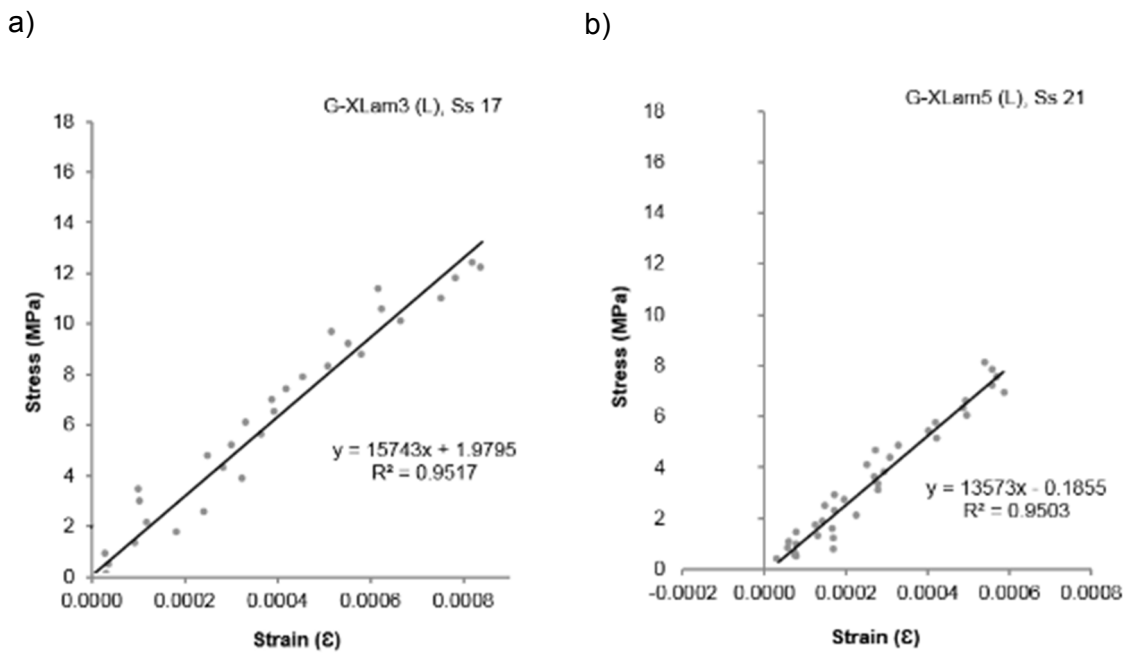

Figure 10-12. Strain-stress graphs of the in-plane compression test of G-XLam panels tested along the Longitudinal (L) or X_1 axis. a) G-XLam3 (L) panel tested along X_1. b) G-XLam5 (L) panel tested along X_1.

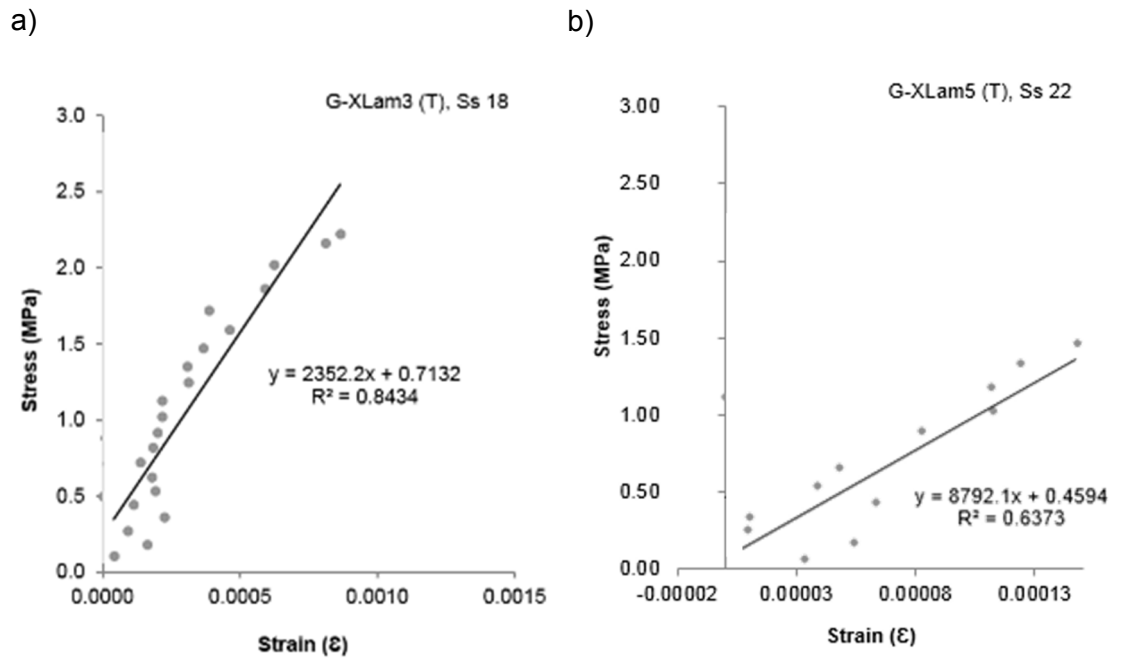

Figure 10-13. Strain-stress graphs of the in-plane compression test of G-XLam panels tested along the Transverse (T) or X_2 axis. a) G-XLam3 (T) panel tested along X_2. b) G-XLam5 (T) panel tested along X_2.

$Ep_{C,0}$ and $Ep_{C,90}$ results for G-XLam3 and G-XLam5 are presented in Table 10-2. As can be observed in this table, MOE values for both panels in the transverse direction ($Ep_{C,90}$) are considerably lower than the analytical predictions and present high coefficients of variation (CoV). This can be attributed to the significant slenderness ratio (λ) of the panels that caused rapid out of plane deformation (buckling) and forced the test to be stopped at low load levels. As a result, strain values from the DIC analysis experienced high scatter. The effect of buckling was critical for the G-XLam3 panels tested in the transverse direction (X_2), which resulted in an extremely low value of $Ep_{C,90}$. Although, $Ep_{C,90}$ results for G-XLam5 panels presented a considerably higher dispersion of values around the mean (CoV∼44%), the buckling effect was minor due to the reduced slenderness ratio, λ=89 for G-XLam3 while for G-XLam5 λ=147.

Table 10-2. Results of MOE in compression for G-XLam panels using DIC.

$Ep_{C,0,90} = \frac{(F_2 - F_1)l}{(u_2 - u_1)A}$	G-XLam3		G-XLam5	
	$E_{pC,0}$ (GPa)	$Ep_{C,90}$ (GPa)	$Ep_{C,0}$ (GPa)	$Ep_{C,90}$ (GPa)
Cycle 1	18.65	2.92	18.53	-
Cycle 2	15.25	3.18	11.42	10.87
Cycle 3	14.20	1.86	14.34	7.24
Cycle 4	15.84	1.64	18.56	5.14
Cycle 5	22.16	2.43	15.67	14.59
Mean	**17.22**	**2.43**	**15.67**	**9.46**
St. dev.	3.22	0.66	3.02	4.16
CoV	19%	27%	19%	44%

Out of plane deformation was recorded by the stereovision cameras and analysed using the DIC method producing 3D strain maps for each panel configuration (Figure 10-14 and 10-15 for G-XLam3 and G-XLam5 panels, respectively). Manufacturing imperfections were observed using the DIC; however, these surface defects did not exceed ±2mm in-plane (measured linearly on the z axis). Maximum in-plane compression load applied to G-XLam3 and G-XLam5 panels along the longitudinal direction (X_1) was seven and four times the load applied transversely, respectively. This allowed small out of plane deflections without failure.

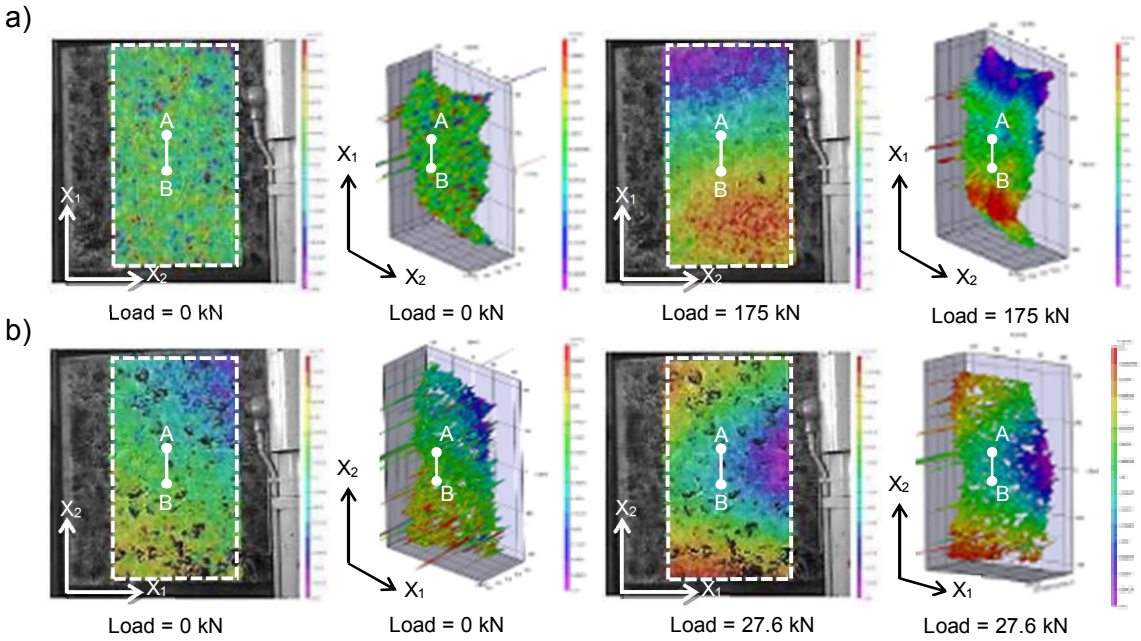

Figure 10-14. Front views and axonometric projections of the 3D strain maps produced using DIC method during in-plane compression test for a G-XLam3 panel. a) G-XLam3 panel tested along the longitudinal (X_1) direction (Ss 17). b) G-XLam3 panel tested along the transverse (X_2) direction (Ss 21).

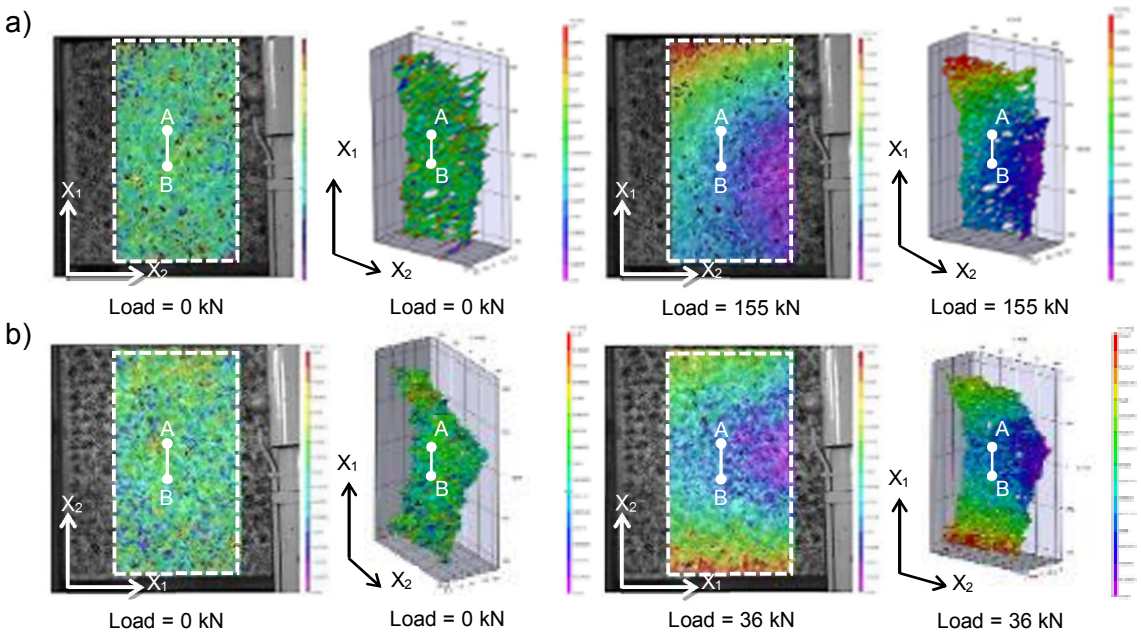

Figure 10-15. Front views and axonometric projections of the 3D strain maps produced using DIC method during in-plane compression test for a G-XLam3 panel. a) G-XLam5 panel tested along the longitudinal (X_1) direction (Ss 18). b) G-XLam5 panel tested along the transverse (X_2) direction (Ss 22).

Strain results from one of the G-XLam3 panel specimens tested in in-plane compression and failed in buckling were discarded for the calculation of the MOE. Figure 10-16 illustrates

this failure and indicates the presence of gaps that triggered the failure.

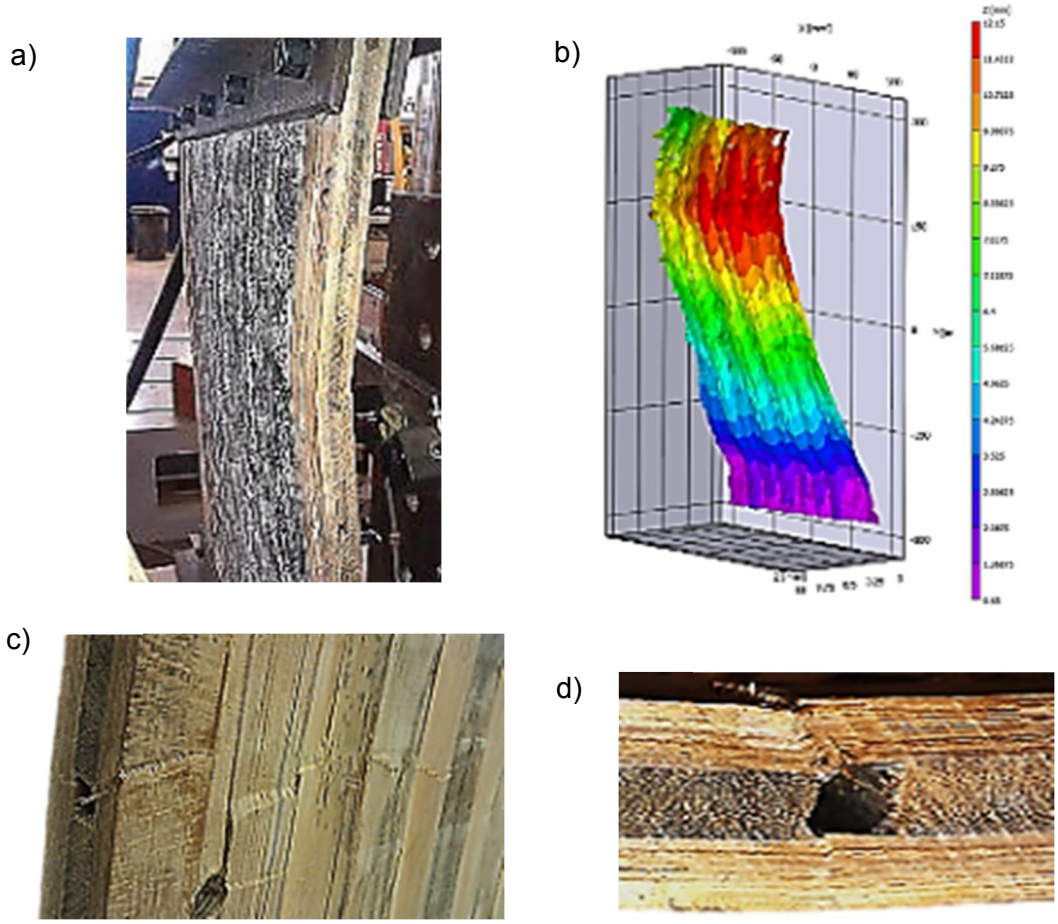

Figure 10-16. G-XLam3 panel discarded for buckling failure during compression test using DIC. a) Failure of panel mounted on the test machine b) 3D-Strain map of the failure c) Detail of the failure area. d) Detail of the shear failure produced by the buckling effect during compression test.

10.3 Compression test using LVDT

In-plane compression test using LVDTs and buckling restraints was undertaken on the same G-XLam3 and G-XLam5 used for the compression tests with DIC technique. The resulting compression moduli of elasticity values were compared with those obtained using the DIC technique.

10.3.1 Materials and methods

Compressive load was applied to two G-XLam (one G-XLam3 and one G-XLam5) panels with a 2,000kN DARTEC universal test machine at a rate of 0.5mm/min (Figure 10-17a). The test was carried out following guidelines given by the BS EN 789 (BSI, 2004) standard for structural timber elements. Each panel was tested in the longitudinal (X_1) and transverse (X_2)

directions (Figure 10-1b & c) as explained in Section 10, and was fixed to the testing machine using the fixture shown in Figure 10-5a (item 2 in Figure 10-17).

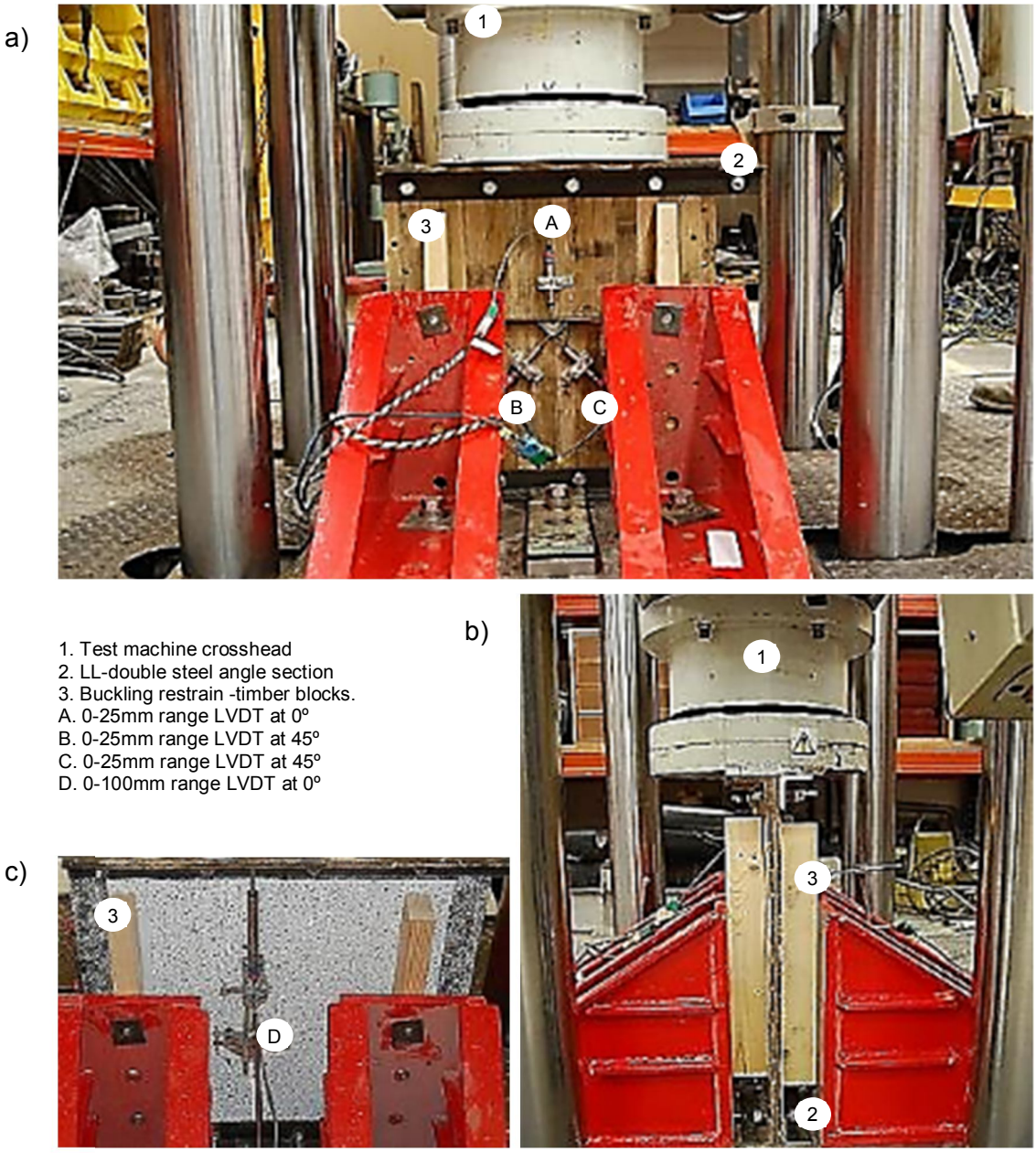

Figure 10-17. In-plane compression test set-up using LVDT and buckling restrains. a) Frontal view. b) Lateral view. c) Back face of the panel under test.

Buckling restraints with Teflon attached to the specimen and wooden blocks were placed vertically (item 3 in Figure 10-17) and deformation at 0º, 45º and -45º of the load application axis was measured by LVDTs (item A, B, C and D in Figure 10-17). LVDTs A, B and C measured displacement variations from zero up to 25mm, while LVDT D had a maximum range of 100mm. Deformation was recorded by a Vishay 5,000 data logger. Data from

seven load cycles for each panel configuration and test direction were collated and load-deformation was plotted (Figure 10-18).

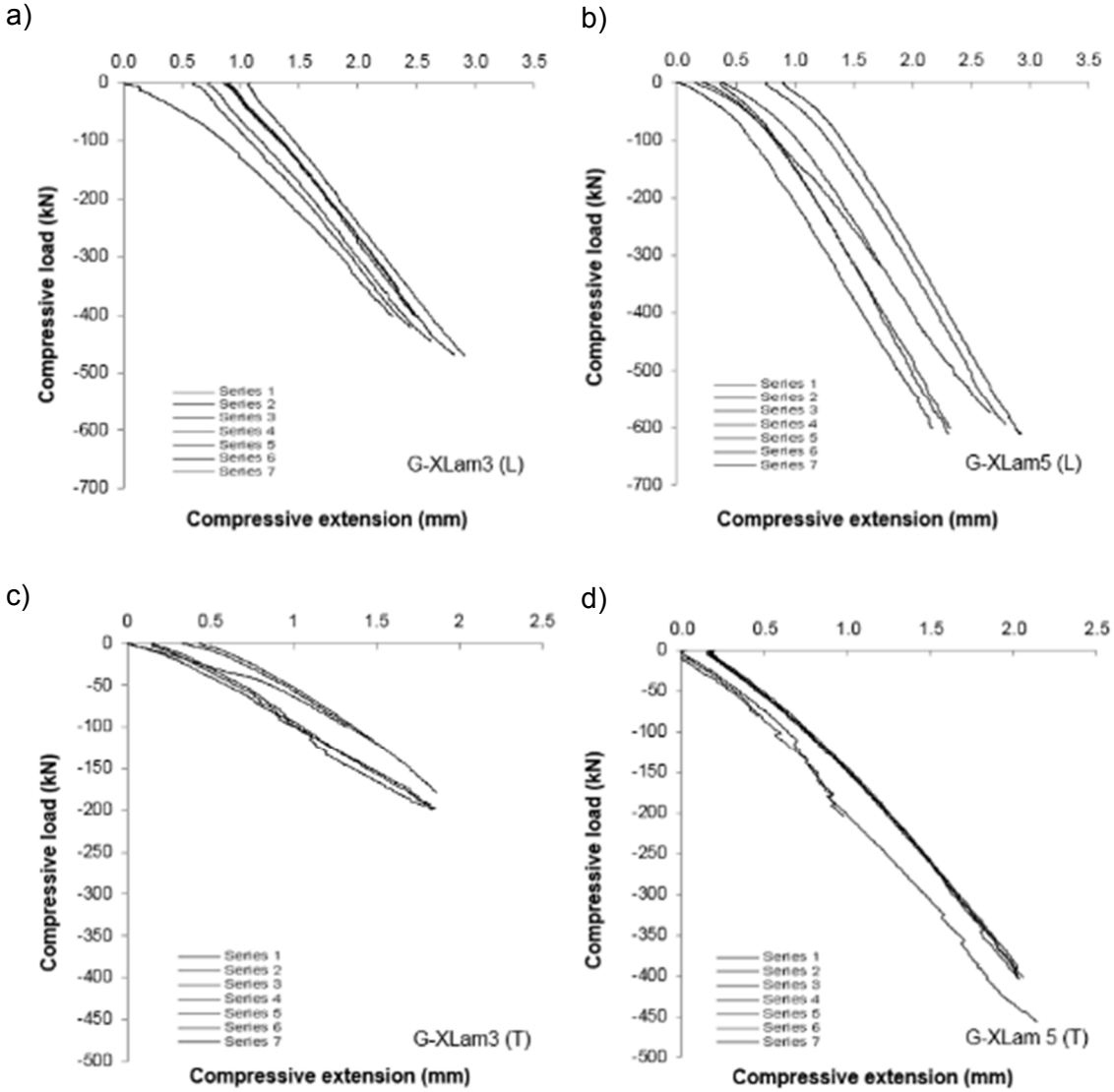

Figure 10-18. Load-deformation graphs for all G-XLam panels tested in compression along L (longitudinal) and T (transverse) directions. a) G-XLam3 (L). b) G-XLam5 (L). c) G-XLam3 (T). d) G-XLam5 (T).

The initial part of these graphs that showed 'parasitic effects' associated with slipping of the test fixture or embedment of the bolts used, were discarded for plotting the stress-strain response of the panels (Figure 10-19). A linear regression analysis was performed for each load cycle and the straight part of these graphs within the elastic region was used for the determination of the longitudinal (L) and transverse (T) moduli of elasticity, MOE (L=$Ep_{C,0}$ and T=$Ep_{C,90}$) of G-XLam3 and G-XLam5 panels. Equation 10-3 was used for calculation of $Ep_{C,0}$ and $Ep_{C,90}$.

Figure 10-19 illustrates the best linear fit with a correlation coefficient (R^2) ≥ 0.90 for all the results of each test configuration.

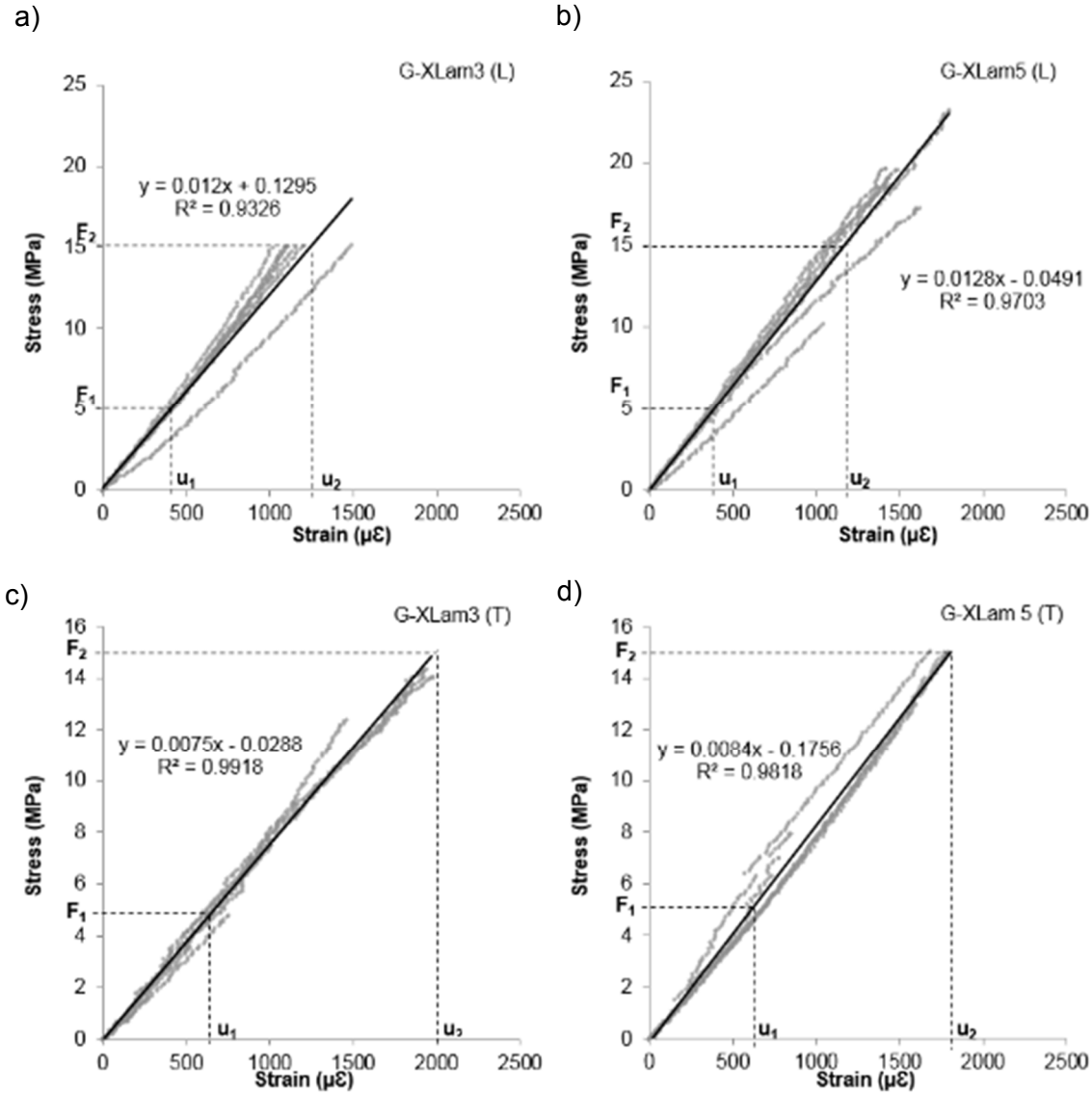

Figure 10-19. Stress-strain graphs of the in-plane compression test of G-XLam panels showing the best linear fit obtained by the regression analysis. a) G-XLam3 (L) panels tested along X_1. b) G-XLam5 (L) panels tested along X_1. a) G-XLam3 (T) panels tested along X3. a) G-XLam5 (T) panels tested along X_3.

10.3.2 Results and discussion

Global compressive deformation of the G-XLam panels recorded from LVDT-D was used for calculating strain and Equation 10-3 for the calculation of the $Ep_{C,0}$ and $Ep_{C,90}$; results are presented in Table 10-3.

Table 10-3. Summary of panel properties chosen for comparison with FE and numerical analysis.

Specimen Property (GPa)	G-XLam3 (L) $Ep_{C,0}$	G-XLam3 (T) $Ep_{C,90}$	G-XLam5 (L) $Ep_{C,0}$	G-XLam5 (T) $Ep_{C,90}$
Mean	14.86	7.43	12.48	8.74
SD	1.17	0.69	0.92	0.76
CoV	8%	7%	7%	9%

Deformation recorded from LVDT A positioned at the centre mid-height point of the panels was not representative for calculating the axial strain of the panel during the compression test. Recorded values from LVDTs A, B and C, were neglected as values obtained for deformation (δ) oscillated between one and ten microns (0.01mm $> \delta \leq$ 0.001mm = 1 micron), which were below the precision range of the LVDTs ($\pm$0.025mm for the 25mm and $\pm$0.2mm for the 100mm range LVDT) and resulted in extremely small strains and hence very large MOE values. This was due to the reduced area in which the axial deformation was recorded that did not experience significant deformation (as observed during compression test using DIC (Figure 10-13)- and the increased stiffness of the panel resulting from the use of buckling restraints. During data analysis, misalignment and embedment effects were accounted for and the linear elastic region of the test was used for the calculation of $Ep_{C,0}$ and $Ep_{C,90}$.

10.4 Picture frame shear test using DIC and LVDTs

The picture frame test provides an experimental method to transfer equal shear forces along the four edges of a thin square panel specimen. The panel is bolted to a hinged-frame, positioned at 45° of its vertical axis and a force is applied diagonally (Figure 10-1e). Deformation occurs by pulling outwards two opposite corners and pushing inwards the other two or vice versa. This deformation is measured as the square deforms into a rhombus and can be transformed into shear strain (Figure 10-20). Evaluation of in-plane shear modulus (G_{xy}) is then possible by calculating the ratio of shear stress (τ) to shear strain (γ) as expressed in Equation 10-4.

$$\gamma_{xy} = \frac{\varepsilon x + \varepsilon y}{2}\left(\tan\theta' + \frac{1}{\tan\theta'}\right); \qquad \tau_{xy} = \frac{0.707\,P}{l\,t}; \qquad G_{xy} = \frac{\tau_{xy}}{\gamma_{xy}} \qquad \text{10-4}$$

where
εx and εy are the measured strains in x and y
$\theta'$the resulting angle for $(dx_1,\ dy_1)$
P is the force applied, l the side-length of the specimen and t the thickness of the panel.

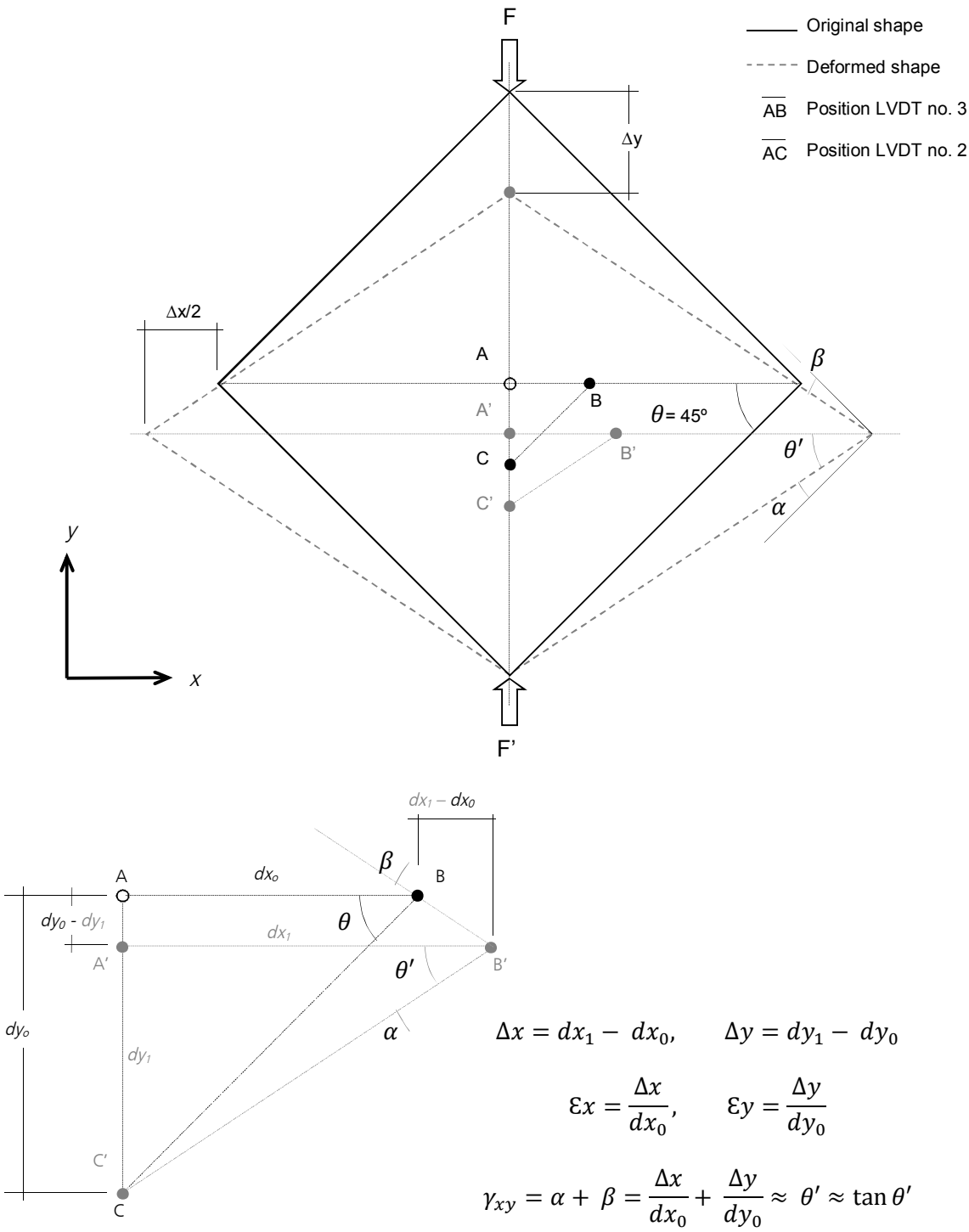

Figure 10-20. Picture frame shear test

The use of this test method in large wooden panels is not widespread either because of the complexity of the test rig or the discontinuation of standard procedures for its application *e.g.* BSI (1969) and ASTM (1972). The suitability of the picture frame method for testing

large plywood panels and the fairly constant strain distribution during testing within the elastic range were highlighted by Youngquist and Kuenzi in 1961 (ASTM, 1961). Furthermore, several researchers have used this test procedure for assessing the shear moduli of advanced composite panel materials (Ambur *et al.,* 2004; Khan *et al.,* 2010; Mastrogiuseppe *et al.,* 2008; Wittenberg *et al.,* 2001). Similar approaches for testing elastic and strength properties of masonry walls have been undertaken by Milosevic *et al.* (2013), Najafgholipour *et al.* (2013) following the current ASTM standard E519-02 (ASTM, 2002). This standard is intended for the determination of the shear strength of this type of structures by inducing a diagonal tension failure using loading pads on top and bottom of large masonry specimens in compression (Figure 10-21a). In addition, the standard provides guidelines for measuring shear moduli.

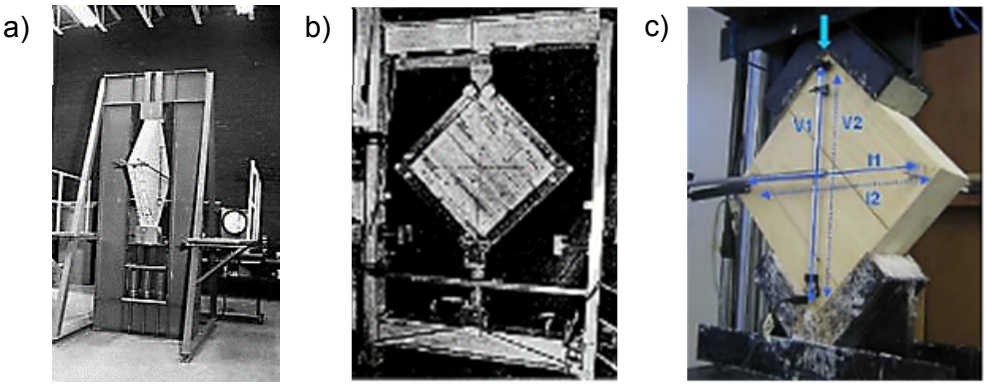

Figure 10-21. a) Diagonal tension test for masonry specimens -picture taken from (ASTM, 2002); b) Picture frame test of layered timber shell elements - picture taken from Moss & Walford (1976); c) Diagonal compression test for determining shear modulus -picture taken from Dujic *et al.* (2007).

Overall, the principle of the test method is to produce a 'close to pure' shear state in the plane of the panel. The picture frame shear fixture has been previously used for the assessment of the elastic properties of timber shell elements (plywood) and cross laminated panels (CLT) by Moss & Walford (1976) and Dujic *et al.* (2007), respectively. These studies used relatively large square specimens (914mm and 300mm, respectively), measured the overall deformation across the specimen using gauges (Figure 10-21b and c) and found good agreement between the experimental results obtained and the standardised results calculated for both elements. The first study utilized the picture frame method whilst the latter used 'shoe' type loading pads.

10.4.1 Materials and methods

Eight back to back rails fabricated from 10mm black mild steel flat bars formed the picture

frame fixture. Each rail had a length of 600mm and a width of 50mm. Ten off-set holes of 10mm diameter drilled across the thickness of the rails were distributed between the 20mm holes for the high tensile (HT) steel pivot pins located at each corner. Class 8.8 high tensile carbon steel bolts, self-locking nuts and washers were used to clamp the panel specimen to the picture frame fixture. Equally rigid fittings were used to secure the picture frame to the top and bottom of the test machine. All these components provided a very rigid frame of higher stiffness than that of the individual panels (Wittenberg *et al.,* 2001) and was appropriate for elastic testing.

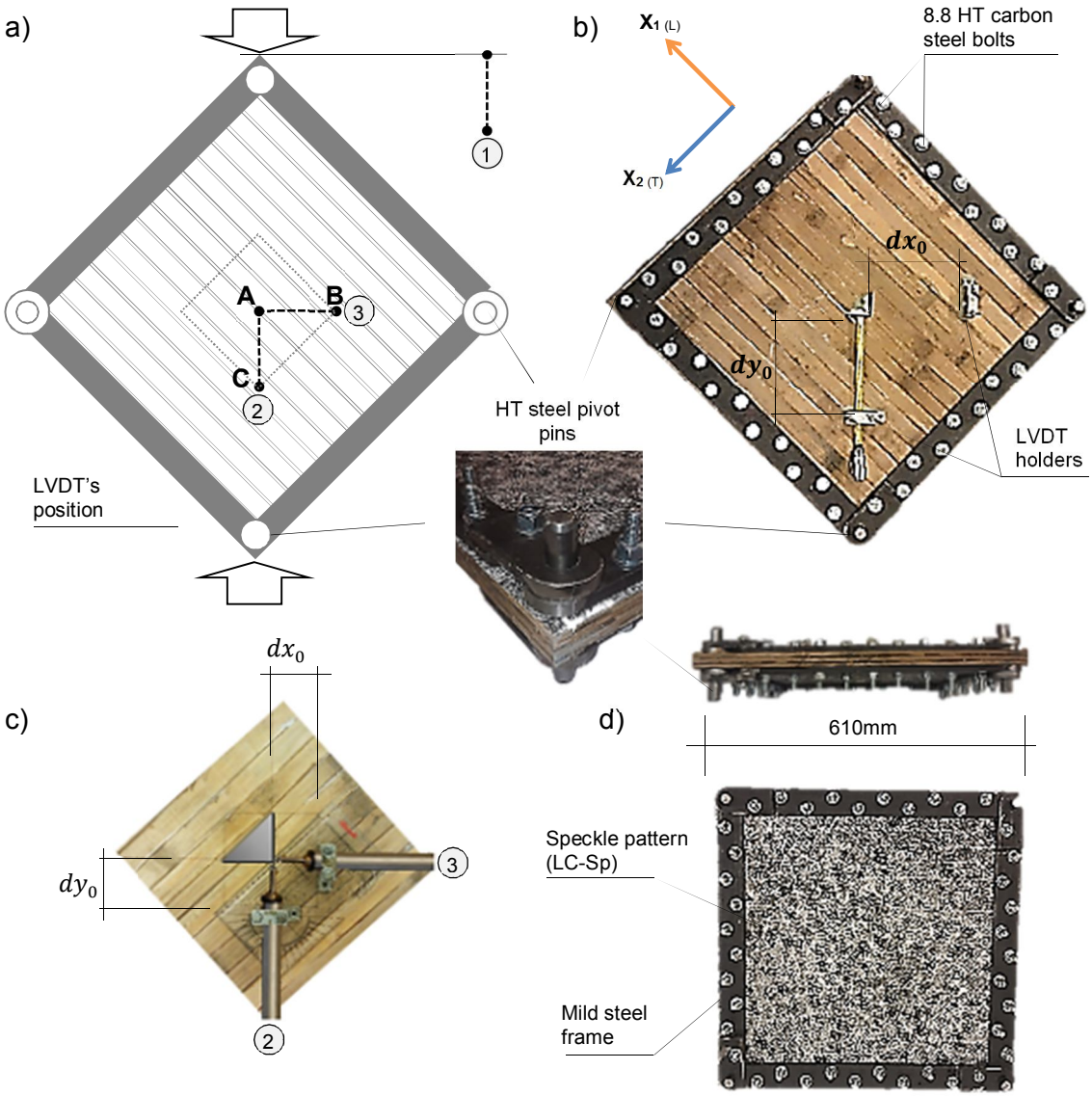

Figure 10-22. Details of the specimen and measurement techniques used for picture frame shear test.

The size of the two G-XLam panels (one G-XLam 3 and one G-XLam5) tested was 610x610mm, which allowed 5mm tolerance at each side of the fixture. Every panel was

positioned in the testing machine at 45° and physical (LVDT, items no. 1 to 3 in Figure 10-22) and virtual methods (DIC, Figure 10-23) were used to measure deformation across the panel diagonals. Both methods recorded the shortening of the vertical diagonal (Δy) and lengthening of the horizontal diagonal (Δx) simultaneously. Five cycles of compressive load were applied with a 2,000kN DARTEC universal test machine at a rate of 0.5mm/min. Figure 10-23 and 10-24 illustrate the test setup on front and back faces of a panel tested in shear.

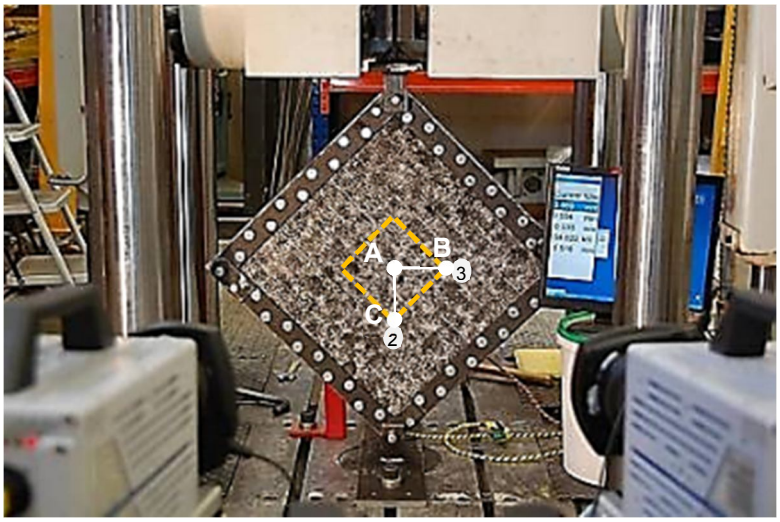

Figure 10-23. Front view of the panel specimen during picture frame shear test showing in orange the AOI (area of interest) and in white the position of the virtual extensometers used for the DIC analysis.

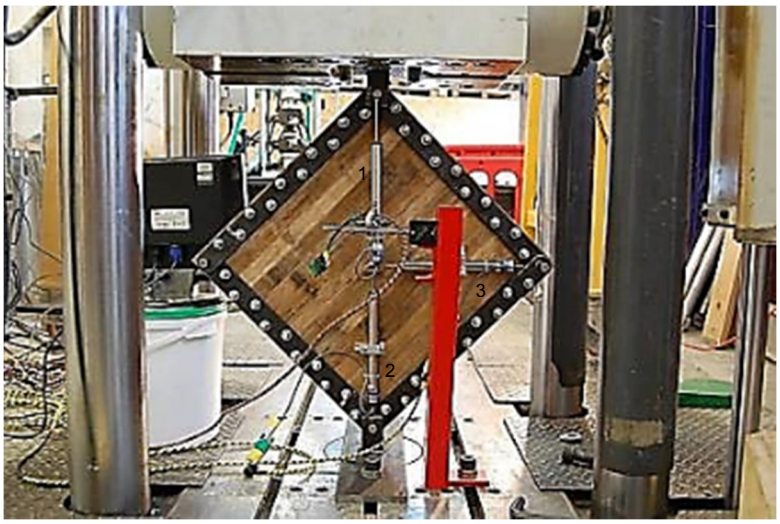

Figure 10-24. View from the back of the panel specimen during picture frame shear test showing the location of the LVDTs used for recording the horizontal and vertical deformation of the panel.

Non-contact measuring technique DIC used the same specifications and equipment employed during the compression tests with DIC, explained in Section 10.2 (see Figure 10-4). Two repetitions of the same test were undertaken maintaining the same parameters, one with a low contrast speckle pattern (LC-Sp Figure 10-23) and other with a high contrast speckle pattern (HC-Sp in Figure 10-17c).

Three LVDTs (1, 2 and 3) of 0-100mm range were attached to the panel during testing of the large panels (Figure 10-22) and connected to a Vishay 5,000 data logger. LVDT-1 measured vertical displacement of the machine cross head and LVDT-2 and LVDT-3 tracked deformation on the panel surface along vertical and horizontal axes, respectively. For the DIC analysis, virtual extensometers (Figure 10-23) recorded deformations at the same orientations of the LVDTs, and gauge lengths (dx_0, dy_0) for both methods were recorded for strain calculation ($\varepsilon x, \varepsilon y$).

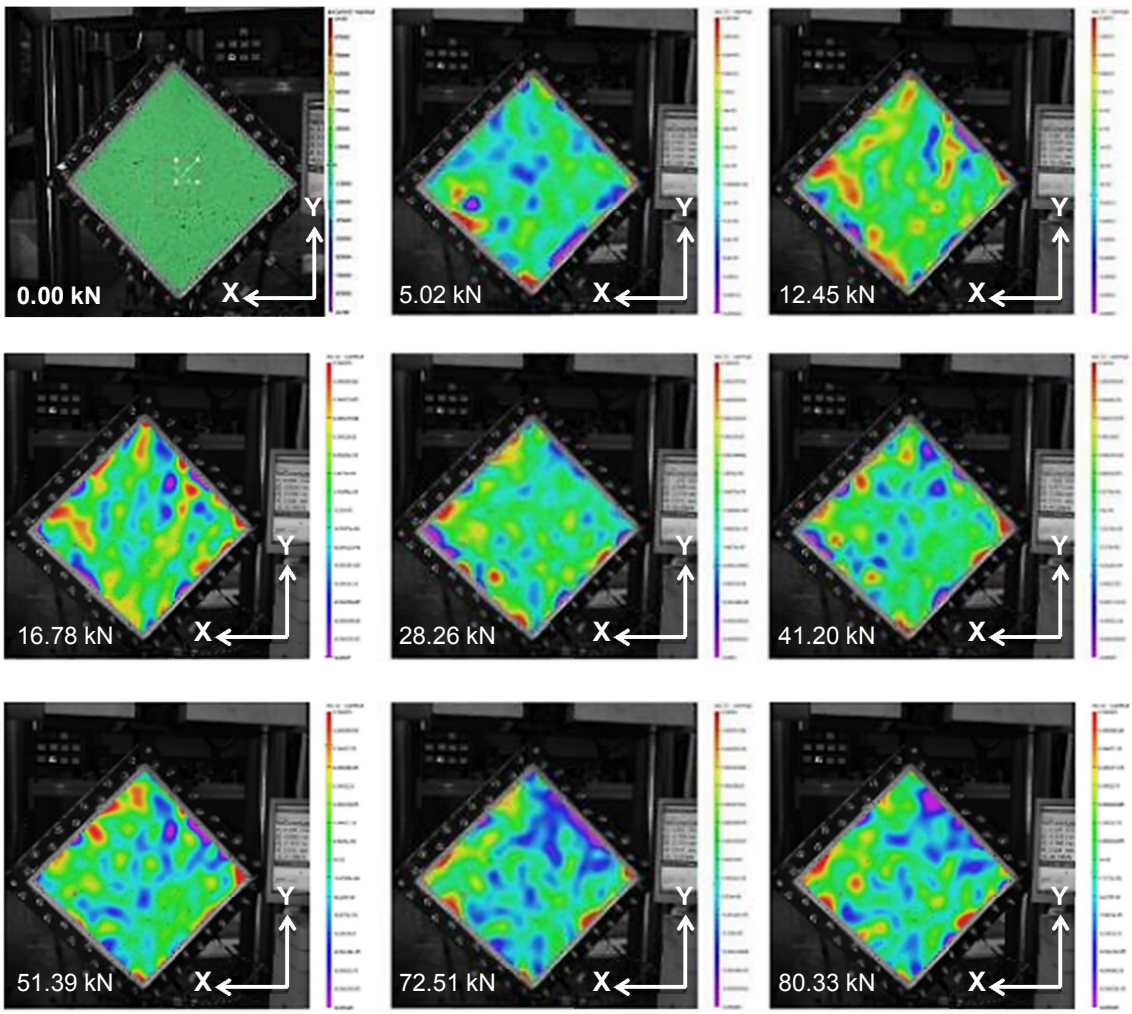

Figure 10-25. Image sequence of the shear strain analysis (εxy-Lagrange) performed by the DIC technique during picture frame shear tests. The image at the top-left is the reference image at 0.00kN with the area of interest (AOI) and the virtual extensometers defined for the DIC analysis.

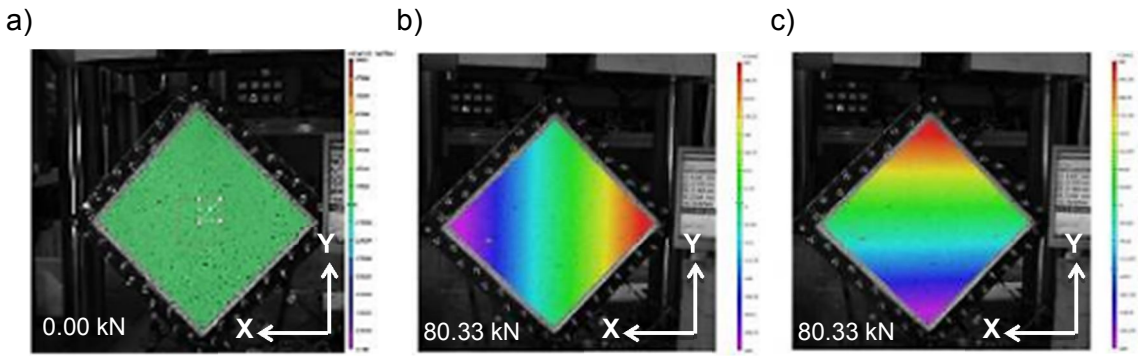

Figure 10-26. DIC deformation maps. a) Reference image. b) Deformation along the X axis. c) Deformation along the Y axis.

Analysis of shear stress (τ), shear strain (γ) and calculation of shear modulus (G_{xy}) followed the method illustrated by Figure 10-20 and Equation 10-4. Displacement and calculated strain values recorded from LVDTs and virtual extensometers were plotted against load (Figure 10-27).

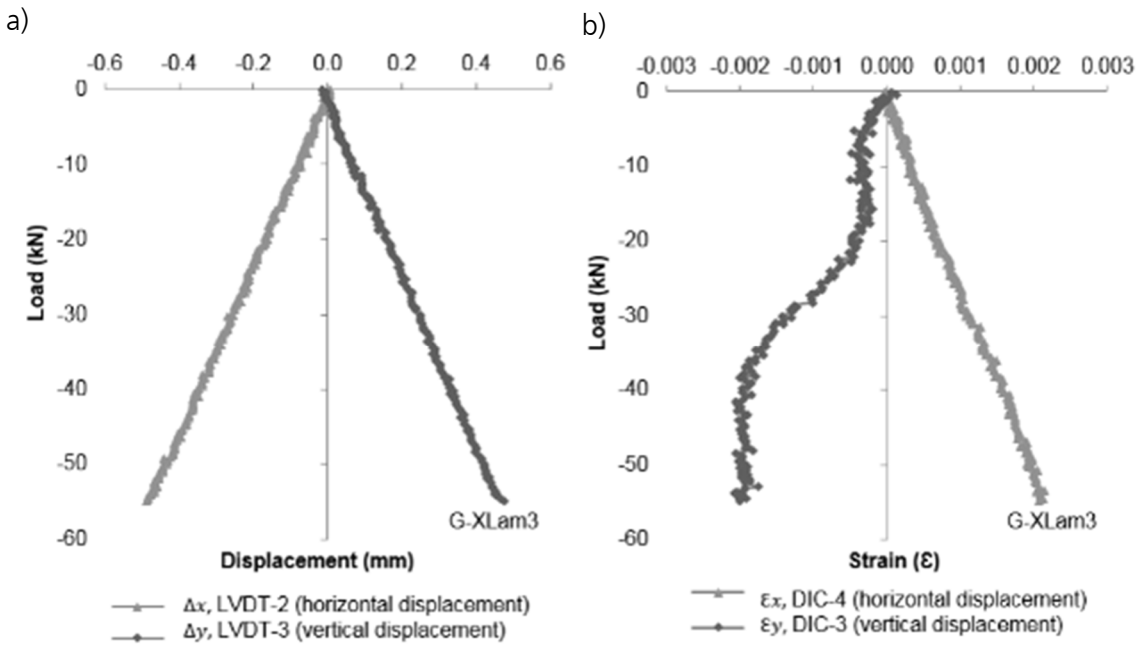

Figure 10-27. Raw data obtained from the picture frame shear test. a) Load vs. deformation using LVDTs. b) Load vs. strain using DIC.

A linear regression analysis was performed for each load cycle and the best linear fit with a correlation coefficient (R^2) ≥0.90 within the elastic region (Figure 10-28 & 10-29) was used for the determination of the shear modulus or G_{xy}.

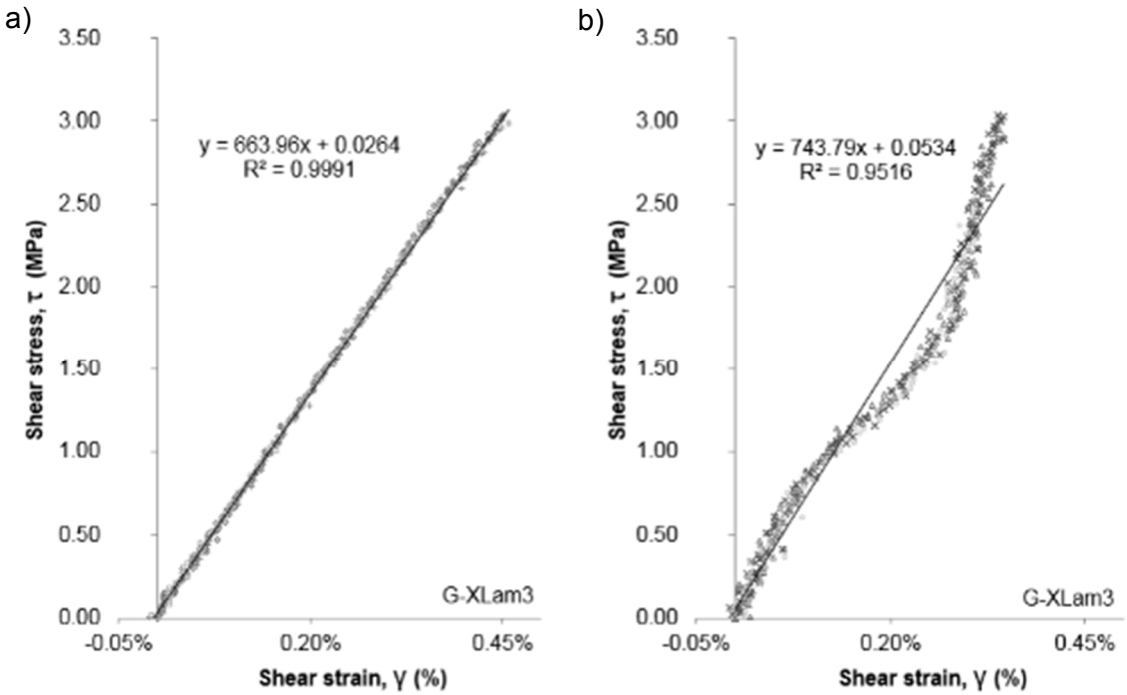

Figure 10-28. Graphs of the typical shear strain vs. shear stress response with the linear trend of a G-XLam3 panel during picture frame shear test using a) LVDTs. b) Virtual transducers on DIC.

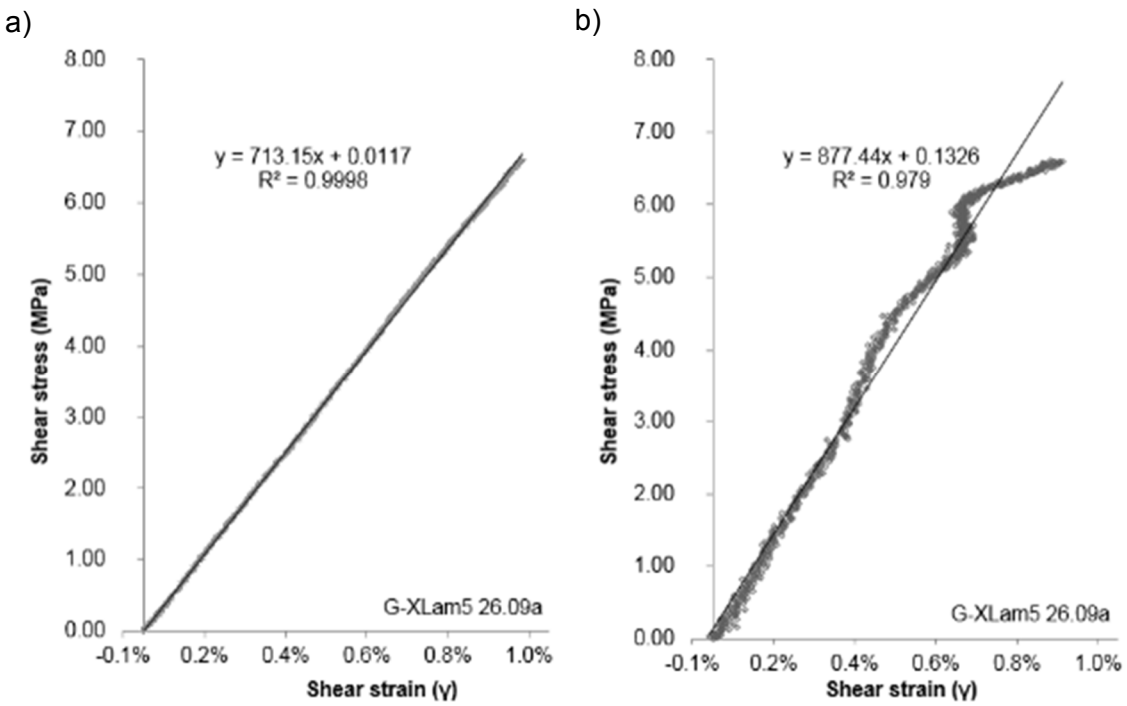

Figure 10-29. Graphs of the typical shear strain vs. shear stress response of a G-XLam5 panel during picture frame shear test using a) LVDTs. b) Virtual transducers (DIC).

10.4.2 Results and discussion

Figure 10-30 illustrates the typical elastic behaviour of G-XLam panels tested in shear using the picture frame fixture and Table 10-4 the values of shear moduli calculated from the strain measurements obtained by DIC and LVDT measurement systems.

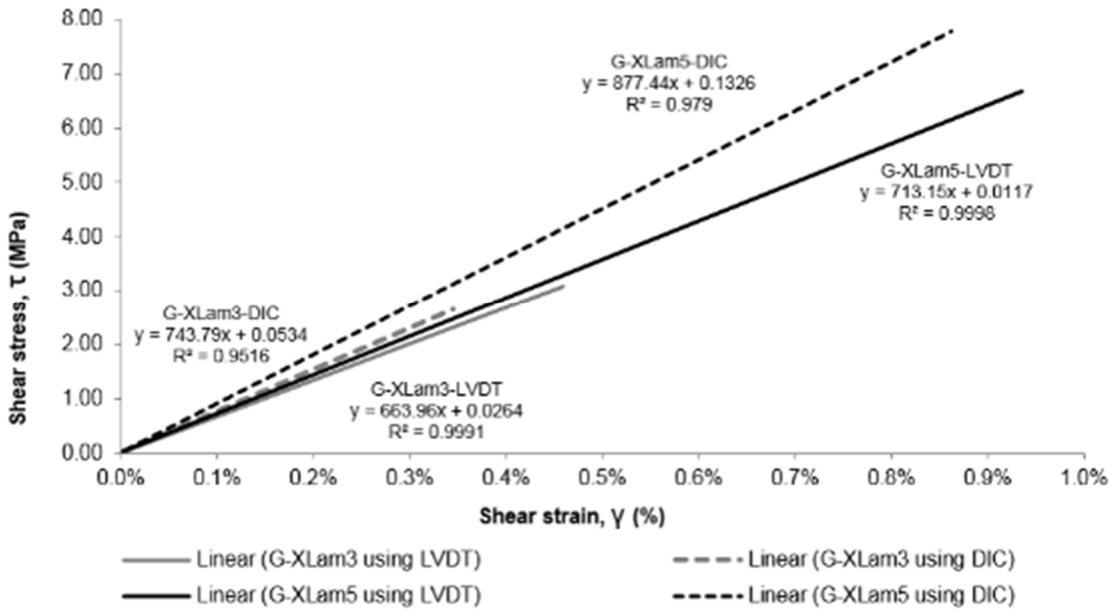

Figure 10-30. Typical shear stress-shear strain graph for G-Xlam3 and G-Xlam5 panels tested using the picture frame fixture and LVDTs and DIC measurement systems.

Overall, shear modulus (G_{xy}) and coefficient of variation (CoV) values obtained using the DIC technique were higher than those measured using linear variation deformation transducers LVDTs (Table 10-4). Mean G_{xy} measured with DIC was 73% and 31% higher for G-XLam3 and G-XLam5 than G_{xy} measured with LVDT.

Table 10-4. Values of shear modulus of G-XLam3 and G-XLam5 panels obtained with the picture frame shear test method using physical and non-contact measurement systems (LVDT and DIC, respectively).

G_{xy}	G-XLam3		G-XLam5	
Test method	LVDT (GPa)	DIC (GPa)	LVDT (GPa)	DIC (GPa)
Mean	0.67	1.16	0.72	0.94
SD	0.02	0.14	0.03	0.09
CoV	2.95%	11.74%	4.28%	9.42%

10.5 Four point bending test

With the aim of assessing the global modulus of elasticity ($Ep_{m,\ global}$) of G-XLam panel specimens and assess potential imperfections or manufacturing defects, a four point bending test was undertaken. $Ep_{m,\ global}$ combines bending and shear deformation. Its calculation considers total deflection over the whole span, which is measured at midpoint (this might be higher due to indentation occurring in the loading points (Nocetti *et al.,* 2013; Raftery & Harte 2011)). Rectangular beam sections of G-XLam3 and G-XLam5 panels were then subjected to bending and deflection at midpoint and load were recorded. Global modulus of elasticity ($Ep_{m,\ global}$), bending strength (MOR), maximum load at break (F_{max}) and moment carrying capacity (M_{max}) were determined. The testing procedure followed European standards for testing structural timber panels (BSI, 2004, 2010).

10.5.1 Materials and methods

Five rectangular beam specimens of both panel configurations (G-XLam3 and G-XLam5) were prepared and conditioned at controlled temperature and relative humidity (27°C±2°C and 70±5%, respectively) prior to four point bending test. Dimensions were checked before the test with digital callipers and a ratio of span (L) to depth (h=thickness) of about 17 was maintained for both specimens. Correspondingly, the distance between rollers was kept at a third of the span, thus the distance between a loading roller and the nearest support was a=L/3.

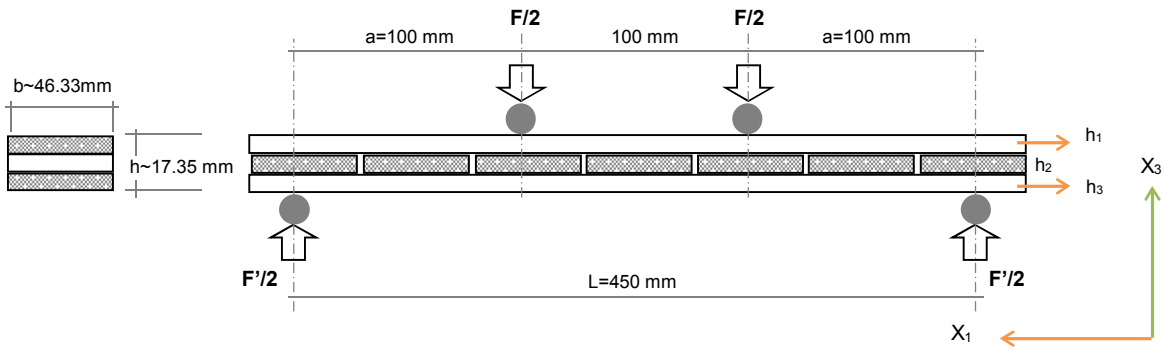

Figure 10-31. Four point bending test diagram of a G-XLam3 panel

G-XLam3 panel specimens for four point bending test had a width (b) and depth (h) of about 46.33mm and 17.35mm, respectively and a span (L) of 300mm (Figure 10-31). While, the set span of the G-XLam5 panel specimens for the same test was 450mm and their average dimensions were 47.24mm in width (b) and 27.25mm thickness (h) (Figure 10-32).

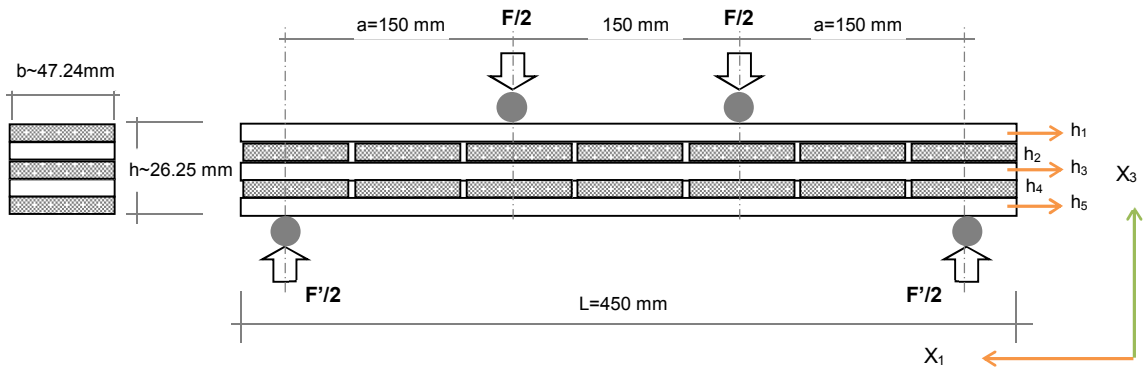

Figure 10-32. Four point bending test diagram of G-XLam5 panel.

The British standards BS EN 408:2010 (BSI, 2010) and BS EN 789:2004 (BSI, 2004) for structural and glued laminated timber were used for setting up the test and determining the elastic and strength properties assessed ($Ep_{m,\ global}$ and MOR). Load along the radial direction (X_3) of the specimens was applied with an INSTRON 5585H floor model testing machine with a 200kN load, using Bluehill control software. A load rate of 2mm/min ensured that failure occurred at 300±120 seconds; temperature during the test was in the range of 27°C±2°C. A linear variable displacement transducer (LVDT) connected to a Vishay System 6000 (Model 6100) Data Logger, was used to measure the deflection occurring at midpoint of the specimens. Steel supports and pads of 12mm width were inserted between the specimen and the rollers at top and bottom to avoid indentation (Figure 10-33).

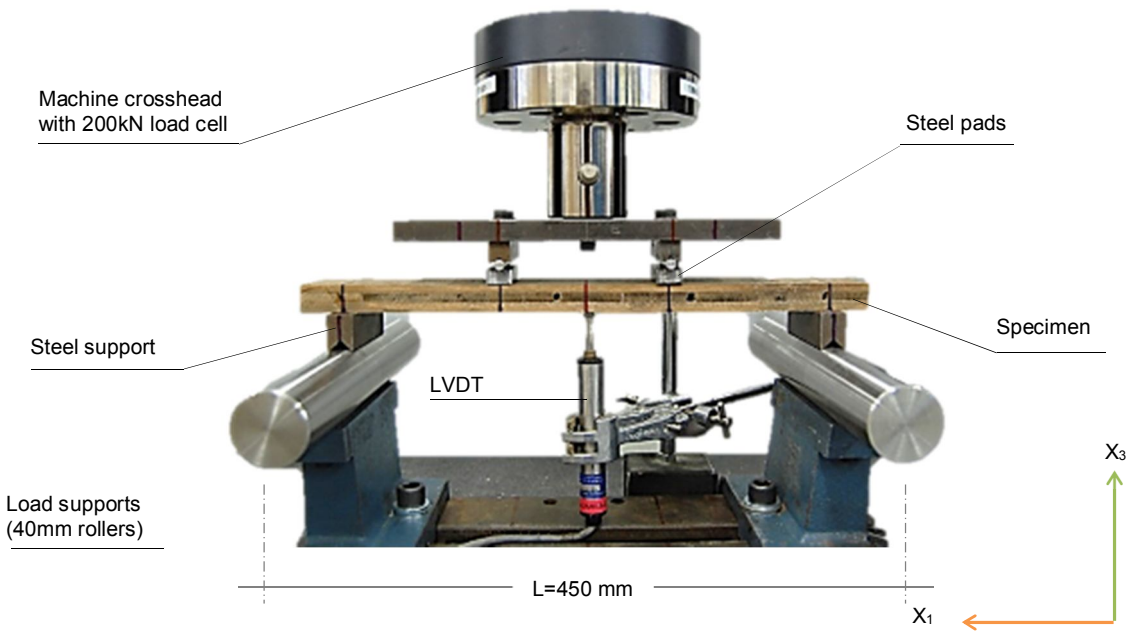

Figure 10-33. Four point bending test setup.

For the determination of global modulus of elasticity in bending ($Ep_{m,\ global}$) the graph load/deformation was plotted and a regression analysis of the straight portion of the line between 0,1F_{max} and 0.4F_{max} (see Figure 10-2) was undertaken. This section with a correlation coefficient ≥ 0,99 was used to calculate $Ep_{m,\ global}$ following Equation 10-5.

$$E \cdot I = \frac{23 \cdot L^3}{1296} \cdot \frac{\Delta F}{\Delta \delta_{centre}} \qquad Ep_{m,\ global} = \frac{23 \cdot L^3}{1296 \cdot I} \cdot \frac{(f_2 - f_1)}{(w_2 - w_1)} \qquad \text{10-5}$$

where
$E \cdot I$ is the bending stiffness,
L is the span,
$f_2 - f_1$ is the increment of load between 0.1F_{max} and 0.4F_{max}
$w_2 - w_1$ is the increment of deflection between $f_2 - f_1$ and
I is the moment of inertia or second moment of area of the beam section ($I = b \cdot d^3/12$).

Maximum load at break (F_{max}) was obtained from test results following the method illustrated in Figure 10-2b. Bending strength (fp_m) and moment carrying capacity (M_{max}) were calculated using Equations 10-6 and 10-7.

$$fp_m = \frac{3\, F_{max} \cdot a}{b \cdot h^2} \qquad \text{10-6}$$

$$M_{max} = \frac{F_{max} \cdot L}{6} \qquad \text{10-7}$$

where
a is the distance between the support and the nearest load application point,
b and h are the width and the depth of the specimen, respectively, and L the span.

10.5.2 Results and discussion

As can be observed in Figure 10-34 the test setup appropriately induced a constant bending moment with peak stresses in the middle section area (between the load points, a=L/3) of the G-XLam3 and G-XLam5 beam specimens. However, shear failure occurred on both sides between the supports and the load application points, which hindered the assessment of bending strength.

a) b)

Figure 10-34. Specimens deflection during four point bending test. a) G-XLam3. b) G-XLam5.

Load-deflection graphs plotted from the four point bending test results are illustrated in Figure 10-35a for G-XLam3 and Figure 10-35b for G-XLam5 specimens; whilst Table 10-5 and Table 10-6 present the calculated values for $Ep_{m,\ global}$, fp_m and M_{max} of both panel configurations, respectively. Values of elastic modulus in bending for G-XLam3 were higher than those for G-XLam5 and correspond to the trend observed with the predicted results in bending (Ep_m), previously analysed in Chapter 9.

a) b)

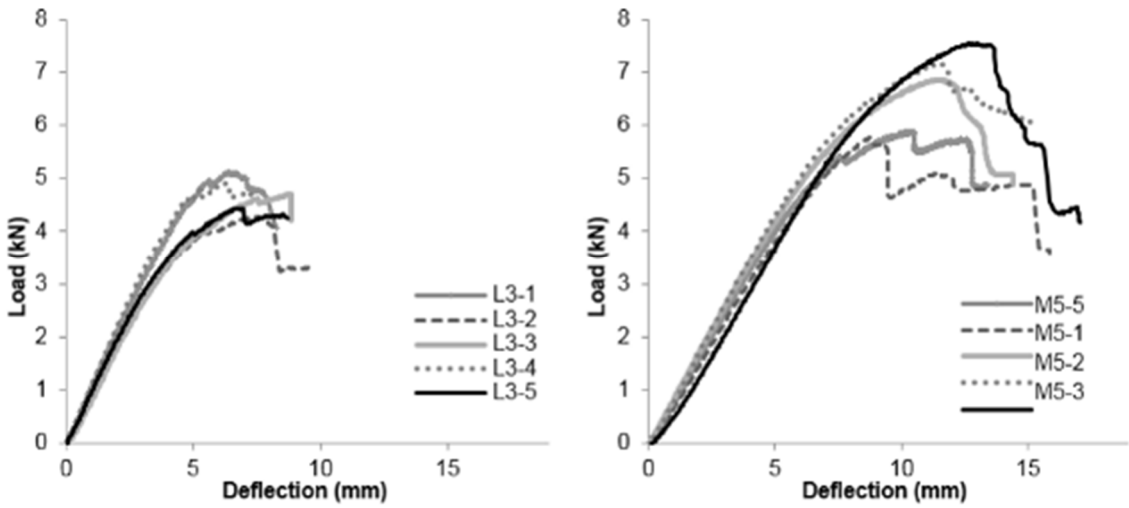

Figure 10-35. Load-deflection graph of the four point bending test for a) G-XLam3 and b) G-XLam5 specimens.

The observed variation on the peak load values (F_{max}) can be attributed to manufacturing defects as gaps, insufficient glue between the lamellas and natural variability of the material. A very low coefficient of variation (CoV) was nevertheless obtained and the linear elastic region presented a consistent gradient between the five test cycles for G-XLam3 and G-XLam5 specimens.

Table 10-5. Mechanical properties of the G-XLam 3 panels subjected to four point bending test.

G-XLam3 Specimen No.	L (span) (mm)	a (mm)	b (width) (mm)	h (depth) (mm)	I (mm^4)	$Ep_{m,\ global}$ (GPa)	F_{max} (kN)	M_{max} (kN x mm)	fp_m (MPa)
L3-1	300	100	46.42	17.35	20,203.30	25.28	5.12	256	109.92
L3-2	300	100	45.61	17.24	19,475.59	22.71	4.281	214.05	94.74
L3-3	300	100	46.51	17.24	19,859.89	23.27	4.693	234.65	101.85
L3-4	300	100	46.61	17.24	21,031.56	24.89	4.906	245.3	102.40
L3-5	300	100	46.52	17.77	21,753.08	22.25	4.441	222.05	90.70
Mean	300	100	46.33	17.37	20,464.68	23.68	4.69	234.41	99.92
SD			0.41	0.23	921.10	1.34	0.34	16.97	7.45
CoV (%)			0.89%	1.32%	4.50%	5.66%	7.24%	7.24%	7.45%

Table 10-6. Mechanical properties of the G-XLam 5 panels subjected to four point bending test.

G-XLam5 Specimen No.	L (span) (mm)	a (mm)	b (width) (mm)	h (depth) (mm)	I (mm^4)	$Ep_{m,\ global}$ (GPa)	F_{max} (kN)	M_{max} (kN x mm)	fp_m (MPa)
M5-1	450	150	47.5	26.25	71,610.99	19.21	5.88	440.63	80.76
M5-2	450	150	46.8	26.25	70,555.67	18.64	5.76	432.08	80.38
M5-3	450	150	47	26.25	70,857.19	20.12	6.86	514.50	95.31
M5-4	450	150	47.5	26.25	71,610.99	20.22	7.17	537.38	98.50
M5-5	450	150	47.4	26.25	71,460.23	18.60	7.54	565.43	103.86
Mean	450	150	47.24	26.25	71219.02	19.36	6.64	498.00	91.76
SD			0.32		483.84	0.78	0.79	59.18	10.66
CoV (%)			0.68%		0.68%	4.04%	11.88%	11.88%	11.62%

The mean value for maximum load at break F_{max} for G-XLam5 (6.64kN) was higher than for G-XLam3 (4.69kN) beams, thus M_{max} resulted also on a higher value (G-XLam3=234.4kN.mm and G-XLam5=498kN.mm, about two fold).

Bending strength (fp_m) values for both panel configurations resulted in similar figures and as expected, much lower values to those predicted in Chapter 9 (almost half). These predictions were based on experimental values of MOR_i resulting from three point bending test of individual layers (i), where the specimens experimented true bending failure instead of shear failure (as evidenced during four point bending test). In Chapter 9, predicted bending strengths (fp_m) were 183.33MPa and 150.78MPa, while experimental results obtained from

the four point bending test were 99.92±7.45MPa and 91.76±10.66MPa for G-XLam3 and G-XLam5 panels, respectively.

Failure in the beams initiated near the loading points and propagated horizontally towards the supports (the areas were the higher shear stresses occur in a four point bending test). These cracks caused the collapse of the lower density material in the cross layers (h_2 and h_4) of G-XLam3 and G-XLam5 beams, delamination and ultimately slip along the sides (Figure 10-36 & 10-37). Apart from specimen L3-5 no-splitting or crushing of the outer lamellas occurred in the compression (h_1 top layer) or tension zone (h_3 and h_5 bottom layers) in any of the panel configurations (G-XLam3 and G-XLam5). The fibre direction of these lamellas was along the beam axis (X_1) and perpendicular to the loading direction (X_3).

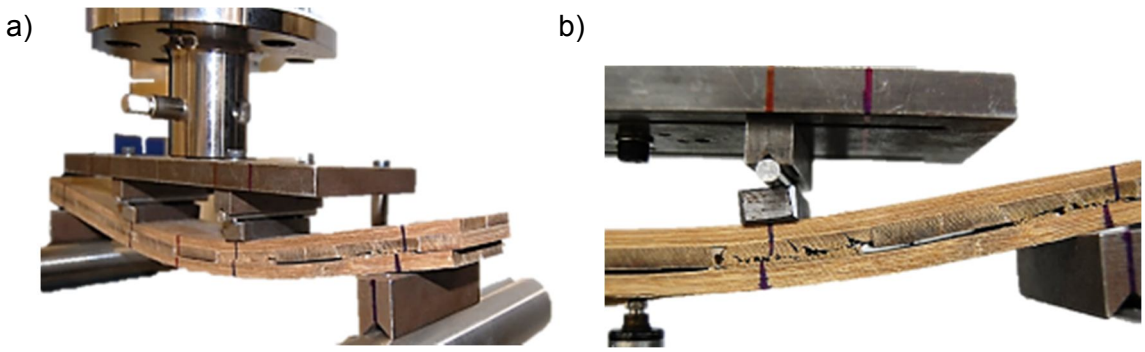

Figure 10-36. Slip and delamination failure mode of specimen L3-5 of a G-XLam3 beam subjected to four point bending test. a) Crack started at the loading points and propagated horizontally across the lower density material, producing delamination and slip. b) Detail of the propagation of the crack and delamination.

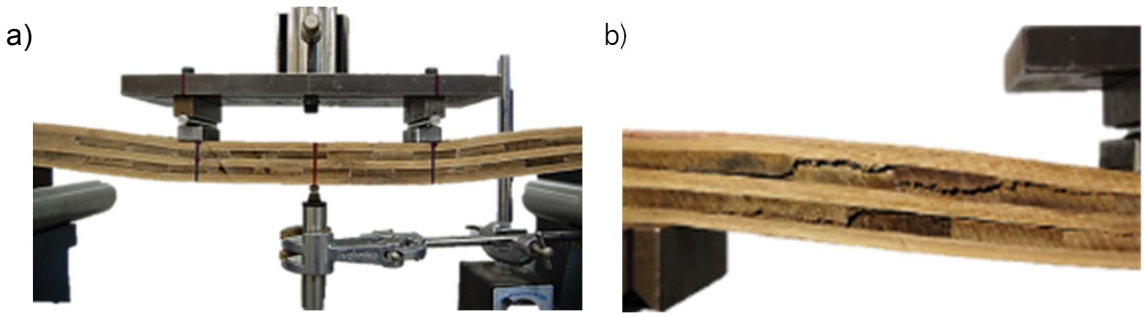

Figure 10-37. a) Shear failure occurred during four point bending test of a G-XLam5 beam. b) Detail of the propagation of the crack mainly along the lower density material.

Specimen L3-5 which had the lowest fp_m presented more gaps towards the middle section between the loading points (due to manufacturing flaws).

Concluding remarks

A set of elastic and strength values for G-XLam3 and G-XLam5 panels were obtained from mechanical testing using physical and non-contact measurement systems. These values are presented in Table 10-7 together with all the values obtained through FE and numerical methods.

Table 10-7. Summary of the results obtained from the testing programme undertaken on G-XLam panels.

	G-XLam3						G-XLam5					
	$Ep_{C,0}$ (GPa)	$Ep_{C,90}$ (GPa)	$G_{xy} = G_v$ (GPa)	Ep_m (GPa)	fp_m (MPa)	M_{max} (MPa)	$Ep_{C,0}$ (GPa)	$Ep_{C,90}$ (GPa)	$G_{xy} = G_v$ (GPa)	Ep_m (GPa)	fp_m (MPa)	M_{max} (MPa)
DIC-Test	**17.22**	**2.43**	1.16	-	-	-	**15.67**	**9.46**	0.94	-	-	-
SD	3.22	0.66	0.14	-	-	-	3.02	4.16	0.09	-	-	-
CoV	19%	27%	11.74%	-	-	-	19%	44%	9.42%	-	-	-
TEST with LVDT	**14.86**	**7.43**	**0.67**	**23.68**	99.92	234.41	**12.48**	**8.74**	**0.72**	**19.36**	91.76	498.00
SD	1.17	0.69	0.02	1.34	7.45	16.97	0.92	0.76	0.03	0.78	10.66	59.18
CoV	8%	7%	2.95%	5.66%	7.45%	7.24%	7%	9%	4.28%	4.04%	11.62%	11.88%
Predicted	**14.83**	**7.93**	**0.92**	**20.97**	183.33	-	**13.45**	**9.31**	**0.84**	**17.43**	150.78	-
FEM (gapless)	**14.95**	**8.05**	-	-	-	-	13.52	9.36	-	-	-	-
FEM (with gaps)	12.75	7.56	-	-	-	-	**12.94**	**8.42**	-	-	-	-

Independently of the method used (DIC, LVDT or Analytical), the values of elastic properties in longitudinal compression ($Ep_{C,0}$) are about 50% and 70% higher than the elastic properties measured in the transverse direction ($Ep_{C,90}$) for G-XLam3 and G-XLam5 panels, respectively.

In spite of the considerably low value for $Ep_{C,90}$ obtained from the DIC test of G-XLam3 panels, in general DIC values were higher than the analytical predictions and test results using LVDT. Additionally, test with DIC resulted on high variability of results; coefficients of variation (CoV) for the compression test values reached up to 44%, while shear moduli values (G_{xy}) were above 10%.

Analytical values provided a reasonably accurate prediction of the elastic properties of G-XLam3 and G-XLam5 panels. Variability of the predicted compressive modulus ($Ep_{C,0}$ and $Ep_{C,90}$) of both panel configurations was below 7%, when compared to the tests results using physical measurement systems (LVDT). Predicted bending modulus (Ep_m) values were in average 12% lower than the LVDT test results; while predicted shear modulus (G_v) values were about 15% and 27% higher than the LVDT test results for G-XLam3 and G-XLam5, respectively. Overall, adequate match between the predictions and the test results using physical measurement techniques was found for assessing the elastic properties of the panels. Differences in the results can be caused by manufacture flaws and thickness variation within the individual lamellas (Figure 10-38) but, unfortunately their influence could not be statistically determined due to the use of only one test specimen per panel configuration (G-XLam3 and G-XLam5). However, simulations undertaken through finite elements (FE) analysis showed the influence that manufacture defects as gaps can have on the final elastic properties of the panels (Section 9.2.1 in Chapter 9).

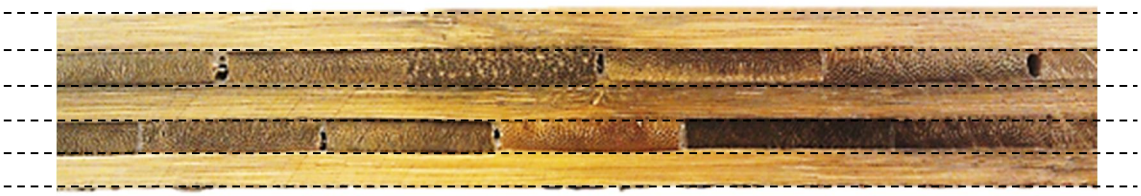

Figure 10-38. Thickness variation and gaps across the section of a G-XLam5 panel.

Finally, predicted fp_m values were higher than the fp_m values obtained through four points bending test due to premature shear failure during testing. In order to avoid shear failure and based on previous experimentation by Dr. Annette Harte's research group at Galway University, Republic of Ireland, advice is given to increase the length of the shear spans to nine times the depth (instead of six), whilst keeping the middle span at six times the depth (between the load points, a=6h). This change to the standard testing method specified by BS EN 408:2010 (BSI, 2010) for CLT induces failure on the zone under bending.

11. Implementation of the G-XLam technology in construction.

Introduction

The THM densification of Guadua has demonstrated the capability to produce flat Guadua strips with a densified profile and improved mechanical properties through a novel straightforward manufacturing process, which has never been applied in Colombia. By contrast TM processes applied to Moso in China are not focussed on enhancing the material's mechanical properties, but its appearance and hardness. These factors are key for commercial flooring applications. Densified flat Guadua strips (FGSs) tackle material and processing related issues such as Guadua's high dimensional variability and the intensive requirement for labour (Table 3-1). In addition, FGSs are potentially more resilient to decay and offer flexibility of use and design. By glue-laminating FGSs with a rigid adhesive in alternating 0-90° layers, G-XLam panels scatter the material variability and result in an engineered Guadua product whose structural performance can be predicted (Chapter 9). The manufacture, testing and structural analysis of cross-laminated Guadua (G-XLam) panels has demonstrated the feasibility of producing dimensionally and structurally stable engineered Guadua products (EGP). As a result, more flexible design and usage opportunities are also possible. Nevertheless, concerns remain over issues related to the spring-back recovery, weathering, fireproofing and machinability of FGSs and the overall environmental impact of G-XLam technologies. Table 11-1 compares the opportunities and threats of using G-XLam technology in construction applications to those issues identified for construction with round Guadua in Chapter 3 (Section 3.2.3) and listed in (Table 3-1). Overall, this Chapter addresses the processing, design and usability potential of G-XLam systems for architectural and structural solutions that could be applied in Colombia. Aspects regarding the implementation of the densification technology at the material's source, achievable size of EGP or G-XLam panels and potential structural systems will be discussed.

Table 11-1. Assessment of the opportunities, risks and key features of using G-XLam technology in construction in comparison to the issues identified with the use of round Guadua in construction.

Item	Issues with round Guadua	G-XLam		
		Opportunities	Risks	Key features
1	Use of non-processed material	Material quality is controlled through standardised processes.	Technological barrier	Appropriate technology
2	Poor design and detailing	Standard details from timber engineering can be implemented. Both processes become more controllable and design and manufacturing platforms such as BIM can be easily used.	Further testing, training of architects and engineers	Standardised
3	Deterioration by weathering and decay	THM densification processes are known to improve the resistance of wood to decay and weathering.	Bio-deterioration and spring-back effect to be investigated	Durable
4	Temporary constructions become permanent	Can be integrated into permanent structural systems	Higher costs than traditional construction.	Permanent
5	Inadequate structural properties when integrated with other conventional materials	Easier to combine with conventional materials and standard construction methods.	Prototyping and product development.	Buildable
6	Intensive labour (handcraft)	The mechanization of the process is increased but highly skilled labour is required.	Heavier and harder material, which will cause intensive wear of tools.	Industrialised process
7	Non-compatibility with building elements	Flat surfaces provide more compatibility with commercially available building elements.	Building systems need to be devised.	Compatible
8	High material variability - Irregularity	Material profile is densified to homogenise its mechanical and physical properties. Irregularity is highly reduced as defects are evenly distributed in the lamination processes.	Control of manufacturing processes and of the efficient use of the material.	Uniformity
9	Deficient maintenance	Increased durability will reduce maintenance and standardised building elements will enhance replacement and retrofit if necessary.	Adequate use of the material to improve durability	Flexible
10	Low-added value	High-added value that can be shared throughout the supply chain and delivered to the final user. High range of applications.	Integration of the supply chain and material availability.	High added value
11	High environmental impact of cement renders	Flat surfaces provided by the panel do not require the use of cement renders and if needed, render thicknesses are reduced. Reduction of the glue-content when compared to commercial products.	LCAs to be undertaken	Social and environmental benefit
12	Highly flexible joints	More rigid connections systems derived from timber engineering can be adopted	Testing of commercial adhesives and connections (e.g. nailed and bolted)	Engineered
13	Insufficient or non-fire proofing	Coatings and fire protection systems can be devised. Fire-resistance of densified product likely to be enhanced.	Fire testing required	Fireproofing through redundancy
14	Structural unpredictability	Panel's structural capacity can be predicted and calculated as part of a structural system that complies with building codes.	Standardisation of the product and acceptance within building codes.	Predictable

11.1 Scaling-up the manufacturing process

Any technology applied to the processing of Guadua has to consider the technical limitations at the point of harvest. Guadua and bamboos in general are grown in developing countries and emerging economies with moderate to low technological development, where the industrialisation of the resource is limited. There are also issues with the location of the plantations within dense forest sites. Natural Guadua plantations in Colombia (Figure 11-1a) are commonly located on steep hills, close to rivers and when not well managed they are difficult to access due to their copious thorny branches that reach breast-height (Figure 11-1b).

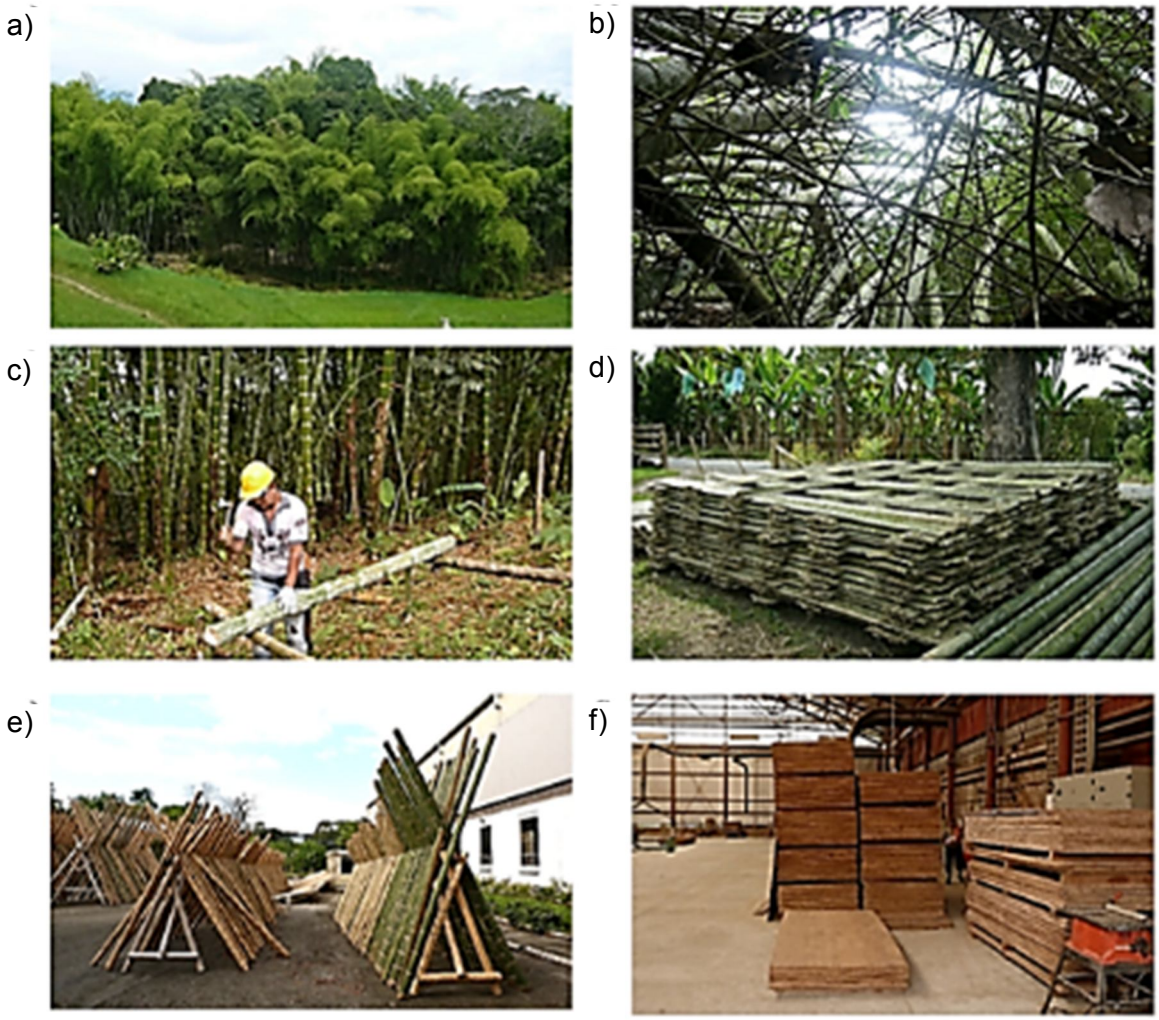

Figure 11-1. a) Natural Guadua plantation in the coffee growing zone in Colombia. b) Thorny branches on a badly managed plantation. c) Manual splitting process of 'esterilla' using an axe. d) Collection site for raw material. e) Selection, preservation and drying processes on a CPP. f) Panelised products manufacture (Riven Guadua boards at the Villegas factory, Colombia).

Normally, the extraction of the material from the plantation is fairly manual; felling is done by hand with machete or chain saw, canes are cut into commercial sizes or converted into 'esterilla' (riven Guadua) in situ (Figure 11-1c) and then transported on mules to the closest collection site (Figure 11-1d). Then, round Guadua culms and riven Guadua boards are transported to centres of primary processing (CPP) where they are dried and preserved (Figure 11-1e) depending on their intended use (see Chapter 3). Further industrial processing into engineered products is rarely undertaken, but initiatives to produce panelised products are under development (e.g. Villegas riven Guadua panels factory in Figure 11-1f).

The transformation of Guadua into engineered Guadua products (EGP) remains a challenge for industry and researchers alike. Chapters 5 and 8 described the processes involved in the manufacture of densified FGS and their lamination into G-XLam panels, respectively. The production of EGP was possible through the use of alternative manufacturing methods that involved thermo-hydro-mechanical (THM) densification treatments, which have not been implemented before in Colombia.

Figure 11-2 illustrates the proposed system for the transformation of round Guadua culms into FGSs, which are the base material of EGPs such as panels, structural elements and shells. The process is subdivided into the three processing stages, previously discussed in Chapter 2. The first stage refers to the extraction of Guadua from the plantation and its sectioning into commercial sizes (if no further processing is required the material is considered as a non-processed product). Once felled and cut, what follows is the moderate processing stage of the material, that can be undertaken partly in the plantation or completely at a CPP. Then, the final stage relates to the transformation of moderately processed Guadua products into highly processed standardised products in a factory (EGP).

The manufacturing system for FGS uses only the middle section of Guadua culms, which are relatively constant in diameter and wall thickness, and with lengths of between six and eight metres. These lengths and the provision of the appropriate equipment throughout the FGS's manufacture will determine the length of EGPs that can be achieved.

11.2 Proposed processing of FGS

On felling and sectioning Guadua in the plantation its cortex needs to be peeled-off. Some vernacular methods use a very sharp machete to slice the outer layer of Guadua when green; however, it is a precarious and highly dangerous procedure that does not provide adequate control over the depth of the removed layer.

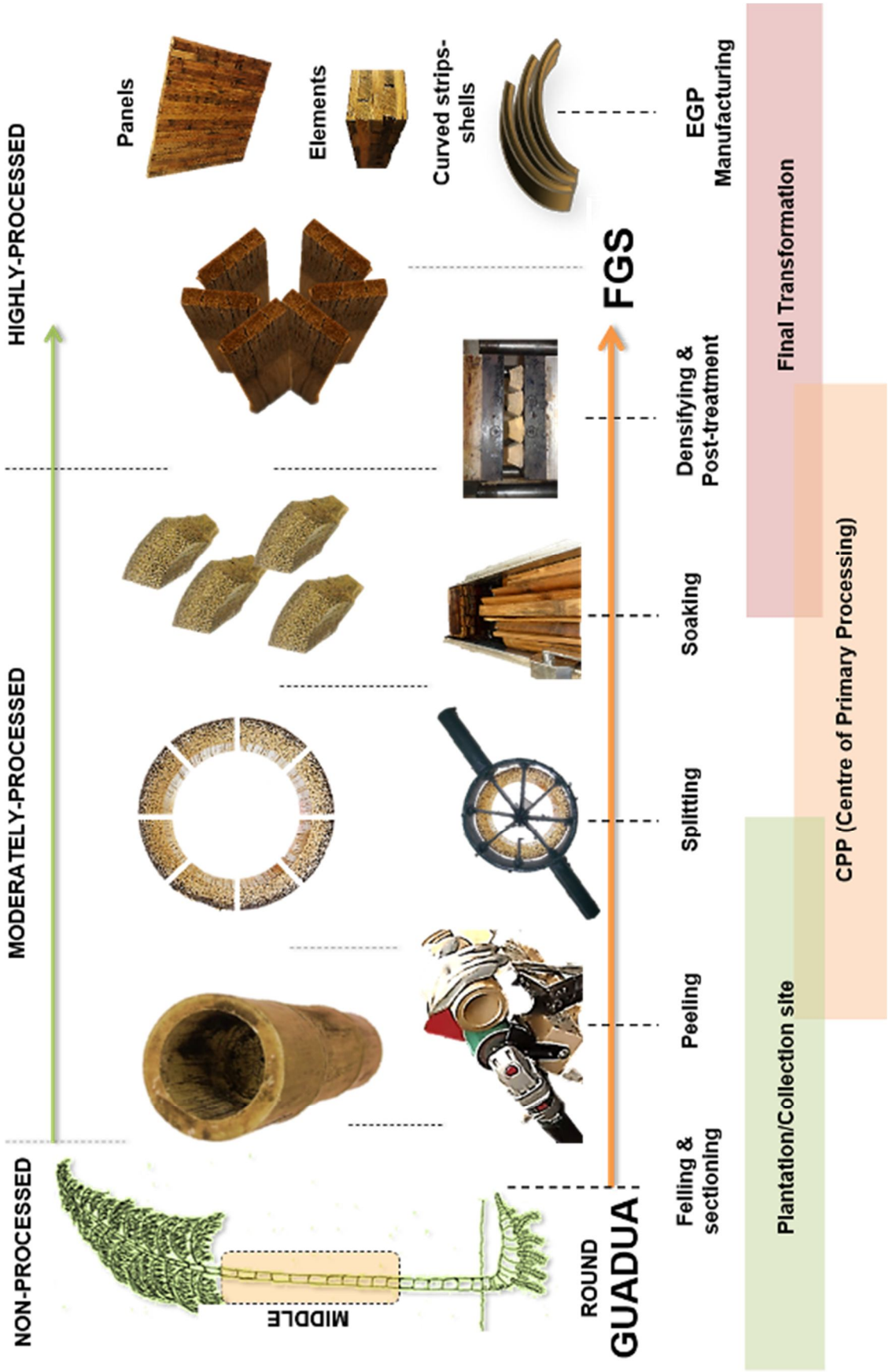

Figure 11-2. Guadua transformation process into FGS (Flat Guadua strips)

Power tools such as the burnisher with a highly abrasive cloth belt used in this study (see Figure 8-1b) are a feasible method for removing the cortex; however, no-experimentation on green specimens has been undertaken. Some commercial products for debarking wood logs can be connected to the chainsaws used in the plantation or installed at CPPs for peeling the cortex of Guadua (Figure 11-3). Peeling the interior layer in the Lacuna would be more challenging, but can utilize similar machinery.

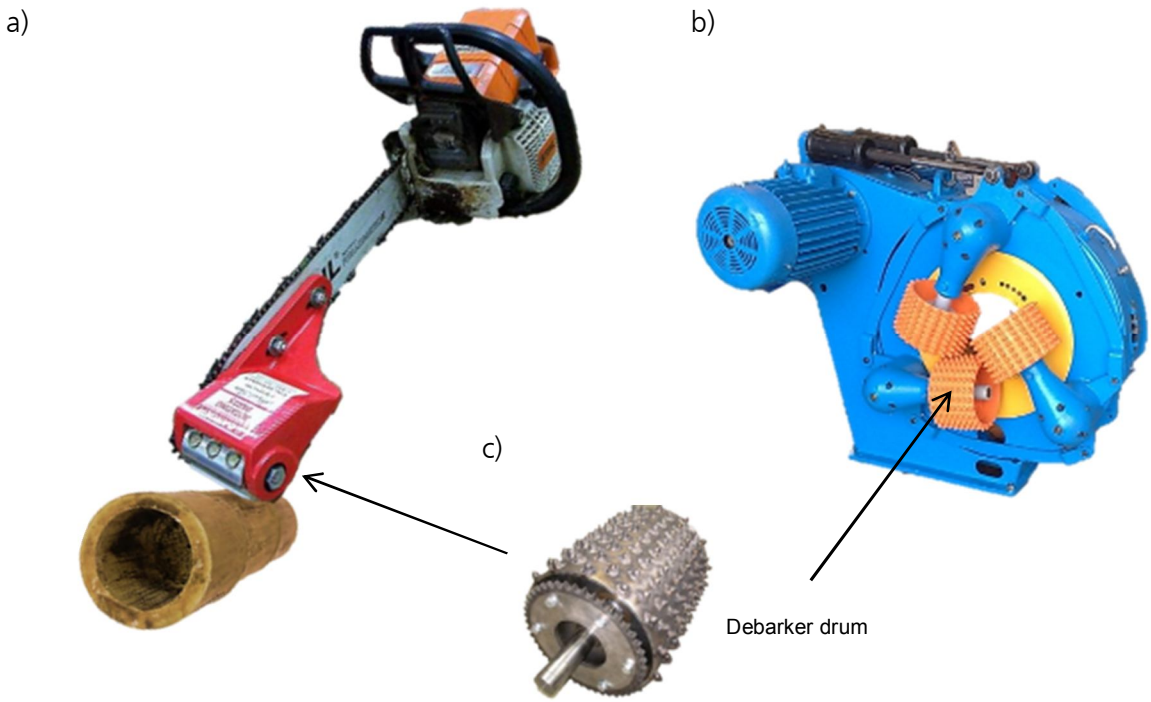

Figure 11-3. Mechanized alternatives for peeling-off the cortex of Guadua. a) Log debarker for sawmill chainsaw (http://www.machine--tools.com/). b) Debarker drum fabricated and machined from scratch by PW Engineering (http://www.pwengineering.co.nz/) with case hardened "teeth" from Morebark. c) Cambio 35 debarker for logs up to 350mm in diameter (http://www.tcr-sawmill.co.uk/).

The processes that follow are the splitting of Guadua into eighths and their soaking in water for 24 hours before densification. The splitting process uses the 'Chinese ring', a metal circular tool with sharp concentric knives that splits the round section of Guadua into eight pieces when culms are pushed through. The cuts spread along the direction of the grain and quarter sections are obtained. Although this could be done manually (Figure 11-4a) with the aim of achieving long regular sections, this system should ideally use an electric or petrol powered device with a guiding rail or a centring plate, like the one shown in Figure 11-4b (long sections could nevertheless, be problematic).

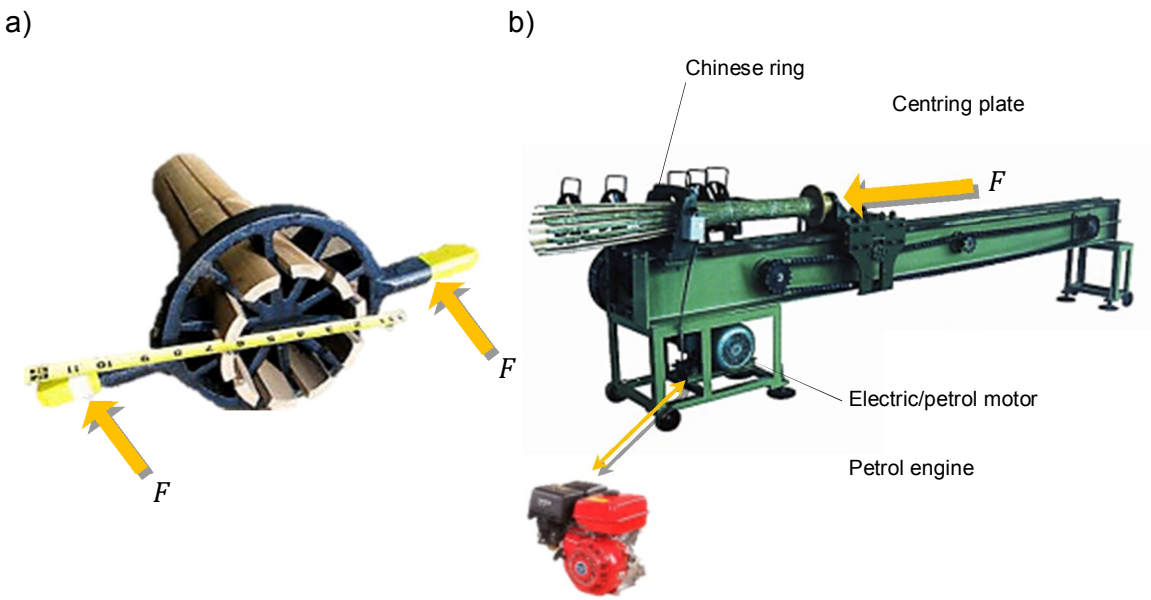

Figure 11-4. Splitting bamboo with the Chinese ring. a) Manual splitting device. b) Mechanized splitting device.

It is assumed that soaking could be avoided by using Guadua in its green condition (over the fibre saturation point FGS>30%), which would require immediate extraction of the material from the plantation for further processing. In general, peeling and splitting devices can be easily implemented close to the plantation or in collection sites. This can reduce transport cost considerably (transporting strips instead of hollow canes) and add value to the product sold by the plantation owner/farmer.

THM densification would then be undertaken in a CPP or a factory at 150°C applying 6MPa of pressure for a total of 20min as explained in Section 5.5. Assuming that the strips of Guadua are still in a green condition, the material will be softer and potentially easier to plasticize during densification. The application of lateral pressure by the use of moulds or lateral restraints is advised to limit side irregularities. If long strips of Guadua (between 6 and 8m long) are to be densified, extremely large hot-press machines will be required. This type of machinery will need to be custom made, as the largest commercially available size of hot platen machines is 2.40m x 1.20m. A more feasible option is the use of pressure rolls and a heat or steam source Figure 11-5. If none of these alternatives is industrially scalable, strips of Guadua could be cut to a maximum of 2.40m in length and densified in conventional hot-presses. As the width of the strips does not exceed 50mm, the use of shorter sections might also ease the application of lateral pressure or the use of moulds. Lengths below 3.00m are commercially available and facilitate local transport (commonly the maximum transported length of raw Guadua is 6.00m).

Figure 11-5. Multi-nip rotary laminator for engineered flooring with hot melt roller coaters (http://www.uniontoolcorp.com) whose design could be adopted for continuous densification of Guadua strips.

Finally, post-densification treatments to fix the compression and avoid the spring back-effect will ensure a suitable dimensional stability of FGSs for the production of engineered Guadua products (EGP). A suggested post-treatment which was not undertaken during this study is the OHT (oil heat treatment) in heated rapeseed oil at 200°C, which has been demonstrated to fix the densification and improve durability (Welzbacher *et al.,* 2007). The use of linseed oil for OHT can also be considered. This oil has been traditionally used for varnishing the surface of Guadua culms in construction.

Once the FGSs are produced, three main applications have been proposed: a) G-XLam panels, whose manufacturing process and mechanical properties were assessed in this study; b) Customised structural elements such as unidirectionally laminated beams that can follow similar manufacturing processes as the G-XLam panels and, c) Curved strip-elements and shells. The use of FGSs as curved strips benefit from the improved elastic properties of the THM modified Guadua. The potential use of these EGP in construction applications is discussed in the following Section.

G-XLam panels

One of the biggest limitations of using round Guadua in construction is height. The Colombian building code allows for a maximum of two floors in residential buildings using plastered cane (bahareque encementado) systems. This is in part due to the dimensional variability of round Guadua culms, which limits standardisation, together with the limited rigidity of the connections within the structural system. Hence, a modular structural system has been devised for tackling these issues using G-XLam panels. A panel system comprised

of two G-XLam faces fastened to a steel frame is proposed. G-XLam panels can provide thin, stiff and strong faces to support in-plane vertical and lateral loads, but their characteristic slenderness makes them vulnerable to out-of-plane action resulting in severe buckling. Thus, distancing the faces and installing horizontal stiffeners increases the second moment of area, which can be calculated using the parallel axis theorem, and the flexural rigidity of the panel system about the neutral axis. Horizontal stiffeners can be manufactured with unidirectionally laminated FGSs (G-ULam) and glued to the faces with the same resin used for the panels. Standard parallel steel flange channels form the frame structure to which the faces are bolted. Threaded pins welded to the top and bottom flanges provide connections to the floor structure. The standard size of the panels is 4ft wide by 8ft height (1.20m by 2.40m) with a thickness of 150mm. The assembly of the panels is illustrated in Figure 11-6.

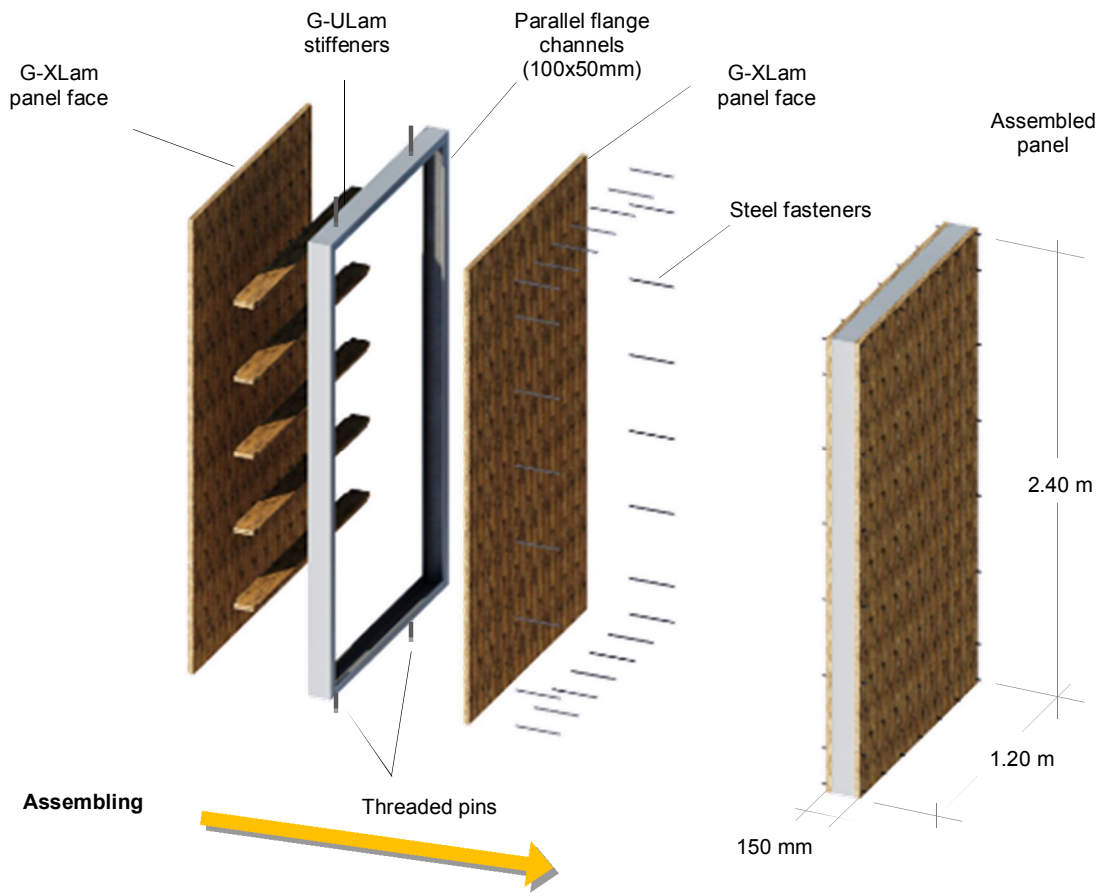

Figure 11-6. Double-faced G-XLam structural panel assembling process.

The steel frame proposed for the panelised system illustrated above can be replaced by a G-ULam frame structure glued to the G-XLam faces and connected to other building elements using connection systems for timber construction; e.g., companies such as Simpson Strong-

Tie Inc. have a broad range of joining systems that are suitable for this purpose. Nevertheless, the use of a steel frame offers easier assembly with conventional reinforced concrete or steel construction. Moreover, the standardised size of the G-XLam panel system can be assembled into standardised container size boxes that are modular and easier to transport. For instance, the standard size of a 20 foot container is 20'x8'x8'6" in length, width and height (l=6.06m, w=2.44m, h=2.59m). These box-type units can be manufactured to high standards in a factory (off-site), shipped to site and crane lifted into place (Figure 11-7).

a)

b)

Figure 11-7. Crane assembly of a box-type unit volumetric prefabricated unit) at a housing community in Vildrosen, Denmark (produced by Kodumaja) (Trubiano, 2015)

Commonly, volumetric units are delivered fully equipped with electrical, gas, and plumbing installations, as well as with building elements such as windows, doors and staircases. These off-site systems enhance the control over the building process and reduce construction times and safety risks on-site (it becomes a systematic factory process instead of an open-air labour intensive construction process). Volumetric units can also be mass customised and engineered to form mid-rise buildings (up to ten stories) (Figure 11-9).

a) b)

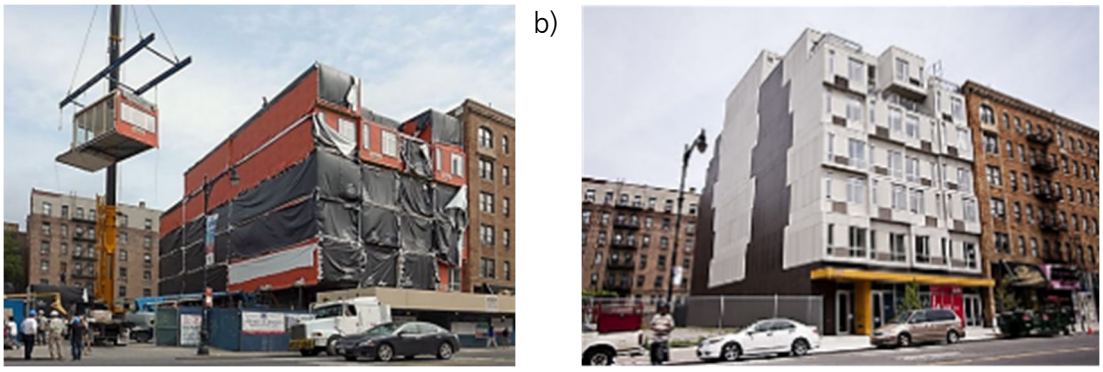

Figure 11-8. The Stack in New York city, a prefabricated seven-story by Gluck+ architects. a) Crane assembly of the volumetric prefabricated unit (www.savemarinwood.org). b) Finished building (www.jcsa.com).

G-XLam panel systems for load bearing walls and slabs can be modularised and assembled into prefabricated volumetric systems (Figure 11-9) and replicated in height (Figure 11-10).

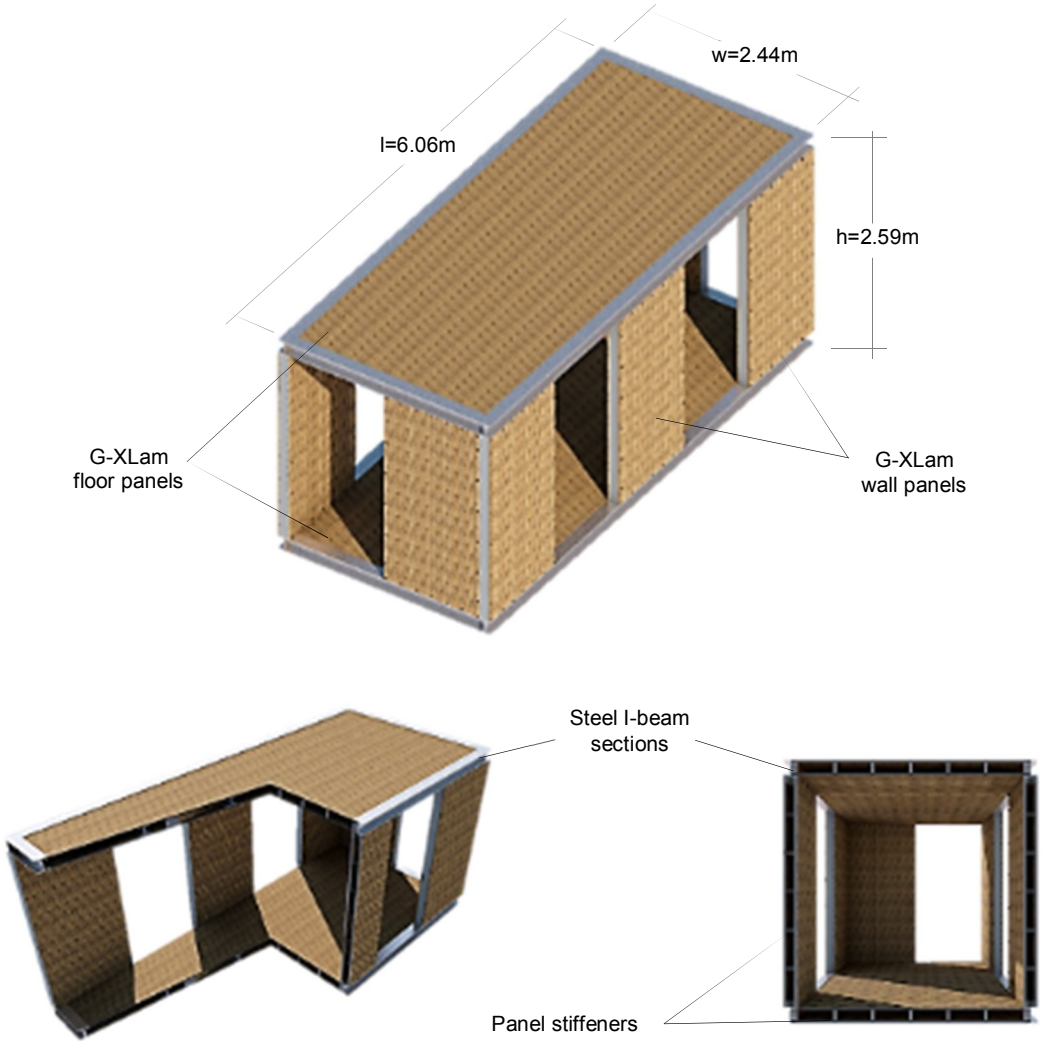

Figure 11-9. 3D views of the modular volumetric unit using G-XLam panels for walls and floors.

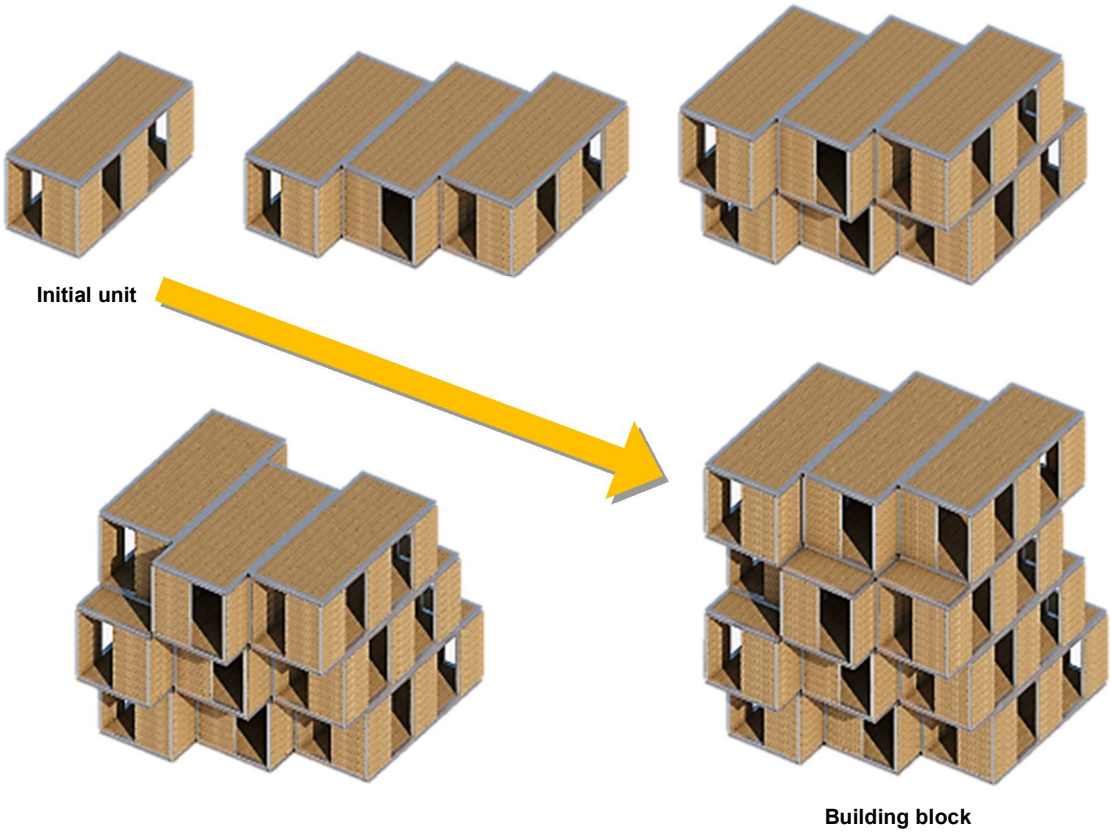

Figure 11-10. Replication of a volumetric unit with the G-XLam panelised system.

Building blocks can be produced from volumetric units and design variations added depending on the structural requirements. Figure 11-11 illustrates a computer-generated image of a four-storey building block.

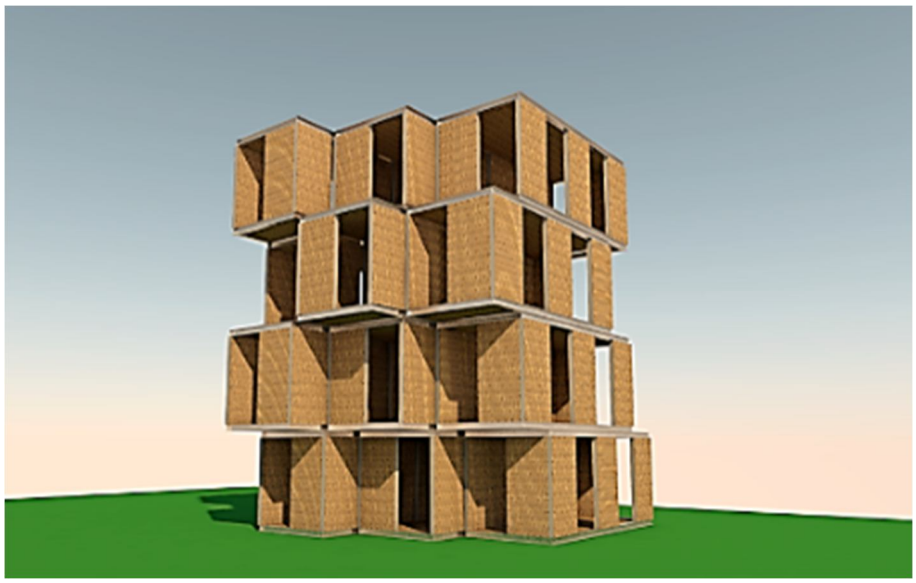

Figure 11-11. Four storey building block using G-XLam panelised system.

Structural insulated panels (SIPs) can also be fabricated using G-XLam panels for the faces and low density natural fibre boards or expanded polyurethane foams for the core. SIPs are considered a composite panel system that homogenously distribute the acting loads throughout the panel area, responding to compression, racking, axial bending and shear loads in high wind and seismic events as a solid one-piece component. Moreover, the characteristic air tightness and insulation capacity of SIPs offer significant advantages when compared to conventional systems.

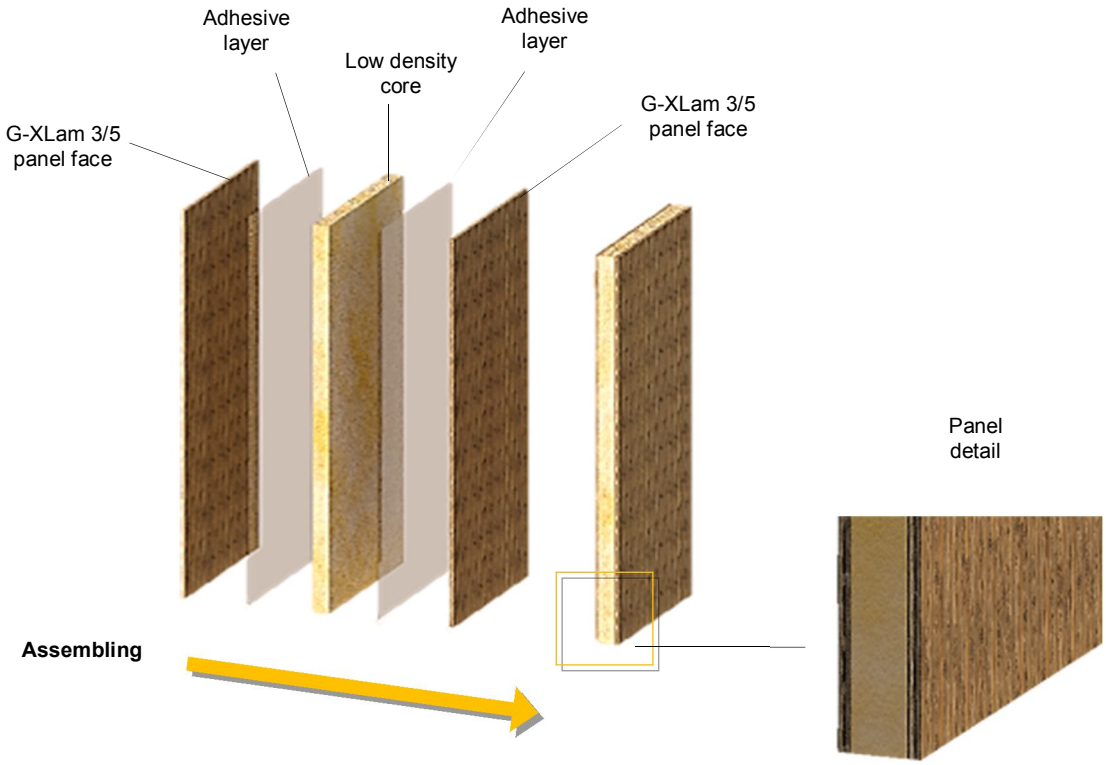

Figure 11-12. Double-faced G-XLam structural panel assembling process.

Curved strip-elements and shells.

G-XLam or G-ULam lamination technologies could be used for individual curved structural elements or to form shells. Flat Guadua sheets (FGS) could be processed to achieve a curved shape and glued or fastened together. This feature is key in providing design flexibility for designers and architects. For instance, some approaches with lightly THM modified bamboo strips (green bamboo bent with a gas flame burner) have been recently undertaken by design practices such as Giant Grass using simple tools (Figure 11-13).

Figure 11-13. Bamboo bent for the roof structure of a tent (http://www.giantgrassdesign.com)

FGS densified through a THM densification process benefits from an increase in mechanical properties, which can be exploited to build vaults and gridshell structures (Figure 11-14).

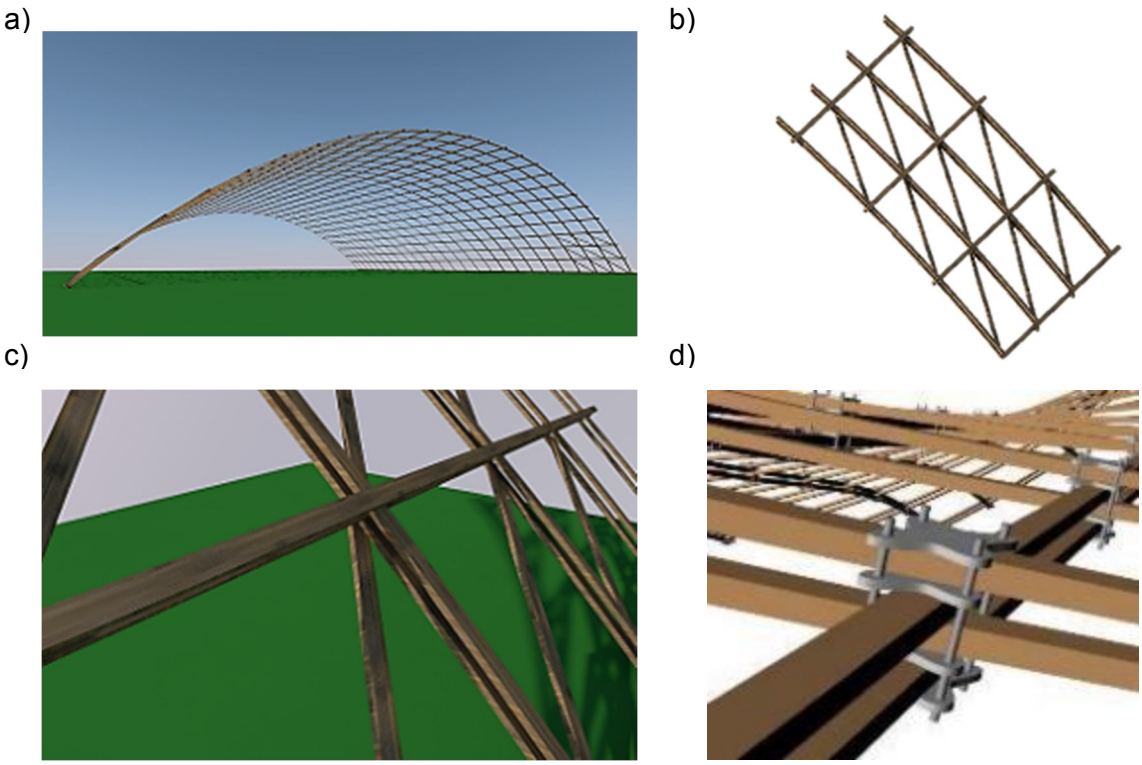

Figure 11-14. Proposed gridshell structure using densified FGS. a) Full structure. b) & c) Structure detail. d) Conventional gridshell connection detail taken from www.grasshopper3d.com.

Combined systems using flat and curved G-XLam panels could also be devised. Stressed-skin structures use a similar structural concept to that of sandwich panels (stiff faces separated by a core or internal structure that increases the second moment of area). Stressed-skin structures such as the 'monocoque' system by Cowley timberwork (Timber engineering connections Ltd) illustrated in Figure 11-15 could be replicated using curved G-XLam panels.

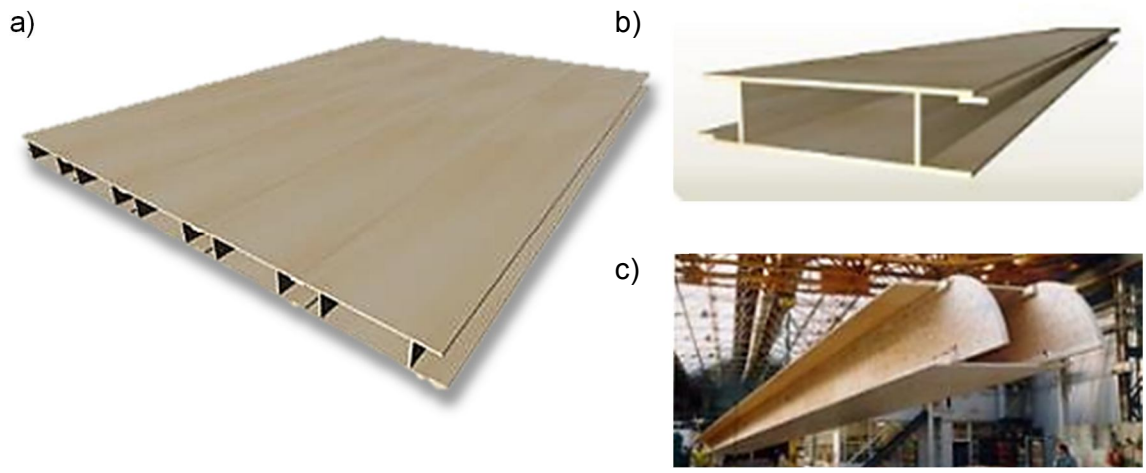

Figure 11-15. Monocoque panels by Cowley timberwork. a) Monocoque panels assembled. b) Monocoque panel unit. c) Prefabricated monocoque panel. Images from (www.cowleytimberwork.co.uk).

These panels have been used for roofs covering large spans and load-bearing walls as shown in Figure 11-16.

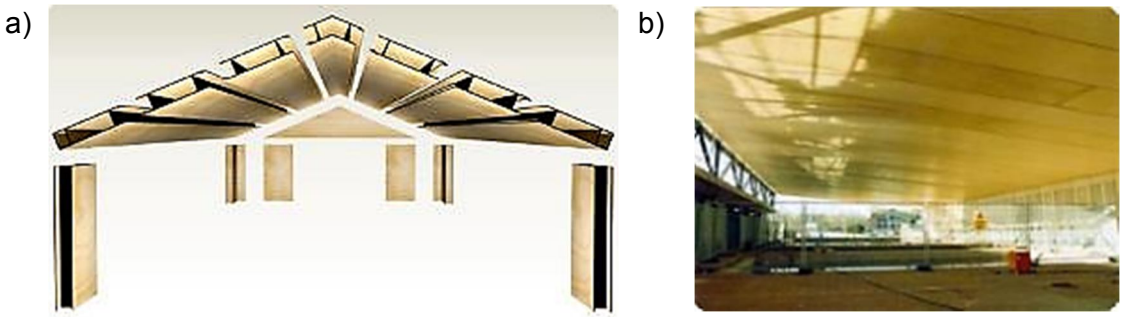

Figure 11-16. a) Roof and wall system using Cowley's monocoque panels. b) Large span covered with Cowley monocoque panels at Darlastan. Images from (www.cowleytimberwork.co.uk).

These monocoque systems use engineered timber products produced by Kerto with exterior quality bonding. Panels are comprised of Kerto 'Q' Laminated Veneer Lumber (LVL) fabricated to maximum sizes of 26m long by 1.8m wide or 20m long by 2.5m. Different roof configurations including barrel vaults can be achieved with these panels. Roof and floor spans of up to 19m and 12m, respectively, can be attained with panel depths of 600mm for maximum loadings of 0.6kN/m^2 and 4kN/m^2, respectively (www.cowleytimberwork.co.uk). The mechanical properties of the Kerto 'Q' LVL elements are comparable to the mechanical properties of the G-XLam panels; however, unidirectional glue lamination increases the axial stiffness per unit area of the structural elements as can be seen in Table 11-2. The values presented on this table for G-XLam panels are not characteristic or five percentile values, but the result of a very small number of mechanical tests with a small statistical significance.

By contrast, Kerto values presented in the same table are the design values for this type of engineered LVL product, which means that a modification factor has been applied to the material's characteristic values.

Therefore, the use of G-ULam panels could provide higher elastic and strength values along the direction of the grain. Finally, as with the case of the G-XLam panels previously presented in this Section, the void spaces inside the panels can be filled with insulating materials for thermal performance.

Table 11-2. Design values of Kerto 'Q' and mechanical properties of G-XLam panels from testing results.

Property	Units	G-XLam3*	G-XLam5*	Kerto 'Q'
Thickness	(mm)	17.5	22.5	27-69
Characteristic density	(kg/m^3)	890	890	480
$Ep_{C,0}$	(GPa)	14.86	12.48	10.5
$Ep_{C,90}$	(GPa)	7.43	8.74	2.4
G_v	(GPa)	0.67	0.72	0.6
Ep_m	(GPa)	23.68	19.36	-
fp_m	(MPa)	99.92	91.76	32
M_{max}	(MPa)	234.41	498.00	-

* TEST with LVDT (Metsä-Wood, 2011)

The design of a pedestrian bridge using the stressed skin system's concept is presented in the following images (Figures 10-15 to 10-17).

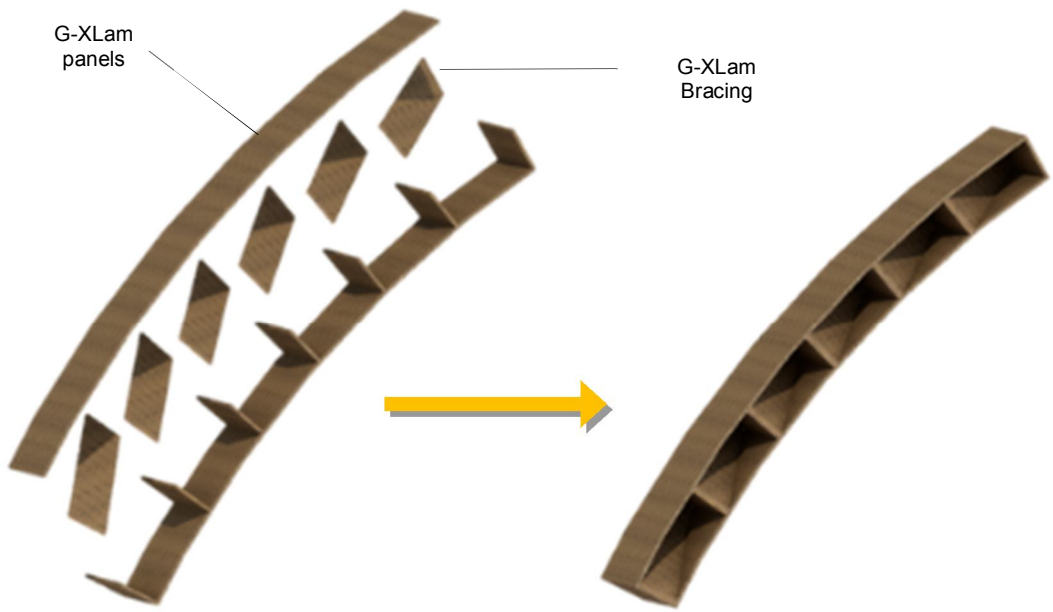

Figure 11-17. Assembling process of stressed skin elements.

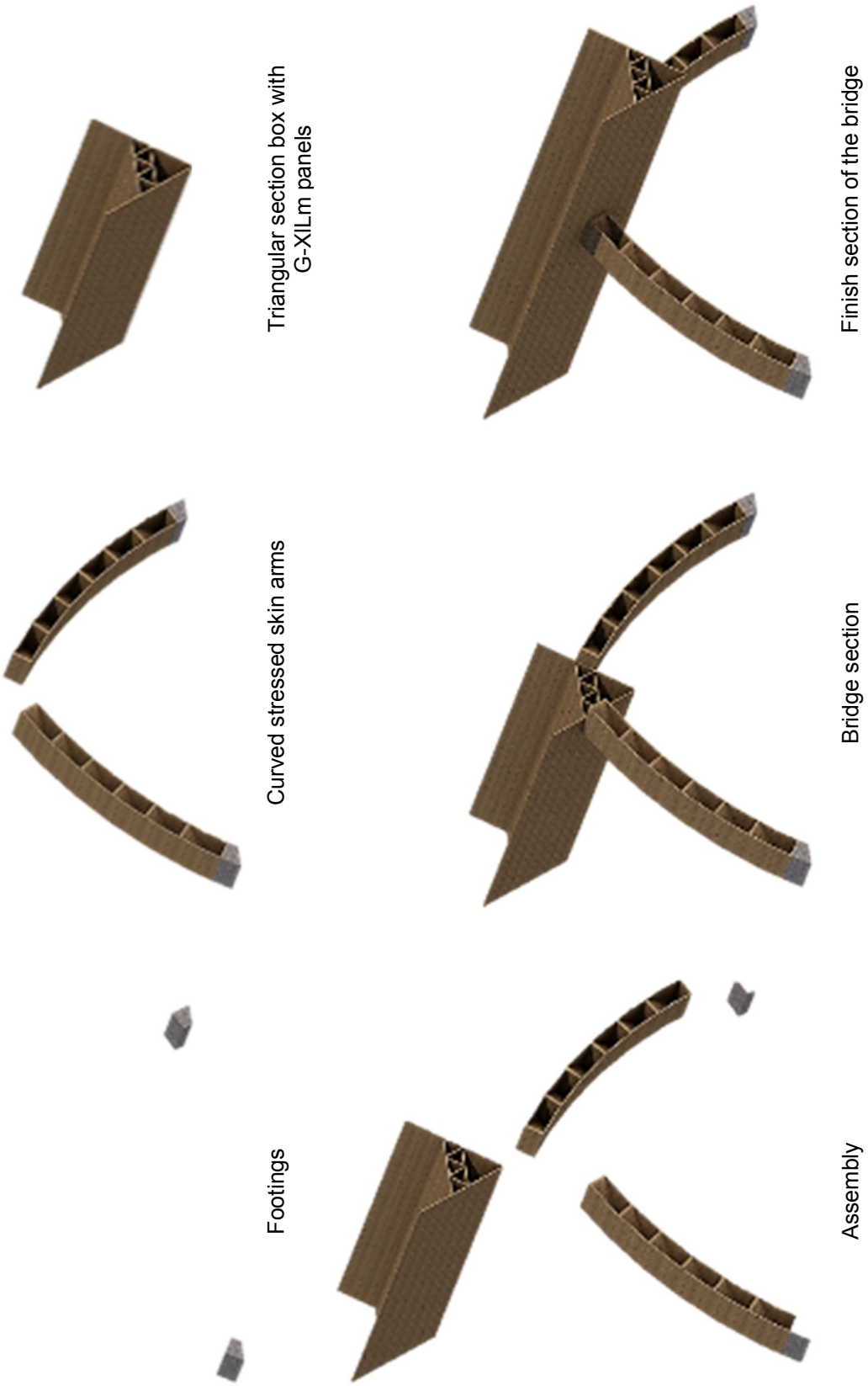

Figure 11-18. Assembling process of a proposed bridge structure using G-XLam panels.

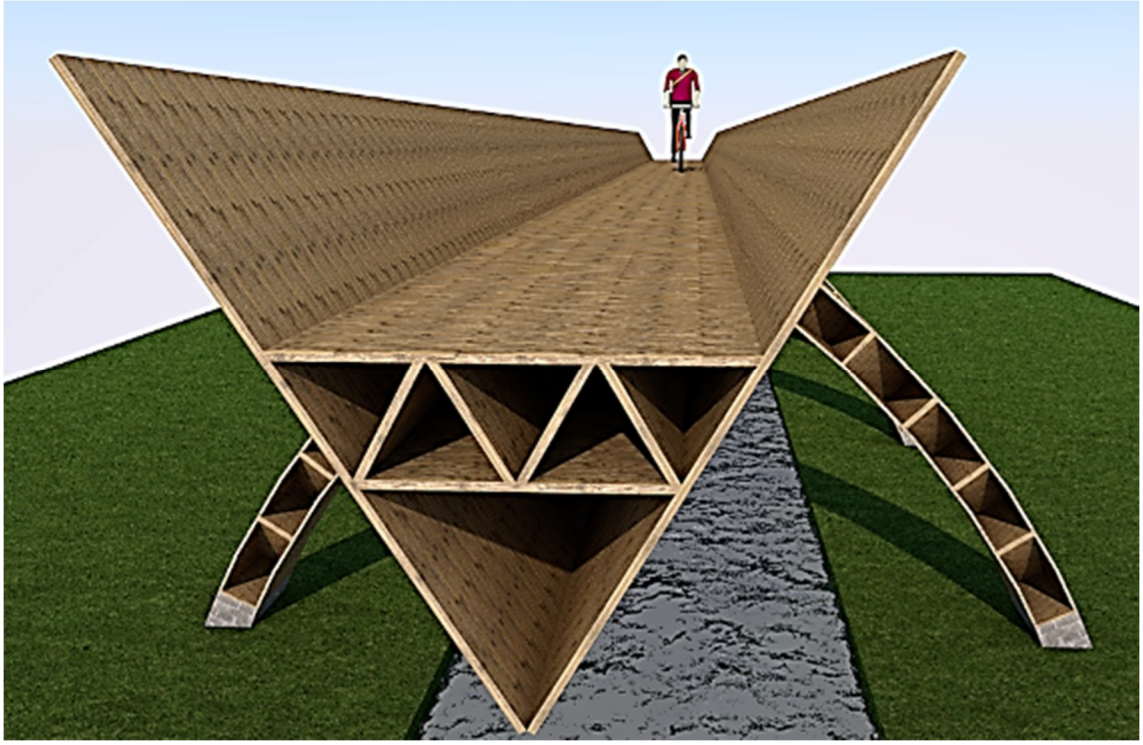

Figure 11-19. 3D view of the G-XLam pedestrian bridge.

Overall, G-XLam panel technologies offer design flexibility for flat and curved strutcural elements, which could use connection systems developed for timber and potentially substitute the use of timber in different applications .

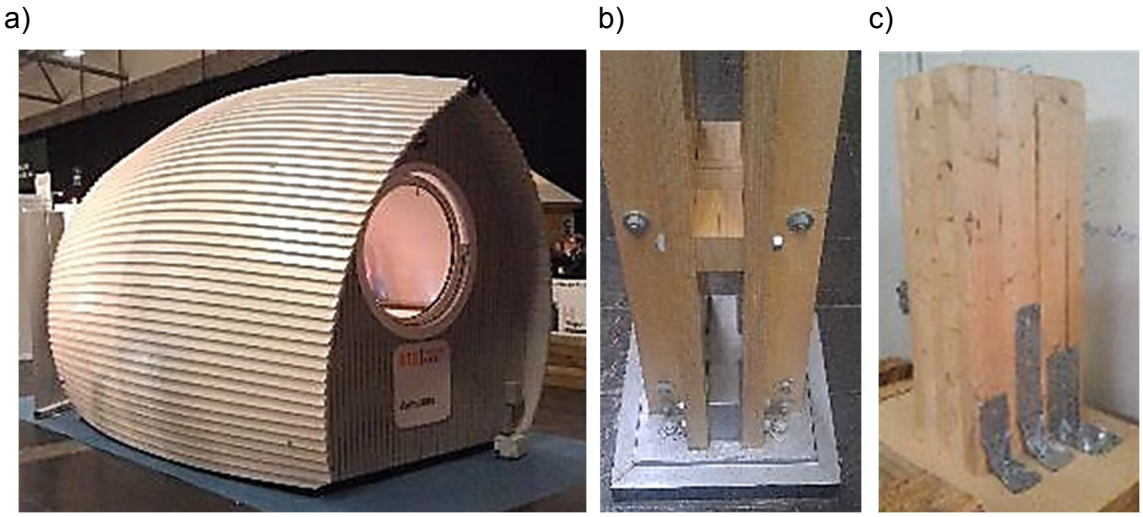

Figure 11-20. Applications and timber connection systems that can be replicated or used in G-XLam panel technologies. a) Armadilla pod at Timber Expo-2012. b) Footing connection of a Glulam column at FP innovations, Quebec.c) CLT floor to wall connection system detail.

Concluding remarks

An assessment of the industrialisation process for G-XLam panels manufacture has been carried out, together with design proposals that illustrate the potential use of G-XLam technologies in a variety of structural solutions.

Guidelines for the implementation of the technology from crop to factory and recommendations regarding the standardisation of the process and the tools and machinery required have also been provided. Maximum sizes of G-XLam elements achievable using the technology presented in this study will depend mainly on the densification process devised and the lamination and clamping methods available. Currently, the maximum commercial length of Guadua strips is 4,50m; however, manufacture of eight metres long strips of Guadua is viable. On the other hand, the maximum length of commercial hot-presses is 2.40m; therefore, alternative densification systems need to be developed. Heated roller systems could provide a continuous method for densifying longer sections of Guadua and producing flat Guadua strips (FGS).

The flatness and dimensional regularity of the G-XLam panels allows for their use in conjunction with conventional materials and structural systems. The potential use of G-XLam panel technology for structural shear wall systems, panelised sandwich systems and volumetric construction has been illustrated through design solutions, which employ standard timber connection systems. Furthermore, the design flexibility of the G-XLam panel technology has been demonstrated. Thanks to the high axial stiffness and bendability of the individual FGS, curved vaulted elements and grid shells are some of the possible design solutions.

Implementation of any of the proposed structural systems will require thorough study of adhesive systems. The epoxy resin system used in this study provided a strong interface between the layers with a low glue content (3%); however, cheaper and more environmentally friendly alternatives could be utilised.

12. Conclusions

A flat cross-laminated Guadua (G-XLam) panel was developed using straight-forward thermo-hydro-mechanical (THM) densification and cold-press glue lamination methods that can be easily applied in industry. G-XLam panels tackle the difficulties of using round Guadua in traditional construction by providing an engineered Guadua product (EGP) whose manufacturing process, size, shape, physical and mechanical properties can be standardised, controlled and tailored for mainstream applications in the new built environment. Additionally, the technology used for the manufacture of G-XLam panels has low environmental impact and wastage when compared to traditional construction and industrialised manufacturing systems applied to Guadua.

Round culms of Guadua were sectioned into strips, soaked and thermo-hydro-mechanically modified. THM densification of these strips resulted in flat, stiff and strong lamellae of Guadua (FGS) with a uniform density profile. Physical and mechanical properties of the densified layers of Guadua were characterised through microstructural image-analysis and mechanical testing. This demonstrated the achievement of a uniform density profile across the section, the density enhancement and the improvement of the elastic properties of Guadua post-densification. Characteristic values permitted the prediction of the mechanical properties of the G-XLam panels through numerical methods and finite element (FE) models. For structural analysis G-XLam panels were considered as multi-layered systems composed of contiguous lamellae with orthotropic axes orientated at 0° and 90°. A perfectly rigid connection between layers was assumed and the effect of glue bonds between layers was neglected. Numerical and FE analyses successfully predicted and simulated the elastic and strength response of G-XLam panels to set axial compression and bending load conditions. These analyses used timber engineering models which are normalized by European standards and applied to cross-laminated panel compositions typical of plywood and CLT (cross-laminated timber) panels.

G-XLam panels of three and five layers were manufactured in large sizes. An epoxy-resin was used during lamination with the aim of attaining a strong interface between the layers and fully exploiting the physical and mechanical properties of the densified layers of Guadua. G-XLam panels were then tested using physical and non-contact measurement techniques, their elastic properties assessed and the results compared to the values obtained through numerical analysis and FE models. An adequate match between the predictions and the test results was found for assessing the elastic properties of the G-XLam panels.

G-XLam panels are slender, stiff and strong laminated systems with high density whose mechanical properties are comparable to engineered timber products such as cross laminated timber (CLT) and laminated veneer lumber (LVL). Assessment of processing, design and usability potential of G-XLam systems resulted in a proposal for their manufacture and architectural and structural solutions.

Overall, the developed cross-laminated Guadua (G-XLam) panels can potentially reduce structural design uncertainties, improve durability, facilitate modularity and prefabrication, enhance the carbon footprint of traditional Guadua construction and offer an alternative to wood products.

Final remarks

- ✓ Bamboo is a structurally graded material whose mechanical properties vary depending on the material orientation. Similarly to wood, bamboo is structurally defined as an orthotropic material with three perpendicular planes of symmetry: radial (R), tangential (T) and longitudinal (L). Elastic properties of wood decrease depending on the orientation following the pattern $E_L > E_R > E_T$, whilst a different trend was found for the elastic properties of the non-modified Guadua sample: $E_L > E_T > E_R$. This might be due to the absence of radial rays in bamboo unlike wood, which weakens its structural response to stresses perpendicular to the grain.

- ✓ The 150°C temperature and 6MPa pressure applied to Guadua in this research together with the increase of its moisture content to about 40% and the removal of its inner and outer 'skins' provided adequate conditions for plasticizing, densifying the material and avoiding considerable cell damage. These Thermo-hydro-mechanical (THM) treatment settings resulted in flattened strips of Guadua with stabilized

cross-sectional density that were appropriated for the development of flat engineered Guadua products. Furthermore, this process is a straight-forward method for transforming round Guadua culms into flat engineered lamellae, which can be used for the manufacture of laminated engineered Guadua products.

- ✓ The densification technology applied to Guadua reduced wastage of material during processing of flat Guadua strips from almost 50% to about 20%. Furthermore, it enhanced its density by about 40% (from 540kg/m^3 to 890kg/m^3), its Young's modulus (E_1) by a factor of two (16.88GPa to 30.72GPa) and its shear modulus (G_{12}) by a factor of three (0.41 to 1.32 GPa).

- ✓ G-XLam panel lamination used 10 times less adhesive for gluing the layers than commercial bamboo-Moso products such as SWB (stranded woven bamboo); thus reducing the potential carbon footprint of G-XLam products.

- ✓ Structural systems using G-XLam panels could make use of connections systems available for timber construction and offer an alternative to engineered timber products.

Future Work

- ✓ Study the microstructural and chemical composition changes caused by the THM modification applied to Guadua to better understand the densification mechanism and determine if preservation methods prior to processing are required or can be avoided.

- ✓ Study the resulting transverse (radial and tangential) Poisson's ratios to determine if bamboos exhibit an auxetic behaviour along these sections.

- ✓ Fully characterise the mechanical properties of Guadua to probe if the matrix of orthotropic properties applied to wood are suitable for the structural analysis of Guadua.

- ✓ Study the effects of the increase moisture and relative humidity on the THM modification of Guadua in depth.

- ✓ Study the recovery spring-back effect of THM densified Guadua and the suitable post-treatment methods (oil, steam or temperature increase) to avoid it.

- ✓ Undertake dynamic shear-racking tests on the wall panels to assess their performance under cyclic loading.
- ✓ Carry out a life cycle assessment of the panels from cradle to cradle considering their recycling alternatives and end of life uses.
- ✓ Assess alternative adhesive systems. The epoxy resin system used in this study provided a strong interface between the layers with a low glue content (3%); however, cheaper and more environmentally friendly alternatives could be utilised.

References

AIS & FOREC. (2002a). *Manual de construcción sismo resistente de viviendas en bahareque encementado*. Bogotá, D.C., Colombia.

AIS & FOREC. (2002b). *Manual de evaluación, rehabilitación y refuerzo de viviendas de bahareques tradicionales (construidas con anterioridad a la vigencia del decreto 052 de 2002)*. Bogotá D.C., Colombia.

Amada, S., Ichikawa, Y., Munetake, T., Nagase, Y. & Shimizu, H. (1997). Fibre texture and mechanical graded structure of bamboo. *Composites Part B: Engineering*, 28(1-2), pp.13–20.

Amada, S. & Lakes, R. S. (1997). Viscoelastic properties of bamboo. *Journal of Materials Science*, 32, pp.2693–2697.

Ambur, D. R., Jaunky, N. & Hilburger, M. W. (2004). Progressive failure studies of stiffened panels subjected to shear loading. *Composite Structures*, 65(2), pp.129–142.

Ansell, M. P. (2011). Wood: A 45th anniversary review of JMS papers. Part 2. Wood modification, fire resistance, carbonization, wood–cement and wood–polymer composites. *Journal of Materials Science*, 47(2), pp.583–598.

Ansell, M. P. & Mwaikambo, L. Y. (2009). The structure of cotton and other plant fibres. In S. J. Eichhorn, J. W. S. Hearle, M. Jaffe & T. Kikutani (Eds.), *Handbook of textile fibre structure* (pp.62–94). Cambridge, UK: Woodhead Publishing Ltd.

Arango-Arango, A. M. (2011). *Posibilidades de la Guadua para la mitigación del cambio climático caso: eje cafetero Colombiano. BSc. Dissertation.* Universidad Tecnológica de Pereira.

Arbeláez A., A., Rodríguez, S. & Hurtado, A. (2001). *Investigaciones sobre Guadua angustifolia* Kunth *realizadas en Colombia (1950-2000)*. Report prepared for Universidad Nacional de Colombia & Corporación autónoma regional del Quindío (CRQ). Medellín, Colombia

Arias-Giraldo, L. M., Camargo-García, J. C. & Cardona-Trujillo, H. (2008). Carbono orgánico hedáfico en rodales de Guadua, *Guadua angustifolia* Kunth, Poeceae y en pasturas arborizadas en la zona cafetera de Colombia. In E. Murgueitio-Restrepo, C. A. Cuartas-Cardona & J. F. Naranjo Ramírez (Eds.), *Ganadería del futuro: Investigación para el desarrollo* (p. 490). Cali, Colombia: Fundación CIPAV.

ASTM. (1961). *Symposium on Shear and Torsion Testing*. Baltimore, USA: American Society for Testing and Materials (ASTM).

ASTM. (1972). *ASTM D 805, Plywood and other glued veneer construction*. West Conshohocken, USA: American Society for Testing and Materials (ASTM).

ASTM. (1998). *ASTM D 5379, Standard test method for shear properties of composite materials by the v-notched beam method.* West Conshohocken, USA: American Society for Testing and Materials (ASTM).

ASTM. (2002). *ASTM E519-02*, *Standard Test Method for Diagonal Tension (Shear) in Masonry Assemblages*. West Conshohocken, USA: American Society for Testing and Materials (ASTM).

Aziz, S. H. & Ansell, M. P. (2004). Green Composites. In C. Baillie (Ed.), *Green Composites* (pp. 154–180). Cambridge, UK: Woodhead publishing Ltd.

Betts, R. (2011). *Behaviour of bamboo nails in multiple nailed timber connections. MEng Dissertation*. University of Bath.

Blass, H. J. (1995). *Timber engineering. - 1: Basis of design, material properties structural components and joints.* Almere, The Netherlands: Centrum Hout.

Blass, H. J. & Fellmoser, D. P. (2004). Design of solid wood panels with cross layers. *8th World Conference on Timber Engineering*, 14, pp.1001–1006.

Bodig, J. & Jayne, B. A. (1982). *Mechanics of wood and wood composites* (Reprint ed.). New York, U.S.A.: Van Nostrand Reinhold Company.

Bonnett, O. T. (1972). *Silicified Cells of Grasses: A Major Source of Plant Opal in Illinois. Agriculture Experiment Station Bulletin 742*. Urbana, Illinois.

Broadmeadow, M. & Matthews, R. (2003). *Forests, Carbon and Climate Change: the UK Contribution. Information note.* Edinburgh, UK.

BSI. (1957). *BS 373:1957 Methods of testing small clear specimens of timber*. London, UK: British Standard Institution (BSI).

BSI. (1969). *BS 4512:1969, Methods of test for clear plywood* (Vol. 3). London, UK: British Standard Institution (BSI).

BSI. (2004). *BS EN 789:2004, Timber structures — Test methods — Determination of mechanical properties of wood based panels* (Vol. 3). London, UK: British Standard Institution (BSI).

BSI. (2008). *BS EN 12369-3:2008, Wood-based panels — Characteristic values for structural design*. London, UK: British Standard Institution (BSI).

BSI. (2009). *BS EN 338: 2009 Structural timber — Strength classes*. London, UK: British Standard Institution (BSI).

BSI. (2010). *BS EN 408:2010, Timber structures — Structural timber and glued laminated timber — Determination of some physical and mechanical properties*. London, UK: British Standard Institution (BSI).

BSI. (2011). *BS EN 14272:2011, Plywood — Calculation method for some mechanical properties*. London, UK: British Standard Institution (BSI).

BSI. (2014). *BS EN 1995-1-1:2004 +A2:2014, Eurocode 5: Design of timber structures — Part1-1: General -Common rules and rules for buildings.* London, UK: British Standard Institution (BSI).

Bystriakova, N., Kapos, V. & Lysenko, I. (2004). *Bamboo biodiversity, Africa, Madagascar and the Americas. UNEP-WCMC/INBAR*. Cambridge, UK: UNEP-WCMC/INBAR.

Bystriakova, N., Kapos, V., Stapleton, C. & Lysenko, I. (2003). *Bamboo biodiversity, information for planning conservation and management in the Asia-Pacific region. UNEP-WCMC/INBAR*. Cambridge, UK: UNEP-WCMC/INBAR.

Camargo-García, J. C., Dossman, M. A., Rodriguez, A. & Arias, L. M. (2009). Integrated Management of Bamboo Resources in the Colombia Coffee Region. In S. Lucas & Liese (Eds.), Proceedings of *8th World Bamboo Congress* (Vol. 1165, pp. 299–321). Bangkok, Thailand: World Bamboo Organization.

CARDER, CRQ, CVC, CORPOCALDAS & CORTOLIMA. (2007). *Norma unificada para el manejo y aprovechamiento de la Guadua*: Publicaciones Bosques FLEGT (1). Pereira, Colombia.

Castaño, F. (1992). Sistemas silviculturales para la propagación del bambú guadua en Colombia. In Proceedings of *I Congreso Mundial del bambú-Guadua. Memorias*. Pereira, Colombia: INCIVA-Instituto Vallecaucano de Investigaciones.

Ceccotti, A. (2008). New Technologies for Construction of Medium-Rise Buildings in Seismic Regions: The XLAM Case. *Structural Engineering International*, 18(2), pp.156–165.

Cherdchim, B., Matan, N. & Kyokong, B. (2004). Effect of temperature on thermal softening of black sweet-bamboo culms (Dendrocalamus asper Backer) in linseed oil. *Songklanakarin J. Sci. Technol*, 26(6), pp.855–866.

Chiang, M. Y. M. & He, J. (2002). An analytical assessment of using the losipescu shear test for hybrid composites. *Composites Part B: Engineering*, 33(6), pp.461–470.

Chung, K. F. & Yu, W. K. (2002) Mechanical properties of structural bamboo for bamboo scaffoldings. *Engineering Structures*. 24(4), pp.429–442 .

Correal, J. F. & Arbeláez, J. (2010). Influence of Age and Height Position on Colombian *Guadua angustifolia* Bamboo Mechanical Properties. *Maderas. Ciencia Y Tecnología*, 12(2), pp.105–113.

Correal, J. F., Echeverry, J. S., Ramírez, F. & Yamín, L. E. (2014). Experimental evaluation of physical and mechanical properties of Glued Laminated *Guadua angustifolia* Kunth. *Construction and Building Materials*, 73, pp.105–112.

Correlated Solutions. (2010). *Vic-3D 2010, testing guide*. Available at: www.correlatedsoultions.com

Crow, E. & Murphy, R. J. (2000). Microfibril orientation in differentiating and maturing fibre and parenchyma cell walls in culms of bamboo (Phyllostachys viridi-glaucescens (Carr.) Riv. & Riv.). *Botanical Journal of the Linnean Society*, 134(1-2), pp.339–359.

Cura, C. (2012). *Improving ductility of reformed bamboo. MEng dissertation.* Bath, UK: University of Bath.

Dayanandan, P., Kaufman, P. B. & Franklin, C. I. (1983). Detection of Silica in Plants. *American Journal of Botany*, 70(7), pp.1079–1084.

De Flander, K. & Rovers, R. (2009). One laminated bamboo-frame house per hectare per year. *Construction and Building Materials*, 23(1), pp.210–218.

Ding, T. P., Zhou, J. X., Wan, D. F., Chen, Z. Y., Wang, C. Y. & Zhang, F. (2008). Silicon isotope fractionation in bamboo and its significance to the biogeochemical cycle of silicon. *Geochimica et Cosmochimica Acta*, 72(5), pp.1381–1395.

Dinwoodie, J. M. (1989). *Wood: nature's cellular polymeric fibre-composite* (Book 420). London, UK & Brookfield, Vermont, USA: Institute of Metals.

Dujic, B., Klobcar, S. & Zarnic, R. (2007). Influence of openings on shear capacity of wooden walls. *NZ Timber Design Journal*, 16(1), pp.5–17.

Düking, R., Gielis, J. & Liese, W. (2011). Carbon Flux and Carbon Stock in a Bamboo Stand and their Relevance for Mitigating Climate Change. *Bamboo Science and Culture*, 24(1), pp.1–7.

Dwivedi, V. N., Singh, N. P., Das, S. S. & Singh, N. B. (2006). A new pozzolanic material for cement industry: Bamboo leaf ash. *International Journal of Physical Sciences*, 1(3), pp.106–111.

Esteves, B. M. & Pereira, H. M. (2009). Wood modification by heat treatment: a review. *BioResources*, 4(1), pp.370–404.

Fang, C., Cloutier, A., Mariotti, N., Koubaa, A. & Blanchet, P. (2010). Densification of Wood Veneers. In *Proceedings of the International Convention of Society of Wood Science and Technology and United Nations Economic Commission for Europe – Timber Committee* (pp. 1–9). Geneva, Switzerland.

FAO. (2006). *Global forest resources assessment 2010, Country report: Brazil*. Rome, Italy: Food and Agriculture Organization of the United Nations.

FAO. (2009). *The poor man's carbon sink, Bamboo in climate change and poor alleviation, Non-Wood Forest Products Document No. 8*. Rome, Italy: Food and Agriculture Organization of the United Nations.

FAO (2010a). *Global forest resources assessment 2010, Country report: China*. Rome, Italy: Food and Agriculture Organization of the United Nations.

FAO. (2010b). *Global Forest Resources Assessment 2010, Main report*. Rome, Italy: Food and Agriculture Organization of the United Nations.

FPL. (2010). *Wood Handbook: Wood as an Engineering Material. General Technical Report FPL-GTR-190*. (p.508). Madison, WI, USA: United States Department of Agriculture (USDA) Forest Service, Forest Products Laboratory.

Gagnon, S. & Pirvu, C. (2011). *CLT Handbook - Cross-Laminated Timber*. (S. Gagnon & C. Pirvu, Eds.) (Canadian ed.). Québec, Canada: FPInnovations.

Ganapathy, P. M., Zhu, H.-M., Zoolagud, S. S., Turcke, D. & Espiloy, Z. B. (1999). *Bamboo panel boards a state-of-the-art review. Technical Report No. 12*. (p.115). Beijing, China; New Delhi, India; Eindhoven, The Netherlands: : International Network for Bamboo and Rattan (INBAR).

García, J. J., Rangel, C. & Ghavami, K. (2012). Experiments with rings to determine the anisotropic elastic constants of bamboo. *Construction and Building Materials*, 31, pp.52–57.

Gédiac, M., Pierron, F. & Vautrin, A. (1994). The Iosipescu in-plane shear test applied to composites: a new approach based on displacement field processing. *Composites Science and Technology*, 51, pp.409–417.

Ghavami, K. (2005). Bamboo as reinforcement in structural concrete elements. *Cement and Concrete Composites*, 27(6), pp.637–649.

Ghavami, K. & Marinho, A. B. (2005). Propriedades físicas e mecânicas do colmo inteiro do bambu da espécie Guadua angustifolia. *Revista Brasileira de Engenharia Agrícola E Ambiental*, 9(1), pp.107–114.

Ghavami, K., Rodrigues, C. S. & Paciornik, S. (2003). Bamboo: Functionally graded composite material. *Asian Journal of Civil Engineering and Housing*, 4(1), pp.1–10.

Goldstein, J., Newbury, D.E., Joy, D.C., Lyman, C.E.,Echlin, P., Lifshin, E., Sawyer, L., Michael, J.R. (2003). *Scanning Electron Microscopy and X-ray Microanalysis* (Third ed., p.689). New York, USA: Springer US.

Gomez-Buitrago, B. (2002). *Evaluación del comportamiento de viviendas de bahareque con el sismo del 25 de enero de 1999. MPhil dissertation.* Universidad Nacional de Colombia.

González, H. A., Montoya, J. A. & Bedoya, J. R. (2007). Resultados del ensayo a flexión en muestras de bambú de la especie *Guadua angustifolia* Kunth. *Scientia et Technica*, Año XIII(35), pp.503–508.

Granta Design Limited (2007). *Granta's CES EduPack*. (Software) Granta Material Intelligence. Available at: http://www.grantadesign.com/education/edupack/index.htm

Gritsch, C. S., Kleist, G. & Murphy, R. J. (2004). Developmental changes in cell wall structure of phloem fibres of the bamboo Dendrocalamus asper. *Annals of Botany*, 94(4), pp.497–505.

Grossman, P. U. A. (1976). Requirements for a Model that Exhibits Mechano-Sorptive Behaviour. *Wood Science and Technology*, 10(November 1975), pp.163–168.

Hawong, J.-S., Shin, D.-C. & Baek, U.-C. (2004). Validation of pure shear test device using finite element method and experimental methods. *Engineering Fracture Mechanics*.

Heger, F., Groux, M., Girardet, F., Welzbacher, C., Rapp, A. O., Navi, P. (2004). Mechanical and Durability Performance of THM-Densified Wood. In Proceedings of *Final Workshop COST Action E22 'Environmental Optimisation of Wood Protection'* (pp. 1–10). Lisboa, Portugal.

Henley, G. & Yiping, L. (2009). *The Climate Change Challenge and Bamboo: Mitigation and adaptation*. (p.17). Beijing, China: International Network for Bamboo and Rattan (INBAR).

Henrikson, R. & Greenberg, D. (2011). *Bamboo architecture in competition and exhibition. Building Design*. Hawaii, USA: Ronore Enterprises, Inc.

Herrera-Giraldo, C., Gómez-Barrera, M., Saavedra-Hernández, M., Fonthal-Rivera, G., Gonzalez-Ceballos, V. E. & Ariza-Calderón, H. (2009). Cuantificación de sílice presente en el follaje de *Guadua angustifolia* del departamento del Quindío. *Revista Investigación Universidad del Quindío*, (19), 14– 17.

Hidalgo-López, O. (2003). *Bamboo: The gift of the gods*. (First ed., p.553). Bogotá D.C., Colombia: D'vinni Ltda.

Hill, C. A. S. (2007). *Wood Modification: Chemical, Thermal and Other Processes*. (First ed., p.260) Chichester, Sussex, UK: John Wiley & Sons.

Hisham, H. N., Othman, S., Rokiah, H., Latif, M., Ani, S. & Tamizi, M. M. (2006). Characterization of bamboo Gigantochloa scortechinii at different ages. *Tropical Forest Science*, 18(4), 236–242.

Hodgkinson, J. M. (2000). *Mechanical Testing of Advanced Fibre Composites* (First ed., p.384). Cambridge, UK: Woodhead Publishing Ltd.

Homan, W. J. & Jorissen, A. J. M. (2004). Wood modification developments. *Heron*, 49(4), 361–386.

Huang, D., Zhou, A. & Bian. (2013). Experimental and analytical study on the nonlinear bending of parallel strand bamboo beams. *Building Materials*, *44*(1), 595–602.

Hunter, I. R. & Junqi, W. (2002). *Bamboo biomass (Working paper No. 36)*. (p.11). Beijing, People's Republic of China: International Network for Bamboo and Rattan (INBAR).

ICONTEC. (2007). *NTC 5301, Preservación y secado del culmo de Guadua angustifolia* Kunth. Bogotá, D.C., Colombia: Instituto Colombiano de Normas Técnicas y Certificación (ICONTEC).

INBAR. (2002). *Industrial utilization on bamboo, INBAR Technical Report No. 26.* (p.207). Beijing, People's Republic of China: International Network for Bamboo and Rattan (INBAR).

ISO. (2004a). *ISO 22157-1: 2004 Determination of physical and mechanical properties - Part 1: Requirements*. Geneva, Switzerland: International Organisation for Standardisation.

ISO. (2004b). *ISO-TR 22157-2, Bamboo-Determination of physical and mechanical properties-Part 2: laboratory manual* (Vol. 2004). Geneva, Switzerland: International Organisation for Standardisation.

Janssen, J. J. A. (2000). *Designing and Building with Bamboo, INBAR Technical Report No.20*. (A. Kumar, Ed.) (p. 211). Eindhoven: INBAR-International Network for Bamboo and Rattan.

Jayanetti, D. L. & Follett, P. R. (1998). *Bamboo in construction, an introduction. INBAR Technical Report No. 15*. (p.120). UK: TRADA Technology Limited, International Network for Bamboo and Rattan (INBAR) & DFID (Department for International Development).

Kaminski, S. (2013). Engineered bamboo houses for low-income communities in Latin America. *The Structural Engineer*, 91(10), pp.14–23.

Kamke, F. A. & Sizemore, H. (2008). Viscoelastic thermal compression of wood. US 7404422 B2. (p.14). USA: United States Patent Office.

Kamruzzaman, M., Saha, S. K., Bose, A. K. & Islam, M. N. (2008). Effects of age and height on physical and mechanical properties of bamboo. *Tropical Forest Science*, 20(3), 211–217.

Kaufmann. (2009). *Manual Cross-laminated timber panels M1 BSP cross plan*. Austria: Mayr-Melnhof Kaufmann Group. Available at: http://www.mm-holz.com/

Khan, M. A., Mabrouki, T., Vidal-Sallé, E. & Boisse, P. (2010). Numerical and experimental analyses of woven composite reinforcement forming using a hypoelastic behaviour. Application to the double dome benchmark. *Journal of Materials Processing Technology*, 210(2), 378–388.

Kitazawa, K., Takahama, M. & Ogawa, H. (2004). Possibility of nosing of common Japanese bamboo. *Journal of Materials Science*, 39(4), 1473–1476.

Kleinhenz, V. & Midmore, D. J. (2001). Aspects of bamboo agronomy. *Advances in Agronomy*, 74, 99–153.

Kleinn, C. & Morales-Hidalgo, D. (2006). An inventory of Guadua (Guadua angustifolia) bamboo in the Coffee Region of Colombia. *European Journal of Forest Research*, 125(4), 361–368.

Krause, J. Q. & Ghavami, K. (2009). TRANSVERSAL REINFORCEMENT IN BAMBOO CULMS. In Proceedings of *11th International Conference on Non-conventional Materials and Technologies (NOCMAT)* (pp. 6–9). Bath, UK.

Kubojima, Y., Yoshihara, H., Ohsaki, H. & Ohta, M. (2000). Accuracy of shear properties of wood obtained by simplified Iosipescu shear test. *Journal of Wood Science*, 46(4), pp.279–283.

Kutnar, A., Kamke, F. A. & Sernek, M. (2008a). Density profile and morphology of viscoelastic thermal compressed wood. *Wood Science and Technology*, 43(1-2), pp.57–68.

Kutnar, A., Kamke, F. A. & Sernek, M. (2008b). The mechanical properties of densified VTC wood relevant for structural composites. *Holz Als Roh- Und Werkstoff*, 66(6), pp.439–446.

Kutnar, A. & Sandberg, D. (2015). Next steps in developing thermally modified timber to meet requirements of European low carbon economy. *International Wood Products Journal*, 6(1), pp.8–13.

Kutnar, A. & Šernek, M. (2007). Densification of wood. *Zbornik Gozdarstva in Lesarstva*, 82, pp.53–62.

Lanning, F. C., Ponnaiya, B. W. X. & Crumpton, C. F. (1958). The chemical nature of silica in plants. *Plant Physiology*, 33(5), pp.339–343.

Li, H. & Shen, S. (2011). The mechanical properties of bamboo and vascular bundles. *Journal of Materials Research*, 26(21), pp.2749–2756.

Li, S. H., Fu, S. Y., Zhou, B. L., Zeng, Q. Y. & Bao, X. R. (1994). Reformed bamboo and reformed bamboo/aluminium composite. *Journal of Materials Science*, 29, pp.5990–5996.

Li, X. B., Shupe, T. F., Peter, G. F., Hse, C. Y. & Eberhardt, T. L. (2007). Chemical changes with maturation of the bamboo species Phyllostachys pubescens. *Tropical Forest Science*, 19(1), pp.6–12.

Li, Z., Lin, P., He, J., Yang, Z. & Lin, Y. (2006). Silicon's organic pool and biological cycle in moso bamboo community of Wuyishan Biosphere Reserve. *Journal of Zhejiang University. Science. B*, 7(11), pp.849–857.

Liese, W. (1985). Anatomy and Properties of Bamboo. In Proceedings of *International bamboo workshop, China* (pp. 196–208). Beijing, People's Republic of China: International Network for Bamboo and Rattan (INBAR).

Liese, W. (1998). *The anatomy of bamboo culms. INBAR Technical Report No. 18*. (p.111). Beijing, People's Republic of China: International Network for Bamboo and Rattan (INBAR).

Liese, W. (2003). *Preservation of bamboo in service (Working paper)*. (pp.1-5). Germany: Hamburg University.

Liese, W. & Grosser, D. (1971). On the anatomy of Asian bamboos, with special reference to their vascular bundles. *Wood Science and Technology*, 5, pp.290–312.

Liese, W. & Weiner, G. (1996). Ageing of bamboo culms. A review. *Wood Science and Technology*, 30(2), pp.77–89.

Lindt, J. W. Van De. (2004). Evolution of wood shear wall testing, modelling, and reliability analysis: Bibliography. *Practice Periodical on Structural Design and Construction*, 9(No. 1, February 1), pp.44–53.

Ling, H., Samarasinghe, S. & Kulasiri, G. D. (2009). Modelling Variability in Full-field Displacement Profiles and Poisson Ratio of Wood in Compression Using Stochastic Neural Networks. *Silva Fennica*, 43(April), pp.871–887.

Lo, T., Cui, H., Tang, P. & Leung, H. (2008). Strength analysis of bamboo by microscopic investigation of bamboo fibre. *Construction and Building Materials*, 22(7), pp.1532–1535.

Londoño, X., Camayo, G. C., Riaño, N. M. & López, Y. (2002). Characterization of the anatomy of *Guadua angustifolia* (Poaceae: Bambusoideae) culms. *Bamboo Science and Culture*: *The Journal of the American Bamboo Society*, 16(1), pp.18–31.

Lou, Y., Li, Y., Buckingham, K., Giles, H. & Zhou, G. (2010). *Bamboo and Climate Change Mitigation Bamboo: a comparative analysis of carbon sequestration. INBAR Technical Report No. 32*. (p.47). Beijing, People's Republic of China: International Network for Bamboo and Rattan (INBAR).

Lux, A., Luxová, M., Abe, J., Morita, S. & Inanaga, S. (2003). Silicification of bamboo (Phyllostachys heterocycla Mitf.) root and leaf. *Plant and Soil*, 255(1), pp.85–91.

Lybeer, B. (2006). *Age-related anatomical aspects of some temperate and tropical bamboo culms (Poaceae: Bambusoideae). PhD Thesis in Biology*. Unversitiet Gent.

Lybeer, B., Acker, J. & Goetghebeur, P. (2006). Variability in fibre and parenchyma cell walls of temperate and tropical bamboo culms of different ages. *Wood Science and Technology*, 40(6), pp.477–492.

Lybeer, B., Koch, G., VAN Acker, J. & Goetghebeur, P. (2006). Lignification and cell wall thickening in nodes of Phyllostachys viridiglaucescens and Phyllostachys nigra. *Annals of Botany*, 97(4), pp.529–539.

Mahdavi, M., Clouston, P. L. & Arwade, S. R. (2011). Development of laminated bamboo lumber: review of processing, performance, and economical considerations. *Journal of Materials in Civil Engineering*, 23(7), pp.1036–1042.

Marcroft, J. (2012). *Concise Eurocodes: Design of Timber Structures. BS EN 1995-1-1: Eurocode 5*. London, UK: British Standards Institution.

Mastrogiuseppe, S., Rogers, C. a., Tremblay, R. & Nedisan, C. D. (2008). Influence of nonstructural components on roof diaphragm stiffness and fundamental periods of single-storey steel buildings. *Journal of Constructional Steel Research*, 64(2), pp.214–227.

Matan, N., Kyokong, B. & Preechatiwong, W. (2007). Softening Behavior of Black Sweet-Bamboo (Dendrocalamus asper Backer) at Various Initial Moisture Contents. *Walailak J Sci & Tech*, 4(2), pp.225–236.

Mead, D. J. (2001). *Mean annual volume increment of selected industrial forest plantation species*. Forest Plantation Thematic Papers, Working Paper 1. Rome, Italy: Food and Agriculture Organization (FAO) of the United Nations.

Mehra, P. N. & Sharma, O. P. (1965). Epidermal Silica Cells in the Cyperaceae. *Botanical Gazette*, 126(1), pp.53–58.

Metsä-Wood. (2011). *KERTO for load- bearing structures*. Technical specifications. Metsä Group. Available at: http://www.metsawood.com/global/

Micro-Measurements. (2014). *Tech Note TN-505-4. Strain Gage Selection: Criteria, Procedures, Recommendations*. Available at: www.micro-measurements.com

Milosevic, J., Lopes, M., Gago, A. S. & Bento, R. (2013). Testing and modelling the diagonal tension strength of rubble stone masonry panels. *Engineering Structures*, 52, pp.581–591.

MinAmbiente. (2010a). *Reglamento Colombiano de construcción sismo resistente, NSR-10*. Bogotá D.C., Colombia: Ministerio de Ambiente Vivienda y Desarrollo Territorial (MinAmbiente).

MinAmbiente. (2010b). *Titulo G-Estructuras de madera y estructuras de guadua. Reglamento Colombiano de construcción sismo resistente (NSR-10)*. Bogotá D.C., Colombia: Ministerio de Ambiente Vivienda y Desarrollo Territorial (MinAmbiente).

Minke, G. (2012). *Building with bamboo: design and technology of a sustainable architecture.* (p.160). Basel, Switzerland: Walter De Gruyter.

Montaño, C. D., Pels, J., Fryda, L. & Zwart, R. (2012). Evaluation of Torrefied Bamboo for Sustainable Bioenergy Production. In Proceedings of *IXth World Bamboo Congress* (pp. 809–818). Antwerp, Belgium.

Montoya A., J. A. (2005). Sap displacement method – Método de desplazamiento de savia (metodo boucherie) para la preservación de la *Guadua angustifolia* Kunth. *Scientia et Technica*, Año XI(28), pp.211–216.

Moore, J.R. (2011) *Sitka spruce in Great Britain: wood properties and uses.* Forestry Commission Research Report 15. (p.48). Edinburgh, UK: Forestry Commission.

Morán-Ubidia, J. A. (2011). *Traditional bamboo preservation methods in Latin America. INBAR Technical report No. 25*. (p.37). Guayaquil, Ecuador: International Network for Bamboo and Rattan (INBAR).

Moreno M., L. E., Osorio Serna, L. R. & Trujillo De Los Ríos, E. E. (2006). Estudio de las propiedades mecánicas de haces de fibra de Guadua angustifolia. *Ingeniería Y Desarrollo*, 20(Julio-Diciembre 2006), pp.125–133.

Morsing, N. (2000). *Densification of wood. The influence of hygrothermal treatment on compression of beech perpendicular to the grain. PhD Thesis.* (Series R No 79, p.138). Denmark: Danmarks Tekniske Universitet, Institut for Bærende Konstruktioner og Materialer.

Moss, P. J. & Walford, G. B. (1976). The testing of layered timber shell elements. *Matériaux et Constructions*, 9(5), pp.347–360.

Murphy, R. J., Trujillo, D. & Londoño, X. (2004). Life Cycle Assessment (LCA) of a Guadua House. In Proceedingd of *Simposio Internacional de Guadua* (pp. 235–244). Pereira, Colombia.

Najafgholipour, M. A., Maheri, M. R. & Lourenço, P. B. (2013). Capacity interaction in brick masonry under simultaneous in-plane and out-of-plane loads. *Construction and Building Materials*, 38, pp.619–626.

Nakajima, M., Furuta, Y. & Ishimaru, Y. (2008). Thermal-softening properties and cooling set of water-saturated bamboo within proportional limit. *Journal of Wood Science*, 54(4), pp.278–284.

Navi, P. (2010). Thermo-Hydro-Mechanical Wood Behaviour and Processing. Report for *COST Action FP0904.* Bern, Switzerland: Bern University of Applied Sciences.

Neelakantan, S., Bosbach, W., Woodhouse, J. & Markaki, A. E. (2014). Characterization and deformation response of orthotropic fibre networks with auxetic out-of-plane behaviour. *Acta Materialia*, 66, pp.326–339.

Nocetti, M., Brancheriau, L., Bacher, M., Brunetti, M. & Crivellaro, A. (2013). Relationship between local and global modulus of elasticity in bending and its consequence on structural timber grading. *European Journal of Wood and Wood Products*, 71(3), pp.297–308.

Nugroho, N. & Ando, N. (2000). Development of structural composite products made from bamboo I: fundamental properties of bamboo zephyr board. *Journal of Wood Science*, 46, pp.68–74.

Nugroho, N. & Ando, N. (2001). Development of structural composite products made from bamboo II: fundamental properties of laminated bamboo lumber. *Journal of Wood Sci Ence*, 47, pp.237–242.

Obataya, E., Kitin, P. & Yamauchi, H. (2007). Bending characteristics of bamboo (Phyllostachys pubescens) with respect to its fibre–foam composite structure. *Wood Science and Technology*, 41(5), pp.385–400.

Okabe, M., Yasumura, M., Kobayashi, K. & Fujita, K. (2013). Prediction of bending stiffness and moment carrying capacity of sugi cross-laminated timber. *Journal of Wood Science*, 60(1), pp.49–58.

Osorio-Saraz, J. A., Vélez-Restrepo, J. M. & Ciro-Velásquez, H. J. (2007). Guadua angustifolia. *Rev. Fac. Nal. Agr. Medellín*, 60(2), pp.4067–4076.

Osorio-Serna, L. R., Trujillo De Los Ríos, E. E., van Vuure, A. W., Lens, F., Ivens, J. & Verpoest, I. (2010). The relation between bamboo fibre microstructure and mechanical properties. In Proceedings of *14th European Conference on Composite Materials* (p. 10). Budapest, Hungary.

Parkkeeree, T., Matan, N. & Kyokong, B. (2014). Flattening of half tubular bamboo culms and fixation of bamboo boards. *Journal of Tropical Forest Science*, 26(1), pp.101–114.

PATH. (2006). Insulated Panels Structural Insulated Panels (manual). [Accessed: 25 August 2011]. Available at: www.pathnet.org

Pierron, F. & Vautrin, A. (1994). Accurate comparative determination of the in-plane shear modulus of T300/914 by the Iosipescu and 45° off-axis tests. *Composites Science and Technology*, 52, pp.61–72.

Poblete, H., Cuevas, H. & Diaz-vaz, J. E. (2009). Property characterization of Chusquea culeou, a bamboo growing in Chile. *Maderas. Ciencia Y Tecnología*, 11(2), pp.129–138.

Raftery, G. M. & Harte, A. M. (2011). Low-grade glued laminated timber reinforced with FRP plate. *Composites Part B: Engineering*, 42(4), pp.724–735.

Ranta-Maunus, A. (2000). Bending and compression properties of small diameter round timber. In Proceedings of *World Conference on Timber Engineering* (pp. 1–8). Whistler, Canada.

Rao, A. N., Rao, V. R. & Williams, J. T. (1998). *Priority species of bamboo and rattan*. (A. N. Rao, V. R. Rao & J. T. Williams, Eds.). (p.95). Serdang, Malaysia: International Plant Genetic Resources Institute (IPGRI) & Beijing, People's Republic of China: International Network for Bamboo and Rattan (INBAR).

Riaño, N. M., Londoño, X., López, Y. & Gómez, J. H. (2002). Plant growth and biomass distribution on *Guadua angustifolia* Kunth in relation to ageing in the Valle del Cauca–Colombia. *The Journal of the American Bamboo Society*, 16(1), pp.43–51.

Robledo-C., J. (1996). *La ciudad en la colonización antioquena: Manizales*. (p.213) Bogotá D.C., Colombia: Editorial Universidad Nacional.

Rojas-Quiroga, R. A., Li, T., Lora, G. & Andersen, L. E. (2013). *A Measurement of the Carbon Sequestration Potential of Guadua angustifolia in the Carrasco National Park, Bolivia*. Development Research Working Paper Series 04/2013 (July). La Paz, Bolivia: Institute for Advanced Development Studies (INESAD).

Rusinque, M. & Takeuchi-Tam, C. (2007). Comportamiento de elementos de *Guadua angustifolia* solicitados a flexión cuando se perforan los tabiques. In Proceedings of *IC-NOCMAT 2007, International Conference on Non-Conventional Materials and Technologies: Ecological materials and technologies for sustainable building.* Maceió, Alagoas, Brazil.

Sánchez-Echeverry, L. A., Aita, G., Robert, D. & Rodriguez-Garcia, M. E. (2014). Correlation between chemical compounds and mechanical response in culms of two different ages of *Guadua angustifolia* Kunth. *Madera Y Bosques*, 20(2), pp.87–94.

Sandberg, D. & Kutnar, A. (2014). Recent Progress in the Industrial Implementation of Thermo- Hydro (TH) and Thermo-Hydro-Mechanical (THM) Processes. (L. Nunes, D. Jones, C. Hill & H. Militz, Eds.). In Proceedings of *The seventh European Conference on Wood Modification (ECWM7)* Lisbon, Portugal.

Sandberg, D. & Navi, P. (2007). *Introduction to Thermo-Hydro- Mechanical (THM) Wood Processing.* (Report No.30, p.167). Växjö, Sweden: School of Technology and Design, Växjö University.

Schneider, M. H. & Phillips, J. G. (1991). Elasticity of wood and wood polymer composites in tension compression and bending. *Wood Science and Technology*, 364, pp.361–364.

Scurlock, J. M. O., Dayton, D. C. & Hames, B. (2000). Bamboo: an overlooked biomass resource? *Biomass and Bioenergy*, 19(4), pp.229–244.

Seborg, R. M., Millet, M. A. & Stamm, A. J. (1956). *Heat-stabilized compressed wood (Staypak). Report No. 1580*. Madison, WI, USA: United States Department of Agriculture (USDA) Forest Service, Forest Products Laboratory.

Steffen, W., Richardson, C., Rockström, J., Cornell, S. E., Fetzer, I., Bennett, E. M., Biggs, R., Carpenter, S., Vries, W., Wit, C., Folke, C., Gerten, D., Heinke, J., Mace, G. M., Persson, L. M., Ramanathan, V., Reyers, B. & Sörlin, S. (2015). Planetary boundaries: Guiding human development on a changing planet. *Science*, 347(6223), pp. 791.

Sulastiningsih, I. M. & Nurwati, P. (2009). Physical and mechanical properties of laminated bamboo board. *Journal of Tropical Forest Science*, 21(3), pp.246–251.

Sutton, A., Black, D. & Walker, P. (2011). *Straw bale, an introduction to low impact building materials. BRE Information Paper 15*. (IP 15/11). Wattford, UK: IHS BRE Press.

Takeuchi-Tam, C. P. (2004). Comportamiento estructural de la Guadua angustifolia. Uniones en guadua. *Revista Ingeniería E Investigación*, (55), pp.3–7.

Takeuchi-Tam, C. P. & González, C. E. (2007). Resistencia a la compresión paralela a la fibra de la *Guadua angustifolia* y determinación del módulo de elasticidad. *Ing. Univ. Bogotá*, 11(1), pp.89–103.

Tanaka, K., Ishitani, J. & Inoue, M. (2008). Improvement of strength performance for bamboo connector by densified technique. *Journal of Structural and Construction Engineering (Transactions of AIJ)*, 73(632), pp.1805–1812.

Thompson, D. A. & Matthews, R. W. (1989). *The storages of Carbon in trees and timber. Research Information Note 160* (Vol. 160). Surrey, UK: Forestry Commission Research Division.

TRADA. (2009). *TRADA Technology Guidance Document 10 (GD10) Cross-laminated Timber (Eurocode 5) Design Guide for Project Feasibility*. High Wycombe, UK: TRADA Technology Ltd.

Trubiano, F. (2015). *Design and construction of high-performance homes: Building envelopes, renewable energies and integrated practice*. (First ed., p.298). Abingdon, UK: Taylor & Francis Group.

Trujillo, D. J. A., Ramage, M. & Chang, W.-S. (2013). Lightly modified bamboo for structural applications. *Construction Materials*, 166(CM4), pp.238–247.

Trujillo De Los Ríos, E. E., Osorio-Serna, L. R., van Vuure, A. W., Ivens, J. & Verpoest, I. (2010). Characterization of polymer composite materials based on bamboo fibres. In Proceedings of *14th European Conference on Composite Materials*, (June). Budapest, Hungary.

UN-HABITAT. (2009). *Global Report on Human Settlements 2009: Planning Sustainable Cities.* London, UK: United Nations Human Settlements Programme (UN-HABITAT).

Van der Lugt, P., Vogtländer, J. & Brezet, H. (2009). *Bamboo, a Sustainable Solution for Western Europe: Design Cases, LCAs and Land-use. Technical report No.30.* (p.87). Beijing, People's Republic of China: International Network for Bamboo and Rattan (INBAR) & Delft,The Netherlands: Delft University of Technology, Faculty of Industrial Design Engineering, Design for Sustainability Program.

Van der Lugt, P., van Den Dobbelsteen, A. & Abrahams, R. (2003). Bamboo as a building material alternative for Western Europe? A study of the environmental performance, costs and bottlenecks of the use of bamboo (products) in Western Europe. *Journal of Bamboo and Rattan*, *2(3)*, pp.205–223.

Villegas, M. (1989). *Tropical bamboo*. (p.176). Bogotá D.C., Colombia: Villegas editores.

Villegas, M. (2003). *New Bamboo. Architecture and Design.* (p.208). Bogotá D.C., Colombia: Villegas editores.

Vogtländer, J. G. & van der Lugt, P. (2014). *The Environmental Impact of Industrial Bamboo Products: Life cycle assessment and carbon sequestration. Technical report No.35.* (p.54). Beijing, People's Republic of China: International Network for Bamboo and Rattan (INBAR)

Vogtländer, J. G., van der Velden, N. M. & van der Lugt, P. (2013). Carbon sequestration in LCA, a proposal for a new approach based on the global carbon cycle; cases on wood and on bamboo. *The International Journal of Life Cycle Assessment*, 19(1), pp.13–23.

Vogtländer, J., van der Lugt, P. & Brezet, H. (2010). The sustainability of bamboo products for local and Western European applications. LCAs and land-use. *Journal of Cleaner Production*, 18(13), pp.1260–1269.

Wahab, R., Mustafa, M. T., Salam, M. A., Sudin, M., Samsi, H. W. & Rasat, M. S. M. (2013). Chemical Composition of Four Cultivated Tropical Bamboo in Genus Gigantochloa. *Journal of Agricultural Science*, *5*(8), 66–75.

Wegst, U. G. K. (2011). Bending efficiency through property gradients in bamboo, palm, and wood-based composites. *Journal of the Mechanical Behaviour of Biomedical Materials*, 4(5), pp.744–755.

Wegst, U. G. K. & Ashby, M. F. (2004). The mechanical efficiency of natural materials. *Philosophical Magazine*, 84(21), pp.2167–2186.

Weinstock, M. (2006). Self-organisation and the structural dynamics of plants. *Architectural Design*, 76(2), pp.26–33.

Welzbacher, C. R., Wehsener, J., Rapp, a. O. & Haller, P. (2007). Thermo-mechanical densification combined with thermal modification of Norway spruce (Picea abies Karst) in industrial scale – Dimensional stability and durability aspects. *Holz Als Roh- Und Werkstoff*, 66(1), pp.39–49.

Wills, C. (2012). *Processing of bamboo into laminated structures. MEng dissertation.* Bath, UK: University of Bath.

Wittenberg, T. C., van Baten, T. J. & de Boer, A. (2001). Design of fibre metal laminate shear panels for ultra-high capacity aircraft. *Aircraft Design*, 4(2-3), pp.99–113.

Wood, L. W. (1960). *Variation of strength properties in woods used for structural purposes.* Madison, WI, USA: United States Department of Agriculture (USDA) Forest Service, Forest Products Laboratory.

Xavier, J. C., Garrido, N. M., Oliveira, M., Morais, J. L., Camanho, P. P. & Pierron, F. (2004). A comparison between the Iosipescu and off-axis shear test methods for the characterization of Pinus Pinaster Ait. *Composites Part A: Applied Science and Manufacturing*, 35(7-8), pp.827–840.

Xiao, Y., Inoue, M. & Paudel, S. K. (2008). Modern Bamboo structures. In Y. Xiao, M. Inoue & S. K. Paudel (Eds.), Proceedings of *1st International Conference on Modern Bamboo Structures (ICBS 2007)* (pp. 5–21). London/UK: Taylor & Francis Group.

Xiao, Y., Yang, R. Z. & Shan, B. (2013). Production, environmental impact and mechanical properties of glubam. *Construction and Building Materials*, *44*(1), 765–773.

Yates, T., Ferguson, A., Binns, B. & Hartless, R. (2013). *Cellulose-based building materials Use, performance and risk*. (p.52). Milton Keynes, UK: NHBC Foundation & IHS BRE Press.

Yoshihara, H., Ohsaki, H., Kubojima, Y. & Ohta, M. (1999). Applicability of the Iosipescu shear test on the measurement of the shear properties of wood. *J Wood Sci*, 45, pp.24–29.

Yoshimura, K., Croston, T., Kagami, H. & Ishiyama, Y. (1999). Damage to Building Structures Caused by the 1999 Quindio Earthquake in Colombia-Report. *Reports of the Faculty of Engineering Research, Oita University*, 40, pp.25–32.

Zea-Escamilla, E. & Habert, G. (2014). Environmental impacts of bamboo-based construction materials representing global production diversity. *Journal of Cleaner Production*, 69, pp.117–127.

Zhang, Y. M., Yu, Y. L. & Yu, W. J. (2012). Effect of thermal treatment on the physical and mechanical properties of phyllostachys pubescen bamboo. *European Journal of Wood and Wood Products*, 71(1), pp.61–67.

Zhou, B., Fu, M., Xie, J., Yang, X. & Li, Z. (2005). Ecological functions of bamboo forest: Research and Application. *Journal of Forestry Research*, 16(2), pp.143–147.

Author's bibliography

Journal papers

Archila-Santos, H.F., Ansell, M.P. & Walker, P., 2014. Elastic Properties of Thermo-Hydro-Mechanically Modified Bamboo (*Guadua angustifolia* Kunth) Measured in Tension. *Key Engineering Materials*, 600, pp.111–120.

Archila-Santos, H.F., Ansell, M.P. & Walker, P., 2012. Low Carbon Construction Using Guadua Bamboo in Colombia. *Key Engineering Materials*, 517, pp.127–134.

Conference papers

Archila H., Brandon, D., Ansell M., Walker P. & Ormondroyd, G. Evaluation of the mechanical properties of cross laminated bamboo panels by digital image correlation and finite element modelling. In Proceedings of *68th FPS-IC and WCTE 2014*, Canada; 08/2014

Archila, H., Takeuchi, C., Trujillo, D. Mechanical and physical characterization of composite bamboo-Guadua products: Plastiguadua. In Proceedings of *68th FPS-IC and WCTE 2014,* Canada; 08/2014

Archila H., Ansell M. & Walker P., Mechanical characterization of engineered Guadua-bamboo panels using digital image correlation. In Proceedings of *Young Researchers' Forum II: Construction Materials*, University College London, London, 02/2014.

Conferences & Workshops

XXIV IUFRO World Congress 2014 *"Sustaining Forests, Sustaining People: The Role of Research"*. [Chair special session] 5-11.10.2014, Salt Lake City, US,

World Conference on Timber Engineering (WCTE 2014), *The renaissance of timber*. [Two oral presentations] 10-14.08.2014, Canada.

Researcher Links Workshop, *Promoting bamboo as a construction material.* [Participation] March 2014, Colombia.

Young Researchers Forum II, *"Mechanical Characterization of engineered Guadua-bamboo panels using Digital Image Correlation"*. [Oral presentation] 19.02.2014 at UCL, London

European Conference on Cross Laminated Timber (CLT) - *Focus Solid Timber Solutions*. [Attendance]. 21.05.2013, Graz, Austria.

14th NOCMAT, *International Conference on Non-Conventional Materials and Technologies.* [Oral Presentation] 24-27.03.2013. Joao Pessoa, Brazil.

9th World Bamboo Congress. [Oral Presentation] 9-15.04.2012. Antwerp. Belgium

13th NOCMAT, *International Conference on Non-Conventional Materials and Technologies*. [Oral Presentation] 22-24.08.2010. Changsha. China.

ECOCOMP 2011, *4th International Conference on Sustainable Materials*, Polymers and Composites. [Oral Presentation] 6-7.07.2011. Birmingham. United Kingdom.

Meeting of minds - University of Bath. [Oral presentation] 9.06.2011. Bath. UK.

BRLSI, *Bath Royal Literary and Scientific Institution*. [Lecture] August 2011, Bath. UK.

IOM3 Conference, *Innovation toward sustainable materials*. Institute of Materials, Minerals and Mining, November 2010. London, UK.

Author's profile

Hector joined the University of Bath in 2010 to carry out a doctoral research programme on structural bamboo composites for construction. Having previously finished a five-year diploma programme in architecture he worked for seven years in the construction industry in Colombia and managed an architectural and engineering practice delivering about 32.000 sq. ft. of new builds.

Hector's practical experience in construction with conventional and non-conventional materials (bamboo *Guadua angustifolia* Kunth -Guadua) and research on bamboo composites have been widely recognized through several awards, including scholarships and travel grants. These have given him the opportunity to support his research studies, network with fellow researchers, and present his work internationally. He has established collaboration with researchers in various research centres, undertaken extensive lab-work and written several journals and conference papers as main author.

During his time at the University of Bath, Hector has carried out engineering labs-teaching, architecture 'crits' and supervision duties for undergraduate and master students across architecture and engineering disciplines. He has also delivered lectures on engineered bamboo products for construction, participated in international workshops and organized academic events with the support of private and public organisations.

Awards & Grants

Wood Preservation Fund Student Scholarship (2014) by the Forest Product Society, Canada.
Gauntlet trust travel grant (2014, 2012 & 2011) by the ARMOURERS & BRASIERS' COMPANY, UK.
Best Oral presentations (2013) at XIV NOCMAT-IC, 27.03.2013, Brazil.
SANTANDER Research grant (2011) Research visit to China, UK.
COLCIENCIAS PhD studentship (2011) - Full scholarship. Becas bicentenario, Colombia.
COLFUTURO Loan Scholarship. (2010) MPhil Architecture & Civil Engineering, Colombia.